Towards all-optical label switching nodes with multicast

Towards All-Optical Label Switching Nodes with Multicast

Ni Yan

Towards All-Optical Label Switching Nodes with Multicast

PROEFSCHRIFT

ter verkrijging van de graad van doctor aan de
Technische Universiteit Eindhoven, op gezag van de
Rector Magnificus, prof.dr.ir. C.J. van Duijn, voor een
commissie aangewezen door het College voor
Promoties in het openbaar te verdedigen
op maandag 14 april 2008 om 16.00 uur

door

Ni Yan

geboren te Hubei, China

Dit proefschrift is goedgekeurd door de promotor:

prof.ir. A.M.J. Koonen

Copromotor:
dr.ir. E. Tangdiongga

The work described in this thesis was performed in the Faculty of Electrical Engineering of the Eindhoven University of Technology and was financially supported by the European Commission through the IST projects STOLAS and LASAGNE, and Network of Excellence ePhoton/ONe (+) program.

Typeset using LaTeX, printed in The Netherlands

CIP-DATA LIBRARY TECHNISCHE UNIVERSITEIT EINDHOVEN

Yan, Ni

Towards all-optical label switching nodes with multicast / by Ni Yan. -
Eindhoven : Technische Universiteit Eindhoven, 2008.
Proefschrift. - ISBN 978-90-386-1834-0
NUR 959
Trefw.: optische schakelaars / optische signaalverwerking / nietlineaire optica /
optische telecommunicatie / computernetwerken ; packet switching.
Subject headings: photonic switching systems / multicast communication /
optical wavelength conversion / optical fibre communication / packet switching.

To Francesco, Angela, and my parents

who have given my life such a colorful spectrum

Samenstelling van de promotiecommissie

voorzitter	**prof.dr.ir. A.C.P.M. Backx**, decaan
	fac. Elektrotechniek
	Technische Universiteit Eindhoven, The Netherlands
promotor	**prof.ir. A.M.J. Koonen**
	afd. Electro-Optical Communication, fac. Elektrotechniek
	Technische Universiteit Eindhoven, The Netherlands
copromotor	**dr.ir. E. Tangdiongga**
	afd. Electro-Optical Communication, fac. Elektrotechniek
	Technische Universiteit Eindhoven, The Netherlands
externe lid	**prof.dr. J. Martí Sendra**
	Centro de Tecnología Nanofotonica
	Universidad Politécnica de Valencia, Spain
externe lid	**prof.dr. M. Pickavet**
	Vakgroep Informatietechnologie
	Universiteit Gent, Belgium
lid TU/e	**prof.dr.ir. J.W.M. Bergmans**
	afd. Signal Processing Systems, fac. Elektrotechniek
	Technische Universiteit Eindhoven, The Netherlands
overige lid	**prof.dr. H.J.S. Dorren**
	afd. Electro-Optical Communication, fac. Elektrotechniek
	Technische Universiteit Eindhoven, The Netherlands
overige lid	**prof.dr.ir. O.J. Boxma**
	afd. Stochastische Besliskunde, fac. Wiskunde & Informatica
	Technische Universiteit Eindhoven, The Netherlands

Summary

Towards all-optical label switching nodes with multicast

Fiber optics has developed so rapidly during the last decades that it has become the backbone of our communication systems. Evolved from initially static single-channel point-to-point links, the current advanced optical backbone network consists mostly of wavelength-division multiplexed (WDM) networks with optical add/drop multiplexing nodes and optical cross-connects that can switch data in the optical domain. However, the commercially implemented optical network nodes are still performing optical circuit switching using wavelength routing. The dedicated use of wavelength and infrequent reconfiguration result in relatively poor bandwidth utilization. The success of electronic packet switching has inspired researchers to improve the flexibility, efficiency, granularity and network utilization of optical networks by introducing optical packet switching using short, local optical labels for forwarding decision making at intermediate optical core network nodes, a technique that is referred to as optical label switching (OLS).

Various research demonstrations on OLS systems have been reported with transparent optical packet payload forwarding based on electronic packet label processing, taking advantage of the mature technologies of electronic logical circuitry. This approach requires optic-electronic-optic (OEO) conversion of the optical labels, a costly and power consuming procedure particularly for high-speed labels. As optical packet payload bit rate increases from gigabit per second (Gb/s) to terabit per second (Tb/s) or higher, the increased speed of the optical labels will eventually face the electronic bottleneck, so that the OEO conversion and the electronic label processing will be no longer efficient. OLS with label processing

in the optical domain, namely, all-optical label switching (AOLS), will become necessary.

Different AOLS techniques have been proposed in the last five years. In this thesis, AOLS node architectures based on optical time-serial label processing are presented for WDM optical packets. The *unicast* node architecture, where each optical packet is to be sent to only *one* output port of the node, has been investigated and partially demonstrated in the EU IST-LASAGNE project. This thesis contributes to the *multicast* aspects of the AOLS nodes, where the optical packets can be forwarded to *multiple* or *all* output ports of a node. Multicast capable AOLS nodes are becoming increasingly interesting due to the exponential growth of the emerging multicast Internet and modern data services such as video streaming, high definition TV, multi-party online games, and enterprise applications such as video conferencing and optical storage area networks. Current electronic routers implement multicast in the Internet protocol (IP) layer, which requires not only the OEO conversion of the optical packets, but also exhaustive routing table lookup of the globally unique IP addresses. Despite that, there has been no extensive studies on AOLS multicast nodes, technologies and traffic performance, apart from a few proof-of-principle experimental demonstrations.

In this thesis, three aspects of the multicast capable AOLS nodes are addressed:

1. Logical design of the AOLS multicast *node architectures*, as well as functional subsystems and interconnections, based on state-of-the-art literature research of the field and the subject.
2. Computer simulations of the *traffic performance* of different AOLS unicast and multicast node architectures, using a custom-developed AOLS simulator `AOLSim`.
3. Experimental demonstrations in laboratory and computer simulations using the commercially available simulator *VPItransmissionMaker*™, to evaluate the *physical layer performance* of the required all-optical multicast technologies. A few selected multi-wavelength conversion (MWC) techniques are particularly looked into.

MWC is an essential subsystem of the AOLS node for realizing optical packet multicast by making multiple copies of the optical packet all-optically onto different wavelengths channels. In this thesis, the MWC techniques based on cross-phase modulation and four-wave mixing are extensively investigated. The former technique offers more wavelength flexibility and good conversion efficiency, but it is

only applicable to intensity modulated signals. The latter technique, on the other hand, offers strict transparency in data rate and modulation format, but its working wavelengths are limited by the device or component used, and the conversion efficiency is considerably lower.

The proposals and results presented in this thesis show feasibility of all-optical packet switching and multicasting at line speed without any OEO conversion and electronic processing. The scalability and the costly optical components of the AOLS nodes have been so far two of the major obstacles for commercialization of the AOLS concept. This thesis also introduced a novel, scalable optical labeling concept and a label processing scheme for the AOLS multicast nodes. The proposed scheme makes use of the spatial positions of each label bit instead of the total absolute value of all the label bits. Thus for an n-bit label, the complexity of the label processor is determined by n instead of 2^n.

Contents

Chapter 1

Introduction

In the last few years, emerging services such as voice-over-IP, video streaming, high definition TV and peer-to-peer file transfer services are becoming increasingly popular on top of the traditional Internet services. All-optical solutions for switching and routing of these packet-based data streams are of crucial importance for realizing a truly intelligent, transparent and broadband optical infrastructure, as they may enable to bypass the opto-electronic bottleneck consisting of optic-electronic-optic conversion, electrical signal processing and electronic switching. The rapidly-developing all-optical label switching (AOLS) technologies have the potential to support low-latency optical packet forwarding and routing based on short packet labels at fiber line-rate. The European Commission 6^{th} Framework Programme IST-LASAGNE (all-optical label swapping employing optical logic gates in network nodes) project, based on the scenario of optical packet-switched networks, proposed an AOLS node architecture for fixed-length optical data packets, which has been one of the first modular AOLS switching nodes of its kind. This chapter presents a brief introduction of the subject and a concise overview of the field, addresses the motivation of the research described in this thesis, and provides a quick reference to the thesis contents. Parts of this chapter are based on publications.[1]

[1] See reference [1, 2].

1.1 Entering the era of optical networking

Telecommunication networks have developed in leaps and bounds since the twentieth century. Communication between entities over networks relies on protocols and physical media. When networks were first implemented by universities and large businesses in late 1980's, the dominant transmission medium was copper wire [3], namely coaxial cable for high-speed data, and twisted copper pair cable for telephony subscriber lines. Nowadays, long-haul transmission networks are based on optical fibers, and many local to metropolitan networks are based on fibers or wireless.

1.1.1 Conventional network reference models

In order to transmit information across the physical medium in form of raw *bits*, layers of protocols have been developed. A set of layers and protocols is referred to as a network architecture [3, 4]. Two of the most important network architectures are based on the Open Systems Interconnection (OSI) reference model and the Transmission Control Protocol (TCP) / Internet protocol (IP) reference model.

a. The OSI reference model

The OSI model has *seven* layers [3, 4]:

1. *Application layer*: ensures compatibility among various entities by defining virtual terminal software to enable them to communication with each other.
2. *Presentation layer*: deals with the syntax and semantics of the information transmitted, i.e. by encoding data in a standard agreed-upon way. Its purpose differs from those of all the layers below, which are only interested in moving bits reliably from one point to another.
3. *Session layer*: allows users on different machines to establish *sessions* between themselves.
4. *Transport layer*: manages network connections from source to destination, such as point-to-point or point-to-multi-point channels, and determines the type of services (ToS), e.g. whether or not to guarantee the order of message delivery.
5. *Network layer*: determines how packets are routed from source to destination based on routing tables, and controls network congestion.

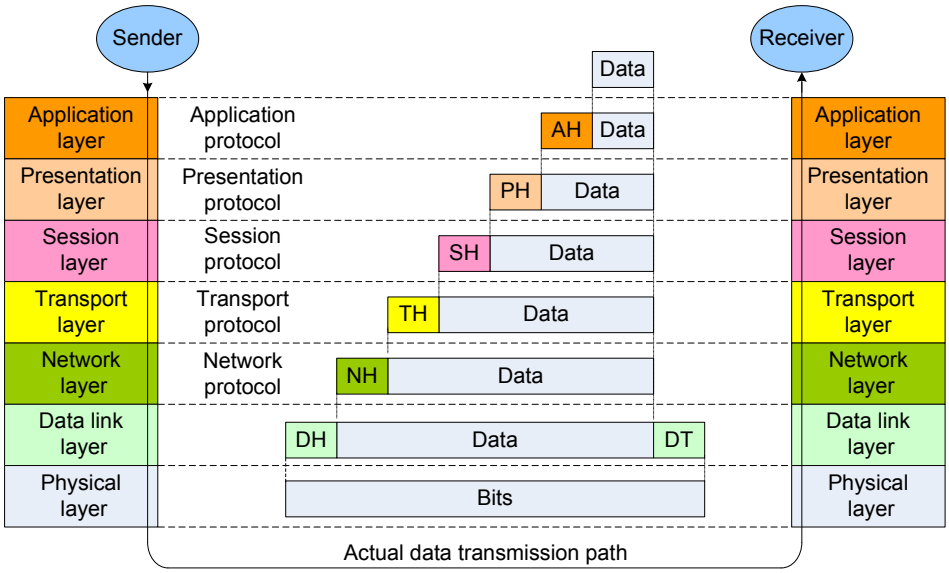

Figure 1.1: Data transmission in the OSI model [3, 4]. Some of the headers may be null. (AH: application header; PH: presentation header; SH: session header; TH: transport header; NH: network header; DH: data link header; DT: data link tailer.)

6. *Data link layer*: creates frame boundaries by attaching special bit patterns to the beginning and the end of the frame, and transmits the frames sequentially.
7. *Physical layer*: transmits raw bits over a communication channel.

Except for the application layer that takes the true user data, each layer takes the data from the layer above, adds its own layer header to it, and gives the result to the layer below, until the data reach the physical layer, where transmission actually takes place. The data transmission process in the OSI model is illustrated in Fig. 1.1.

Experience with the OSI model has proven that some of its layers are of little use to most applications [3]. Moreover, having so many layers working together introduces a large amount of overhead on top of the actual user data. The overhead can count for a significant small portion of the total number of bits transmitted. Most of the physical communication channel bandwidth is used to carry the header information of all the stacked layers. Besides, individual header processing at each

layer prolongs the handling *latency* of the user data. From the network perspective, latency, also called delay, corresponds to how long it takes a message to travel from one end of a network to the other [4]. From the system perspective, latency can refer to the delay that data experience to travel from an input to an output of the system, due to the processing time required to make the right decision which output the data are destined for, plus the executing time required to perform the switching of data. In short, data overhead and latency considerably limit the efficiencies of networks with many layers.

b. The TCP/IP reference model

With the rapid development of Internet, the OSI protocols have quietly vanished, and the TCP/IP protocol suite has become dominant and is often used for Internet [3, 4]. One of the major design goals for the TCP/IP reference architecture is to connect multiple networks together in a seamless way [3]. Some of the OSI layers are not present in the TCP/IP model. The TCP/IP reference model has *four* layers:

1. *Application layer*: contains all the higher-level protocols including virtual terminal *telnet*, file transfer protocol (FTP), simple mail transfer protocol (SMTP) for emails, and hypertext transfer protocol (HTTP) for accessing Web via different application programs.
2. *Transport layer*: allows peer entities on the source and destination hosts to carry on a conversation, the same as in the OSI transport layer. TCP is defined in this layer for reliable byte stream delivery without error.
3. *Internet layer*: delivers packets sent by hosts independently to the destinations without caring about the order of the delivery, and avoids congestion. The higher layers need to rearrange the packets if desired. This layer defines the official IP packet format and protocol. Sometimes it is referred to as the IP layer where the IP packet routing takes place.
4. *Host-to-network layer*: connects the host to the network so that it can send IP packets over it. Not much has been defined about this layer in the TCP/IP model.

Figure 1.2 shows the functionality correspondence of the TCP/IP model to the OSI model [3].

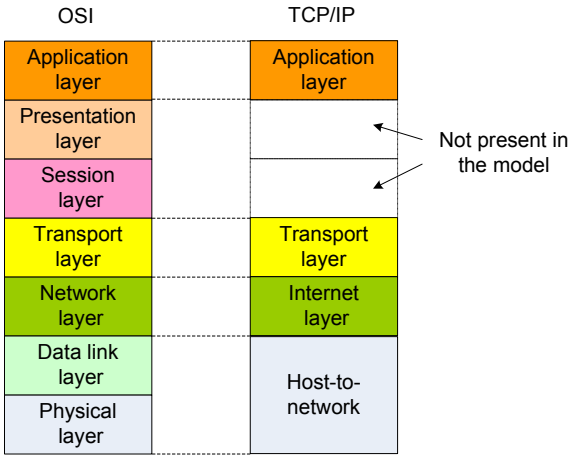

Figure 1.2: The TCP/IP reference model in relation to the OSI model [3].

1.1.2 Telecom network hierarchy

The OSI and TCP/IP reference models have much in common, as both represent the layered hierarchy of telecommunication networks. In practice, most telecom networks can be conceptually described by a simplified *three*-layer hierarchy:

1. *Application layer* or *service layer*: employs different high-level protocols to provide various data services to end users via software and applications.
2. *Network layer*: delivers the data information units in form of electronic or optical packets, cells or frames by processing the data unit headers. It also controls network congestion. The functionalities of this layer correspond to those of the network layer in the OSI model or of the Internet layer in the TCP/IP model. Routing, switching or forwarding in this layer can be in either electronic or optical domain. Increasingly, various switching functionalities are being taken over by optics.
3. *Physical layer*: transmits the data information bit by bit via various physical media such as optical fibers and copper wires.

Such a network hierarchy is visualized in Fig. 1.3. The entities in layers are *logically matched*, but *physically* do not necessarily have a *one-to-one relation*. Except in the physical layer, where the nodes are actually connected to each other via physical media, the communications in the network and application layers are *virtual*, and rely on the services provided by the layer(s) below.

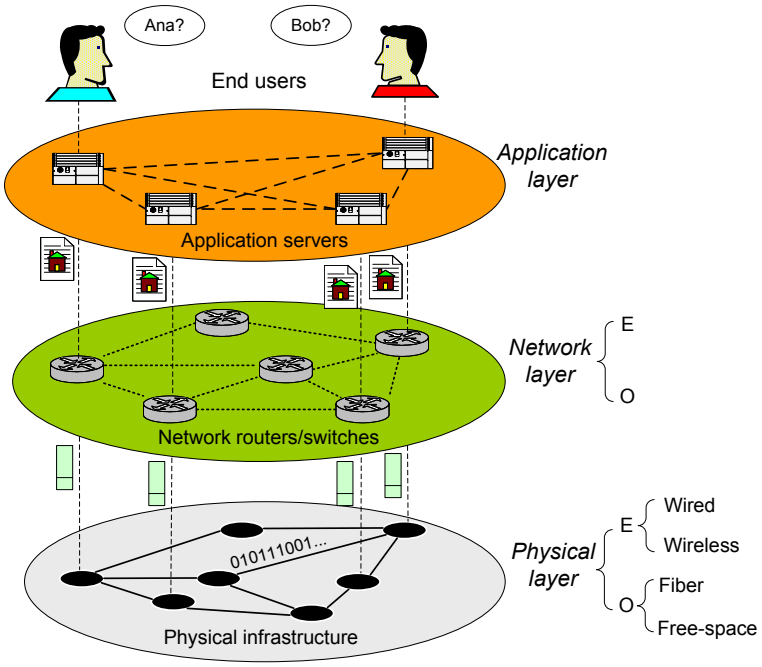

Figure 1.3: Conceptual telecom network hierarchy. (E: electronic; O: optical.)

a. Network functionalities in electronic domain

In the current Internet network architecture, routing decisions are made in the electronic domain by the IP routers. Most of the network functions such as ToS, unicast, multicast or broadcast are performed by electronics.

For *unicast* operation, the information is only sent to *one* destination. *Multicast* is a mode of operation where the same information is sent to *a selection of* destinations, usually at the same time. *Broadcast* is a special case of multicast where the same information is sent to *all* the destinations connected to the network.

IP plays a key role as the major network layer protocol for realizing such functionalities in the electronic domain. An IP diagram consists of a header and payload. An IP header includes information such as the version of the protocol, ToS, time-to-live (TTL), source address, and destination address. The ToS field allows the host to tell the subnet what kind of service it wants. Various combinations of reliability and speed are possible. The TTL field is a counter used to limit

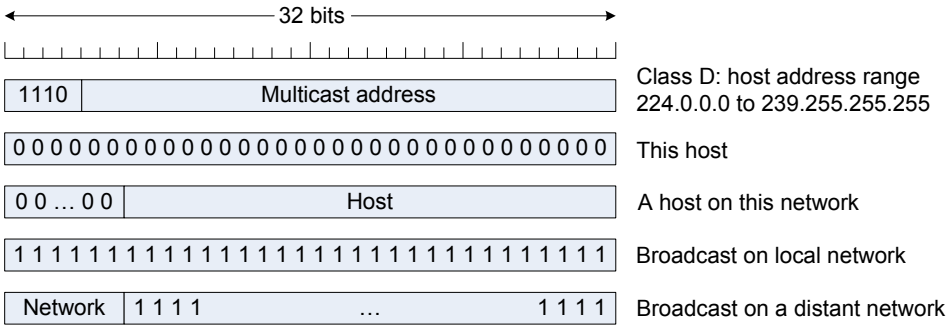

Figure 1.4: Multicast and some special IPv4 address formats [3].

the number of hops that the packet can experience [3], in order to avoid a packet going into an endless *dead* loop.

IP addresses are used in the source and destination fields of an IP packet header. In an IP address, the network number and the host number is encoded. The combination of these two numbers is globally unique for each individual machine that is connected to the Internet in the public domain. An IP version 4 (IPv4) address is 32-bit long. At the time of writing, IP version 6 (IPv6) has been defined to deal with the scaling problems caused by the Internet's massive growth. IPv6 provides a 128-bit address space [4]. There will probably be a long transition period for the hosts and routers that run IPv4 only to be IPv6 compatible [4].

IPv4 addresses are categorized into different *classes*. In IPv4, *class A, B, C* of IP addresses are for different network scales, e.g., wide area networks (WANs), metropolitan area networks (MANs), and local area networks (LANs). The multicast addresses are in a separate class, *class D*, and are in the range from 224.0.0.0 to 239.255.255.255. Broadcast is indicated by a series of value 1 as the host number or the whole IP address for *all* hosts on the specified network. A series of zeros in an IP address indicates *this* network or *this* host. In Fig. 1.4, multicast and some special IPv4 address formats are shown [3].

b. Network functionalities in optical domain

In the first-generation optical networks, which are still widely deployed, the optical layer has little or no intelligence. The main function of such optical layer is to carry raw bits via point-to-point fiber links. In other words, the traditional optical layer is only responsible for transmission, not switching. At each switching point,

the optical data are converted to electronic data, and routing decisions are made using electronic processing based on the header information. Afterwards, if the data have not reached their final destination, they are converted back to the optical domain to be transmitted to the next node. The same process repeats until the data arrive at the destination node(s).

The rapid growth of Internet and multimedia data traffic poses a potential challenge for such telecom transport networks. The enormous increase of data traffic demands the future backbone transport networks to deliver multiplexed high bit-rate data packets with higher efficiency. The huge bandwidth of optical fiber which can be exploited by means of the wavelength division multiplexing (WDM) technologies has greatly increased the transmission link capacity. However, the present optical layer is still static or quasi-static, with limited switching functionalities. In order to improve the network efficiency, more *intelligent* optical layer functionalities need to be introduced to reduce and minimize the optic-electronic-optic (OEO) conversion, so that end-to-end optical transparency can be achieved. As a matter of fact, more and more conventional network layer functionalities are being moved from the electronic domain towards the optical domain, and many of them can nowadays be realized by optics. The evolution of telecommunication networks is migrating from electronic domain networking to optical domain networking, with increasingly sophisticated optical layer functionalities and *smart* optical decision circuits.

1.1.3 Network structure

a. Backbone networks

Telecom transport networks consist of *backbone* networks and *edge* networks. The *backbone* networks, conventionally comprise *core* and *metropolitan* networks, transmit aggregated and multiplexed data traffic from the edge networks at high speeds across a spine structure that interconnects various lower speed edge networks. A core network usually spreads over a large area, corresponding to the size of WANs, and is used for national or international backbone transmissions. Fig. 1.5 shows the European backbone network, which is an example of a core network. The main switching nodes in a core network are referred to as *core nodes*, or sometimes as *core routers* or *core switches*.

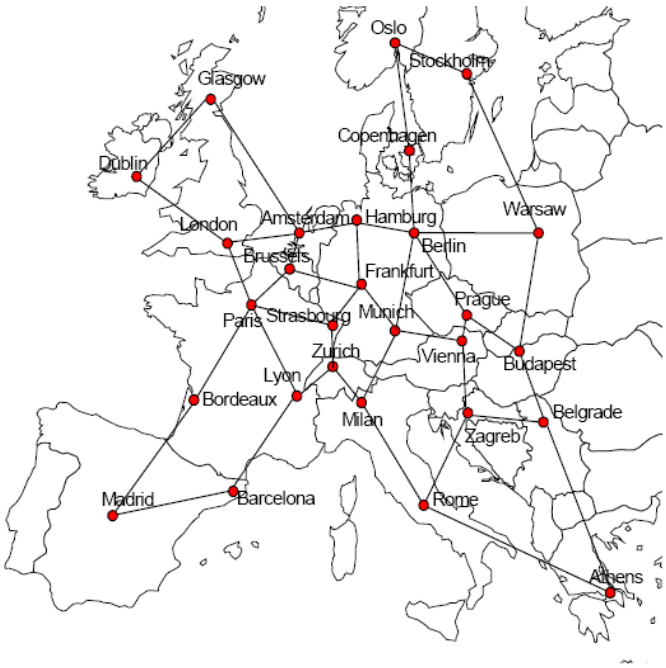

Figure 1.5: Example of a core network: the European backbone network.

b. Edge networks

An *edge* network should aggregate data directly from end users. An edge network usually covers a relatively small geographical area, and has the size of a LAN or an access network. Data traffic in an edge network is always at a lower speed than in the backbone networks. In practice, the edge networks have certain tasks such as aggregating and multiplexing the data traffic from the end users, classifying and prioritizing them before having them sent over the backbone networks. Besides, the edge networks also receive and demultiplex the data traffic from the backbone networks, and distribute them to the destination end users. The nodes or routers that perform such functionalities are referred to as *edge nodes* or *edge routers*. The edge routers that aggregate the data traffic from the end users and multiplex them into the *add* traffic for the backbone network are called *ingress* edge routers. The edge routers that demultiplex the *drop* data traffic from the backbone network and deliver them to the end users are called *egress* edge routers.

1.1.4 Optical switching techniques

In the Internet, traffic originates from end-users in the access and low-speed LANs, to MANs, and finally aggregates at the edge router of the core networks in the WANs. In an edge router, the aggregated data traffic is classified by destination and multiplexed into high-speed optical data. The multiplexed data are transmitted through the optical core network, where switching and routing of the data takes place, until the data reach the destination edge router. At the destination edge router, the optical data are converted back into the electronic domain and delivered to the correct destination LANs or access networks, and finally to the end-users.

Traditionally, the switching of optical data in the core networks is either static, or if dynamic, carried out in the electrical domain. Considerable efforts have been made to keep to the data in the optical domain as much as possible all the way from source to destination, and to perform the data switching *optically*. To this end, various optical switching techniques have been proposed and developed.

a. Optical circuit switching (OCS)

Current optical core networks deploy mostly optical circuit switching (OCS) or point-to-point wavelength channels. OCS is comparatively easy to implement as it requires only slow optical components, usually at millisecond speeds [5]. Due to the present technical limitations on optics, wavelength-routed networks based on OCS are expected to prevail for the near future. However, OCS or wavelength routing results in relatively poor bandwidth utilization because of its infrequent reconfiguration, e.g. from every few days to months, and dedicated use of wavelengths. It is hard for OCS networks to respond to fast changing traffic demands. Therefore, it is expected that the next generation optical Internet will evolve towards optical networks based on optical burst switching (OBS) or even optical packet switching (OPS) in the long run [5].

b. Optical burst switching (OBS)

OBS is a technique for transmitting *bursts* of traffic through an optical transport network by setting up a connection and reserving end-to-end resources for the duration of the burst. A burst is a set of packets. Buffering at the optical layer is not required [6]. OBS can achieve higher bandwidth utilization, and at the same time, can be implemented with currently available optical technology, as in

Table 1.1: Characteristics of optical switching schemes [5].

Scheme	*Utilization*	*Granularity*	*Implementation*	*Adaptability*	*Latency*
OCS	low	coarse	easy	low	low
OBS	moderate	moderate	moderate	moderate	moderate
OPS	high	fine	difficult	high	low

OCS [5]. It also offers better granularity than OCS. Being an optical switching technology, OBS mainly relies on the computation and control complexity in the electrical domain.

c. Optical packet switching (OPS)

Like electrical packet switching, and even more due to the additional wavelength dimension, it is generally believed that OPS will further significantly improve the optical network throughput, efficiency and bandwidth utilization [6, 7], and at the same time offer the network providers a cost-effective solution to keep their broadband and multimedia data services affordable for the end-customers [2]. Based on optical *packets*, OPS offers the finest granularity among the three optical switching concepts. In the OPS scenario, the packet switches can be *hybrid packet switches* with OEO conversion, electronic packet processing and buffering, or *optical packet switches* with electronic packet header processing but transparent optical payload forwarding, or *all-optical packet switches* with packet label processing and packet forwarding purely in the optical domain. Compared to OBS and OCS, OPS is the most flexible and also the most demanding switching scheme [5].

Table 1.1 summarizes the characteristics of OCS, OBS and OPS [5].

1.2 Evolution of label switching

1.2.1 Concept of label switching and terminologies

In the Internet, a conventional IP router makes packet forwarding decisions based on the destination *network* number, *subnet* number and *host* number. Each IP router needs to keep an updated *routing table* with a list of surrounding networks, subnets and all the host IP addresses on the subnet [3]. Matching a globally

unique IP address to an entry of the routing table can be rather exhausting. If the destination address is not from the host's network and subnet, the packet is forwarded to the next IP router according to its network and subnet number, until it reaches the router of the desired network and subnet where the destination address matches one of its host addresses.

Label switching is a technology that is developed to enable very fast forwarding at the cores and conventional routing at the edges [5]. This is realized by assigning short, local *labels* to packets based on their forwarding equivalent classes (FECs) as they enter the core network, and switching the packets based on these short labels instead of the globally unique IP addresses in the core network. A *label* is different from a *header*. A *header*, e.g. IP packet header, can include several fields with different purposes; while a *label* is only used as an index for making quick forwarding decision. A *label* can be a specific field inside a *header*.

For the core routers, making forwarding decisions according to local labels is much faster than using IP addresses. Fig. 1.6 illustrates the concept of label switching. As a packet enters the core network consisting of label switching routers (LSRs), a label is added to the packet by the label edge router (LER) according to its FEC. Based on the destination address, the LER decides a label-switched path (LSP) for the packet to travel through the core network. The IP packet header only needs to be examined once by the LER as it enters the label-switching domain of the core network [5]. This way, the complex computational process is left to the LERs, and fast packet forwarding can be achieved by the LSRs across the core network solely on the basis of the labels.

In the core network, each LSR has its own *lookup* table. LSRs use a label distribution protocol to inform others of their label to FEC bindings [5], which is similar to the updating of routing tables among IP routers. A lookup table of an LSR contains a list of entries, where the incoming labels (ILs) are matched with outgoing labels (OLs) and output ports (OPs) of the LSR. Therefore, the labels only have a *local* meaning to that LSR, and the same label may have different meanings to different LSRs. Because the labels are local, they can be very short, and readily be matched with one of the entries in the lookup table. The labels generally serve as indices for the entries of the lookup table. A lookup table in an LSR has a similar function to the routing table in an IP router, but with much fewer entries as it only needs to keep track of the possible destination LSRs, not all the subnets and hosts on the local network. No complex searching algorithms are required for indexing the routing table as in IP routers. In label-switching

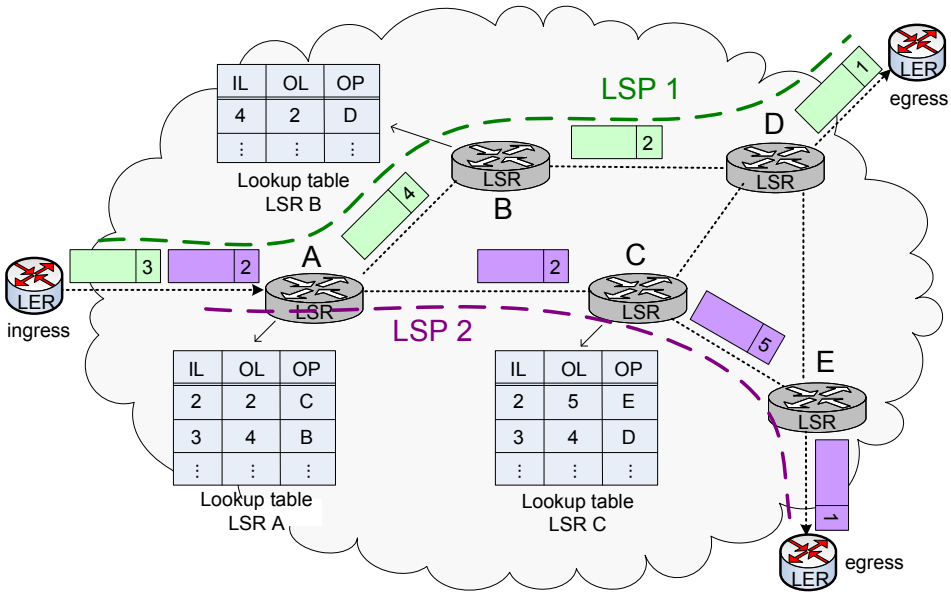

Figure 1.6: Label switching concept. (LER: label edge router; LSR: label switching router; LSP: label-switched path; IL: incoming label; OL: outgoing label; OP: outgoing port.)

terminologies, the lookup table is also sometimes referred to as a *forwarding table*.

To realize label switching, two approaches have been proposed. Most label switching systems employ *label swapping* techniques [8–15]. In the *label swapping* scenario, at each LSR, the incoming label is erased, and a new outgoing label is generated according to the lookup table and added to the data packet. In other words, the label is *swapped*. Each time, the packet label contains only necessary information for the next LSR to make a forwarding decision and generate a new label. The length of a label is determined by the actual required bit-length for every LSR along the LSP to make its forwarding decision.

Label stripping [16] is another concept where *end-to-end concatenated labels* are pre-defined at the ingress LER, which includes all the short *local labels* for every intermediate LSR on a pre-defined LSP decided by the LER. Each LSR along the LSP simply *strips* off one *local label* for forwarding decision making. Consequently, no outgoing label is generated at each LSR. In the *label stripping* scenario, the LERs compute the LSPs across the whole core network and insert

the *end-to-end labels*. The length of an *end-to-end label* is determined by the total bit-length of all the *local labels* for every LSR along the pre-defined LSP. For large core networks, the *stripping* approach may lead to long label fields, and is less scalable to large networks, but it can considerably simplify the core router design with respect to the label swapping approach, as no outgoing labels need to be generated and inserted to the data packets.

1.2.2 Development of label switching

The label switching concept was first implemented in the multi-protocol label switching (MPLS) technology, using the label swapping approach. The term multi-protocol came from the fact that this technique can be used with any network layer protocol and is not restricted to IP [5]. With the rapid development of optical switching technologies, the success of the MPLS has brought the label switching concept from the electronic layer to the optical layer. Multi-protocol lambda switching (MPλS), generalized MPLS (GMPLS), optical label switching (OLS) and all-optical label switching (AOLS) have been successively proposed. MPλS and GMPLS are being gradually standardized and even taken into account in some commercialized optical cross-connect nodes. While MPλS is still for OCS networks, OLS and AOLS have been primarily researched for OPS networks. GMPLS, on the other hand, is more a control plane technology rather than a switching technology, and is emerging as a common control and signaling protocol to take care of optical switching and routing at various levels such as fiber, wavelength, packet, and even time slot level [5].

a. Multi-protocol label switching (MPLS)

The advancements in electrical label switching technologies such as MPLS [8–10] have considerably boosted the packet handling speed at the core nodes. MPLS emerged from a need to support any type of traffic on a large IP network to minimize the limitations of different routing protocols, transport layers and addressing schemes, so that routing costs can be reduced [10]. It can adapt data of any type into one packet format and does not need a centralized management. MPLS implements LSPs as *virtual* connections in the network through LSRs [6]. It also provides traffic engineering in a packet-based network.

The MPLS protocol encapsulates IP packets that have the same destination and FEC by assigning a *label* in the MPLS *header* and attaching this header

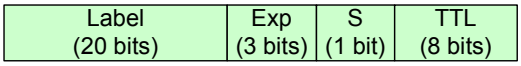

Figure 1.7: MPLS header format [10].

to all these IP packets [10]. An MPLS header comprises the following fields, as illustrated in Fig. 1.7:

1. **Label**: 20-bit field that carries the value of the label.
2. **Experimental use (Exp)**: 3-bit field reserved for experimental use.
3. **Bottom of Stack (S)**: 1-bit used for label stack purposes.
4. **TTL**: 8-bit field for encoding a time-to-live value.

Forwarding traffic under the MPLS framework is accomplished by using simple local lookup tables or node forwarding tables to define or discover a specified LSP over the IP network, and comply with traffic engineering constraints including *bandwidth*, *acceptable network resources*, and *quality of service* (QoS) [10]. QoS is implemented in MPLS to guarantee some transmission quality assurance by, for example, reserving bandwidth along the LSPs [17]. The LSPs are also known as *tunnels*, which are explicit routes over which aggregated traffic flows are mapped based on traffic conditions and availability of network resources. As a result, traffic management is simplified and traffic congestion is minimized. Tunneling data traffic between customer sites sets up a virtual private network (VPN). MPLS enhances the ability of a VPN to establish, maintain, and guarantee QoS for an LSP [10].

b. Multi-protocol lambda switching (MPλS)

Packet switching and forwarding based on swapping short local labels instead of locating the globally unique IP addresses has dramatically enhanced network throughput [4, 10, 17]. Nevertheless, the MPLS protocols have been only employed for electronic routers that deal with electronic data packets such as IP packets.

MPLambdaS, or MPλS, brings the advances in the MPLS traffic engineering control plane technology and enables dynamic connectivity at the optical layer [10]. MPλS uses wavelengths, i.e. lambdas (λs), as labels. Consequently, an LSP becomes a λ switched path (λSP).

c. Generalized multi-protocol label switching (GMPLS)

GMPLS is an extension of the MPLS architecture that supports multiple types of switching, including MPλS [5]. It is investigated as the control plane of optical networks, tailored to their specific requirements. In optical networks, a FEC may be mapped in many different ways, not necessarily packet based. For example, switching in the optical layer can take place in form of fibers, wavelengths, packets or time slots. A FEC may be associated with a *lightpath*, i.e., a wavelength channel, so that a packet on this lightpath can be routed end-to-end in the optical layer. In GMPLS, the label values are implicit since the LSPs are identified by the transport media or methods [5].

d. Optical label switching (OLS)

While MPLS is implemented for electronic packet switched networks such as the IP networks, the optical layer using MPλS is still a circuit switched network. Once the circuit is established, all the resources of the circuit switched path are dedicated to it. If the enormous capacity of each wavelength is not fully utilized, the optical bandwidth is partially wasted [5].

OLS is an attractive technology for accommodating IP-over-WDM using explicit *optical packet labels*, which allows seamless interoperability with OPS, OCS as well as OBS on a single WDM platform [18]. It applies label switching to *optical packets*, and thus combines the advantages of MPLS efficiency and OPS granularity. In [19], the first demonstration of OLS for packet-switched WDM networks is documented.

Benefited from various optical labeling techniques and the power of electronic processing [2, 20, 21], current proof-of-principle OLS routers can offer transparent optical packet payload forwarding based on electronic or electro-optical handling of packet headers [18, 22–24]. By keeping the high-speed packet payload in the optical domain, the header processing is done at medium speed, usually of megabit per second (Mb/s) range, employing low-cost and mature electronic techniques. In this way, the OEO conversion of the headers has negligible influence on the packet throughput of the OLS nodes, as the major portion of the optical packet, the optical payload data, is kept intact [2]. To date, various network functionalities that are implemented in the electronics, have been demonstrated by researchers in OLS nodes. Such examples include QoS, optical TTL, multicast and multimedia applications [22].

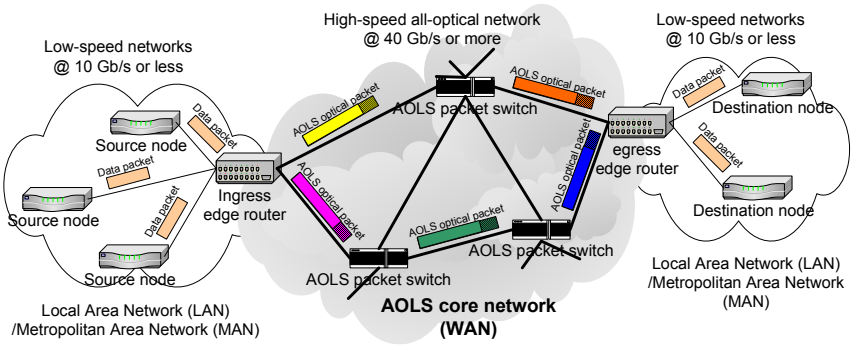

Figure 1.8: AOLS network scenario.

e. All-optical label switching (AOLS)

To support optical packet switching and forwarding at fiber line-rates up to Terabit/s, OPS core nodes that can realize packet handling directly in the optical layer are desirable [21, 25]. As the label speed becomes higher, the latency from the header OEO conversion and electronic processing starts to influence the packet forwarding efficiency. Electronic header processing for the high bit rate core networks will no longer meet the speed and capacity demands [2]. AOLS is a new concept of implementing label switching techniques for optical packets by doing the label processing fully in the optical domain [21, 26, 27]. AOLS technologies combined with OPS could be a solution for the next generation optical networks.

As depicted in Fig. 1.8, AOLS packet switches can be used in the optical core network within WANs to interconnect low-speed LANs/MANs, or even high-speed "optical islands" in the future, for multiplexed data traffic in national or international backbone transmission. In the ingress edge router of the AOLS core network, the aggregated data traffic is classified by destination, prioritized and encapsulated into optical packets with optical labels. At each AOLS core node, the packet label is processed all-optically, a forwarding decision is then made based on the incoming label, and the packet might be converted into a different wavelength to travel to the next AOLS node. The LSPs inside the AOLS core network are thus pure optical layer LSPs. The optical packet remains in the optical domain until it reaches the destination egress edge router, where the optical label is removed and the high-speed optical packet is demultiplexed into lower speed packets to be processed electronically and delivered via the local networks to their end users.

1.2.3 Optical labeling techniques

In the past years, various optical labeling techniques have been proposed and investigated for hybrid electro-optical and all-optical data switching. They can be classified into the five categories summarized in this section. In [2], these labeling techniques are extensively discussed and compared with respect to their technologies, advantages and disadvantages.

a. Time-domain multiplexing (TDM) labeling

Time-serial or time-domain multiplexing (TDM) labeling [13, 16, 21, 26–28] is one of the most widely employed labeling technique, and is used also in the electrical domain. In time-serial labeling, the label is usually placed before the payload on the same wavelength in the time domain. A guard band is required for separating the label and the payload in time for the label extraction. The bit-length of the guard band may be less when optical signal processing is used. This method requires strict synchronization between the label and the payload, but it is easy to implement as the packet label and payload can be generated using the same light source and intensity modulator. With all-optical processing of the labels at packet data rate, time-serial labeling does not suffer from bandwidth overhead.

b. Subcarrier multiplexing (SCM) labeling

With *Subcarrier multiplexing (SCM) labeling* [21, 25, 29–31], the label is on a subcarrier outside the payload spectrum, while the label and payload data are still multiplexed on the same wavelength, i.e., optical carrier. This is achieved by encoding the payload data at the baseband while encoding the label bits on a chosen subcarrier frequency at a lower bit rate [5]. This method requires extra spectrum for the label, and thus creates some bandwidth overhead. Moreover, if the payload data rate is increased, the baseband will expand and may eventually overlap with the subcarrier frequency, so the potential payload data rate is limited [5].

c. Optical code division multiplexing (OCDM) labeling

With *Optical code division multiplexing (OCDM) labeling* [32–35], the label is encrypted on the payload data using OCDM technologies by scrambling the label with a code key data sequence. This method increases sizeably the line rate and also requires bit-level synchronization.

d. Wavelength division multiplexing (WDM) labeling

With *Wavelength or WDM labeling* [12, 36, 37], the label is on different wavelength channel(s) running in parallel to the data channel. This method offers easy extraction of the optical labels by optical filtering.

Wavelength labeling can be either in-band or out-of-band. *In-band* wavelength labeling can be used for high bit rate payload, where the labels can be placed within the payload spectrum [12]. The higher the payload bit rate, the wider the payload spectrum. *Out-of-band* wavelength labeling can be implemented by, for instance, dedicate a separate, common wavelength channel for transmitting the optical labels for the payloads in the other wavelength channels [2]. The labels are time-division multiplexed and need to be carefully synchronized with the respective payloads.

e. Orthogonal labeling

With *Orthogonal labeling* [2, 23, 24], the label is in an independent modulation dimension different from the one of the payload. For example, the label can be frequency shift keying (FSK) modulated while the payload is intensity modulated (IM) [2]. This method may suffer from signal degradation due to the interferometric FSK-IM conversion, which can generate crosstalk between the label and payload [2].

1.3 This thesis

1.3.1 Groundwork: European IST projects

In 2004, an AOLS node architecture was proposed in the European Commission (EC) funded FP6 IST-LASAGNE (all-optical label swapping employing optical logic gates in network nodes) project, with the network scenario of WDM packet-switched networks implementing label swapping technique for fixed-length optical data packets at a targeting data rate of 40 Gb/s [38]. Although there had been research activities in the field of time-serial optical label swapping before [21, 26–28], the IST-LASAGNE project was the first to investigate a modular WDM time-serial AOLS packet switching node design with all-optical label processing [13, 16]. This project was successfully concluded by the end of 2006. The AOLS core system, a proof-of-principle all-optical label processing unit based on integrated

semiconductor optical amplifier – Mach-Zehnder interferometers (SOA-MZIs), was demonstrated for all-optical unicast forwarding of nanosecond-range packets at 40 Gb/s based on arrayed waveguide grating (AWG) passive routing [14, 39].

The label-controlled optical packet switching node architecture by means of wavelength conversion and AWG passive routing has been previously employed and demonstrated by the EC FP5 project IST-STOLAS (switching technologies for optically labeled signals), except that in the STOLAS project, electronic processing of orthogonal labels was used [2, 23, 24]. The IST-DAVID (data and voice integration over DWDM) [40, 41] is another EC FP5 project that investigated optical packet switching with MPLS control plane for MANs/WANs, applying time-serial labeling. Both the STOLAS and DAVID projects utilized electronics as well as optics for optical packet switching and wavelength routing, differing from the all-optical approach in the IST-LASAGNE project.

1.3.2 Contributions to the field

The research described in this thesis was initiated by the IST-European project LASAGNE, one of the world's first attempts to develop and demonstrate a truly all-optical packet switching system. The main contribution of the thesis is on the *multicast* aspects of the AOLS nodes and technologies. Apart from that, other engineering aspects of the AOLS nodes such as all-optical node contention resolution, scalability issues, are also discussed.

a. All-optical packet unicast, multicast and broadcast

With the rapid development of Internet and modern data services, emerging applications such as voice/video-over-IP, video streaming, high definition TV, multiparty online games and peer-to-peer file transfer services are becoming increasingly popular on top of the traditional Internet services. In order to deliver large amounts of data more efficiently, more and more networking functions that are currently performed by electronics are being moved to the optical layer. All-optical solutions for *switching*, *routing* and *multicasting* are of crucial importance for realizing a truly intelligent, transparent and broadband optical infrastructure. Despite that, most of the solutions studied so far support only unicast operation. There is a strong need for efficient optical layer multicast technologies driven by all the entertainment and business applications such as video conferencing and optical storage area networks [11, 22].

In this thesis, issues concerning multicast capable AOLS nodes are addressed and their performance are evaluated (Chapter 3). All-optical multicast technologies are also summarized and investigated (Chapter 4∼7).

b. Contention resolution

In an OPS network, contention occurs at a switching node whenever two or more packets try to exit the same output port on the same wavelength, at the same time. Contention can result in loss of data packets due to packet collision, as well as network congestion, and requires re-transmission of the optical packets.

In electronic switches such as asynchronous transfer mode (ATM) [42] switches, contention can be solved by queueing the packets, or *cells* in ATM terminology, in the *time* domain. Queueing of the electronic packets or cells can be placed at either the input or the output side of the switch, referred to as *input queueing* and *output queueing*, respectively. Output queueing is generally more efficient than input queueing because of an effect called *head-of-line (HOL) blocking*, where the packets being held up block the progress of any packets behind it, even if they could otherwise be switched [3]. On the other hand, input queuing allows some degree of traffic shaping, which to a certain extend can alter the received traffic statistics, and thus reduce possible congestion at the output.

In optical switches, any or a combination of *time*, *space* and *wavelength* domain can be used to resolve optical packet contention. Depending on where the optical buffering is implemented in the optical node, optical contention resolution approaches can also be categorized into *input-buffering* and *output-buffering*. Most OLS and AOLS nodes rely on electronic processing to detect and resolve optical packet contention [30]. At the time of writing, there is no solution for a complete all-optical contention resolution solution on the AOLS node-level.

As AOLS node contention resolution is out of the LASAGNE project scope, a technical solution for the AOLS output-buffered contention resolution on the node level had not been addressed in the project. This thesis presents a possible architecture of the output-buffered contention resolution block and the corresponding algorithm. Two buffering strategies are investigated and evaluated through traffic performance simulations. These two strategies evolve either increasing the number of *one-slot buffers* or increasing the number of *slots in one buffer* for each AOLS output fiber. At this moment such algorithm shall require electronic processing (Chapter 8).

c. Scalability issues

For either AOLS nodes or networks, scalability is one of the most important issues. Scalability can refer to node and network dimension regarding the number of physical ports or links, wavelength capacity, data bit rate per wavelength, and ability of handling extra traffic employing the same or minimum additional hardware. The node and network dimension scalability is directly linked to the physical resources required for implementing and processing longer labels without significant hardware footprint expansion, complexity multiplication and performance degradation. Current AOLS technologies are still too expensive to be commercialized. Therefore, alternative solutions that ease the scalability bottlenecks are vital for the deployment of the AOLS technologies.

In this thesis, several aspects of improving the scalability of the LASAGNE AOLS nodes are addressed, including an alternative label/keyword generation scheme (Chapter 2), a feed-forward AOLS multicast scheme (Chapter 3), and a highly-scalable spatial labeling concept and label processing scheme (Chapter 9).

1.3.3 Framework of research

The following aspects are addressed in the thesis:

- General AOLS node design: architecture, technologies, and traffic performance – Chapter 2
- Multicast AOLS node design: architecture, technologies, and traffic performance – Chapter 3
- All-optical multicast technologies based on selected multi-wavelength conversion (MWC) technologies: simulation and experimental performance – Chapters 4∼7
- AOLS contention resolution: output-buffering strategies, traffic performance – Chapter 8
- Scalable multicast AOLS node design: spatial labeling concept, spatial label processing scheme and technologies, scaling feed-forward multicast traffic performance – Chapter 9.

Regarding these aspects, three research approaches have been used:

1. *Logical design* and *engineering* concerning node architectures, as well as functional subsystems and interconnections, based on state-of-the-art literature research of the field and subject.

2. *Computer simulations*:

   (a) Using a custom-made AOLS simulator `AOLSim` for traffic performance evaluation of various proposed node architectures, based on C++ programming in a Linux environment. The `AOLSim` has been designed with specific characteristics of the AOLS nodes and tailored to its label switching process [43, 44].

   (b) Using the commercially available simulator *VPItransmissionMaker*™ *WDM* for physical layer performance evaluation of various MWC schemes and setups, based on standard *VPI* components with customized simulation parameters.

3. *Experimental validation*, *characterization* and *performance evaluation* in laboratories for proof-of-principle demonstrations of MWC technologies and techniques.

In this thesis, the proposed *logical node architectures* (1) are supported by *literature*, *simulation* (2) and *experimental results* (3).

1.3.4 Outline of thesis

According to the subject addressed and the relevant research approaches, the thesis can be divided into three parts:

Part I: Logical unicast/multicast AOLS node design and traffic performance
System level design and simulations – Chapter 2, 3.

Chapter 2 introduces the LASAGNE AOLS node architecture and its unicast operation principle. Traffic performance simulations of the unicast architecture are also presented. Chapter 3 describes the feedback multicast operation proposed for the AOLS node, and introduces a more scalable, economical and efficient AOLS multicast approach – feed-forward multicast. These two multicast approaches are compared in terms of cost and traffic performance based on simulations.

Part II: All-optical multicast technologies by MWC
Physical layer simulations and experiments – Chapter 4, 5, 6, 7.

Chapter 4 summarizes the state-of-the-art technologies for all-optical multicast, focusing on various reported MWC techniques. Chapter 5 addresses general

requirements on multicast components for optical switches, with a few experimental validations of four different MWC approaches. In Chapter 6, extensive simulation and experimental characterizations of single SOA-MZI-based MWC at 10 Gb/s and 40 Gb/s data rate are presented, as SOA-MZIs are one of the basic building blocks of the LASAGNE AOLS nodes with great integration potential. In Chapter 7, experimental results of fiber-based MWC using four-wave mixing (FWM) are shown. The FWM MWC technique was chosen for its bit rate and data modulation format transparency.

Part III: Buffering for contention resolution, spacial label processing
System level design and simulations – Chapter 8, 9

Some other aspects of the AOLS node design are also discussed in this thesis. Two output buffering strategies for AOLS node contention resolution and their traffic performance are presented in Chapter 8. The effectiveness of these two buffering strategies is assessed through `AOLSim` simulations for different traffic models.

Another important aspect of the AOLS node design is the scalability and complexity regarding the number of active components required. Chapter 9 proposes a simple labeling concept and a spatial label processing scheme based on serial-to-parallel conversion of the label bits. This scheme is highly scalable and can be applied to different labeling formats.

Finally, Chapter 10 summarizes the conclusions drawn in this thesis. Recommendations for future research are also given.

Chapter 2

Unicast all-optical label switching nodes and performance

All-optical label switching (AOLS) technologies can support ultra-fast and high-capacity all-optical packet forwarding with low latency, full transparency and high efficiency. This chapter presents the unicast AOLS node architecture investigated in the LASAGNE project, explains the AOLS node operation principle, and describes in detail the all-optical label processing concept. The LASAGNE AOLS technologies enable the AOLS nodes to forward fixed-length optical packets at 40 Gb/s based on the processing of the optical time-serial labels directly in the optical domain. This all-optical label processing is performed in each all-optical label swapper (AOLSW) of an AOLS node. In this chapter, the original AOLSW design is discussed and an alternative AOLSW design is proposed. In addition, the optical packet format for the LASAGNE AOLS nodes is specified. Finally, traffic performance evaluation results are shown for a 3-port unicast AOLS node in terms of the packet loss ratio and network throughput. Parts of this chapter are based on publications.[1]

[1] See references [1, 45–47].

2.1 Introduction

All-optical label switching (*AOLS*) has rapidly become a research focus during the last five years [11–16]. Unlike optoelectronic or electronic label processing, AOLS eliminates the needs for optical-electronic-optical (OEO) convertors and high-speed electronic processors, whose fabrication complexity, installation and operational cost, footprints, as well as power consumption start to multiply for high data rates from 40 Gb/s upwards. Moreover, AOLS supports ultra-fast packet routing and forwarding directly in the optical layer independent of packet payload bit rate and format, which is a feature highly desirable for system and network operators, as necessary hardware replacement due to every gradual change and upgrade in their network can be reduced to a minimum.

Inherited from the multi-protocol label switching (MPLS) concept, most AOLS systems employ *label swapping* techniques [11–15]. In the *label swapping* scenario, at each AOLS node, the old optical label is extracted, and a new label is generated and added to the high bit-rate optical packet. Apart from making a switching/forwarding decision based on the incoming packet label, the AOLS node also needs to generate a new label and attach it to the optical packet. The length of the labels is determined by the actual required bit-length for each AOLS node to make a forwarding decision.

Label stripping has also been proposed for AOLS networks [16]. In the label stripping scenario, no new label generation functionality is required at each AOLS node and the core node complexity can be reduced. The edge nodes compute the LSPs across the whole AOLS core network and insert the *end-to-end labels* as the optical packets enter the AOLS core network. The length of the *end-to-end label* is determined by the total bit-length of all the *local labels* for every AOLS node along the pre-defined LSP. For large AOLS core networks, the *stripping* approach may lead to long label fields. On the other hand, due to current limited optical intelligence, this approach can considerably simplify the AOLS core node design.

In this chapter, the unicast AOLS node architecture based on optical logic gates for fixed-length wavelength division multiplexed optical packets at 40 Gb/s is presented. Sec. 2.2 describes the unicast AOLS node architecture and its operation principle. Sec. 2.3 explains in detail the essential component of the switch, that is, the all-optical label swapper (AOLSW). Sec. 2.4 discusses the AOLS packet format. Sec. 2.5 presents traffic performance of the unicast AOLS node architecture. Finally, Sec. 2.6 concludes the chapter.

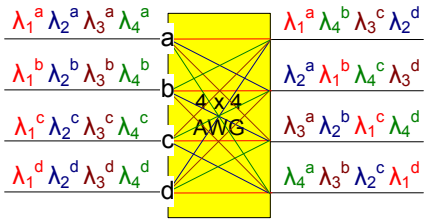

Figure 2.1: Schematic of a 4×4 AWG routing operation.

2.2 Unicast AOLS nodes

The optical label switching node architectures investigated in this thesis are based on the AOLS node architecture and function blocks studied, validated and demonstrated in the IST-LASAGNE project [13, 14, 16, 38, 39]. In the LASAGNE project, we mainly investigated AOLS nodes with a dimension of *two input* fibers, *two output* fibers, *one add* fiber to the ingress edge router, and *one drop* fiber to the egress edge router. In general, according to the network dimension and scenario, an AOLS node needs at least around *four input* fibers, *four output* fibers, *one* or *two add* fibers, and *one* or *two drop* fibers. For example, in the backbone European network, the core nodes in central Europe are connected to three to five adjacent core nodes on average, as shown in Fig. 1.5. In some cases, it is possible for an AOLS node to have up to *eight* pairs of *input/output* fibers and more *add/drop* fibers, according to the traffic load and network topology.

The LASAGNE AOLS nodes include the following functional stages: *input fiber ports*, *wavelength demultiplexers* (demux's), *all-optical label swappers* (*AOLSWs*), *arrayed waveguide grating* (*AWG*) *routers*, *contention resolution blocks*, *wavelength multiplexers* (mux's), and *output fiber ports*. As in the STOLAS project [2, 23, 24], the LASAGNE project focuses on a *four-wavelength* wavelength-division multiplexing (WDM) network scenario [13, 16]. The main operating principle of the node is to use all-optical eXclusive OR (XOR) correlators [39, 48] to match the incoming label with the keyword indexes of the node forwarding table, wavelength convert the whole label-swapped optical packet, and then route the new packet to the desired output port according to its wavelength by an AWG.

An AWG is a *passive* waveguide router that routes light signals from its inputs to its outputs on the basis of signal *wavelength* and *input position*, as illustrated in Fig. 2.1. Consider an AWG as a black box where an input wavelength λ_a that

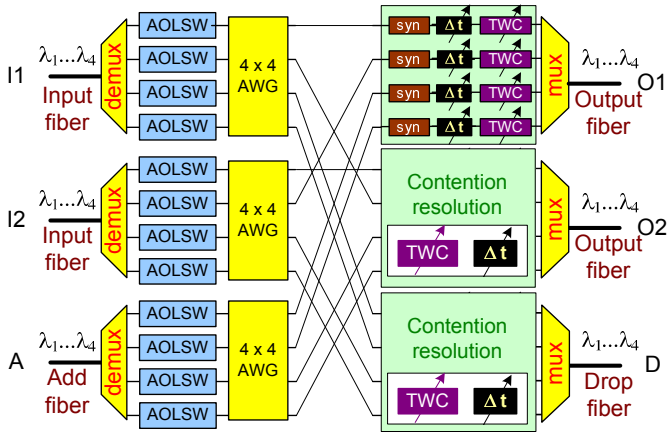

Figure 2.2: 2×2 AOLS unicast node architecture. (AOLSW: all-optical label swapper; AWG: arrayed-waveguide grating; syn: synchronization; Δt: packet buffering; TWC: tunable wavelength converter.)

enters the AWG input i goes out at the AWG output j. An AWG has a *cyclic* nature. This means there exists a $\Delta\lambda$ for which if a wavelength $\lambda_b = \lambda_a + k\Delta\lambda$ ($k \in \mathbb{Z}$), λ_b is routed by the AWG exactly the same way as λ_a is. In other words, if λ_b enters the AWG input i, it also exits on the AWG output j. In fact, all the wavelengths that show the same behavior in the AWG as λ_a are spaced by a multiple of $\Delta\lambda$, that is, $k\Delta\lambda$ ($k \in \mathbb{Z}$).

Figure 2.2 presents the schematic diagram of a basic 2×2 AOLS unicast node for four-channel WDM AOLS networks, including an *Add* fiber port for connecting to an ingress edge router and a *Drop* fiber port to an egress edge router for local traffic, similar to the node architecture investigated in the STOLAS project [2, 23, 24].

The node processes optical packets in the following procedure: at the input line ports, the WDM channels are demultiplexed into packets of single wavelengths. From each output of the demux an optical packet enters an AOLSW. Inside the AOLSW, the packet label is extracted and compared with a list of keywords, which are generated locally according to the forwarding table and serve as its lookup indices. Each keyword maps a corresponding entry, where a new label pattern and an internal packet wavelength are specified. The new label is inserted in front of the payload, and the whole packet is converted to the internal wavelength. Follow-

ing the AOLSW, the AWG routes the new packet to the desired output(s) of the switch. To avoid packet collision, contention resolution is required. As illustrated in Fig. 2.2, the contention resolution blocks need to include the functions of packet synchronization (syn), variable packet buffering (Δt) and tunable wavelength converters (TWCs). In the top-right contention resolution block, a possible internal circuit diagram is shown. For simplification purpose, the inner details of the second and the third contention resolution blocks are not shown. The TWCs near the outputs are employed to convert the optical packets from internal wavelengths for the AWG routing onto acceptable vacant external wavelengths for the AOLS core network. In the LASAGNE project, such a complete output-buffered contention resolution block has not been investigated. This output-buffered contention resolution requires electronic processing to detect packet contention and configure the packet buffering as well as the TWCs. Reference is made to Chapter 8 for more details on the output-buffer AOLS contention resolution.

2.3 All-optical label swapper (AOLSW)

The AOLSW has six subsystems, namely the *label extraction*, *label comparison*, *new label generation*, *label insertion*, *control block* and *wavelength conversion* subsystems. In this section, two AOLSW configurations based on different label generation techniques are presented and discussed.

2.3.1 AOLSW original configuration

Figure 2.3 presents the block diagram of the proposed AOLSW design in the LASAGNE project. Before explaining in detail how the function of each block is implemented, we first discuss the interrelation of these functions. When an AOLSW receives an optical packet, the optical label of the packet is separated from the payload by the *label extraction* circuit [49]. After the label extraction, the packet payload is delayed by optical delay lines (ODLs) to allow for the processing time of the label. The optical label goes into the parallel *label comparison* subsystem, and an optical pulse is generated if an address match is found [39, 48]. This optical pulse then sets the *control block* to emit a continuous wave (CW) signal of a certain wavelength for the *wavelength conversion* of the optical packet. The optical pulse from the label comparison subsystem is also used together with ODLs for the *new label generation* [28, 50]. After that, the new label is sent to

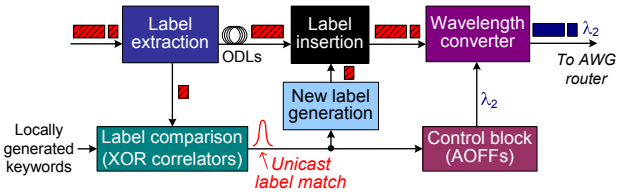

Figure 2.3: AOLSW subsystems interrelation: original configuration. (AOFF: all-optical flip-flop; AWG: arrayed waveguide grating.)

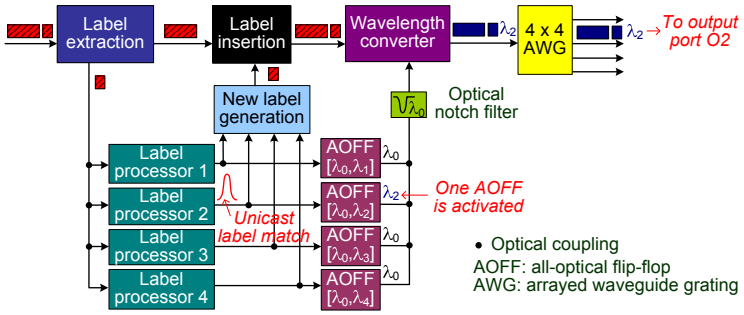

Figure 2.4: AOLSW label processing logical connections: original configuration.

the *label insertion* subsystem, and placed in front of the payload by means of an optical coupler or a semiconductor optical amplifier - Mach-Zender interferometer (SOA-MZI) optical gate. Finally, the whole packet is converted to the desired wavelength for the AWG routing. The logical connections for the label processing procedure is illustrated in Fig. 2.4.

The details of the AOLSW are shown in Fig. 2.5. The *label extraction* circuit is coordinated by an *all-optical packet-rate clock recovery* circuit [51] and an *all-optical AND logic gate*, which is required for the label extraction according to the time-domain multiplexing (TDM) approach. On packet detection, a single pulse is also produced by the *single pulse generation* block. This pulse is divided into $2N$ copies where N is the total number of possible labels. In Fig. 2.5, $N = 4$. N copies of the pulse are used to generate local keyword bit patterns via sets of pre-defined ODLs [28, 50], as illustrated in Fig. 2.6. The other N copies of the pulse are sent to the *control block* for resetting the all-optical flip-flops (AOFFs) [52]. The above described process of the pulse division and distribution is exhibited in Fig. 2.7.

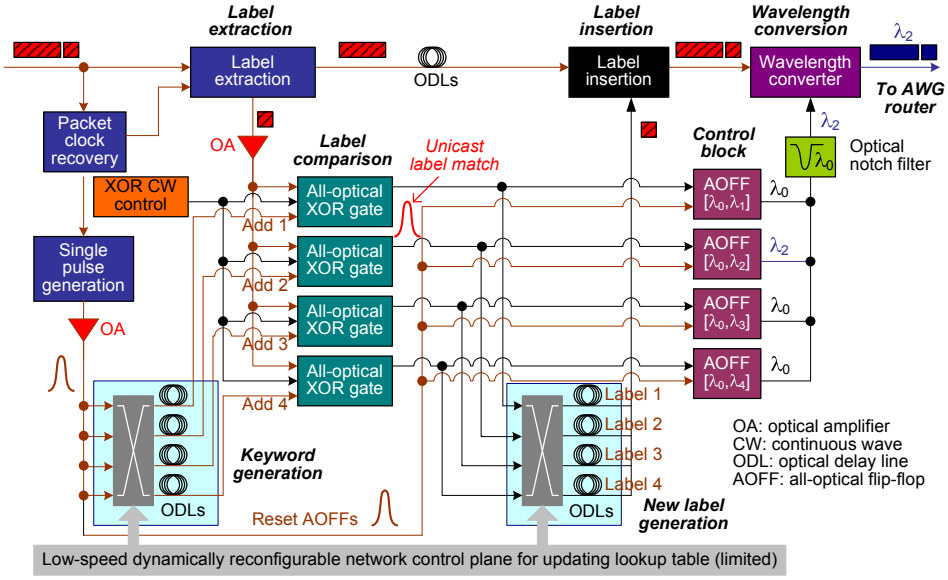

Figure 2.5: AOLSW details: original configuration.

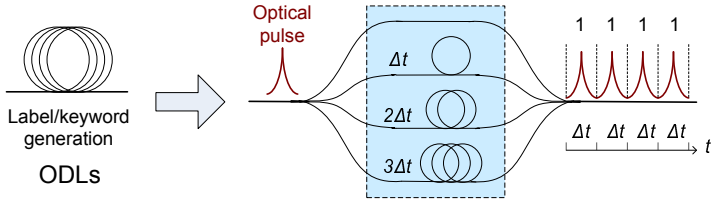

Figure 2.6: Keyword and label generation by ODLs. (example shows how the optical code "1111" is generated from a single pulse.)

In the *label comparison* subsystem [39, 48], the label bits are copied and XOR correlated with the locally generated optical keywords according to the forwarding table, using SOA-MZI-based optical logic gates. When there is an address match, the relevant XOR gate produces another optical pulse, which is used to create a new label in the same way as the *keyword generation* presented in Fig. 2.6. A copy of this XOR-correlated pulse sets one related AOFF [52] in the *control block*. This process is illustrated in Fig. 2.8.

The AOFFs have two states with a different wavelength each. They are de-

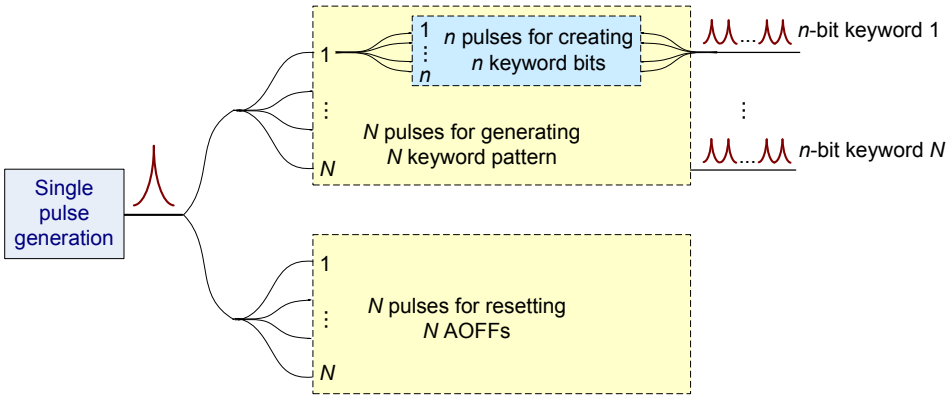

Figure 2.7: Single pulse generation for keyword generation and resetting AOFFs.

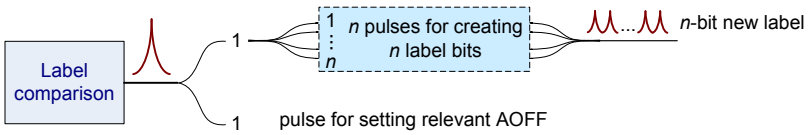

Figure 2.8: Label comparison for new label generation and setting AOFF.

signed to be triggered by optical pulses from one state to the other, and they emit one of the two wavelengths alternately. For each AOLSW, upon receiving optical packets, the original states of all the N AOFFs are set to λ_0 by N copies of the pulse produced by the *single pulse generation* block, as described earlier. Following the *label comparison*, one of the AOFFs is set to change state and emits another wavelength if there is an address match. After a notch filter at λ_0, only this new wavelength enters the wavelength converter as the CW control signal for the *wavelength conversion* [14, 53]. In the example shown in Fig. 2.3 and Fig. 2.5, the second AOFF is triggered into its λ_2 state.

It is worth mentioning that in the case of no address match, no optical pulse is generated from the *label comparison* subsystem. Consequently, all the AOFFs remain in their original reset states of emitting λ_0, which is then removed by the notch filter. If counter-propagation scheme is used for the *wavelength conversion*, the packet is *erased* from the network by the AOLS node. This prevents optical packets with wrong addresses keep looping in the network, resulting in unwanted

dead, legacy traffic that occupies and exhausts the available AOLS network resource.

Keyword and label generation by ODLs shown in Fig. 2.6 offers little flexibility because of the fixed fiber delay lengths and predefined coupling configurations for every possible label patterns. Each of the N copies from the optical pulse for the keyword generation needs to be further divided into n pulses, where n is the label bit-length and $N = 2^n$. In the example illustrated in Fig. 2.6, $n = 4$ and $N = 16$. Each of the n pulse copies travels through a fiber delay path of a different physical propagation length. All these n pulse copies have to be well aligned at the bit level so that when they are combined at the output of the ODL coupling, they form a bit-synchronized label pattern in the time domain. The physical length of *one-bit* fiber delay line l is decided by the label bit rate r and the light propagation speed in the fiber medium v: $l = v/r$. Assuming the fiber refraction index to be 1.5, $v = c/1.5 = 2 \times 10^8$ m/s. Thus, for optical labels at 40 Gb/s, $l = 5$ mm. The corresponding *one-bit delay*, Δt in Fig. 2.6, is decided by $\Delta t = l/v = 1/r = 2.5 \times 10^{-11}$ s = 25 ps.

Like in electronic packet-switched networks, the routing table of a switching node may need to be updated from time to time to adapt to changes occurred in the network configurations and traffic situations. In order to provide the possibility of upgrading the forwarding table in the AOLS node, two low-speed electronic switches are included in the AOLSW: one for the *local keyword generation* block, and one for the *new label generation* block, as shown in Fig. 2.5. The switching matrices of these two electronic switches are dynamically reconfigurable by the network control plane. They allow exchange of the forwarding table entries among the existing keywords and new labels for different decision making and packet forwarding possibilities. It is not possible, however, to introduce new keywords and label patterns or adding more bits to the labels, because the ODL lengths and configurations are already fixed. New keywords and labels require completely new ODL blocks.

Synchronization among the subsystems is realized by including proper guard-bands between the packet label and payload, and adjusting the physical propagation delay within and among all the subsystems. The AOLS nodes are for fixed-length optical packets. The processing time of each AOLSW subsystem as well as the total packet processing time are also constant and can be measured. Therefore, for a fully-interconnected AOLSW module, synchronization within the AOLSW can be achieved on the hardware level.

2.3.2 AOLSW alternative configuration

Recent demonstrations of interconnected as well as individual working subsystems have proved the feasibility of AOLSW original configuration with *two-bit* label length for the proof-of-principle [14, 39, 48, 49, 51, 53]. However, keyword and label generation relying on a locally generated optical pulse to be split and combined via predefined ODL modules [28, 50] cannot scale efficiently as the number of label bits increases. As we know, label generation by means of optically splitting, delaying and combining an optical pulse to create a label pattern has a potential problem regarding the power budget and requires strict synchronization at bit level. At each coupler, the optical power is distributed and optical amplifiers are needed to maintain an even optical power level among the label bits. Furthermore, updating the label patterns requires a completely new ODL combination. All these requirements place limitations on the optical power budget, signal quality, node performance and dynamic node re-configuration complexity. Therefore, a second AOLSW design with label generation by means of external modulation [54–56] is proposed here for avoiding the ODLs, where predefined electrical label patterns are deployed for the external modulators and synchronized locally with the label processing procedure, so that the label swapping still happens seamlessly. Although electrical data inputs are used, no OEO conversion is introduced, so the label processing remains all-optical.

All-optical bit pattern generation at 10 Gb/s has also been reported in [57] using an optical loop memory. It was stated that the demonstrated technique of generating bit patterns from noise in a fiber loop memory could be easily adopted at bit rates up to 100 Gb/s. However, no further advances have been found so far in literature using this technique.

Figure 2.9 shows the block diagram of such an AOLS design. In this configuration, the CW light from the control block, instead of the optical pulse from the label comparison as in Fig. 2.3, is used for the new label generation. Thus the new label is generated directly on the new packet wavelength, so that the wavelength converter converts only the packet payload. After that, the label insertion combines the new label and payload properly in the time domain.

The corresponding AOLSW details are illustrated in Fig. 2.10. For the keyword generation before the label comparison, a local CW light source is introduced and externally modulated by the electrical label bit patterns. For the new label generation before the label insertion, the CW light from the optical flip-flop is

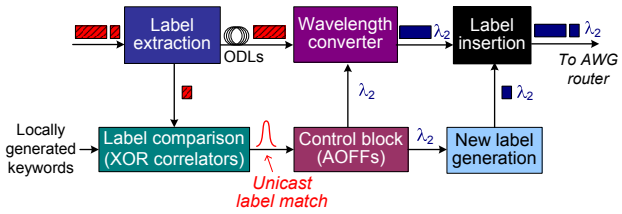

Figure 2.9: AOLSW subsystems interrelation: alternative configuration.

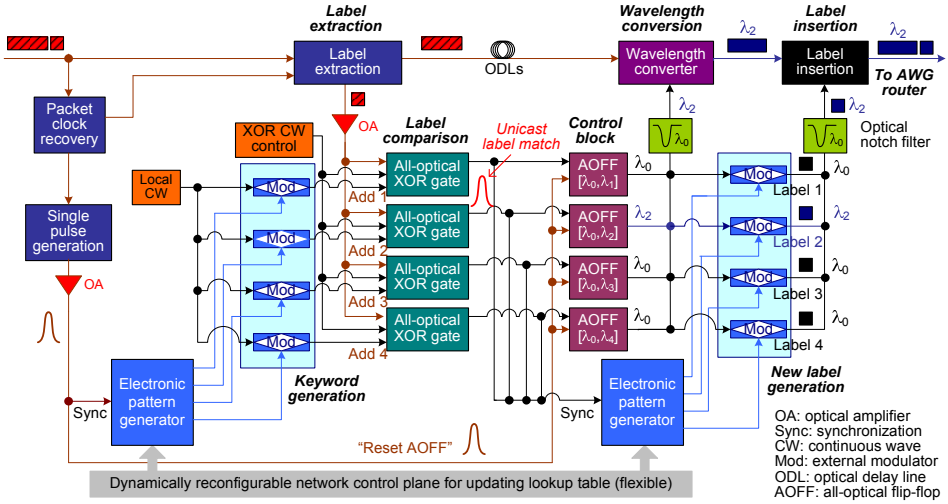

Figure 2.10: AOLSW details: alternative configuration.

employed. The optical power level of the keywords or the new labels can be tuned by adjusting the power level of the CW light injected into the external modulators. Updating the node lookup table can be realized simply by modifying the electronic label patterns. No hardware needs to be replaced as in the case of label generation by ODLs. Another advantage of this AOLS unit design is that the new label will be generated directly on the desired wavelength, which means that the wavelength converter does not need to be optimized to convert an optical packet with packet label and payload on different wavelengths. Thus the requirements for the wavelength range can be more relaxed.

In Fig. 2.10, the generation of the keywords and the new label by the electronic pattern generators need to be synchronized with the rest of the packet processing

subsystems. Just as in the AOLSW original configuration, the optical pulses from the *single pulse generation* block and the *label comparison* subsystem can be utilized to trigger the two electronic pattern generators to generate the keywords and the new label, respectively. As the outputs of the preceding function subsystems, these two pulses indicate the timing for the processes that follow.

In Fig. 2.9 and Fig. 2.10, the packet payload delay by ODLs is required for compensating for the latency of the *label comparison* and adjusting the timing for the *label insertion*. These ODLs can be placed once just before the *wavelength converter* to compensate for the total latency of both subsystems, or separately before and after the *wavelength converter*. This is because, following the *label comparison*, the address matching pulse sets the relevant AOFF and this AOFF stays in the *set* state until the next incoming packet resets it. As the *wavelength conversion* happens on-the-fly, it does not matter if the packet timing for the *label insertion* is adjusted before or after it.

Compared to label generation by ODLs, the external modulation scheme is more controllable and versatile. Although the label pattern is generated electrically, there is no OEO conversion involved for the label processing, and the incoming labels remain in the optical domain. External modulations such as LiNbO3-based Mach-Zehnder modulators (LN-MZMs) are widely used for 40 Gb/s transmission experiments. Other external modulators at 40 Gb/s include semiconductor-based Mach-Zehnder modulators (MZMs) and semiconductor-based electroabsorption modulators (EAMs) [54]. The high-speed external modulators support all-optical and seamless label processing without loss of speed, as current all-optical label processing by means of bit-correlation using SOA-MZIs is also limited to 10 Gb/s to 40 Gb/s operation speed due to the SOA carrier dynamics. Finally, this approach also allows sharing of a common CW laser source for all the keyword generators of different electrical pattern inputs.

2.4 AOLS packet format

The following specifications have been decided for the LASAGNE AOLS packet format:

- *40 Gb/s Label bit-rate (10 Gb/s for the demonstration).* This limitation is imposed by the label processing technique implemented in the LASAGNE project, which is all-optical bit-correlation using cascaded SOA-MZIs. Em-

ploying fast SOA-MZIs with high switching performance will in principle enable such label processing scheme to operate at 40 Gb/s. However, at the moment of writing, higher label bit-rate would require different labeling techniques and label processing schemes. Some suggestions and recommendations are given in Chapter 9.

- *40 Gb/s Payload bit-rate.* This limitation is imposed by wavelength conversion subsystems. The LASAGNE project aims at exploiting the ultrafast phase dynamics of SOAs in interferometric arrangements. Wavelength conversion of the optical packets including the payload is realized via cross-phase modulation inside an SOA-MZI [58]. The current commercially available SOA-MZIs can operate at 40 Gb/s in a differential mode [59, 60]. SOA-MZIs are expected to move to higher rates operation as SOA technology evolves. Photonic integration of arrayed SOA-MZIs will also result in easier handling, more stability, higher power efficiency, smaller footprints and lower cost. Although higher bit rate wavelength conversion has been reported for 160 Gb/s or even 320 Gb/s using a single SOA and detuned optical filtering techniques [61, 62], this filtered chirp technique suffers from large power penalties and thus at this moment is not yet mature enough for real AOLSW implementation. Moreover, multi-wavelength conversion (MWC) [59, 60] using the filtered chirp technique has not been demonstrated, while MWC can be employed for optical layer feed-forward packet multicast in the AOLS nodes, as will be introduced in Chapter 3∼7.

- *Fixed-length packets.* A fixed-length packet format is preferred for the potentially simpler packet format, AOLS node design, and network protocol definitions compared to a variable-length packet format. It also makes the synchronization within the AOLS node much easier, in particular for the alignment of the packets at the various input ports and wavelength channels. Deploying fixed-length AOLS packets reduces not only the general AOLS node complexity, but also the complexity of the required label format and the all-optical label processing circuit, as there is no need to include an extra field in the label regarding the packet length, and extract and "read" this field all optically. Furthermore, it is practical and commercially attractive to integrate the AOLSW into a plug-in module for the designed packet length, which consequently can improve the scalability of the AOLS nodes. In the LASAGNE demonstrations, optical packets of nanosecond-range at 40

Gb/s were deployed [14]. The minimum packet length is limited by the rise and fall time of the fabricated AOFFs, which are about 2 ns each [52, 63]. As far as the AOFFs are concerned, technically there is no upper limit for the packet length.

2.5 Unicast traffic performance evaluation

Previously, to the best of the author's knowledge, no study has been reported on the performance of AOLS nodes under various data traffic patterns. Traffic analysis of AOLS node architectures and network topologies is essential in designing high performance all optical packets switches and network strategies.

To this end, a custom-made simulator `AOLSim` was designed and developed to accommodate the features of AOLS nodes and network scenario depicted in Fig. 1.8, using the C++ language [43, 44, 47]. The simulator runs on a *Linux* platform (Suse v.10) with command line interface. No graphic interface has been developed yet. The current simulator consists of a kernel, interfaces and internal library.

A discrete time approach is applied in the simulations, in which time is divided into equal-sized slots. A *packet duration* is the smallest unit of information transferred over the network, and it occupies exactly *one time slot*.

A *traffic model* represents the mathematical characteristics of the traffic at each input wavelength to an input fiber of a switching node. The traffic model used in the simulations is one of the factors that influence the results obtained. Several traffic models have been studied in literature. To evaluate and compare the traffic performance of the node architectures presented in this thesis, the way optical packets are sent to the AOLS node needs to be set beforehand. In this thesis, AOLS node performance under *Bernoulli* and *self-similar* traffic models are investigated and discussed. For details of these two traffic models, reference is made to Appendix A.

Traffic load is the quotient between the number of time slots where a packet is present and the total number of time slots. It is a measurement of the usage of a channel. In the simulations, a traffic load of "1" means that a packet is present in every time slot, while a traffic load of "0" means that no packet is generated and transmitted.

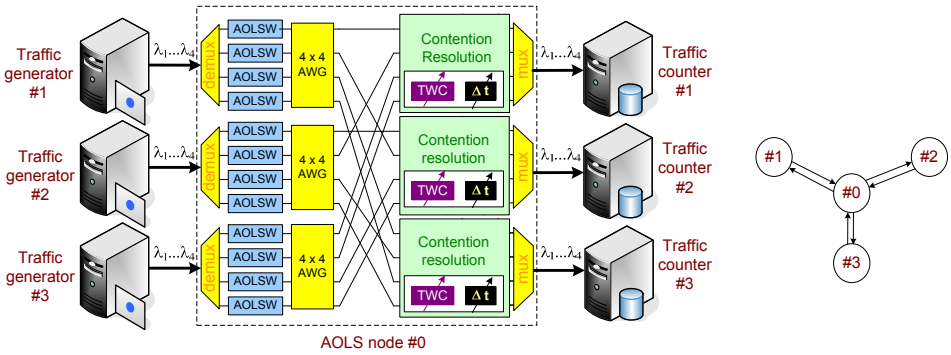

Figure 2.11: Simulated AOLS node with three input/output fiber ports [47].

2.5.1 Simulator design

The `AOLSim` is developed to facilitate user-defined AOLS simulations. In `AOLSim`, each user module of network elements such as AWGs, AOLSWs and optical fibers, is completely independent of the simulation core, and can be modified for each set of simulations. The user programs a shared library, which is loaded dynamically at runtime [43].

To run each AOLS simulation, the user writes one or several ASCII files containing a description of the simulated AOLS node or network with the simulation parameters as the simulation input [43]. In this description, the user can specify parameters such as the *AOLS node dimension* (the number of fiber ports), the *AWG dimension* (the number of AWG ports), *network capacity* (the number of WDM wavelengths), the *buffer depth* (how many time slots of packet delay), whether or not to use *wavelength conversion* for contention resolution, and the node *lookup table* (which output port the packet is to be forwarded according its label).

In the user file, the simulated AOLS nodes need to be fully connected. For isolated AOLS node simulations, each input fiber port of the node should be connected to a *traffic generator*, and each output fiber port to a *traffic counter*. The add/drop fiber ports are also treated in the same way as the input/output fiber ports. In this way, the AOLS node in Fig. 2.2 shall be connected to *three* traffic generators and *three* traffic counters, as shown in Fig. 2.11. The traffic generator generates packets according to the network load in each time slot and sends them to the AOLS node input fiber ports. Every packets is assigned randomly a *label*

from a *label pool*, where a defined number of labels are kept. According to the node lookup table specified by the user, the simulated AOLS node passes the packets to the correct output ports, where a user-defined contention resolution strategy is implemented. After the contention resolution, the packets that are successfully delivered shall be collected and counted by the traffic counter.

Each object in a simulated AOLS node and network is a representation of real network objects. From the component point of view, the following objects can be used: *traffic generators*, *traffic counters*, *AOLS nodes* and *fiber delay lines* [43].

2.5.2 Simulation parameters and conditions

a. Unicast forwarding

Unicast packets are forwarded to only *one* of the output ports of AOLS node. In a unicast AOLS node lookup table, which is defined manually by the user of the `AOLSim` simulator, each label should match only *one* output port of the AOLS node where the packet is to be sent.

The number of labels for each simulated AOLS node architecture depends on the number of input/output ports that the AOLS node has. For an AOLS node with P input/output ports, each input port is assigned P dedicated labels. So there are in total P^2 labels used for the whole AOLS node. Note that this way of *simulating* the labels is different from *practice*, where in total only P labels are necessary for the whole AOLS node.

In the simulation carried out, *nine* labels, namely, from 0 to 8, are defined in the lookup table. Every *three* labels are dedicated to *one* of the *three* output fiber ports in Fig. 2.11. A randomly generated packet at an AOLS input fiber port carries a label that is taken *by chance* from a label pool of three labels. All the labels in the unicast AOLS node lookup table are *unicast* labels.

b. Measured performance parameters

Packet loss ratio (PLR) and *network throughput* (NT) are the two parameters that are mostly used in assessing network traffic performance in an optical packet-based environment. They indicate network reliability and utilization [64]. The LASAGNE AOLS nodes were designed for fixed-length optical packets. In all our simulations, we deployed a packet length of an average IP packet size, which is 512 bytes. However, the exact value of this parameter is not relevant for the PLR

and NT estimation.

PLR is defined as *the total number of dropped packets divided by the total number of packets generated* (#: the number of):

$$PLR = \frac{\#packets_{dropped}}{\#packets_{generated}}. \tag{2.1}$$

The dropped packets are the packets that are discarded due to congestion.

For the PLR calculation, the AOLS node, or several AOLS nodes if a network simulation is to be carried out, is considered as a "*black box*". The PLR is then an estimation of the probability of any packet that enters the node(s) being dropped.

NT is *the fraction of the network resources*, in this case the node resource, *that successfully delivers packets* [64]. According to this definition, different measurements can be implemented for evaluating NT. For example, in [64], the *ideal average hop distance of the simulation* was included under the condition that longer fiber spans without packets is more costly than shorter spans. In our simulator `AOLSim`, only three parameters have been taken into account: the *number of packets delivered*, the *number of packets generated*, and the *number of null packets*, i.e. void time slots when there are no packets generated [43].

The simulated NT is calculated as:

$$NT = \frac{\#packets_{delivered}}{\#packets_{generated} + \#null_{generated}}, \tag{2.2}$$

where $\#null_{generated}$ is the number of null packets.

In this case, the NT parameter and the PLR parameter is related. If we define the normalized network load (NNL) as

$$NNL = \frac{\#packets_{generated}}{\#packets_{generated} + \#null_{generated}}, \tag{2.3}$$

NT can also be expressed in PLR and NNL as

$$NT = \frac{1 - PLR}{1 + \frac{\#null_{generated}}{\#packets_{generated}}} = NNL \times (1 - PLR). \tag{2.4}$$

The reasons of using the above NT definition are:

i) The parameter *fiber span length*, which is the lengths of optical fibers between the AOLS nodes within a network, does not apply to isolated AOLS node simulations. For AOLS unicast network simulations, the fiber span length is also not an influential factor on the results obtained. In four-wavelength

AOLS networks, the simulated PLR and NT performance difference between 0 and 5000 slots delay is negligible [43]. At 40 Gb/s, with the typical value of light propagation speed in fiber $v = c/1.5 = 2 \times 10^8$ m/s and a packet duration of 512 bytes, the above simulated span difference is 100 kilometers; Moreover, if for future network simulations, span length between nodes is considered, the NT can be still easily upgraded from the current definition to a more complex form as in [64].

ii) For the simulator development, it is important to leave some redundancy in the software to help spot and correct possible errors. This means in the current `AOLSim`, the results obtained for PLR and NT should be related by the function defined by Eq. 2.4.

c. Assessed contention resolution schemes

Three approaches to contention resolution are applied to the unicast node architecture in Fig. 2.2, which are:

- `NoCR` (*no contention resolution*): No contention resolution implemented. In case of packet contention, the lower priority packet(s) will be dropped.

- `WC` (*wavelength conversion*): Only wavelength conversion is implemented for contention resolution. In case of contention, the node tries to convert the contending packet(s) onto one of the available output wavelength channel(s), or drops the lower priority packet(s) when all the output wavelengths are occupied.

- `WCFB` (*wavelength conversion + fiber buffering*): In case of contention, the node will first look for an available output wavelength. If this is not possible, the node can buffer the lower priority packet(s) in an ODL for one packet duration. In the next time-slot, the packet(s) that is/are in the buffer will have higher priority to be forwarded than the incoming packet.

In all these cases, a policy is applied that the optical packets on the shorter wavelengths have the higher priority to be forwarded. For more information on contention resolution, reference is made to Chapter 8.

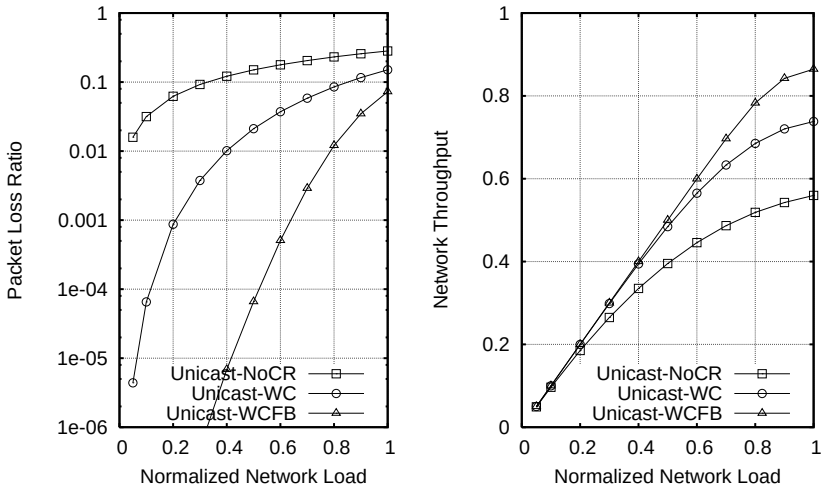

Figure 2.12: Simulation results of unicast node performance under Bernoulli traffic.

2.5.3 Simulation results

In simulations of the unicast architecture illustrated in Fig. 2.2, at each time slot, i.e., the duration of the 512-byte fixed-length packet, maximum *twelve* synchronized packets are generated and sent to the node. Of these *twelve* packets, *four* each are sent to the first two *input* fibers, and the last *four* are for the *add* fiber.

Figure 2.12 and 2.13 present the *PLR* and *NT* performance of the unicast node under Bernoulli and self-similar traffic conditions, respectively. We can observe that introducing a one-slot buffer into the contention resolution scheme is less efficient with the self-similar traffic than with Bernoulli traffic. This is because of the difference between the traffic model characteristics. Self-similar traffic sends a burst of packets during an *ON* period, during which the one-slot buffer is likely to be constantly occupied so that when more packets come in they can only be dropped. Therefore the *PLR* starts to increase quickly and the *NT* does not experience much improvement, while in an *OFF* period the buffering resource is not utilized efficiently. Bernoulli traffic has a homogeneous nature, which spreads packets over all the simulation time slots for a certain load to avoid packet bursts. Consequently, the packets that are stored in the buffer can be forwarded quickly and the slot is available again for upcoming contended packets.

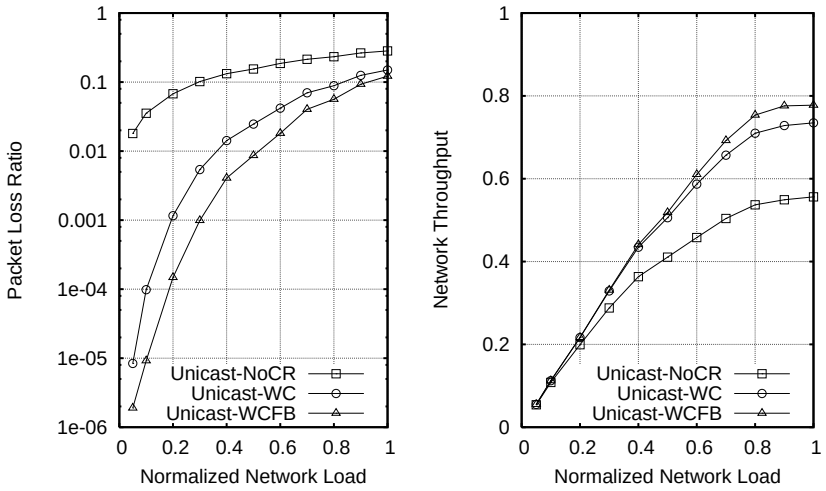

Figure 2.13: Simulation results of unicast node performance under self-similar traffic.

The *PLR* and *NT* indicate the AOLS node traffic performance under the specified *node dimension* and *architecture* shown in Fig. 2.2, with the evaluated *contention resolution* schemes. The absolute values of the *PLR* and *NT* are not important when not configured with node dimensions or contention resolution schemes according to the real network demands and performance requirements. Rather, in this thesis these *unicast* simulation results are obtained as a baseline for the AOLS *multicast* traffic performance under the same node dimension and intended network throughput, which is presented in Sec. 3.4.2, to investigate the influence of the multicast traffic on the AOLS node performance.

In general, the developed `AOLSim` simulation platform can be used to evaluate the traffic performance of various AOLS node dimension, architectures and network topologies with commercial parameters and network specifications by changing the number of AOLS input/output ports, node buffering position and strategies, network topology design, etc. The *PLR* and *NT* may vary whenever one or more of the following configurations or parameters are modified: AOLS node dimension, wiring matrices between the AWGs and the output ports, contention resolution schemes, buffering depths, and other AOLS node and network specifications such as the number of internal and external wavelengths. To improve the AOLS node performance under the same conditions, the most straightforward

way is to *employ wavelength conversion* and to *increase the buffer depth* for the contention resolution [43, 44] to achieve the desired PLR and NT.

2.6 Summary and discussions

In this chapter, the AOLS node investigated in the LASAGNE project is described. The AOLS node forwards optical packets by wavelength conversion and passive AWG routing. The processing of optical time-serial labels and decision making are done in the optical domain without any OEO conversion. The $AOLSW$, one of the most important functional components of the AOLS node, is especially looked into. This chapter presented and discussed two layouts of the AOLSW and their principal operation.

The AOLS nodes as well as the AOLSWs shown in this chapter are for unicast operation. To evaluate the traffic performance of the AOLS nodes, Bernoulli and self-similar driven simulations were carried out for different contention resolution schemes. The simulation results indicate similar performance under these two traffic models when no contention resolution is used and when only wavelength conversion contention resolution is applied. The effect of further adding optical buffering is traffic pattern dependent. For realistic bursty traffic such as self-similar traffic, the fiber buffering is significantly less efficient for AOLS nodes than Bernoulli traffic with a homogeneous nature.

In the hierarchial telecom networks, the transmission errors of the *lower layers*, such as the optical layer, are generally corrected via the network control and monitoring of *upper layers*, such as the ATM and IP layer. In the AOLS networks, with the current AOLS technologies, lost or dropped optical packets shall be detected by the upper layers. As optical device technologies, AOLS labeling and all-optical label processing techniques advance, more fields can be included in the optical header for controlling the packet quality and the correct delivery of the optical packets, as in the case for the MPLS applications [8–10] and research optical label switching (OLS) demonstrations with electronic header processing [22]. Unlike *bit error rate* (BER), i.e., the number of erroneous bits received divided by the total number of bits transmitted, which is the lowest level error control, PLR indicates the *network layer* reliability rather than the *physical layer* transmission correctness. In the AOLS scenario, the network layer refers to the optical networks consist of interconnected AOLS core nodes.

Chapter 3

Multicast all-optical label switching nodes and performance

Multicast all-optical label switching (AOLS) is desirable for multicast packet forwarding directly in the optical layer at high speeds, as it bypasses the optical-electronic-optical conversion of the optical packets and the electronic processing of the packet headers. In this chapter, two multicast AOLS node architectures are discussed, referred to as the feedback multicast (FBM) and the feed-forward multicast (FFM), respectively. Compared to FBM, FFM is a simpler, faster, more efficient and more economical multicast concept for passive waveguide-based optical label switching nodes. We analyze its advantages in terms of hardware requirements and traffic performance under different contention resolution schemes in comparison with the FBM nodes. An analytical study shows that an FFM AOLS node requires considerably fewer physical components than an FBM AOLS node of the same node dimension. Traffic performance evaluation regarding packet loss ratio and network throughput proves the performance enhancement of FFM over FBM to be also significant. Parts of this chapter are based on publications.[1]

[1] See references [46, 65].

3.1 Introduction

With all the significant developments in all-optical label switching (AOLS) technologies, more and more networking functions are being realized in the optical layer. Particularly, multicast capable AOLS [11, 13, 16] has attracted great interest as it is of crucial importance for coping with the steeply increasing number of multicast applications such as high-definition TV, multi-party online games, video conference and optical storage area networks.

Most of the AOLS or optical label switching (OLS) nodes investigated so far provide only limited multicast functionalities employing *broadcast-and-select* schemes [66] or *feedback multicast* (*FBM*) configurations [2, 13, 16, 22, 23]. The *broadcast-and-select* schemes result in a large amount of unwanted network traffic, create network congestions, and suffer from excessive optical losses due to the passive optical power splitting via the distributors [66]. The *FBM*, also sometimes referred to as the *recirculation multicast*, has been the most exploited multicast method for AOLS and OLS nodes studied and demonstrated in the last 5∼10 years [2, 13, 16, 22, 23].

There are mainly *two* node configurations using the FBM approach:

i) The *first* configuration deals with the multicast traffic by directing them to a feedback structure consisting of fiber delay lines or optical waveguides, where the multicast packets are looped back to some multicast capable ports at the node input side. This multicast capable ports can then process the multicast packets, copy the multicast information, and forward the same data information to several output ports simultaneously [22].

   In the first FBM configuration, the multicast packet processing is at the node *input* side, by additional *multicast capable ports*.

ii) The *second* configuration relies on an extra multicast switch at the output side. All the multicast packets are routed to this switch, where the the multicast packet information is copied into several and all the copies of the multicast packets are looped back separately via feedback fiber lines to dedicated node input ports. Each of these node input ports forwards a copy of the multicast packet to one of the multicast destination output ports [2, 13, 16, 23]. These node input ports do not have to be multicast capable, but just as the other unicast input ports, because the processing and copying procedure is already carried out at the multicast switch.

When there are only two possible multicast destinations, as in [13, 16], the multicast switch can be replaced by an optical coupling structure with proper amplification. This is the simplest multicast case that requires the least amount of packet processing. When there are more than two possible multicast destinations, the multicast switch needs to be able to process the multicast packet label and make copies of the multicast packet data according to the label information. Such processing has been done electronically in [2, 23].

In the second FBM configuration, the multicast packet processing is at the node *output* side, by an additional *multicast switch*.

The main disadvantage of the FBM configurations is that it can support only limited multicast traffic depending on the number of feedback loops and extra input ports installed in the node. Moreover, by implementing feedback structures, multicast traffic experiences longer delay, encounters more optical losses and goes through more active components, which also reduce the packet handling efficiency and optical node transparency. Finally, to compensate the power losses, multicast packets need to pass through multiple optical amplifiers, which shall consequently suffer from optical signal-to-noise ratio degradation (OSNR) due to the amplified spontaneous emission (ASE) noise from the amplifiers.

In Sec. 3.2, we discuss the FBM scheme, and introduce another multicast scheme: *feed-forward multicast* (*FFM*) [65]. The FFM scheme eliminates the feedback structure by supporting multicast functionality directly in the optical layer inside the label processor before the arrayed waveguide grating (AWG). In Sec. 3.3, we analyze its hardware savings in comparison with the FBM scheme. In Sec. 3.4, we investigate the impact of various contention resolution schemes on the packet loss ratio (PLR) and network throughput (NT) of the FFM and the FBM nodes, and prove the superior traffic performance of the FFM node to the FBM node under the same conditions. In Sec. 3.5, the main issues addressed in this chapter are summarized and discussed. Our simulation results prove that FFM is simpler, faster, more efficient and more economical for passive waveguide-based OLS nodes. From the physical layer point of view, FFM does not need additional optical amplification like broadcast-and-select and FBM do, so the multicast packets shall not experience further OSNR degradation due to the ASE noise. Employing certain multi-wavelength conversion (MWC) technologies in the FFM scheme, optical signals can even be regenerated with an improved OSNR [67, 68].

3.2 Multicast AOLS nodes

The evaluated multicast OLS node architectures were based on the AOLS node architecture and function blocks studied, validated and demonstrated in the European Commission funded FP6 project IST-LASAGNE [13, 14, 16].

3.2.1 Multicast labeling

Multicast labels do not have to be special labels different in nature from the unicast ones. For a node with P output fiber ports, excluding "*not forwarding*", there are $2^P - 1$ possible different ways of *forwarding* an incoming packet: P of them are for unicast to each output fiber port, and $2^P - P - 1$ for multi- or broadcast.

The 2×2 AOLS nodes investigated in the LASAGNE project has *three* output fiber ports: *two* output line ports and *one* drop port. Strictly speaking, there are *seven* ways of forwarding an incoming packet: *three unicast* forwarding to either of the three output fiber ports, *three multicast* forwarding any two of the three output fiber ports, and *one broadcast* forwarding to all the three output fiber ports. However, in the LASAGNE project, only *one* of the *four* multicast cases is considered, which is the multicast forwarding to both output line ports and not the drop port. Therefore, for the LASAGNE 2×2 AOLS nodes, in total only *four* ways of forwarding a packet are taken into account. For this purpose, a minimum *two-bit* label length is required to cover the *four* possibilities, namely, 00, 01, 10, and 11. A LASAGNE 2×2 multicast AOLS node can use any *three* of these four labels for unicast, and the other *one* for multicast. *Which three* for unicast and *which one* for multicast are not important, as long as they are defined accordingly in the AOLS node lookup table.

3.2.2 Feedback multicast (FBM) AOLS

In the LASAGNE project, the second FBM configuration is applied, where the multicast packet processing is at the node *output* side, by an additional *multicast switch*, as illustrated in Fig. 3.1. FBM AOLS in a 2×2 node is performed by directing *one* of the multicast packets received at the *input fiber ports I1* and *I2* to a 2×2 multicast switch or a 2×2 coupler, where the packet is duplicated, and recirculating the duplicated multicast packets via two feedback loops to two unicast input ports of the switch in order to have them forwarded to both *output fiber ports O1* and *O2*. Fig. 3.2 shows the all-optical label swapper (AOLSW) label

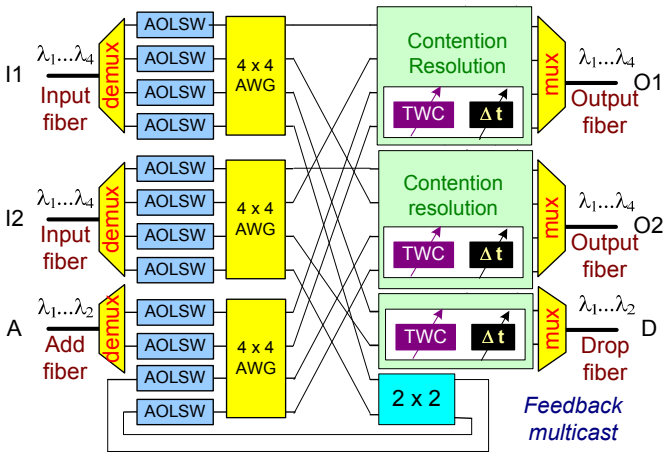

Figure 3.1: 2×2 FBM AOLS node architecture [13]. (AOLSW: all-optical label swapper; TWC: tunable wavelength converter.)

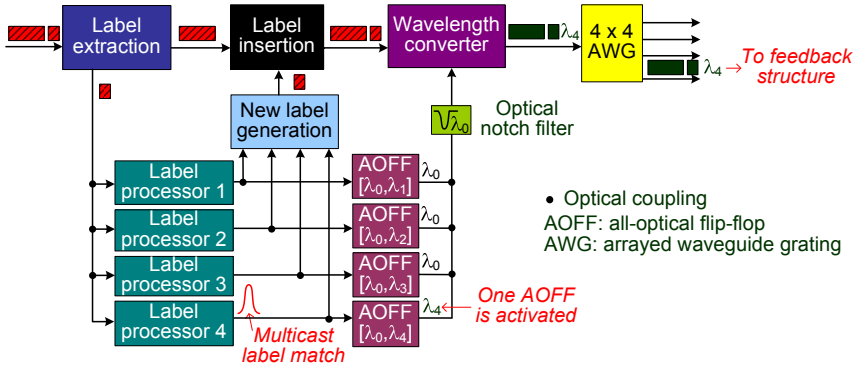

Figure 3.2: AOLSW label processing logical connections for FBM.

processing logical connections for an FBM AOLS node, which employs the same subsystems as the unicast AOLSW presented in Fig. 2.4 in Sec. 2.3. In Fig. 3.2, the *multicast label*, as should be specified in the AOLS node lookup table, can be any of the four combinations of the two label bits. Thus it is not different in nature from the *unicast label* in Fig. 2.4. As a matter of fact, they can even have the same *label pattern*, but this label pattern has a different meaning in the lookup tables for an AOLS unicast node as for an FBM AOLS node.

For a node with P output fiber ports, with the FBM approach, all the packets with the $2^P - P - 1$ multicast labels are sent to the multicast switch or the recirculation loops in order to be further processed. Multicast by means of feedback configurations must be executed at the *node* level, in this case the AOLS node level. With a limited number of feedback loops and dedicated AOLSWs for multicast, as in the case shown in Fig. 3.1, it is not possible for the FBM AOLS node to have all the multicast possibilities. For example, the FBM AOLS node in Fig. 3.1 can neither deal with multicast packets from the *Add* fiber port, nor can it send any multicast packets to the *Drop* fiber port. Moreover, part of the node resources needs to be dedicated to the re-processing and the recirculation of the multicast packets, therefore, the percentage of the resources that is used for forwarding the packets to the next nodes is lower. Hence, the NT of such multicast nodes is lower, and the efficiency is reduced.

Another drawback of the multicast node architecture shown in Fig. 3.1 is that this switch can only process *one* multicast packet from both input fiber ports at a time, as the feedback loops can only accommodate *one* multicast connection. This way, the switching is envisaged to be able to keep the packet loss ratio low only when the number of multicast packets represents a relatively small fraction of the total number of generated packets. If the multicast traffic constantly occupies a large portion of the total traffic, apart from *increasing the dimension of the AWGs* and *introducing more 2×2 couplers*, *additional input ports and the corresponding number of AOLSWs* for multicast purpose are also required for the AOLS node be able to handle the extra amount of multicast traffic. Besides, a relevant number of *optical feedback loops* needs to be set up. This means that the packet forwarding efficiency and the NT of the AOLS node is further reduced. Therefore, scalability is a serious issue for the FBM nodes.

3.2.3 Feed-forward multicast (FFM) AOLS

The architecture of a 2×2 FFM AOLS node is the same as a 2×2 AOLS unicast node, as presented in Fig. 3.3. The difference between an FFM AOLS node and a unicast AOLS node is determinded by the way each AOLSW handles an optical packet. In the cases of unicast and FBM, the AOLSW can only convert the packet onto one single wavelength [13, 14]. Consequently, the optical packet is routed to only *one* output of the AWG, and hence to either *one* of the output fiber ports of the AOLS node or the feedback circuit; while in the case of FFM, the AOLSW is

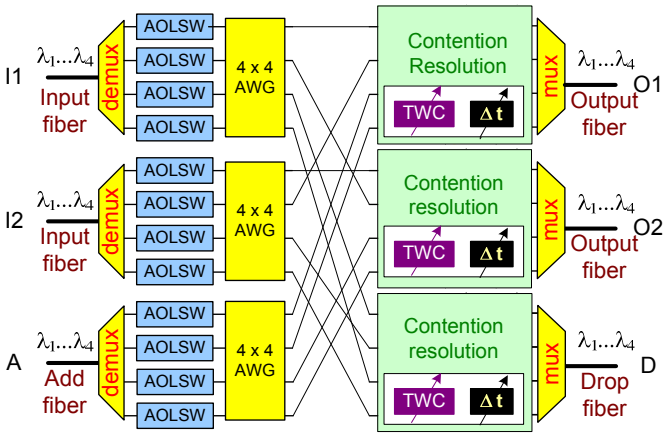

Figure 3.3: 2×2 FFM (unicast) AOLS node architecture.

able to convert the packet onto multiple appropriate wavelengths specified by the all-optical flip-flops (AOFFs) in the control block. These AOFFs are set by the label processors [65]. The same optical data information on different wavelengths is then simultaneously forwarded to different outputs of the AWG that are connected to different output fiber ports of the AOLS node.

Figure 3.4 shows the AOLSW label processing logical connections of an FFM AOLS node. FFM AOLS is executed at each AOLSW level by all-optical MWC [60, 67–70], which is achieved by driving the wavelength converter in the AOLSW with multiple continuous waves (CWs) on the desired wavelengths when a label is matched to a multicast entry defined in the node lookup table [65]. Such AOLSWs can still employ all the function subsystems as in the unicast and FBM nodes [13, 14], except that the wavelength converter can also convert the optical packet simultaneously onto multiple wavelengths [60, 67–70]. Operation of MWC inside the AOLSW is realized by activating multiple corresponding AOFFs on detecting a multicast label. As in the case of FBM, a multicast label for FFM can be specified in the AOLS node lookup table with *any label pattern* chosen from all the possible label pattern combinations made up by the defined number of label bits. The details of an FFM AOLSW are shown in Fig. 3.5.

For a node with P output fiber ports, with the FFM approach, all the $2^P - P - 1$ multicast possibilities are already taken into account at the first label processing stage before the AWGs. Consequently, multicast is executed at the *label processor*

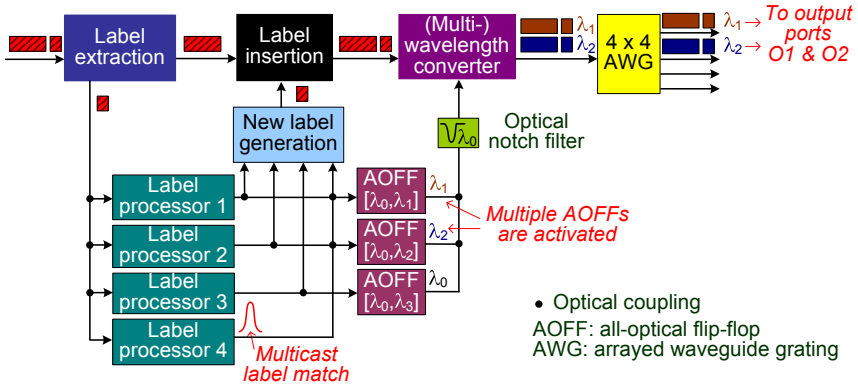

Figure 3.4: AOLSW label processing logical connections for FFM.

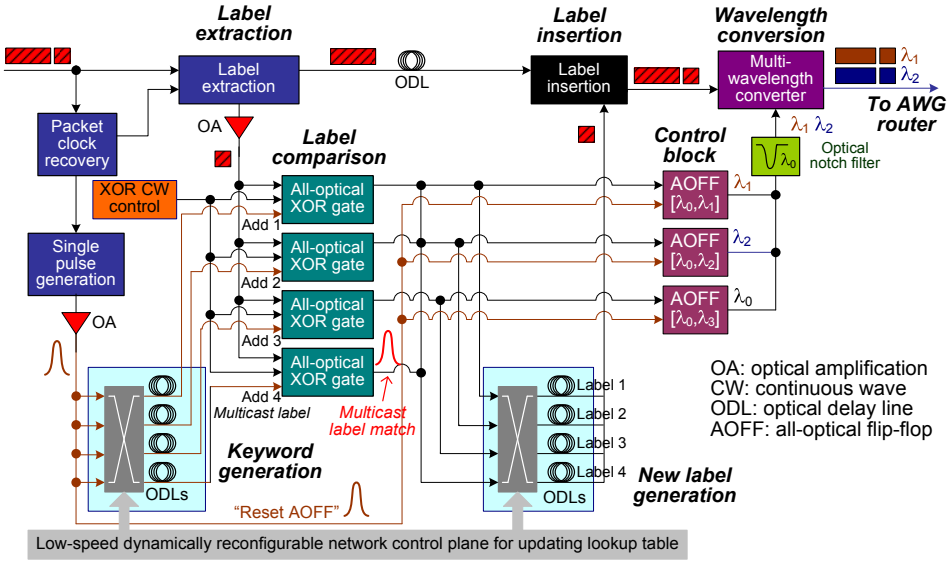

Figure 3.5: AOLSW details for FFM.

level, e.g. the AOLSW level, instead of the *node* level, e.g. the AOLS node, as in FBM.

So far, one-to-eight MWC has been reported based on a single semiconductor optical amplifier – Mach-Zehnder interferometer (SOA-MZI) [71], proving

good feasibility for current OLS node multicast applications. A proof-of-principle demonstration of the AOLSW has also been realized for unicast in the laboratory [14].

Comparing the FFM AOLSW in Fig. 3.4 to the FBM AOLSW in Fig. 3.2, it can be seen that the FFM AOLSW requires one AOFF less than the FBM AOLSW. This is because for each FBM AOLSW, a fourth AOFF is necessary to convert the multicast packet onto the fourth input wavelength of the AWG, in order for the AWG to route the packet to its relevant output that is connected to the multicast switch and the feedback loops. In the FFM node, multicast is implemented at each AOLSW and no feedback configuration is used, so the fourth input wavelength of the AWG for addressing the feedback configuration in the FBM AOLS node is not anymore essential for the FFM AOLS node to be able to forward multicast packets. This results in considerable physical component saving on AOFFs in each AOLSW of the AOLS node.

This fourth input wavelength of the AWG, however, can be utilized either to provide extra connectivity in the AOLS node to improve the node throughput, or to serve as AOLS node internal backup connections, which is generally a network-layer decision dependant of the actual traffic conditions. Comparing the FFM node in Fig. 3.3 to the FBM node in Fig. 3.1, instead of linking the fourth AWG outputs after both input fiber line ports to the *multicast switch* and the *feedback loops*, these AWG outputs are linked to the *drop fiber port* to provide extra or backup connections for the drop traffic in the FFM node.

3.3 Comparison of hardware requirements

As mentioned in Sec. 3.2, the FFM AOLS approach brings various benefits including physical component savings. It not only necessitates less AOFFs at the AOLSW level, but also eliminated the feedback loops, the multicast switch and the extra AOLSWs dedicated for multicast packets, at the AOLS node level. Moreover, it also allows downsizing of the AWGs because less AWG internal wavelengths are required to route the multicast packets to the feedback configuration, and thus less AWG ports are needed.

Table 3.1 presents the calculation of the *minimum* resource requirements of the FBM and the FFM approaches for AOLS nodes with P_1 number of *input/output fiber line ports* and P_2 number of *add/drop fiber ports*, in a network of W wavelengths. Here, P_1 and P_2 indicate the AOLS *node dimension*.

Table 3.1: Minimum hardware requirements per FBM and FFM node. (P_1: number of AOLS node input/output fiber ports; P_2: number of AOLS node add/drop fiber ports; W: number of AOLS network wavelengths.)

	FBM	FFM	***Savings***
AOFFs	$(4P_2+W)P_1^2+(P_2+1)WP_1$	$(P_2+W)P_1^2+WP_1P_2$	$\boldsymbol{3P_1^2P_2+WP_1}$
AWG ports	$(W+2P_2)P_1$	$(W+P_2)P_1$	$\boldsymbol{P_1P_2}$
AOLSWs	$(W+2P_2)P_1$	$(W+P_2)P_1$	$\boldsymbol{P_1P_2}$
Feedback loops	P_1	0	$\boldsymbol{P_1}$
Multicast switch	1 (with dimension: $P_1 \times P_1$)	0	**1**

To simplify the calculation for the FBM node in Table 3.1, as in the LASAGNE FBM AOLS node in Fig. 3.1, multicast situations to only the *output fiber line ports* are considered, and no multicast packets can be sent to the *drop fiber ports*. Moreover, the number of the add/drop wavelengths per add/drop fiber port is equal to the number of output fiber line ports per AOLS node, so that *add traffic* can be sent to all the P_1 *output fiber line ports*. In this way, the complexity and hardware requirements for the FBM AOLS node is reduced, at the cost of limited multicast forwarding possibilities. Note that if all the multicast possibilities are taken into account for an FBM AOLS node, there will be in total $2^{P_1+P_2} - (P_1+P_2) - 1$ multicast forwarding possibilities for the FBM node to handle, as stated in Sec. 3.2.1, instead of $2^{P_1} - P_1 - 1$ possibilities considered in this section. Consequently, the minimum physical resource requirements per FBM AOLS node shall increase dramatically when the extra $2^{P_1}(2^{P_2}-1)-P_1$ multicast possibilities are considered.

Taking the LASAGNE AOLS nodes as an example, each node has *two* input/output fiber line ports with *four* network wavelengths, and *one* add/drop fiber ports with *two* add/drop wavelengths. FBM and FFM nodes under *minimum* hardware configuration are presented in Fig. 3.1 and Fig. 3.6, respectively. In this example, $P_1 = 2$, $P_2 = 1$, and $W = 4$. Table 3.2 shows the minimum hardware requirements for these FBM and FFM AOLS nodes.

In Table 3.2, the entries of *AWG ports*, *AOLSWs*, *feedback loops* and *multicast switch* are clearly visible from the AOLS node level, and can be easily confirmed

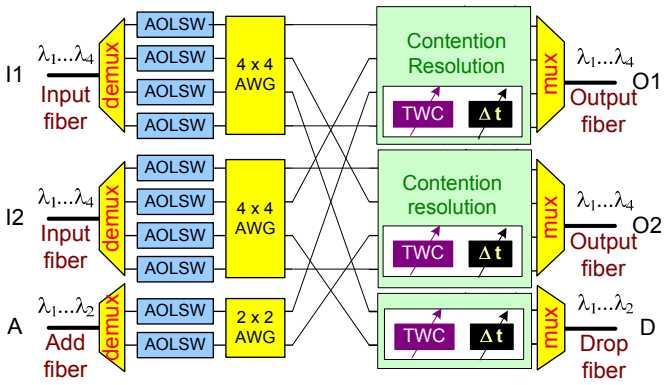

Figure 3.6: 2×2 FFM (unicast) AOLS node architecture with two add/drop wavelengths.

Table 3.2: Minimum hardware requirements per FBM and FFM node. Each node has 2 input/output fiber ports with 4 wavelengths each, and 1 add/drop port with 2 wavelengths.

	FBM	FFM	***Savings***
AOFFs	48	28	**20**
AWG ports	12	10	**2**
AOLSWs	12	10	**2**
Feedback loops	2	0	**2**
Multicast switch	1 (with dimension: 2×2)	0	**1**

from Fig. 3.1 and Fig. 3.6. The entry of *AOFFs* is the total number of AOFFs from all the AOLSWs in the AOLS node. For the FBM node in Fig. 3.1, there are 12 AOLSWs, and each AOLSW has 4 AOFFs as in Fig. 3.2. Therefore, the total number of AOFFs per FBM node is: $12 \times 4 = 48$. For the FFM node in Fig. 3.6, the first 8 AOLSWs of the *input line fiber ports* require *minimum* 3 AOFFs each as in Fig. 3.4, and the last 2 AOLSWs of the *add fiber port* require only 2 AOFFs each to address the two input wavelengths of the 2×2 AWG. Hence the total number of AOFFs per FFM node is: $8 \times 3 + 2 \times 2 = 28$. This verifies the *AOFFs* entry of Table 3.2.

From Table 3.1, we can observe that in general, with the FFM scheme, considerable physical components can be spared. On the AOLS node level, for the number of AWG ports, and AOLSWs required, the resource reduction is *proportional* to the *product* of P_1 and P_2; for the number of feedback loops required, the resource reduction is *proportional* to P_1. On the AOLSW level, for the number of AOFFs required per AOLS node, the resource reduction is *quadratic* in P_1 when P_2 and W are fixed, and *proportional* to the network wavelengths W when the node dimension parameters P_1 and P_2 are fixed.

3.4 Multicast traffic performance evaluation

To evaluate and compare the traffic performance of the two multicast node architectures under different contention resolution schemes, as in Chapter 2, simulations deploying *Bernoulli* and *self-similar* traffic models were carried out.

3.4.1 Simulation parameters and conditions

a. Multicast forwarding

Multicast packets are forwarded to more than *one* output ports of AOLS node. In the LASAGNE AOLS nodes, only one multicast possibility, which is multicast forwarding to the first two output fiber ports, is considered.

In a multicast AOLS node lookup table, there are labels that match *only one* output port of the AOLS node, as well as labels that match *more than one* output ports of the AOLS node. As in the unicast simulations, the lookup table is defined manually by the `AOLSim` user.

In the simulation carried out, for an AOLS node with three input/output ports, *one* of the *three* labels per port is defined as the multicast label in the lookup table. A multicast packet is forwarded to both the first and the second output fiber ports. Therefore, in this case, the possibility of generating a multicast packet is configured to be on average *one* in every *three* packets per multicast input fiber port. This multicast probability, regardless of the wavelength channels at the input port, can be modified by introducing more labels for unicast and multicast purposes. The 1/3 multicast factor is employed to keep the simulation runtime under reasonable measure of hours. Increasing the number of labels allows finer tuning of the multicast factor, but results in higher complexity in the simulated system, which consequently lengthens the simulation runtime.

b. Measured performance parameters

The measured performance parameters were still *PLR* and *NT*, the same as in the unicast case in Sec. 2.5.2. However, in a multicast possible environment, a randomly generated packet can be either unicast or multicast. Moreover, for each multicast packet, it needs to be copied and forwarded to several outputs at the same time.

Under the multicast configuration, the $packets_{generated}$ variable in Eqs. (2.1) and (2.2) become

$$packets_{generated} = packets_{generated} + packets_{duplicated}. \tag{3.1}$$

c. Assessed contention resolution schemes

The same contention resolution schemes were applied to each node architecture, which are:

- `NoCR:` No contention resolution implemented. In case of contention, the packet(s) will be dropped.
- `WC:` Only wavelength conversion is implemented.
- `WCFB:` In case of contention, the node will first look for an available output wavelength. If this is not possible, the node can buffer the packet for one packet duration. In the next time-slot, the packet that is in the buffer will have higher priority to be forwarded than the incoming packet.

3.4.2 Simulation results

a. One multicast port

Multicast performance of the feedback and feed-forward architectures, shown in Fig. 3.1 and Fig. 3.3, are assessed. The FBM and FFM nodes employ the same number of AOLSWs and the same AWG dimension. However, in the FBM node, two of the AOLSWs are dedicated for the multicast function; while in the FFM node, these two AOLSWs are used as the rest of the AOLSWs for both unicast and multicast forwarding. Therefore, the *input* capacity for these two nodes are different. At each time slot, maximum *ten* synchronized packets for Fig. 3.1 and *twelve* for Fig. 3.3 are generated and sent to the nodes, as allowed by the node input capacity. In this set of simulations, we only configured the first input fiber port

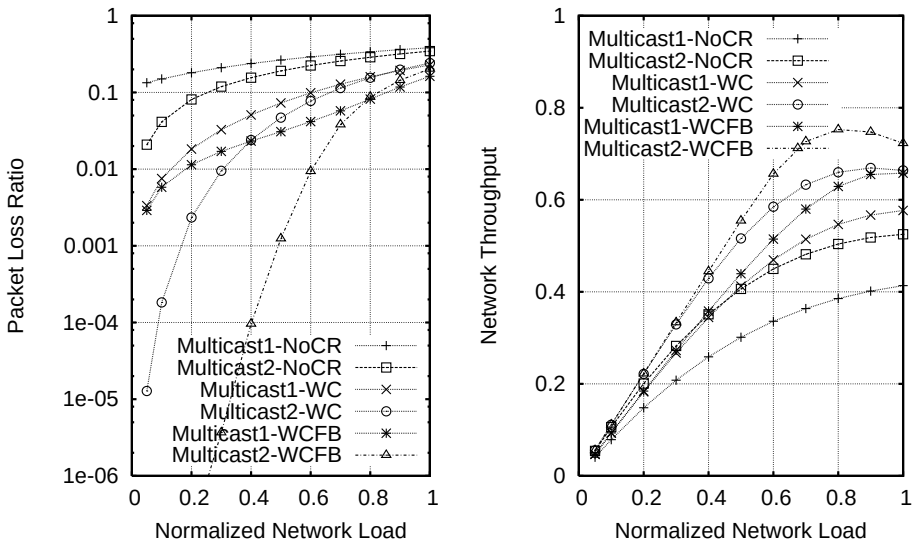

Figure 3.7: Simulation results of multicast node performance under Bernoulli traffic. (`Multicast 1`: FBM; `Multicast 2`: FFM.)

of each node with multicast traffic, while the second input fiber port receives only unicast traffic. Whenever a multicast label is detected, the packet is forwarded to both output fiber ports. The FBM and FFM are referred to as `Multicast1` and `Multicast2`, respectively. The simulation results of the FBM and FFM nodes are plotted in Fig. 3.7 and Fig. 3.8.

Comparing the traffic performance of the multicast architectures with Bernoulli traffic and self-similar traffic, we perceived again that when fiber buffering is introduced, both multicast nodes perform better with the Bernoulli traffic pattern than with the self-similar one. The reason is the same as that in the unicast case, which is determined by the traffic model characteristics.

From the Bernoulli traffic driven results in Fig. 3.7, we also observed that as the network load becomes higher, the network reliability of the `Multicast1-WCFB`, indicated by the *PLR* curves, started to outperform both `Multicast2-WC` and `Multicast2-WCFB`. This is because at a high network load, the feedback configuration also serves as a buffer for the congested situation. Therefore, `Multicast1` physically have more packet buffers than `Multicast2`, which tries to forward the packets straight to the output fiber ports. As Bernoulli traffic model distributes the

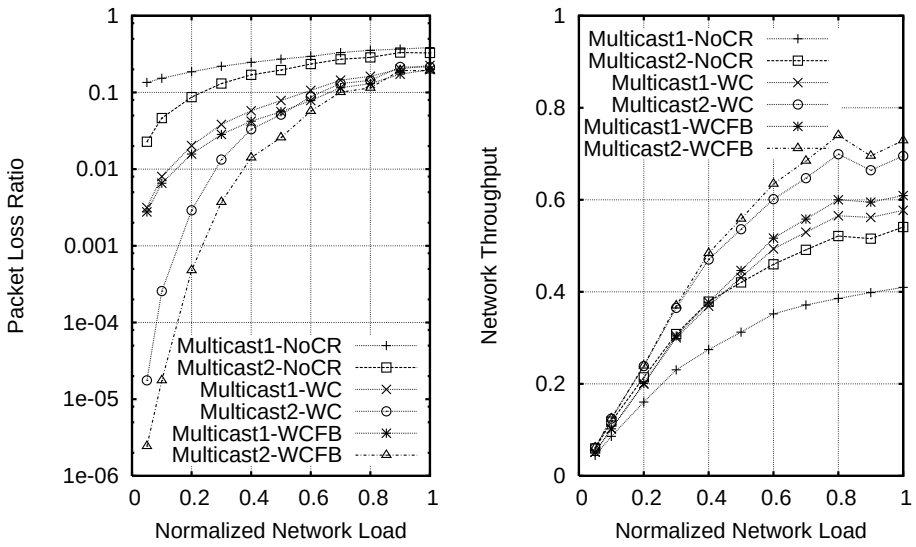

Figure 3.8: Simulation results of multicast node performance under self-similar traffic. (`Multicast 1`: FBM; `Multicast 2`: FFM.)

traffic load evenly across all the simulation time slots, the packets that are in the buffer and feedback circuit can seek the next available time slots to be forwarded to the output fiber ports instead of being dropped. As a result, `Multicast1-WCFB` also has a better NT performance. In the case of self-similar traffic, the feedback circuit do not improve much the `Multicast1` performance when functioning as a buffer due to the bursty nature of the traffic. The explanation is similar as in the unicast case in Sec. 2.5.3.

In Fig. 3.7, the network throughput of `Multicast2-WCFB` shows a *saturation* point at high network load where the FFM node performance reaches a maximum and then decreases. This can be explained by the NT definition Eq. 2.2. For an FFM node, the number of the packets to be delivered includes the number of duplicated multicast packets. The duplication of the multicast packets is executed at the AOLSWs. When the network load increases, the number of multicast packets also increases. At a certain point, there will be more *packets in the FFM node to be delivered* than the actual *forwarding capacity of the FFM node*, so that the FFM node NT becomes saturated and the number of packets delivered ($\#packets_{delivered}$) in Eq. 2.2 will not increase anymore, but maintains at a

level that is equal to the full forwarding capacity of the FFM node for that particular contention resolution scheme. However, the number of packets generated ($\#packets_{generated}$) plus the number of null packets generated ($\#null_{generated}$) in Eq. 2.2 continues to increase as the network load goes up. Therefore, the network throughput of the FFM node starts to decrease after the saturation point.

Note that this saturation situation will not happen for unicast and FBM nodes. For unicast nodes, the number of packets to be forwarded in the node cannot be *constantly* more than the forwarding capacity of the node. It can however occur, *temporally*, when there are already packets in the buffers waiting to be delivered from the previous time slot. In this aspect, an FBM node behave very similar to a unicast node, as the duplication of the multicast packets only take place *once* in every time slot, and there are dedicated feedback loops acting as a buffer to store the duplicated packets, with dedicated AOLSWs to process them. An FBM node does not duplicate more multicast packets than what it can handle, instead, it discards the multicast packets that it cannot handle. Therefore, as in the unicast case, the FBM node forwarding capacity does not reach a full saturation. This also indicates that the FBM node cannot make use of the resource to a full extend, and thus is less efficient than the FFM node.

From the self-similar traffic driving results in Fig. 3.8, it can be seen that the network throughput of the multicast nodes experiences some fluctuations at high network loads. This is due to the *bursty* nature of the self-similar traffic and the simulation *stop* conditions. Because self-similar traffic is bursty and unpredictable, the results for a given load may vary with each run of the same simulation. On the other hand, a simulation for a given load stops when the packet loss parameter converges to a number according to statistical analysis. At higher network loads, there are more packets in the node and the chance of each packet getting discarded is greater, the packet loss parameter converges more rapidly, so that the number of simulated time slots becomes less. Therefore, the higher the network load, the larger the variation can be due to the decreased simulation runtime slots. Consequently, the simulation results at higher network loads shows a more *incidental* behavior. The node architecture that can duplicate and handle more multicast packets also experiences larger degrees of fluctuations.

The self-similar traffic driven results presented in Fig. 3.8 prove that with bursty traffic, the FFM node performs considerably better under the same contention resolution conditions, even with just *one* multicast port. Moreover, the FFM node with only `WC` contention resolution already achieve significantly better

performance than the FBM node with WCFB. The limited performance of the FBM node can be expected. As discussed in Sec. 3.2.2, the FBM node can only process *one* multicast packet at each time slot to be forwarded at the next time slot; while the FFM node can process *as many* multicast packets *as required* at each AOLSW in the same time slot. With one multicast port, at each time slot there can be *more than one* and *up to four* multicast packets. In an FBM node, all the multicast packets except for *one* have to be dropped. That is why the packet loss ratio of the FBM node is much higher than that of the FFM node. For the same reason, there are much less packets, including multicast packets, that can be actually delivered by the FBM node, and the delivery of the duplicated multicast packets can only take place at the next time slots. Therefore, the network throughput of the FBM node is also much worse than that of the FFM node.

With both multicast architectures, introducing WC is always more efficient in solving the contention than introducing FB. As in the unicast case, buffering demonstrates to have only minor improvement in the node performance for the self-similar traffic.

b. Two multicast ports

In this set of simulations, both input fiber ports can receive multicast traffic with 1/3 probability. However, instead of comparing the two multicast architectures with the same number of active components as in Fig. 3.1 and Fig. 3.3, we compare two multicast architectures with the same *intended throughput* as in Fig. 3.1 and Fig. 3.6. This means for both multicast configurations, at every time slot only maximum *ten* synchronized packets are generated and sent to each node: *four* each to both input fiber ports, and *two* to the add fiber port. Only self-similar traffic is deployed as it is more realistic for network analysis [72–74].

The results are shown in Fig. 3.9. We observe that when both input fiber ports receive multicast packets, the performance of the FBM node becomes much worse, while the FFM node can still retain similar *PLR* and a slightly degraded *NT*.

As in the case with one multicast port, the high *PLR* obtained for the FBM node is due to the fact that it can process only *one* multicast packet per time slot. Now that there are two multicast ports, the maximum possible number of multicast packets generated at each time slot becomes *eight* instead of *four*. Still *all but one* of these multicast packets have to be discarded. In order to lower the *PLR*, more feedback loops are required [22], which leads to further increase

in the number of active components and physical resources in Table 3.1 such as AOFFs, AWG dimensions and AOLSWs, as well as node internal wavelengths. In order to keep the node size, complexity and cost reasonable, so far only limited multicast functionality could be realized for a basic 2×2 OLS node [22]. Such limitations can be on the number of multicast forwarding possibilities for each multicast packet [13, 16], as well as on the number of simultaneously processed multicast packets at a time for each AOLS or OLS node [13, 16, 22]. Most of the time it is both, as leaving all the multicast processing to extra dedicated feedback loops and multicast processors is very physical resource demanding, in terms of both component complexity and quantity. On the other hand, the FFM node can process as many multicast packets as needed in each time slot, as the multicast function is integrated inside each AOLSW.

For the FFM node, the *PLR* degradation due to the additional multicast port is only visible at high network loads. This is because as the network load increases, both the number of generated packets ($\#packets_{generated}$) and the number of dropped packets ($\#packets_{dropped}$) in Eq. 2.1 increase. Until the amount of traffic inside the FFM node reaches the node forwarding capacity, the rate of $\#packets_{dropped}$ accretion shall be proportionate to the rate of $\#packets_{generated}$ accretion. When the FFM node cannot deliver all the packets that it receives and duplicates, the rate of $\#packets_{dropped}$ accretion starts to excel the rate of $\#packets_{generated}$ accretion, which is why the *PLR* with two multicast ports is worse than that with one multicast port just at high network loads. Under similar reasons, the *NT* degradation is also more prominent at high network loads. This degradation is caused by the almost doubled amount of multicast packets. When the network load becomes higher, because of the increased number of multicast packets, the FFM node reaches a saturation of its forwarding capacity slightly earlier. After the network load exceeds the saturation load, it is not possible for the FFM node to successfully deliver all the duplicated packets. Also from Eqs. (2.2) and (3.1), we can expect a lower *NT* when more input ports are configured as multicast ports.

Fig. 3.9 also indicated that under such conditions, `Multicast2` without any contention resolution strategy can already attain similar results to `Multicast1` with `WC` and `WCFB` in both *PLR* and *NT* simulations. When `WC` is introduced to `Multicast2`, significant improvement is achieved. Further introducing one-slot optical buffering to `Multicast2` shows additional performance enhancement, which is much more noticeable than that with `Multicast1`.

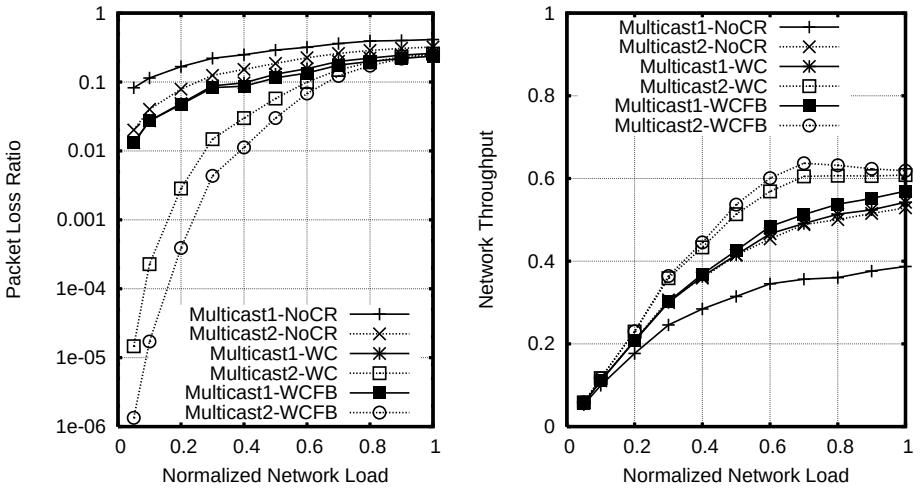

Figure 3.9: Simulation results of multicast node with self-similar traffic with the same intended throughput.

3.5 Summary and discussions

In this chapter, we discuss the FBM AOLS node architecture and operation principle. We further introduce a novel multicast scheme, FFM, for passive waveguide grating router based optical label switching node. An analytical study shows that the FFM scheme requires considerably fewer physical components than the conventional FBM approach.

Moreover, traffic performance of the two AOLS multicast architectures is evaluated. Bernoulli and self-similar traffic driven simulation results are presented under three contention resolution conditions: `NoCR`, `WC` and `WCFB`. We evaluate two parameters: *PLR* and *NT*, which represent network reliability and utilization, respectively [64].

The investigated AOLS architecture performs best when configured as a unicast node. When it is configured into the FBM or FFM multicast node, a multicast packet is to be sent to both output ports but not the drop port, i.e., with a multicast factor of 2. With 1/3 multicast traffic per multicast port, the FFM structure is significantly more efficient regarding the *PLR* and *NT* performance than the FBM structure, under both Bernoulli and self-similar traffic. Compared to a unicast node of the same dimension, the FFM node can achieve similar *PLR* per-

formance, and comparable NT performance when there is only one multicast port among the three input ports. The performance difference between the feedback and feed-forward schemes becomes more prominent as the multicast probability per port increases, and as number of the multicast ports per node increases, due to the limited multicast capacity of the FBM node.

In current `AOLSim`, the multicast probability per port is determined by the fraction of defined *number of multicast labels* over the *total number of labels*. This probability applies to all wavelength channels at an input port. In practice, an alternative can be to use certain wavelength channel(s) of an input port for pure multicast traffic to support video and data storage applications, whereas the other wavelengths channels of the same port for unicast traffic. In this alternative case, the multicast quotient per port is determined by the ratio of the *number of multicast channels* to the *total number of wavelength channels*. Note that using dedicated wavelengths for multicast can be considered as a case of *circuit* switching. There is less flexibility and granularity in this option than using optical packet labels to define multicast, which is purely *packet* switching. If a multicast wavelength channel is under-unutilized, some optical bandwidth is wasted. Or, if all the multicast wavelength channels are fully occupied, additional multicast traffic cannot be delivered. On the other hand, multicast based on optical packet labels does not have such limitations. At a random moment, the multicast traffic can be 60% of the total incoming traffic, all carrying multicast labels; while at the next moment, the multicast traffic can be only 10% of the total traffic.

Chapter 4

All-optical multicast technologies

Future all-optical networks will incorporate more and more networking functionalities that used to be performed in the electrical domain but now can be directly realized in the optical domain. An example of such networking functionalities is multicast. Transparent optical-layer multicast by multi-wavelength conversion (MWC) has revealed a brand-new way to implement data multicast in the optical domain without passing through any electronics, at reduced cost and with lower power consumption. In this chapter, all-optical multicast technologies are reviewed. In particular, MWC state of the art is summarized. Both multiple-to-multiple and single-to-multiple conversions are addressed. For each MWC technique, advantages and disadvantages are discussed. In the end, a summation of reported single-to-multiple MWC techniques is given. Except for Sec. 4.3 in this chapter, throughout the rest of the thesis, when MWC is mentioned, it refers to single-to-multiple conversion. Parts of this chapter are based on a publication.[1]

[1] See reference [75].

4.1 Introduction

Data multicast at the optical layer enables a broad range of telecommunication network applications, simplifies electronic data packet formats and network layer protocols, and provides new visions of optical network designs. Performing data multicast directly in the optical domain eliminates the needs for optic-electronic-optic (OEO) conversion from the optical layer up to the network layer and backwards, thus improving the optical network switching and forwarding efficiency, transparency, and scalability [76].

The future telecommunications optical network hierarchy can be roughly divided into three levels - optical backbone networks, optical metropolitan networks and optical access networks [77]. Optical multicast supports point-to-multipoint connections directly in the physical layer for transmission of information in the form of light signals from a source node to multiple destination nodes simultaneously. Light paths enhance optical network connectivity by using virtual connections among network nodes. All-optical networking by means of transparent light paths avoids the need of implementing costly high-speed electronics at intermediate nodes to perform OEO conversions and electronic signal processing, allowing fast optical networking to be more cost-effective. Applications for optical multicast include teleconferencing, video distribution, multi-party gaming and global enterprise virtual private networks (VPNs), etc.

To realize optical layer multicast, two lines of research for different network scenarios have been progressing in parallel: optical multicast by *passive light splitting*, and by *multi-wavelength conversion* (MWC). In optical packet switching (OPS), packet multicast in a broader sense involves not only creating multiple copies of the packets, but also assigning multicast labels to these packets. However, in Chapters 4∼7, the term *multicast* only refer to the physical layer operation of generating multiple copies from an input signal.

4.1.1 Passive light splitting

The first approach, *passive light splitting*, uses optical splitters to split the light signal into multiple optical fibers, as illustrated in Fig. 4.1 (a). This is a *colorless* and *color-blind* approach, which is neither *sensitive to* or *aware of* the wavelength carrier. This approach is mostly employed for shorter-range optical access networks, such as passive optical networks (PONs). When incoming data are in form of wavelength division multiplexed (WDM) signals, optical data on all the wave-

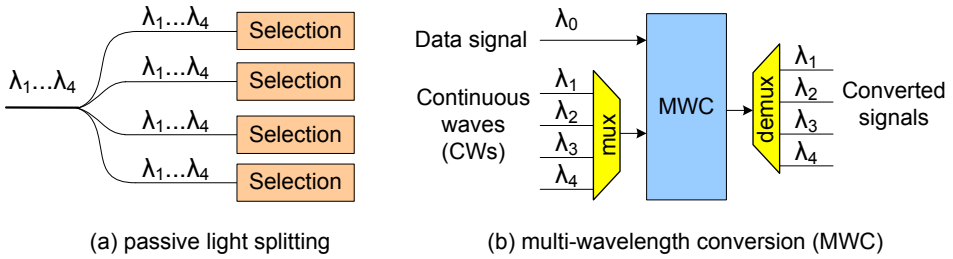

Figure 4.1: Two common all-optical multicast approaches.

length channels are coupled onto all the outputs, as shown in Fig. 4.1 (a). In many cases, although the process itself is passive, considerable amplification is required afterwards due to inherent splitting losses [76–78]. Therefore, for optical metro and core networks, this approach is disadvantageous.

With passive split, selection mechanisms at the receiving terminals are needed to realize broadcast, multicast or unicast. These mechanisms may for example deploy information in the packet header, which is used in time-division multiple access (TDMA) PONs [79].

Passive light splitting can also be applied in broadcast-and-select architectures to provide multicast function [5]. A broadcast-and-select architecture consists of two stages: the *broadcast* stage and the *select* stage. The *broadcast* stage makes use of passive optical couplers, such as star-couplers and power splitters, to divide the incoming light signals to all the switches on the *select* stage. The *select* switches select one or many optical packets or signals by means of crossbar-like switching fabric and optical filters [5]

4.1.2 Multi-wavelength conversion

The second multicast approach, by means of MWC, is preferable for larger networks across long distances, i.e. metro and core networks. MWC is a *color*-aware technology that is compatible with *wavelength*-sensitive applications, such as wavelength-routed communication systems, which have been extensively explored for future dynamic WDM optical networks. As for the optical control plane, as explained in Chapter 1, generalized multi-protocol label switching (GMPLS) allows a wavelength channel to tunnel a set of multi-protocol label switching (MPLS) label-switched paths (LSPs) and enlightens the possibility of traffic grooming for the

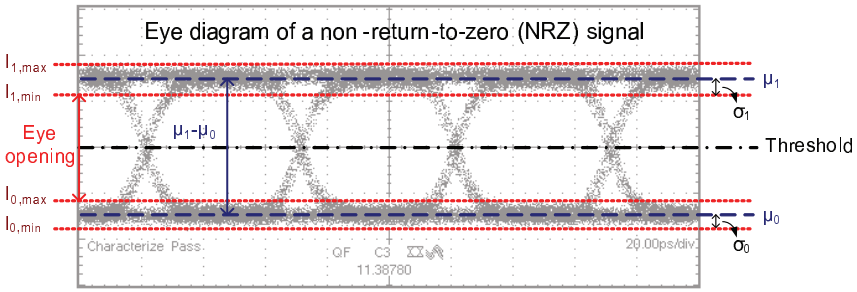

Figure 4.2: Eye diagram of a non-return-to-zero (NRZ) signal.

data streams with common destinations [76]. Moreover, passive optical wavelength routers such as *arrayed waveguide gratings* (*AWGs*), have become one of the most basic building blocks for optical switches, since they can behave simultaneously as *passive routers*, *multiplexers*, *demultiplexers* and *optical filters*. Transparent optical wavelength multicast can be easily realized by all-optical one-to-many MWC followed by an AWG, as illustrated in Fig. 4.1 (b).

In this chapter, we focus on all-optical MWC technologies. Firstly, in Sec. 4.2, a few standard parameters and typical performance measures for optical data signals are introduced. Secondly, in Sec. 4.3, state-of-the-art technologies and methods for MWC are reviewed, summarized and discussed. Finally, in Sec. 4.4, main characteristics of various single-to-multiple conversion technologies are compared.

4.2 Performance measuring of optical data signals

4.2.1 Eye diagram

A key indicator of optical signal quality and noise is the *eye diagram* [80]. Eye diagram is a superposition of bit periods on an oscilloscope, a quick and qualitative measure of the quality and integrity of the received signal [81]. It is measured in the electronic regime and provides a virtual way of monitoring the receiver performance [82]. Fig. 4.2 shows the eye diagram of a non-return-to-zero (NRZ) signal and parameters of an eye diagram.

As indicated in Fig. 4.2, the eye opening is defined as the difference of the minimum current threshold for logic 1 $I_{1,min}$, and the maximum current threshold for a logic 0 $I_{0,max}$ [81]:

$$E_{eye} = I_{1,min} - I_{0,max}. \tag{4.1}$$

In practice, the decision threshold I_D shown in Fig. 4.2 is optimized to minimize detection errors [82]. When the standard deviations for 1 and 0 symbols are equal ($\sigma_1 = \sigma_0$), the decision threshold is $I_D = (I_1 + I_0)/2$, where I_1 and I_0 are the average values of the sampled values for 1 and 0 symbols, respectively [82].

4.2.2 Quality factor (Q factor)

The quality factor (Q factor), is closely related to the quality of the optical signal in terms of signal-to-noise ratio (SNR) in the time domain [80–82]. It is defined as the difference of average for 1 and 0 symbols ($\mu_1 - \mu_0$) divided by the sum of the standard deviations for 1 and 0 symbols ($\sigma_1 + \sigma_0$):

$$Q = \frac{\mu_1 - \mu_0}{\sigma_1 + \sigma_0}, \tag{4.2}$$

where μ_1 and μ_0 are the average values of 1 and 0, respectively, while σ_1 and σ_0 are the standard deviations for 1 and 0 respectively.

4.2.3 Extinction ratio (ER)

Most transmitters emit some power even in the OFF state [82]. Semiconductor lasers emit low-power light when the bias current is below their lasing threshold. This power during the 0 bits is due to the *spontaneous emission* [80, 82]. In this case, the optical power level at the OFF state P_0 is very small compared to that of the ON state P_1. However, P_0 can be a significant fraction of P_1 is the laser if the laser is biased close to but above the threshold [82].

In telecommunications, extinction ratio (ER) is defined as the ratio of two optical power levels at logical 1 and 0 [82, 83]. In other words, the ER is basically the ratio of the desired modulated light and the unmodulated light [80]. If P_1 is the optical power level of the ON state, e.g., when the light source is "*on*", and P_0 is the optical power level of the OFF state, e.g., when the light source is "*off*", the ER r_{ex} is defined as a fraction [82, 83]:

$$r_{ex} = \frac{P_0}{P_1}. \tag{4.3}$$

The ER defined in Eq. 4.3 varies between 0 and 1. However, Eq. 4.3 is not a universal definition for the ER. In many cases in the literature, the *reciprocal* of

Eq. 4.3 is used [80, 83], in which case the ER is defined as [80, 81, 83]:

$$r_{ex} = \frac{P_1}{P_0} \tag{4.4}$$

if expressed as a ratio, or

$$r_{ex} = 10\log(\frac{P_1}{P_0})(\text{dB}) \tag{4.5}$$

if expressed in dB. In this case, the ER ranges between 1 and ∞ [83]. The ERs for directly modulated lasers are from 9 to 14 dB, whereas externally modulated lasers can exceed 15 dB [80]. In an oscilloscope, the ER can be measured from an eye diagram. The ER measured with an oscilloscope is calculated by measuring the average 1 and 0 optical power levels in the center 20% of the eye, setting the oscilloscope upper bandwidth to three-quarters of the bit rate [84].

4.2.4 Signal-to-noise ratio (SNR or S/N)

Signal-to-noise ratio, often abbreviated as SNR or S/N, is an *electrical engineering* concept. SNR is defined as the ratio of the signal power P_s to the unwanted noise power P_n [80]:

$$\text{SNR} = \frac{P_s}{P_n}. \tag{4.6}$$

In SNR, both signal and noise power must be measured at the same or equivalent points in a system, and with in the same system bandwidth. In many cases, SNRs are expressed in dB scale:

$$\text{SNR} = 10\log(\frac{P_s}{P_n})(\text{dB}). \tag{4.7}$$

4.2.5 Optical signal-to-noise ratio (OSNR)

When the SNR is applied to optical signals and noise, it is referred to as optical signal-to-noise ratio (OSNR). OSNR is the measure of the ratio of signal power to noise power in an optical channel [84]. In other words, ONSR indicates of the "clarity" of the transmitted optical signal, although when the optical signal arrives at the photo detector (PD), the receiver itself also adds several sources of noises, including thermal noise [81].

In optical systems, the *signal* is usually modulated light superimposed on a background comprised of mostly unmod8ulated optical power distributed over a broad wavelength range including the signal wavelength [84]. The noise arises

typically from optical amplification which is a source of amplified spontaneous emission (ASE). In most cases, the noise is better thought of as a power density rather than a total power [84].

OSNR can be measured with an optical spectrum analyzer (OSA) and is defined as [84]:

$$\text{OSNR} = 10\log(\frac{P_{os}}{P_{on}})(\text{dB}), \tag{4.8}$$

where P_{os} represents the (linear) optical signal power, and P_{on} is the (linear) optical noise power [84].

In an optical system with cascaded amplifiers, noise is added to the signal with each amplification and is also amplified along with the signal by the next amplifier. Therefore, the OSNR tends to degrade as the signal passes through the system.

4.3 Multi-wavelength conversion: state-of-the-art

All-optical wavelength conversion (AOWC) as an essential functionality for optical nodes enables wavelength reuse in different light paths, eases wavelength contention issues, and provides new ways for optical $1 + 1$ protection as well as transparent optical data forwarding without OEO conversions. $1 + 1$ protection is one of the most commonly deployed protection architectures for failure recovery [5]. In $1 + 1$ architecture, data are transmitted in both primary and secondary paths to ensure fast restoration when failure actually occurs. AOWC can realize $1 + 1$ protection by having the same data transmitted on a second wavelength-routed path.

Up to now, studies have mainly concentrated on converting one single wavelength channel into another [61, 85, 86]. However, along with the rapid development of AOWC technologies, there has also been research on MWC from one set of wavelength channels into another set ever since as early as the 90's [85, 87–93]. Despite that, one-to-many MWC only started to attract attention at the beginning of the 21st century, when simultaneous conversion of a single wavelength channel into multiple wavelength channels created a new path for transparent optical network multicast. Within less than a decade, it has advanced rapidly as it can potentially cut down the number of converters in a routing node, and allow data multicast directly in the optical domain without passing through any electronics. It has become an especially appealing technology for optical switches based on passive waveguides, because with no added complexity in the switch design, optical layer

multicast functionality can be easily introduced and implemented inside the nodes.

In this section, various all-optical MWC approaches are reviewed. Both *multiple-to-multiple* conversion and *single-to-multiple* conversion are addressed.

4.3.1 Multiple-to-multiple conversion

a. Overview of reported approaches

Most of the reported demonstrations of simultaneous wavelength conversion of multiple inputs to multiple outputs utilized second- or third-order optical nonlinearity such as difference frequency generation (DFG) or four-wave mixing (FWM) [85, 87–93]. They belong to the *wave-mixing* wavelength conversion category. Within this category, *nonlinear optical wave-mixing* results from nonlinear interactions among the optical waves present in a nonlinear optical material, and can provide large frequency translation required for WDM [85].

The utilized mixing functions in DFG and FWM are *parametric* [85]. *Parametric processes* are in a class of nonlinear phenomena where the nonlinear optical materials such as optical fibers play a passive role except for mediating interaction among several optical waves. They are referred to as parametric processes because they involve modulation of a medium parameter such as the fiber refractive index [94].

MWC from multiple to multiple channels is one unique feature common to this category. Phase matching is normally required for efficient wavelength conversion to take place. Generally speaking, *phase matching* requires matching of the frequencies as well as of the wave vectors. The latter requirement is often referred to as phase matching [94]. However, in contrast to the *cross modulation* or *gating* wavelength conversion category such as cross-gain modulation (XGM) and cross-phase modulation (XPM), the operation of such wavelength converters preserves both amplitude and phase information, and thus is strictly transparent to the modulation formats of the signal. Furthermore, they support data bit rates up to terabit per second (Tb/s) [85]. If semiconductor optical amplifiers (SOAs) are used, speed limitations are normally imposed by SOA carrier dynamics to around several tens of gigabit per second (Gb/s) depending on the SOA characteristics [95]. This kind of wavelength converters has *spectral inversion effects* on the converted signals, as shown in Fig. 4.3, where both the order of the channels and the shape of the signals are *inverted* in the *spectral* domain. Despite that, the original data information, transmission bit rate and modulation format are

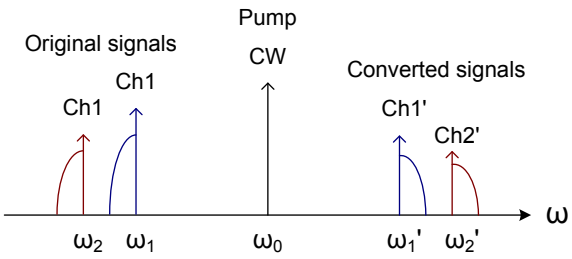

Figure 4.3: Spectral inversion effects of parametric wavelength conversion.

transferred onto the converted signals. For WDM system applications, the spectral inversion effects may be not desirable as it makes the management of WDM channel wavelengths more difficult.

b. DFG in $LiNbO_3$ or AlGaAs waveguides

DFG is a *second-order* nonlinear process that has been demonstrated using periodically poled $LiNbO_3$ (PPLN) waveguides and AlGaAs waveguides [87–89]. DFG is a consequence of nonlinear interaction of the material with a pump wave and a signal wave [85], in which a new optical frequency is generated at the *difference frequency* between the pump wave and the signal wave [93].

The DFG is based on the second-order nonlinear susceptibility [93]. In general, susceptibility of a material describes how this material responds to a field that is applied to it [96, 97]. Compared to FWM, which is a third-order parametric process, DFG has a number of attractive attributes: i) DFG is free from satellite signals that appear in FWM. Thus it has low cross talk and no intrinsic chirp. A *chirp* is a signal in which the frequency increases or decreases with time, referred to as up-chirp and down-chirp, respectively. ii) DFG offers strict transparency, polarization diversity and polarization independent conversion efficiencies. iii) DFG has extremely wide conversion bandwidths covering the gain bandwidth of standard C-band erbium-doped fiber amplifiers (EDFAs) and can be easily shifted into the S- or L-band or further. In optical communications, C-band is the *conventional* wavelength region from approximately 1530 to 1570 nm, S-band is the *short*-wavelength region extending from approximately 1470 to 1520 nm, and L-band is the *long*-wavelength region from approximately 1570 to 1610 nm [82]. Fig. 4.4 presents the conversion efficiency as a function of the input wavelength published

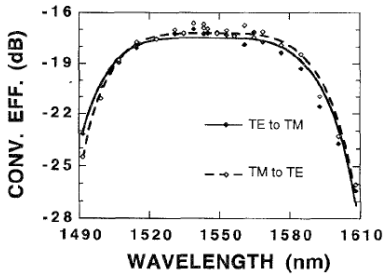

Figure 4.4: DFG conversion efficiency curves for transverse electric (TE) and transverse magnetic (TM) input polarizations as function of input wavelength in AlGaAs waveguide. (After Ref. [85]; ©1996 IEEE.)

in [85]. Conversion efficiency is defined as a ratio of the output converted signal power with respect to the input signal power [85]. It shows conversion bandwidths exceeding 90 nm and polarization diversified operation. iv) DFG is also capable of chirp-reversal and MWC. Nevertheless, phase matching and low insertion loss for DFG wavelength converters have to be achieved by careful fabrication, which are the main drawbacks of this method. These factors generally impose limitations on the conversion efficiency of such converters [85, 87].

c. FWM in SOA or fibers

Compared to DFG, FWM in SOAs and non-linear optical fibers for multiple-to-multiple wavelength conversion has been explored by more researchers because of the widely available devices and easier phase-matching conditions [90–93]. FWM is based on the third-order nonlinear susceptibility [93]. Signal and pump wavelengths, power levels and polarizations have to be properly balanced to eliminate or minimize in-band crosstalks due to high-order FWM products. Apart from these general characteristics, FWM phenomena in SOAs and nonlinear fibers have a number of distinct differences due to the different attributes of the physical media used.

FWM in semiconductor gain media

FWM in SOAs has been extensively studied because for most applications, SOAs have several good intrinsic characteristics such as operation with relatively low input power, small size and integration potential. However, the conversion range in an SOA is limited to a few nanometers, and the conversion efficiency decreases

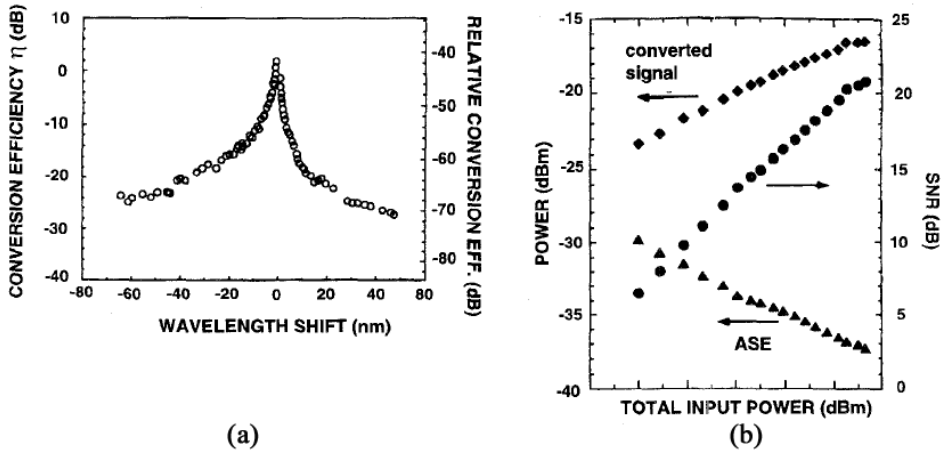

Figure 4.5: Wavelength conversion characteristics by FWM in SOA (After Ref. [85, 98]; ©1996 IEEE.): (a) conversion efficiency as function of signal detuning from the pump wavelength; (b) conversion efficiency, gain and signal-to-noise ratio (SNR) as function of input optical power.

steeply with detuning of the signal wavelength relative to the pump wavelength, as shown in Fig. 4.5. At large detuning, the conversion efficiency is significantly lower than the peak value. Therefore, only a limited number of channels can be applied at the same time. This non-flat and asymmetric conversion efficiency is the main problem for multi-channel FWM wavelength conversion in semiconductor gain media [93].

Moreover, carrier dynamics of SOAs generally limit the operation data rate to a few tens of gigabit per second (Gb/s) [95]. Although high-order nonlinear processes in an SOA can support bit rate far beyond that, they are limited by the low conversion efficiency that causes bad OSNRs in converted signals.

Furthermore, Multiple-to-multiple wavelength conversion by FWM in SOAs can also suffer from XGM-induced crosstalk because of the fast gain compression feature of SOAs. To reduce this crosstalk due to the SOA gain compression, the power of the WDM signals has to be carefully controlled [90]. On the other hand, to compensate the degradation in signal OSNRs due to the low conversion efficiency of the FWM process, it is desirable to have higher input signal power. Thus a proper balance of the FWM and XGM effects in SOAs can be particularly

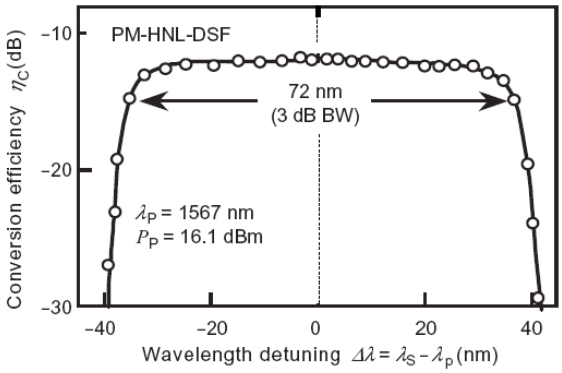

Figure 4.6: Conversion efficiency as function of signal detuning from the pump wavelength. (After Ref. [93]; ©1999 Fujitsu.)

crucial in order to produce high quality signal copies [85, 90, 93].

Generally speaking, SOAs with higher nonlinearities and higher saturation power give better performance in terms of number of simultaneously converted channels using FWM for multiple-to-multiple conversion [78].

FWM in nonlinear fibers

A more efficient solution for simultaneously converting a large number of channels is to use nonlinear optical fibers such as dispersion-shifted fibers (DSFs) or highly-nonlinear (HNL)-DSFs. Compared to semiconductor-based FWM, FWM in DSF or HNL-DSF has symmetric and relatively flat band conversion efficiency around the pump wavelength if placed at the zero-dispersion wavelength of the fiber, as shown in Fig. 4.6. These characteristics of FWM in nonlinear fibers enable a more practical WDM multi-channel wavelength conversion. For FWM in nonlinear fibers, usually several kilometers of DSF fiber is used. Studies have shown that a DSF of over 10 km is normally required to generate sufficient conversion due to the small third-order optical nonlinearity of silica fibers [92]. A HNL-DSF can have five to eight times' higher nonlinearity coefficient than conventional DSF, so that it can provide the same conversion efficiency at a much shorter length such as several hundreds of meters. Nevertheless, comparing a fiber length of hundreds of meters to a semiconductor length of few hundred microns, *phase matching* among the input wavelength channels is an important issue for efficient FWM in optical fibers [92]. To achieve significant phase matching in fiber, not only the polarizations of

the input waves needs to be matched, the pump wavelength also needs to be adjusted to the average zero-dispersion wavelength of the fiber [94]. HNL-DSF to DSF is normally preferred because of the difficulty in controlling precisely the zero-dispersion wavelength fluctuation along the fiber. The main disadvantages of FWM in fibers are that there is a restriction on the pump wavelength that this wavelength must be placed around the (average) zero-dispersion wavelength of the fiber, and the bulkiness of the kilometers-long optical fibers. The latter issue can be eased by further increasing the nonlinearity of the fiber to shorten the fiber-length [92, 93].

With HNL-DSFs, a 320 Gb/s (32 × 10 Gb/s) conversion in a 1-km polarization-maintaining HNL-DSF with a nonlinearity constant of 11 $W^{-1}km^{-1}$ has been achieved. The 3 dB conversion bandwidth for this fiber was 72 nm. All channels were converted with a power penalty of less than 2.6 dB [93]. Moreover, successful simultaneous wavelength conversion and optical phase conjugation of 200 Gb/s (5 × 40 Gb/s) WDM signals have been demonstrated using a 750-m HNL-DSF with a nonlinear coefficient of 20.4 $W^{-1}km^{-1}$ [92].

Comparison of conversion media for WDM conversion

Both FWM in SOAs and in optical fibers have their own pros and cons. In general, the non-flat and asymmetric conversion efficiency with SOA-based FWM can be improved by increasing the third-order susceptibility for a large detuning. This can be achieved by, for example, using different semiconductor gain media such as quantum dot [93]. As for fiber-based FWM, further increase of the third-order susceptibility in HNL-DSF can potentially decrease the fiber length to several tens of meters and obtain a better tolerance of the pump wavelength with respect to the zero-dispersion wavelength of the fiber [93]. However, increasing the third-order susceptibility also increases the optical loss considerably, as in photonic crystal fibers. Therefore, a proper balance between the desired fiber length and the tolerable attenuation is an important consideration.

4.3.2 Single-to-multiple conversion

a. Overview of reported approaches

Simultaneous single-to-multiple conversions have been demonstrated with various methods. The reported approaches are mostly based on FWM [70, 78, 99–101], XPM [59, 60, 67–69, 71, 102–107], XGM [75, 104, 108–112], cross-absorption modulation (XAM) [113–116], nonlinear polarization switching (NPS) [117], supercon-

tinuum (SC) generation [99, 118, 119], and mode-locking in Fabry-Pérot (FP) – laser diodes (LDs) [77]. Each of them is reviewed in the following subsections.

b. FWM in SOA or fibers

One-to-many MWC by FWM can be realized if multiple pumps are injected together with the signal channel into an SOA [78, 104] or fibers [70, 75, 99–101, 104]. Wave mixing can result in one-to-many MWC through different nonlinear effects.

Multiple FWM in SOA

In [78], one-to-five MWC by FWM in an SOA was demonstrated at 10 Gb/s with one input NRZ signal and three pumps. The five copies together with the original signal channel were compliant with the International Telecommunication Union (ITU) 200 GHz channel grid. After the MWC, all the six channels were successfully transmitted over a metro-like system. In this scheme, illustrated in Fig. 4.7 (a), one pump P1 was aligned in the same polarization of the signal (TM polarization) with a spacing of 100 GHz from the signal channel. The other two pumps P2 and P3 were both placed in the orthogonal polarization of the signal (TE polarization) with a spacing of 400 GHz from the first pump, one at each side. Output converted wavelengths can be tuned by moving P2 and P3 as long as they lie within the gain curve of the SOA. The five copies, shown in Fig. 4.7 (b), were generated due to different nonlinear effects so that two of them were linear copies of the signal and the other three were spectrally inverted. The average conversion efficiency of the five copies is around -25.5 dB. The number of the obtainable copies is mostly limited by the low OSNR and the moderate FWM conversion efficiency. The success of such MWC strongly relies on careful planning and alignment of the input channel wavelengths, as well as fulfilling the phase matching conditions.

It is worth mentioning that, when the wavelength conversion medium is an SOA, multiple pumps can also be deployed for flattening the conversion efficiency response of the SOA for single wavelength conversion. By placing the pumps nanometers to tens of nanometers apart from each other, under proper conditions, a wider and flatter conversion efficiency of an SOA can be obtained [120].

Optical parametric amplification in fibers

In [99, 100], twelve first-order converted signals, including six signal and six idler channels at ITU 100 GHz grid, were obtained from FWM in a highly nonlinear fiber (HNLF) and a HNL-DSF, shown in Fig. 4.8 (a), with one input NRZ channel

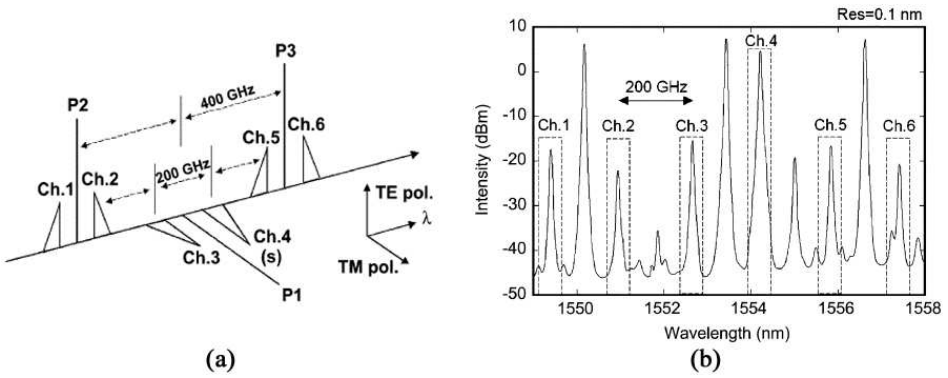

Figure 4.7: Multiple FWM in SOA [78]: (a) position of the input signal channel and three pumps; (b) output optical spectrum after SOA. (Ch.: channel; P: pump; pol.: polarization.)

at 10 Gb/s bit rate, and two pumps of 100 GHz spacing located in the region of anomalous dispersion of the nonlinear fibers. The MWCs were based on optical parametric amplification (OPA) in fibers. The nonlinear fibers were functioning as fiber optical parametric amplifiers. The pump wavelengths were combined to form the beat signal, phase modulated and amplified by an EDFA. When the signal wavelength was anchored to the ITU grid and the two pump wavelengths were wavelength stabilized with 100 GHz separation, the converted waves were positioned at ITU grid frequencies [99, 100]. The advantage of OPA-based MWC is that it can generate simultaneous copies on several channels with considerable net gain, usually of more than 10 dB [99, 100]. However, it requires two high power pumps at specific wavelengths to provide gain to the converted channels on particular wavelengths, and the conversion efficiency varies largely among the MWC channels, as presented in Fig. 4.8 (b).

First-order FWM in SOA or fibers

Figure 4.9 (a) shows the conventional FWM schematic with two inputs of one *pump* and one *signal*. The *pump* wavelength usually has much higher power than the *signal* wavelength, so that the stronger first-order *converted* product, whose optical power is proportional to the square of the *pump* power, is selected. The weaker product that is generally referred to as the *satellite* is usually neglected because of its low power. The optical power of this weaker product, on the other

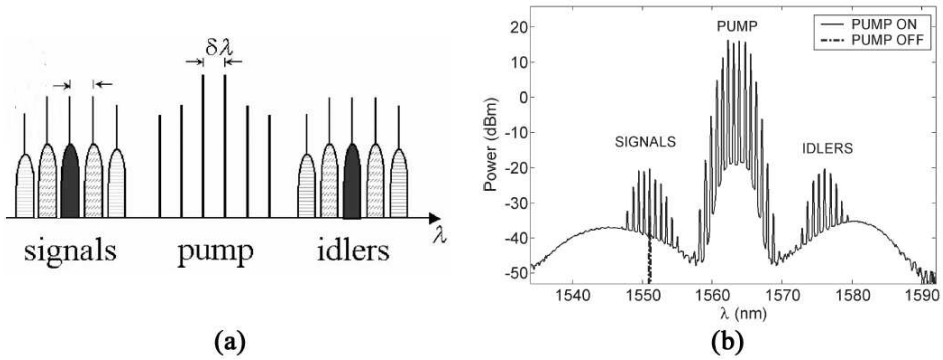

Figure 4.8: Optical parametric amplification in fiber optical parametric amplifier [100]: (a) position of the input signal channel and two pumps; (b) output optical spectrum after the optical parametric amplifier.

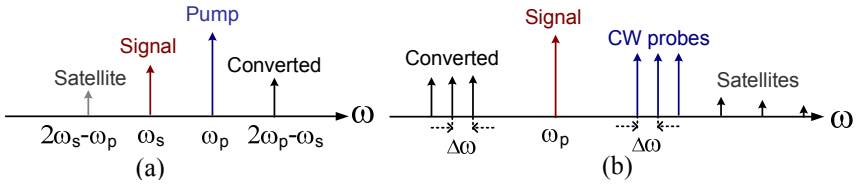

Figure 4.9: FWM wavelength conversion: (a) conventional FWM schematic; (b) first-order FWM MWC ($\Delta\omega$: frequency spacing between MWC channels).

hand, varies with the square of the input *signal* power [95].

According to this principle, one-to-many MWC by FWM can also be achieved by placing the modulated signal on the pump wavelength instead of the probe wavelengths, as illustrated in Fig. 4.9 (b). Copies can be generated by satisfying the phase matching between the modulated pump and the lower power continuous wave (CW) probe wavelengths. With nonlinear fibers, due to its flat conversion efficiency response around the zero-dispersion wavelength, a much higher number of channels can be simultaneously converted. Several experiments based on SOAs or fibers have been carried out to evaluate the performance of such FWM schemes [70, 75, 101, 104], in which one-to-one first-order MWC channels are generated spectrally inverted to each injected CW probe. The results are discussed partly in Chapter 5 and extensively in Chapter 7.

c. XPM in SOA-based interferometers or fibers

MWC by XPM in SOA-based interferometers has been much exploited [59, 60, 67–69, 71, 102, 103]. Mostly, a semiconductor optical amplifier – Mach-Zehnder interferometer (SOA-MZI) is employed [59, 60, 67–69, 71, 103]. In [102], an SOA delay interferometer was employed to achieve MWC based on similar effects. The operation principle under *standard* configuration is as follows. A data signal is injected only into one of the two arms to induce a phase change, and is transferred into multiple CW probe wavelengths simultaneously due to the small phase-shift dependence on wavelengths. With an SOA-MZI, both inverted and non-inverted copies of the original data can be obtained at the two output arms. A compact scheme with integration potential is an obvious advantage of such MWC technologies.

At 10 Gb/s, up to eight channels MWC of both NRZ and return-to-zero (RZ) has been demonstrated with an external assist light [71]. The proposed multi-wavelength converter was claimed to be able to accommodate more than eight CW channels [71]. In [67, 68], regenerative one-to-four MWC by XPM in an SOA-MZI at 10 Gb/s was reported without any assist light. In general, under standard configuration, this MWC method can achieve negative to low power penalties and negligible difference in channel performance, with relatively low input optical power requirement of 0-dBm range for data and CW inputs [67, 68, 71, 103].

At 40 Gb/s, due to the slow SOA gain recovery time of the current commercially available SOA-MZIs, usually a differential scheme is applied [59, 60, 69]. Up to four-channel MWC was demonstrated with moderate power penalties at ITU standard 200 GHz channel spacing [60, 69]. The input power requirement for 40 Gb/s operation is still much lower compared to most other MWC technologies. Less than 10 dBm total input optical power per port has been used in the reported experimental validations [59, 60, 69].

Disadvantages of the scheme include: i) the maximum operation speed is intrinsically restricted by the SOA carrier dynamics to a few tens of Gb/s; ii) the maximum number of channels is expected to be around ten limited by the SOA gain spectrum and input power limit [59, 71].

XPM in optical fibers can also be employed to realize MWC [105–107]. It offers more bit-rate independent conversion. In [106], one-to-eight conversion was achieved at the bit rate of 40 Gb/s. In [107], MWC to more than 20 channels has been demonstrated with error-free operation at up to 10 Gb/s.

d. XGM in SOAs

XGM in SOAs can be a very practical method to obtain MWC because of its simplicity, compactness, stability and polarization independence. MWC approaches based on XGM in SOAs can be grouped into two: single or double-stage XGM in SOA(s) [75, 104, 108, 109], and XGM of SOA ASE spectrum [110–112].

Single or double-stage XGM in SOA(s)

Conventional XGM wavelength conversion can be realized by injecting a data signal coupled with a CW into an SOA. The CW is then subject to the gain modulation and carries the complementary bit patterns as the data signal. Therefore, in principle, when more CWs are injected along with the data signal into the SOA, the data pattern will be copied onto all the wavelengths of the CWs. By means of co- or counter propagating XGM in an SOA, MWC can be achieved easily [75, 104, 108].

In *co-propagation* scheme, the data signal and the CW(s) enter the wavelength converter from the same side and they propagate *alongside* each other in the same direction inside the wavelength converter. At the output of the wavelength converter, usually an optical filter or an AWG is required to select the desired converted wavelength channel(s). In *counter-propagation* scheme, the data signal and the CW(s) enters the wavelength converter from the opposite sides and they propagate *against* each other inside the wavelength converter. The converted channels can be retrieved on the other side of the wavelength converter opposite to the input side of the CW(s), without any optical filtering. In many cases, counter-propagation is implemented as it separates automatically the input data channel and the desired converted channel(s).

However, this technique suffers from detrimental waveform distortion related to the semiconductor gain dynamics and poor output ERs, even for single wavelength conversion [86, 108, 121]. If MWC is performed, the ERs of the converted copies shall drop significantly from the single wavelength conversion as the XGM response is then shared by all the CWs. The more CWs are used, the more depleted are the output ERs, OSNRs and Q factors of the MWC channels, since the above negative effects are further emphasized when working with multiple wavelengths, and the FWM byproducts start to interfere with the original wavelengths in the probe signals [75, 104, 108, 109].

Although the FWM induced intraband crosstalk is inevitable, other aspects of the MWC signal degradation can be improved by introducing a second-stage SOA

to regenerate the multiple output channels [108, 109]. By implementing double-stage XGM in SOAs, 8 up to 16 channels MWC has been achieved at 10 Gb/s [108, 109]. However, this technique requires higher input signal power due to the splitting of the data signal to both SOA stages [108]. Moreover, it is likely to face a bottleneck of maximum operational bit rate, although lengthening the SOA chip will provide a temporary solution [109].

XGM of ASE spectrum in SOA

XGM of the SOA ASE spectrum followed by spectrum slicing has been proposed as a simple MWC scheme without the need of any probe light source [110–112]. It makes use of the fact that the level of the ASE in an SOA can be modulated by a high-intensity pump signal. Therefore, when the input power is low, the ASE level is high; while the input power is high enough, the ASE level is highly compressed. The proposed method treated a band of ASE as converted signal, as long as the level difference of ASE between the two input states is large enough at the desired wavelengths. Multicast function is then realized by filtering out multiple wavelengths from the ASE band. The bandwidth of ASE with a level difference over 10 dB was more than 80 nm [111]. However, due to the limitation of the SOA carrier recovery time, this technique suffers intrinsically from the SOA patterning effects. Successful demonstrations with bit error rate (BER) measurements using this method have only been reported for bit rate of up to 622 Mb/s with $2^{15} - 1$ pseudorandom bit sequence (PRBS) signals [110, 111], though with low power penalties and no sign of error floors. In [112], 10 Gb/s operation has been demonstrated for pre-defined bit patterns.

The advantage of this approach is that it requires no CW probe lights; however, the MWC bit rate and performance are limited by the SOA carrier recovery time and ASE spectrum response to XGM [110–112].

e. XAM in electroabsorption modulators

Wavelength conversion can be realized in an electroabsorption modulator (EAM). It works on the principle of cross-absorption saturation. An EAM can block the CW signal because of high absorption except when the arrival of 1 bits from the data signal channel saturates the absorption [82].

Several six to eight-channel MWC for RZ signals based on XAM in a single EAM have been demonstrated at bit rate of up to 40 Gb/s [113–116]. In these experiments, 200 GHz channel spacing was deployed and a counter-propagation

scheme was implemented. EAMs offer advantages such as compactness, integration potential, stable converted output polarization, and stability against environmental conditions such as temperature fluctuations and physical vibrations. An EAM can also have a good high-speed performance, low-chirp characteristics, and capability of all-optical signal regeneration. Furthermore, if a dense WDM configuration such as 0.8 nm channel spacing is applied, the number of converted channels can be possibly further increased. At 10 Gb/s, EAM-based MWC has even revealed signal regeneration properties when a degraded input signal with an ER of around 5 dB was applied [116].

The main disadvantage of most EAMs is the insertion loss. A high input power of more than 10 dBm is generally required for XAM applications [113–115]. Moreover, insufficient XAM also results in decreased ERs of the MWC channels. By reducing the insertion loss of the EAM through careful design and fabrication of the device, XAM efficiency, output power level and the output OSNR can be improved [113, 114]. However, the conversion efficiency of this method is not very high [115] and only MWC of RZ signals has been reported [113–116].

f. NPS in SOA

NPS in an SOA requires local polarization-controlled CWs and a polarization-controlled output to a polarization beam splitter (PBS). A driving signal produces a change of the effective refraction indices of the two orthogonal modes of the SOA, so that the transverse electric and transverse magnetic modes of a co-propagating signal experience a net phase difference and interfere in the PBS. High-speed operation and both inverted and non-inverted switching modes are possible [117].

Ref. [117] explored the potential of NPS at 40 Gb/s in an SOA under a standard configuration by utilizing an SOA optimized for high gain figure and fast saturated gain recovery time. One-to-four MWC of NRZ data was achieved with moderate OSNR penalties. Using current commercially available SOAs, this is close to the upper limit for the MWC possibilities. The scheme requires high input power of more than 10 dBm and suffers from significant FWM byproducts generated inside the SOA. Besides, the polarization sensitive nature of the method is one big disadvantage for applications in most arbitrary polarization state systems. Finally, the system demonstrated MWC conversion efficiencies in a range between -8.5 and -10.5 dB, which indicated its considerably lower power efficiency than that of XPM in an SOA-MZI.

g. SC in fibers

MWC by SC generation followed by spectral slicing has a long tradition [99, 118, 119]. SC is generated through a multitude of nonlinear effects when a seed light is amplified to a sufficient level in a fiber amplifier. These nonlinear effects include FWM, self-phase modulation, XPM, and stimulated Raman scattering, together with the effects of dispersion [94]. The seed light can be CW light, continuous ASE or optical pulses with nanosecond or picosecond pulse duration [99]. In theory, this technique has no speed limitations. High quality SC generation with bandwidth exceeding 50 nm was achieved when a HNLF was pumped with 25 dBm average power [99]. Such high pump power requirement is one of the main disadvantages of the scheme, which results in very low optical power efficiency. More than 200-nm-wide SC has also been generated with 210 mW input optical power [82, 94].

h. Mode locking in laser diodes

One-to-eight MWC at 10 Gb/s using an FP-LD has been reported [77]. This approach can be low-cost with no high-speed driving circuits, but a dc-bias is needed for the FP-LD operation. An input signal with 0 dBm power and 13.5 dB ER was coupled with eight 200-GHz-spaced CWs as inputs to the FP-LD. The CW power per channel was about -3 dBm. The average power penalty of the eight converted channels was around 2.5 dB at a BER level of 10^{-9}. The output ER was around 12 dB. The maximum number of channels for the MWC is determined by the gain spectrum of the FP-LD. Measurements of that FP-LD indicated that the wavelength conversion range was about 32 nm for an output ER of over 10 dB. The outputs of the MWC exhibited stable amplitude and single polarization. A disadvantage of such a scheme is that an arbitrary input wavelength within the injection-locking range of one of the modes of the FP-LD has to be supported by temperature-tuning of one of the FP modes. The longitudinal mode spacing of the FP-LD must also match the channel spacing of the CW probes [77].

4.4 Summary and discussions

This chapter reviews all-optical multicast technologies, especially all-optical MWC technologies, from the *technique* point of view. Various ways of realizing MWC via different *nonlinear processes* in materials or optical components are summarized. Operation speed limits apply for applications based on these nonlinear processes.

Table 4.1: Comparison of all-optical multi-wavelength conversion techniques. (IM: intensity modulation; PM: phase modulation; FM: frequency modulation; *: theoretical values based on the wavelength conversion principles [82, 93]; **: demonstrated values for MWC operations. For FWM in an SOA, the theoretical maximum speed is around 100 Gb/s [82].)

Principle	Data format	λ flexibility	Efficiency	Speed
FWM	IM, PM, FM	limited	low	$\sim$ Tb/s *
XPM	IM	SOA gain spec.	high	$\leq$ 40 Gb/s **
XGM	IM	SOA gain spec.	limited	$\leq$ 10 Gb/s **
XAM	IM	EAM bandwidth	low	$\leq$ 40 Gb/s **
NPS	IM	SOA gain spec.	low	$\leq$ 40 Gb/s **
SC	IM	SC spec.	low	$\leq$ 1 Tb/s *
mode locking	IM	restricted	limited	$\leq$ 10 Gb/s **

Parametric processes are the only wavelength conversion category that can be used for converting one waveband into another, namely, multiple-to-multiple channel conversion. The transparent operation of such wavelength converters preserves both amplitude and phase modulation, and allow simultaneous conversion of WDM channels with different data formats into spectrally-inverted WDM channels.

As for single-to-multiple conversion, Table 4.1 provides a comparison of the MWC properties of the above discussed techniques based on their underlying principles. Among the reported techniques, FWM MWC is the method that offers the most transparency in bit rates and modulation formats, but its conversion efficiency is rather low. XPM and XAM-based MWC can be realized by compact and integrable devices, and both potentially support simultaneous conversion of about eight channels or more for bit rates up to 40 Gb/s. However, high-speed SOA-MZIs and EAMs supporting 40 Gb/s operation are very expensive. Besides, EAM MWC also suffers from the high insertion loss. Current commercially available SOAs limit XGM-based MWC to around 10 Gb/s data rate. NPS in an SOA has been demonstrated at 40 Gb/s but is highly polarization dependent. SC provides transparent MWC at high speed, however, its power efficiency is very low. Finally, FP-LD MWC can be a low cost solution and offers good output ERs, but it has poor wavelength flexibility.

Chapter 5

Multi-wavelength conversion for optical nodes

Multicast in the current Internet infrastructure is implemented in the Internet layer by optic-electronic-optic (OEO) conversion of the Internet data and by processing the multicast Internet protocol (IP) addresses in the IP packet headers in the electrical domain. Internet layer multicast based on electronic header processing is going to be the bottleneck of the next-generation optical Internet. Optical switching nodes with optical-layer multicast capability will become the new focus to overcome the speed limit of the OEO conversion and electronic processing, and simplify the telecommunication network architecture and hierarchy. Although passive optical splitting has been proposed for certain multicast optical node architectures such as broadcast-and-select, it necessitates large-scale amplification to compensate the power losses. In this chapter, all-optical multi-wavelength conversion (MWC) techniques are analyzed with regard to their suitability for performing the multicast functionality in optical switching nodes. Three possible multi-wavelength converters are further discussed. Afterwards, experimental performance of four potential MWC techniques employing these multi-wavelength converters is tested at 10 Gb/s with non-return-to-zero (NRZ) signals. Next, a few promising MWC techniques for optical switching nodes are suggested. Finally, several novel all-optical applications enabled by MWC technologies are proposed. Parts of this chapter are based on publications.[1]

[1] See reference [60, 104].

5.1 Towards optical layer multicast nodes

Optical wavelength division multiplexing (WDM) systems have been deployed in data transmission links over the last decade to meet the rapidly increasing bandwidth demands [85]. The exponential growth of Internet and multimedia traffic poses a potential challenge for the telecommunication transport networks. Emerging voice-over-Internet protocol, video streaming, high-definition TV and peer-to-peer file transfer services are becoming widely available on top of the traditional Internet services. In order to deliver large amounts of data efficiently, more and more networking functions that are currently performed by electronics are to be moved to the optical layer. Telecommunication networks are undergoing major transformations driven by new all-optical technologies for WDM applications. All-optical solutions for switching, routing and multicasting become of crucial importance for realizing a truly intelligent, transparent and broadband optical infrastructure.

Wavelength conversion is a key WDM functionality for network interoperability and scalability. It can be used to route and switch wavelengths, resolve contention, reduce node blocking probabilities, increase optical transparency, and enable dynamic network wavelength assignments and allocation capability [85, 122]. Many optical and optoelectronic devices and components have been investigated for wavelength conversion. In WDM transponders, simple optoelectronic conversion is implemented [5]. However, this approach requires optical-electronic-optical (OEO) conversion of the optical signal, which consumes power and reduces the optical transparency. As all-optical wavelength conversion (AOWC) technologies were walking into a mature stage of high bit rates at 10∼40 Gb/s and successful research demonstration at 160∼320 Gb/s [61] crossing the last two decades, all-optical one-to-many multi-wavelength conversion (MWC) began to attract increasing interest during the last five to seven years due to several advantages. Firstly, instead of deploying large amounts of OEO converters and WDM transponders, all-optical MWC can be realized in a single device, saving operational cost and reducing system complexity. Secondly, all-optical MWC provides more independency on bit rate, protocol, modulation format and utilized bandwidth. Unlike with OEO MWC, physical resources for all-optical MWC do not need to be replaced, upgraded or multiplied whenever a change takes place concerning the above mentioned system parameters. Finally, all-optical MWC has also facilitated many new applications, such as optical layer wavelength multicast [2, 60, 65, 78], grid networking [99, 109] and service multi- or broadcast in access networks [60].

Optical layer multicast by MWC is particularly suitable for optical switching nodes that employ passive waveguides such as arrayed waveguide gratings (AWGs). Up to date, the demonstrated MWC and multicast approaches have been based on one of the following devices or components, as summarized in Sec. 4.3: semiconductor optical amplifiers (SOAs) [78, 108–112, 117], SOA – Mach-Zehnder interferometers (SOA-MZIs) [59, 60, 67–69, 71, 103] or SOA delay interferometers [102], nonlinear fibers [70, 99–101, 105–107, 118, 119], electroabsorption modulators (EAMs) [113–116], injection-locked Fabry-Pérot (FP) – laser diodes (LDs) [77], and fiber optical parametric amplifiers (OPAs), etc.

Each MWC technique has its advantages and disadvantages. Therefore, not all of them are suitable for multicast applications in optical nodes. In Sec. 5.2, general requirements on multicasting components for optical cross-connects and switching nodes are addressed. In Sec. 5.3, the basic characteristics of three possible MWC media are described. In Sec. 5.4, experimental validations of a selection of MWC techniques based on these three MWC media are demonstrated and discussed. In Sec. 5.5, a few other applications enabled by all-optical MWC are proposed. Finally in Sec. 5.6, conclusions are drawn based on the observed experimental performance and some suitable MWC technologies for optical nodes are suggested.

5.2 Requirements on multicast components

A multi-wavelength converter must process certain intrinsic physical characteristics to be practically suitable as a built-in switching component for optical layer multicast. This section discusses the requirements on multicast components for optical nodes.

Firstly, multicast operation requires reasonably *uniform optical power levels* of all multicast channels. Concerning this aspect, OPA-based MWC suffers from a large range of conversion efficiencies and power penalties among the MWC channels, which result in significant optical power difference in these channels. Secondly, a good *extinction ratio (ER)* and *Q factor* of the output signals are necessary to allow for long distance propagation between the nodes without OEO conversion or optical regeneration. As for the performance of MWC, modulation of an SOA amplified spontaneous emission (ASE) noise can not satisfy this. Thirdly, *wavelength flexibility* is essential for dynamic optical communication systems. In real networks, the wavelength carriers of the signals can hardly be predicted, although most systems have adopted the International Telecommunication Union (ITU)

wavelength grid. However, for an FP-LD, an arbitrary input wavelength within one of its modes' injection-locking range has to be supported by temperature-tuning of one of the FP modes. The mode spacing of the FP-LD must also match the channel spacing of the continuous wave (CW) probes [77]. These place several restrictions on wavelength freedom. Finally, a reasonably *wide wavelength conversion range* with a *flat conversion efficiency response* is important for WDM transmissions. SOA-based four-wave mixing (FWM) MWC can only perform effective MWC in very near field of the pump signal, or several pumps need to be used to obtain even conversion efficiencies [78].

Apart from these essential requirements, there are two other conditions that, if met, hold extra advantages for potential multicast technologies to be applied in optical switches. The first one is *compactness*. Bulky components can not be easily integrated. They are far less attractive than their integrated equivalents that can offer the same performance. The second one is *low optical power budget* with *high conversion efficiency*. Power-economical and efficient MWC saves the trouble for other add-ins such as erbium-doped fiber amplifiers (EDFAs) to boost the power level as well as optical filters to remove the out-of-band noise afterwards. As an example, for simple NRZ/RZ modulated one-to-many MWC at a bit rate no higher than 40 Gb/s, MWC by cross-phase modulation (XPM) in an SOA-MZI is much more promising than by FWM in fibers because of the SOA-MZI's integration potential, and than by cross-absorption modulation (XAM) in an EAM because of the power efficiency of the scheme.

Furthermore, ideal multicasting functionalities call for even higher requirements, which have not yet technically been fulfilled by most MWC technologies. To name a few, low cost, polarization insensitivity, stability to temperature, moisture and bias current fluctuations, etc., are the ones mostly concerned by manufactures and operators. However, to the author's knowledge, none of the reported technologies combine all these attractive properties.

5.3 Possible candidates

In this section, we introduce the basic characteristics of the MWC components whose performance is experimentally validated and presented in the next section. These components or devices are selected for MWC experiments because of their availability in the laboratory.

5.3.1 Nonlinear fibers

As discussed in Chapter 4, FWM in nonlinear fibers offers a large conversion bandwidth with flat and symmetric conversion efficiency, around the zero-dispersion wavelength of the fiber. This feature enables nonlinear fibers to convert a large number of wavelength channels simultaneously. In principle, wavelength converters based on optical fibers can operate at bit rates up to 1 Tb/s because of the fast nature of their nonlinear response [82].

However, FWM process in optical fibers is polarization sensitive, as signal polarization is not maintained in normal optical fibers. Such random variations of the signal polarization affect the FWM efficiency and make the standard FWM technique unsuitable for practical purposes [82]. Therefore, fibers with very high nonlinearities are preferred for FWM applications because they can achieve the same nonlinear effects with much shorter fiber span length. The higher the nonlinearity of the fiber, the shorter the fiber length, and the better the phase matching for the FWM can be maintained along the fiber, as phase matching is strongly related to the polarization states of the input waves [93].

5.3.2 SOAs

Like all other lasers, semiconductor lasers act as amplifiers close to but before reaching threshold [82]. Although semiconductor lasers were invented in 1962, SOAs were only developed for practical applications motivated largely by their potential applications in lightwave systems during the 1980s [82].

Optical amplifiers without feedback are called *traveling wave* (TW) amplifiers to emphasize that the amplified signal travels in the forward direction only [82]. TW SOAs can be made if the reflection feedback from the end facets is suppressed. Semiconductor lasers experience a relatively large feedback because of reflections occurring at the cleaved facets, which can be used as amplifiers when biased below threshold [82].

SOAs are polarization sensitive. The amplifier gain can differ for the transverse electric (TE) and transverse magnetic (TM) modes by up to 5∼8 dB [82]. This property is undesirable for optical system applications as the polarization state of lightwave changes while propagating along the fiber, unless polarization-maintaining fibers are used. Employing certain SOA designs or system configurations can reduce the polarization sensitivity [82].

FWM in SOA

As discussed before, FWM can also be generated in an SOA. The obvious advantage for using an SOA is that the wavelength converted signal(s) can be generated in a device of about 1-mm long. Typically the conversion efficiency is higher than that of FWM in a fiber because of the amplification. However, this advantage is offset by the relatively large coupling losses from the SOA to the fiber [82].

The nonlinearity responsible for the FWM in an SOA occurring at a time scale of 0.1 ps [82]. For this reason, this technique can work at bit rates up to 100 Gb/s and is transparent to both the data rate and format [82]. However, in practice, to the best of the author's knowledge, MWC based on FWM in an SOA has not been reported for data rate above 40 Gb/s. Moreover, For MWC, this technique suffers from the non-flat and asymmetric conversion efficiency and a narrow conversion bandwidth as discussed in Sec. 4.3 [85, 93]. This undesired feature can be relaxed by employing multiple pumps with carefully planned polarizations and channel spacing relative to the input data signal, but the conversion efficiency was less than -20 dB [78].

XGM in SOA

When cross-gain modulation (XGM) is used for wavelength conversion in an SOA, both co- and counter propagation scheme can be implemented. In XGM, the intensity-modulated signal modulates the gain in the SOA. Due to gain saturation, one or more CW signal(s) can be modulated by the gain variation so that the same information is carried also on the CW wavelength(s) [5].

However, the XGM technique generates *inverted* signals compared to the original input signal. This means a converted data signal by XGM has reversed polarity such that 1 and 0 bits are interchanged [82]. Moreover, XGM usually suffers from ER degradation for an input signal converted to a signal of equal or longer wavelength, often referred to as *up-conversion* [5]. Furthermore, XGM in an SOA produces relatively low ON-OFF contrast of the converted signal and is impaired with degradation due to spontaneous emission [82]. Finally, XGM also experiences phase distortion in an SOA [82].

XGM in an SOA as a wavelength conversion technique has been widely investigated and can work at bit rates as high as 40 Gb/s [82]. It can also provide net gain and can be made nearly polarization insensitive [82]. Nevertheless, MWC by XGM in SOAs have only been demonstrated with operation speeds up to 10 Gb/s [75, 104, 108–112].

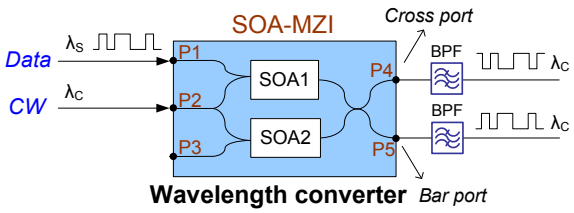

Figure 5.1: Co-propagating XPM in SOA-MZI with standard configuration.

5.3.3 SOA-MZIs

Today, one all-optical wavelength conversion technique approaching maturity is based on XPM in SOA interferometric configurations [5]. Interferometric structures can convert XPM into intensity modulation. Among all the interferometric structures, the MZI structure is often used in practice because it can be easily integrated by using SiO_2/Si or InGaAsP/InP waveguides, resulting in a compact device [82]. The Mach-Zehnder configuration with one SOA in each arm of an MZI, can be monolithically or hybrid integrated. Wavelength conversion based on XPM in an SOA-MZI can solve the problem of low ON-OFF contrast with XGM in an SOA and provide non-inverted bit conversion [82].

In the standard configuration for wavelength conversion in an SOA-MZI illustrated in Fig, 5.1, intensity-modulated data at wavelength λ_S is sent to one arm of the SOA-MZI. At the same time, a CW signal at wavelength λ_C enters the middle arm of the SOA-MZI and is split by the coupler. The split CWs propagates simultaneously in the two arms. In the absence of the data signal, the CW signal exists from the *cross* port of the SOA-MZI. When the data signal is present, all 1 bits are directed to the *bar* port because of the refractive-index change induced by the data signal. The physical mechanism behind this behavior is the XPM [82].

In Fig. 5.1, the duration of the tailing edges of the converted pulse depends on the effective carrier lifetime of the SOA1 [123]. In general, carrier dynamics of SOAs allow XPM-based wavelength conversion to operate at high bit rate of above 10 Gb/s and up to even 40 Gb/s [5]. This speed limitation can be relaxed by a method called differential mode operation [123]. In [82], it is stated that up to 80 Gb/s operation can be achieved. Often, the device is utilized for regeneration of an input signal, including signal power, reshaping, ER improvement [5]. Thus it can act as an optical regenerator, although the ASE from the SOAs sometimes

does affect the optical signal-to-noise ratio (OSNR) of the converted signal [82].

In an SOA-MZI, standard wavelength conversion can be realized with either co- or counter propagation scheme. With XPM wavelength conversion in an SOA-MZI, an incoming signal can modulate the refractive index and thereby results in phase modulation of a CW signal coupled into the converter [5]. The output converted signal can be either inverted or non-inverted. If the SOA-MZI structure has both cross and bar output ports, usually one port yields a non-inverted signal and the other yields an inverted signal. Compared to the XGM technique, the XPM can be very power efficient [121], and has also been found to be able to improve the signal quality by reducing the noise in the converted signal [124].

The main disadvantage of the XPM scheme is a narrow dynamic range of the *input power* since the phase induced by the SOA(s) depdends on it [82]. Another disadvantage is that XPM has limited transparency, and can be applied only to intensity-modulated data [85].

5.4 Experimental validation

Four potential MWC techniques were tested in the laboratory at 10 Gb/s to evaluate their performance. In this section, these experimental results are presented. These techniques are based on: FWM in a dispersion-shifted fiber (DSF) and in an SOA, XGM in an SOA, and XPM in an SOA-MZI. FWM was investigated for its conversion transparency. XGM and XPM can be easily realized in an SOA. As SOA is one of the most basic and widely available switching component, we studied the XGM and XPM effects in an SOA for MWC applications. Experimental performance of the other MWC techniques have not been explored due to the unavailability of laboratory facilities.

In order for results to be comparable, experimental apparatus for the performance validation of these MWC schemes were largely kept the same, as shown in Fig. 5.2. Different power levels were applied and monitored for different MWC media and the principles on which the MWC nonlinear processes were based. Except in the experiment MWC via an SOA-MZI, where four CW lasers were applied, in the other three experiments only two CW lasers were utilized for the MWC evaluation due to the availability of the laboratory facilities at that time. For the same reason, no bit error rate (BER) measurements were taken for the other three experiments. For BER results of the MWC via an SOA-MZI, reference is made to Chapter 6.

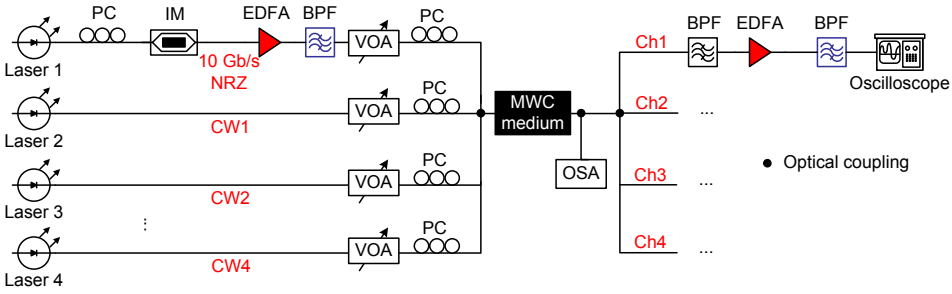

Figure 5.2: General experimental setup for evaluation of MWC employing different wavelength conversion media. (PC: polarization controller; IM: intensity modulator; EDFA: erbium-doped fiber amplifier; BPF: bandpass filter; VOA: variable optical attenuator; OSA: optical spectrum analyzer; NRZ: non-return-to-zero; CW: continuous wave; Ch: channel.)

The output signal from a laser was encoded with $2^{31}-1$ pseudorandom binary sequence (PRBS) by an intensity modulator (IM) to form the 10 Gb/s nonreturn-to-zero (NRZ) data signal, and then was optically amplified by an EDFA. Another two to four lasers were used as CWs. Polarization controllers (PCs) were included to adjust the polarization of each laser at the input of the multi-wavelength converter because all the approaches involve polarization-sensitive processes. Couplers or multiplexers were employed to combine the optical sources and inject the multiple wavelengths into the device or component where the MWC took place. An optical spectrum analyzer (OSA) monitored the output spectrum. The converted wavelength channels were selected through an optical band-pass filter (BPF). Afterwards, a second EDFA was used as a preamplifier for the oscilloscope detection. A few other optical BPFs were placed after the each EDFA to remove the out-of-band ASE noise from the EDFAs. Variable optical attenuators (VOAs) were utilized to adjust optical power levels of each input channel.

5.4.1 FWM in a DSF

Among the MWC principles discussed so far, the FWM process for wavelength conversion offers the highest level of transparency in both data rate and modulation format. AOWC by means of FWM in an SOA may still suffer from bit rate restrictions due to the SOA operation speed or patterning effect. AOWC by FWM

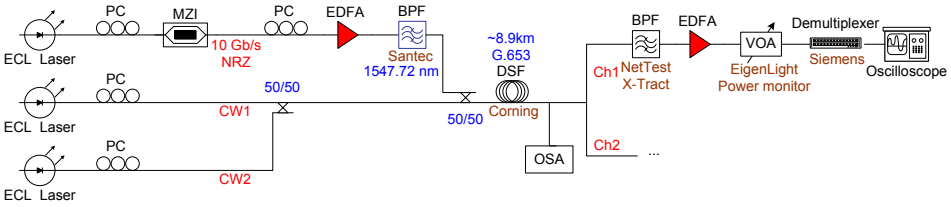

Figure 5.3: Experimental setup for MWC by FWM in DSF. (ECL: external cavity laser; MZI: Mach-Zehnder interferometer.)

in non-linear fiber is believed to have no such limitations.

We choose first-order FWM replicas as converted channels [70, 75, 101, 104]. The difference of this approach from the other reported FWM-based MWC approaches [78, 99, 100] is that we modulated the pump signal which usually has much higher power in the conventional FWM scheme, and injected this modulated pump signal together with two CW wavelengths into the DSF. As a result, the FWM products generated closer to the modulated pump have much higher power than the ones closer to the CWs. Therefore the replicas closer to the modulated pump were selected as converted signal channels.

The experimental setup is illustrated in Fig. 5.3. An extended cavity laser (ECL) laser was modulated in an MZI to form the 10 Gb/s PRBS pump NRZ data, and then was amplified by an EDFA to increase the power as the modulated pump signal. Two other ECL lasers were used as CWs. PCs were used to adjust the polarization of each laser of the inputs in order to maximize the phase-matching condition of the input channels in the DSF, as FWM in DSF is polarization sensitive. Two 50/50 couplers were used to combine the wavelengths, and at the same time due to wavelength transparency, provide the flexibility of tuning the modulated pump around the zero-dispersion wavelength of the DSF and optimize the position of the two CWs. After the DSF, an OSA was used to monitor the output spectrum of the fiber. Another EDFA was used for the converted signal to allow proper detection by the oscilloscope. The optical filters placed after the EDFAs were to remove the out-of-band ASE noise from the EDFAs.

In this experiment, we used a commercially-available DSF of the ITU G.653 standard. The data signal wavelength was tuned to 1547.72 nm. The output power of all the lasers was set to be 7 dBm. The MZI was designed for 40 Gb/s operation. A 40 Gb/s pattern generator was used to generate the 10 Gb/s data,

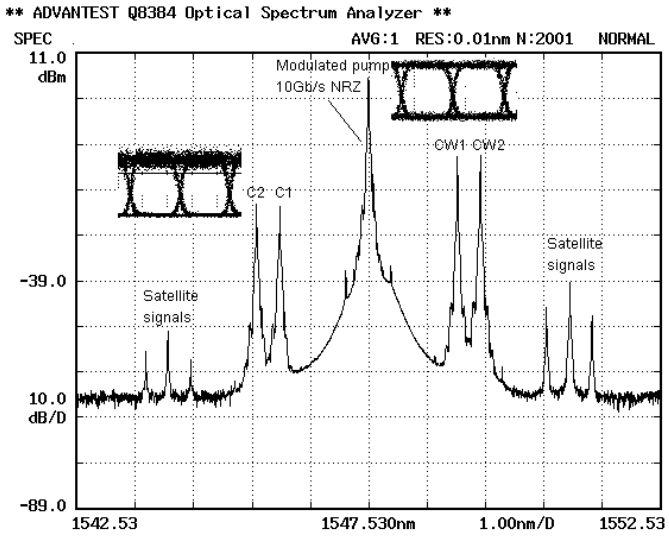

Figure 5.4: Spectrum of MWC by FWM in DSF. (eye diagram insets: source signal Q = 11.3; converted signal Q = 11.5.)

to allow easy adaption to higher operation speed for testing bit rate transparency and the extendibility of the scheme. The source signal at 10 Gb/s had a Q factor of 11.3.

The output spectrum is presented in Fig. 5.4, with the input data channel and one of the converted channel eye diagrams shown as insets. Under optimized polarization conditions, the converted signal exhibited a clear eye opening with a Q of 11.5. The increase in the Q factor was due to the quadratic-power nature of the copies selected, which is responsible for the signal regeneration effect at the logical *zero* level. As the optical power of the selected MWC channels is *proportional* to the optical power of the modulated pump signal, the power difference at logical *one* level is increased while the power difference at logical *zero* level is decreased. This quadratic effect also resulted in a lower crossing point in the eye diagram. The measured average MWC conversion efficiency, in this case defined as converted signal power divided by input CW power, was around −13.5 dB within the wavelength range from 1543.73 to 1551.72 nm.

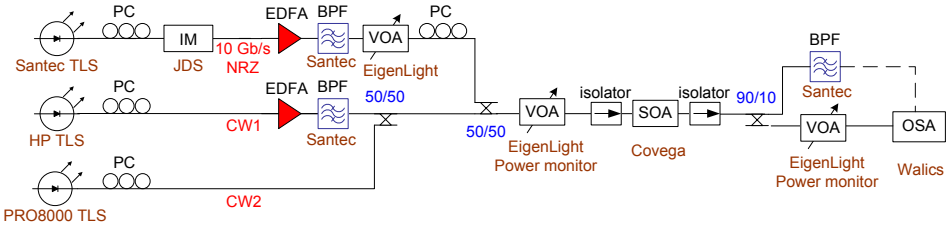

Figure 5.5: Experimental setup for MWC by FWM in SOA. (TLS: tunable laser source.)

5.4.2 FWM in an SOA

In principle, MWC by FWM in a nonlinear SOA should offer higher conversion efficiency, due to the SOA gain. It also requires less input optical power. Unlike fibers, SOAs can be easily monolithically-integrated into optical switches.

The experimental setup is shown in Fig. 5.5. We experimented with a *COVEGA* 1550-nm nonlinear SOA. Three tunable laser sources (TLS's) were used, for the signal channel and two CW probes. The data wavelength was set to 1548.51 nm, the gain peak of the SOA. The power of this laser was 7 dBm. Two fixed lasers with 3 dBm optical power at 1551.72 nm and 1553.33 nm were used as CW sources. After coupling, the total input power to the SOA was 1.1 dBm.

Fig. 5.6 shows the spectrum after the SOA. The measured average MWC conversion efficiency was less than -30 dB. One of the reasons could be the choice of the SOA, whose nonlinearity is not sufficient for efficient wavelength conversion. Another reason could be that the phase-matching conditions for this MWC could not be well satisfied. There are two reasons for this: i) For efficient FWM in an SOA, the input wavelength channels need to be placed very close to each other, but this is not possible in our scheme because strong crosstalk between adjacent channels as well as strong satellite signals will appear; ii) The optical power of the channels were very low when they entered the SOA due to the coupling processes. These low-power waves could not interact efficiently for strong FWM to occur. Apart from this, due to the non-flat conversion efficiency of FWM in an SOA explained in Sec. 4.3.2, the conversion efficiency decreased noticeably as we placed the CWs further away from the modulated signal.

Two other disadvantages of using an SOA for MWC were discovered in this experiment: i) because SOAs have different gain for different wavelengths, it is fairly

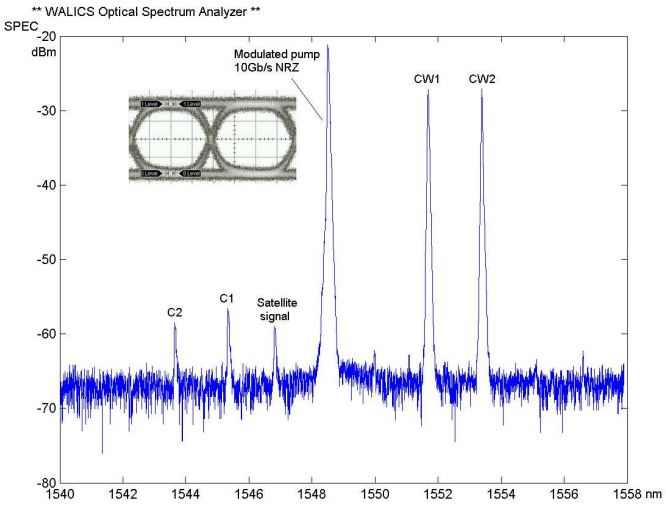

Figure 5.6: Spectrum of MWC by FWM in SOA. (eye diagram inset: source signal S/N = 14.6 [linear scale], ER = 16.7 dB.)

difficult to find the optimum optical power levels for different CWs to achieve flatter conversion efficiency curve among only a few converting channels; ii) the conversion efficiency of the two MWC channels was very unequal, and was much lower than that of the single wavelength conversion utilizing the same SOA. Therefore, we expect that as the number of channels increases, these two problems will become more prominent.

The eye diagrams of the converted signals could not be monitored because their optical power was too weak to be extracted and examined via the oscilloscope.

5.4.3 XGM in an SOA

Conventional XGM single-channel WC can be realized by injecting a data signal coupled with a CW into an SOA. The CW is subject to the gain modulation and carries the inverted bit patterns as the data signal. In this experiment, we injected two CWs along with the data signal into an SOA. The inverted data pattern were transferred onto both wavelengths of the CWs.

The experimental setup is illustrated in Fig. 5.7. One ECL laser encoded by a MZI to form the 10 Gb/s data signal, and two other ECL lasers used as CWs. PCs were also placed after each input channel because the SOA is polarization

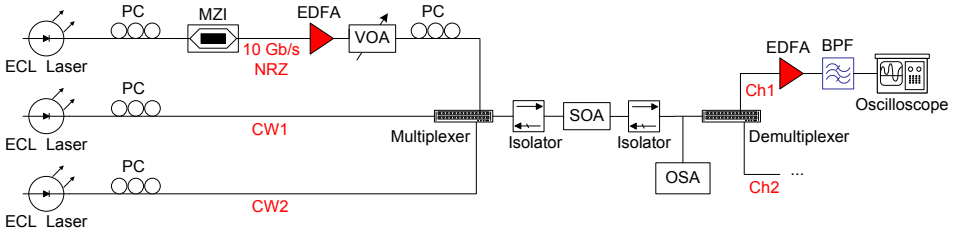

Figure 5.7: Experimental setup for MWC by XGM in SOA.

sensitive. Isolators at the input and output of the SOA were deployed to avoid reflections. A multiplexer and a demultiplexer were used instead of optical filters and couplers, because unlike the FWM process, the XGM operation is insensitive to wavelengths. By employing multiplexers with insertion loss of just ∼1 dB per port, we could reduce optical power losses in the setup.

The MZI in this experiment was designed for 10 Gb/s operation driven by a 10 Gb/s pattern generator. The source signal had only a Q factor of 6.5 because of the reduced bandwidth of the MZI. It was not necessary to use the 40 Gb/s data generator because the SOA we used for this experiment was from former *Optospeed Inc.* and was designed for operating at 2.5 Gb/s. However, by properly positioning the multiplexer at the input and the demultiplexer at the output, the SOA operation speed can be improved to accommodate 10 Gb/s wavelength conversion [125].

The output spectrum after the SOA and the eye diagram of one of the channels are shown in Fig. 5.8. The source and one of the converted eye diagrams are included as insets. The converted signal had clear eye opening with an improved Q factor of 9.7. However, the ER was largely degraded. This was mainly due to two reasons: i) the operation of the SOA led to a high penalty in the converted signals when the power of the modulated signal was very high; ii) due to the nature of the XGM process, the gain modulation in each CW became much weaker as the XGM effect was then shared by both CWs. Nevertheless, from the eye diagrams we noticed a signal regeneration effect.

The output ER of this scheme can be greatly improved if a faster SOA is used. The wavelengths can then be placed in the center of the demultiplexer filtering band, so that the large power loss from the filter positioning can be avoided, and only the insertion loss would be introduced.

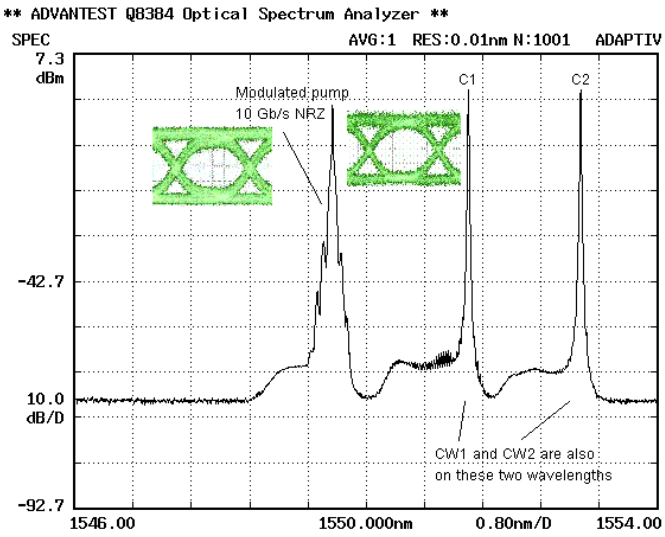

Figure 5.8: Spectrum of MWC by XGM in SOA. (eye diagram insets: source signal S/N = 6.5 [linear scale], ER = 8.3 dB; converted signal S/N = 9.7 [linear scale], ER = 1.7 dB.)

5.4.4 XPM in an SOA-MZI

Finally, we investigated MWC by XPM in an SOA-MZI. This approach has been reported with good performance [59, 60, 67–69, 71, 103]. An SOA-MZI is compact and easy to integrate. Moreover, SOA-MZI-based technologies have many applications in optical switches, including wavelength conversion. Large scale integration of SOA-MZIs is being investigated by the industry and academia.

The experimental setup is shown in Fig. 5.9. The SOA-MZI used was an AOWC with data rate transparency up to 20 Gb/s, fabricated by the Heinrich Hertz Institute (HHI). A co-propagation scheme was implemented. A laser tuned at 1541.35 nm was encoded to form the data. Four other tunable lasers were used as CWs. The channel wavelengths employed were of the ITU 200 GHz standard. VOAs reduced the optical power of the lasers so that the final input power to the SOA-MZI ports was around 0 dBm. A four-to-one coupler was used to combine the CWs. After the SOA-MZI, an optical filter of 0.3 nm bandwidth was used to select one copy at a time to be received by the digital clock recovery (DCR) circuit, and finally to be tested by an error detector (ED).

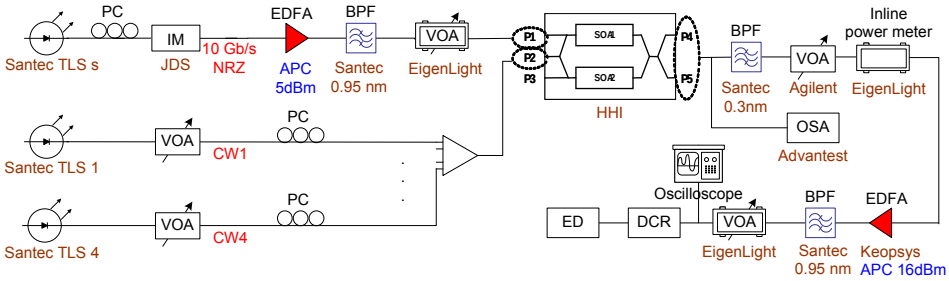

Figure 5.9: Experimental setup for MWC by XPM in SOA-MZI. (DCR: digital clock recovery; ED: error detector.)

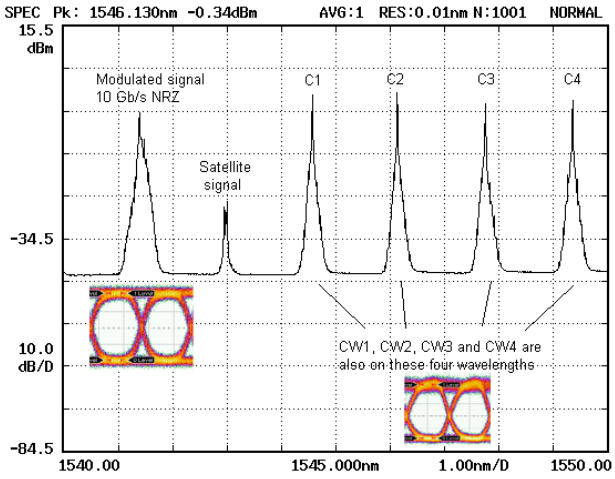

Figure 5.10: Spectrum of MWC by XPM in SOA-MZI. (eye diagram insets: source signal S/N = 13.9 [linear scale], ER = 12.3 dB; converted signal S/N = 11.3 [linear scale], ER = 11.0 dB.)

The output spectrum is illustrated in Fig. 5.10. The extracted converted channels had clear open eyes. Eye signal-to-noise ratio (S/N) values of the four channels were around 10∼11 and the ER was around 10∼11 dB, measured by the oscilloscope. Further BER measurements proved that the converted channels could be recovered with negligible power penalties of around 0.5 dB or less. The complete results are presented in Chapter 6.

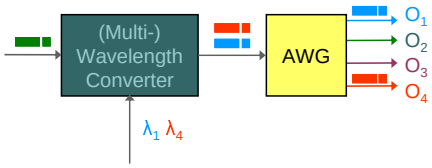

Figure 5.11: Optical packet multicast by MWC in optical packet switches based on passive waveguides such as arrayed waveguide gratings (AWGs).

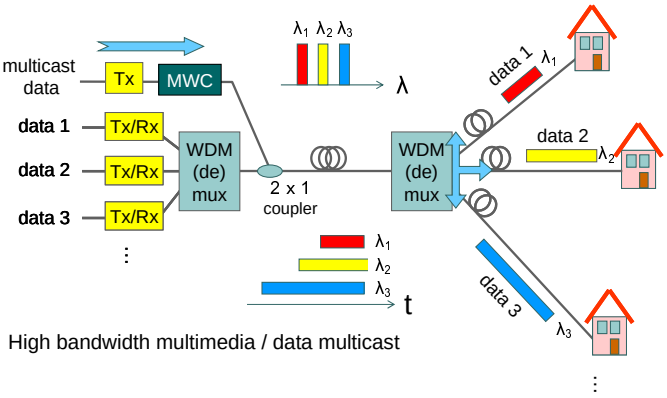

Figure 5.12: High bandwidth data multicast in WDM passive optical networks. (Tx: transmitter; Rx: receiver.)

5.5 Other multi-wavelength conversion applications

Apart from optical layer wavelength multicast, which can be implemented either in the WDM core networks for wavelength routed scenarios or optical switches based on passive waveguides as shown in Fig. 5.11 [46, 65], or in WDM passive optical networks (PONs) [79] as shown in Fig. 5.12, there are a number of other desirable all-optical functionalities that can be enabled by MWC technologies.

All-optical multi-slot reflective packet buffering can be realized by MWC followed by a fiber Bragg grating (FBG). Gratings for different wavelengths can be written on a fiber at several intervals to retrieve packets in different time slots on multiple converted lambdas [60], as illustrated in Fig. 5.13.

More but not exhaustive MWC applications include $1 + 1$ link protection [76] and grid networking that rely on high speed data multicasting [99, 109].

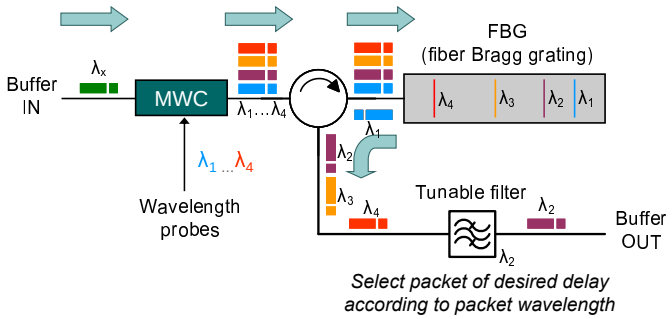

Figure 5.13: All-optical multi-slot reflective packet buffering by MWC followed by a FBG.

5.6 Summary and discussions

This chapter discusses a selection of all-optical MWC technologies, from the point of view of the physical medium in which the MWC take place. Requirements for possibly suitable MWC components for optical nodes are summarized. Experimental validation of four approaches utilizing three MWC media is presented. These four approaches are based on: FWM in a nonlinear fiber, FWM in an SOA, XGM in an SOA and XPM in an SOA-MZI. Table 5.1 shows a comparison of the performance and general characteristics of the investigated MWC approaches using a DSF, an SOA and an SOA-MZI.

Among the above investigated MWC approaches, XPM in an SOA-MZI is the most promising one for multicast purposes. Comparing to nonlinear fibers, an SOA-MZI excels in its compactness and conversion flexibility in wavelengths. SOA-MZI-based MWC also has an advantage over the other MWC techniques for they only require very low optical input power, which prevents by itself possible strong crosstalk caused by FWM among the multicast channels. Experimental validation further proved the promising performance of the SOA-MZI MWC with negligible power penalty both among the converted channels and relating to the back-to-back signal. Reference is made to Chapter 6 for more extensive simulation and experimental evaluation on SOA-MZI-based MWC performance.

A disadvantage of SOA-MZIs for optical multicast is that an optimized balance between the converted eye S/N and ER value has to be found by setting the right current control to the SOAs in both arms when the conditions of the

Table 5.1: Comparison of all-optical MWC performance and characteristics using different MWC media. (IM: intensity modulation; PM: phase modulation; FM: frequency modulation; η: conversion efficiency; *: theoretical values based on the wavelength conversion principles [82, 93]; **: demonstrated values for MWC operations.)

MWC media	DSF	SOA	SOA	SOA-MZI
Principle	FWM	FWM	XGM	XPM
Data format	IM, PM, FM	IM, PM, FM	IM	IM
Operation speed	$\sim$ Tb/s *	$\leq$ 100 Gb/s * $\leq$ 40 Gb/s **	$\leq$ 40 Gb/s * $\leq$ 10 Gb/s **	$\leq$ 80 Gb/s * $\leq$ 40 Gb/s **
λ flexibility	λ_0; spec. inversion	$\lambda_{sig.}$; spec. inv.	SOA gain spec.	SOA gain spec.
Input power	$>$ 10 dBm	$\sim$ 0 dBm	$\sim$ 0 dBm	$\sim$ 0 dBm
Conversion efficiency η	$\ll$ 0 dB (very low); flat; symmetric	$<$ 5%; non-flat; asym.	$<$ 0; flat	good; flat
ER improv.	$\sim$ 0	$\sim$ 0	$<$ 0	possible
Compactness	no	yes	yes	yes
η with respect to channel no.	not affected	strongly influenced	strongly influenced	stable within SOA gain spec.

experiment are changed. However, this problem exists in general even for single-channel wavelength conversion using an SOA-MZI. The solution is to find the best operating point where all the wavelength channels covered by the application can be on average well converted. In this setup, the polarization of the CWs also plays a role in minimizing crosstalk among the converted channels. Therefore, another room for improvement is to develop a polarization-insensitive scheme or device. Nevertheless, all the MWC techniques reported to date rely on PCs to achieve good performance.

From the experimental results, we can see that both FWM in a DSF and XGM in an SOA have benefits from certain signal regeneration effects for reshaping the converted eye diagrams. Our FWM scheme of putting the modulated signal in the pump has the advantage of noise suppression at logical *zero* level. However the quadratic effect to the signal power also amplified the noise at logical *one* level

and caused signal distortion where the crossings of the converted eye diagram was lower than the normal threshold level. The signal regeneration in the XGM scheme preserved perfectly the shape of the original signal with an increase in the Q factor from 6.5 to 9.7, but the ER of the converted copy dropped significantly from the value of the original signal. Moreover, XGM produces *inverted* signal which usually requires a second inverting stage.

Concerning the possible number of converted channels, from the experiments we noticed that for the FWM scheme, the conversion efficiency, Q factor and ER of one converted channel had little dependence on the existence of the other, so the maximum number of possible converted channels is mainly restricted by the conversion efficiency response of the DSF around the zero-dispersion wavelength. The higher is the nonlinearity of the fiber, the wider and flatter the bandwidth of its conversion efficiency will be, and thus the more channels can be included. On the contrary, in the XGM experiment, a strong dependence of the converted ER on the number of the channels has been noticed. If one CW was switched off, the measured converted ER of the other channel increased from 1.7 dB to 3.0 dB, while the conversion efficiency and the Q factor were not that much affected. Therefore, the maximum number of possible converted channels should mainly be determined by the ER tolerance of the receivers. The low ERs were due to the detuned filtering while extracting the MWC channels. Generally speaking, with an SOA of higher operation speed, normal filtering can be performed and the ERs of the converted signals can be greatly improved.

The conversion efficiencies of the XGM and XPM scheme were much higher than those of the FWM scheme. This is partially due to the fact that the SOAs had contribution in optical gain, while the DSF only attenuated the signals. In general, XGM in an SOA and XPM in SOA-based interferometers are also more power-efficient solutions because there is a limit on the total input power into the SOAs, which in the above cases was about 5 dBm in order to have the SOA work most effectively. In the XGM scheme, the converted signals after the SOA and the isolator still had optical power of about -1 dBm. On the other hand, FWM in nonlinear fibers requires generally very high optical power of at least 10 dBm. Although FWM in an SOA also has an input power limit, the FWM process in either nonlinear fibers or SOAs normally only has a conversion efficiency of around -15 to -20 dB.

Moreover, FWM in a nonlinear optical fiber needs the modulated pump signal to be placed around the zero-dispersion wavelength of the fiber. FWM in an SOA

has an asymmetric conversion efficiency response around the modulated pump and a small convertible wavelength range, while XGM is more tolerant to the wavelengths of the signal and the CWs as long as they are located inside the gain curve of the SOA.

However, from the transparency point of view concerning bit rate and modulation formats, FWM is more promising than XGM and XPM. Highly nonlinear fibers (HNLFs) can have more than 70 nm flat conversion efficiency response around its zero-dispersion wavelength [85, 93], much more than the total gain bandwidth of a common SOA, which is typically around 30∼50 nm. The number of converted channels also has little impact on the conversion efficiency and the Q factor of the converted signals. The main drawback of the FWM wavelength conversion is its low conversion efficiency.

It is worth mentioning that EAM could be another option as a wavelength multicast component for optical switches. Although it has not been investigated by us, in literature EAM-based MWC demonstrated good attributes comparable to SOA-MZI-based MWC, but it suffers from large power losses in the EAM and only return-to-zero (RZ) signal format was used [113–116], while SOA-MZI-based MWC has been reported to work for both RZ and NRZ formats [59, 60, 67–69, 71, 103].

Chapter 6

SOA-MZI-based multi-wavelength conversion via XPM

Multi-wavelength conversion (MWC) techniques with large wavelength flexibility, good performance and a compact scheme are desirable for various multicast applications such as video conferencing and grid networking. Single semiconductor-optical amplifier – Mach-Zehnder interferometer (SOA-MZI) – based MWC via cross-phase modulation (XPM) possesses these attractive characteristics. This chapter presents extensive simulation and experimental characterizations of a single SOA-MZI-based MWC of non-return-to-zero (NRZ) data at 10 Gb/s and return-to-zero (RZ) data at 40 Gb/s under various conditions with International Telecommunication Union (ITU) standard 100 and 200 GHz channel spacings. The performance impairment caused by the high-order four-wave mixing interference are analyzed in particular. The simulation results indicate the promising performance of the MWC to up to eight channels at both 10 Gb/s and 40 Gb/s. Further experimental demonstrations show four-channel 10 Gb/s error-free MWC with signal regeneration possibilities and 40 Gb/s MWC with moderate penalties, employing commercially-available integrated SOA-MZIs. Parts of this chapter are based on publications.[1]

[1] See references [60, 67–69, 103, 126].

6.1 Introduction

Among the various all-optical multi-wavelength conversion (MWC) techniques demonstrated in recent years, promising results have been shown based on technologies in the following categories: four-wave mixing (FWM) [70, 78] or supercontinuum [99], cross-phase modulation (XPM) [59, 60, 67, 69, 71, 102], cross-gain modulation (XGM) [108, 109], cross absorption modulation (XAM) [113, 116] and fast nonlinear polarization switching (NPS) [117]. However, FWM is limited by its low conversion efficiency and wavelength inflexibility [70, 78]. XGM by double-stage SOAs requires high input optical signal power because of the data splitting process to both SOAs [108, 109]. XAM suffers from large insertion loss of electroabsorption modulators and only MWC of return-to-zero (RZ) signals has been demonstrated [113, 116]. The NPS technique is polarization sensitive, requires high input power and consequently is also penalized by the significant FWM byproducts generated inside the SOA [117].

In comparison, XPM-based multi-wavelength converters using a single SOA-MZI outperform the others by offering the greatest combination of desirable features, including [59, 67, 69, 71]: high integrability, satisfactory and flat conversion efficiency, low power consumption, wide conversion bandwidth covering the SOA gain spectrum, simultaneous conversion of a considerable number of channels, wavelength flexibility, commercial product availability, compactness, supporting both RZ and non-return-to-zero (NRZ) data format, possible signal regeneration and noise suppression, and high operation speed. With RZ data, SOA-MZIs also can be deployed with a differential scheme to operate beyond the speed limitation of the SOAs in the standard scheme to up to 80 Gb/s [82]. Moreover, SOA-MZI is a switching element that is widely used in a broad area of applications in optical communications, which allows massive production to reduce the cost. In the LASAGNE project, almost all the subsystems consist of signal or cascaded SOA-MZIs for various functionalities, such as *label/payload separation*, *label comparison*, *all-optical flip-flops* and *wavelength conversion*. Several SOA-MZIs can be integrated on a single chip. Furthermore, the working principle and schematic of XPM in an SOA-MZI are simple and straightforward, requiring no more complexity than any of the other methods reported. MWC can be easily achieved by providing a data signal and several continuous waves (CWs) on the desired probe wavelengths to the interferometric ports of an SOA-MZI device.

Previous demonstrations using SOA-MZIs for MWC were reported as individ-

ual experiments [59, 60, 67, 69, 71]. In [71], an additional high-power assist light was employed for MWC at 10 Gb/s. In [59], differential mode was used for 10 Gb/s operation, and no BER results were shown for 40 Gb/s operation. Moreover, with the unequal channel spacing and large signal detuning employed in [59], the negative influence of the FWM interference could not be identified and evaluated.

In this chapter, systematic simulation and experimental characterizations on the performance and limitations of ITU standard 200 and 100 GHz spaced MWC at 10 Gb/s and 40 Gb/s based on single SOA-MZIs are presented. The behaviors of the MWC regarding the channel performance variations under different parametric conditions are analyzed. It is identified and proved that high-order FWM interference is an important performance limiting factor for the maximum number of simultaneously converted channels under equal wavelength spacing. The chapter is organized as follows. In Sec. 6.2, we describe the general setup and explain the operation principle. In Sec. 6.3, simulations results on SOA-MZI-based MWC are presented and discussed. In Sec. 6.4, experimental performance is demonstrated and analyzed. Finally, Sec. 6.5 summarizes and concludes the chapter.

6.2 Setup and operation principle

In order for the results to be comparable, simulation and experimental parameters and configurations for the performance evaluation were largely kept the same, as shown in Fig. 6.1. In both simulations and experiments, ITU standard channel spacing of 200 or 100 GHz were employed. Slightly different power levels were applied in simulations and different sets of experimental measurements for characterization and optimization purposes. Regarding the experiments, due to the limited number of laser sources, only one-to-four MWC was investigated. As for the simulations, MWC to four and eight channels was analyzed.

The data signal (Tx) was generated by externally intensity-modulating a CW tunable laser source or a train of optical pulses with a pseudorandom bit sequence (PRBS) to obtain NRZ and RZ signals, respectively. The signals were then optically amplified by an erbium-doped fiber amplifier (EDFA). Four CWs or more were combined and launched in the co-propagating direction with the data signal. Polarization controllers (PCs) were included to adjust the polarization of each channel in order to optimize the performance. Right after the SOA-MZI, an optical spectrum analyzer (OSA) was placed to monitor the output spectrum of the MWC. Finally, the converted wavelength channels were individually selected by

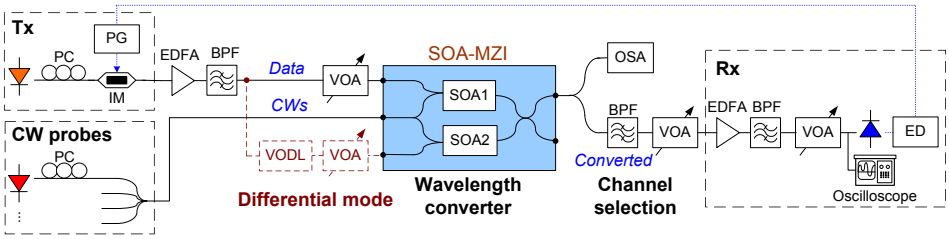

Figure 6.1: General setup for simulations and experiments of MWC via an SOA-MZI. (Tx: transmitter; PC: polarization controller; IM: intensity modulator; PG: pattern generator; CW: continuous wave; EDFA: erbium-doped fiber amplifier; BPF: band-pass filter; VOA: variable optical attenuator; VODL: variable optical delay lines; OSA: optical spectrum analyzer; Rx: receiver; ED: error detector.)

an optical bandpass filter (BPF) and detected by a pre-amplified receiver (Rx) for bit-error rate (BER) tests. The other BPFs in the setup were used to remove the out-of-band amplified spontaneous emission (ASE) noise from the EDFAs. Variable optical attenuators (VOAs) were deployed in several parts of the setup to adjust the optical power to appropriate values. When differential mode was configured, a variable optical delay line (VODL) and a VOA were employed to tune the time and optical power difference between data streams traveling in the upper and lower arms of the MZI.

MWC performance evaluation at both 10 Gb/s and 40 Gb/s was carried out. At 10 Gb/s, the SOA-MZI was operated in the standard configuration where NRZ-coded data were sent to only one of the two data input arms. Wavelength conversion is obtained through phase shift on the CWs injected into the middle arm, induced via XPM. The MZI translates the phase modulation into an amplitude modulation [58]. As the phase change is only weakly dependent on the wavelength, input data can be simultaneously transferred onto the multiple probe wavelength channels [71]. At 40 Gb/s, the differential mode was employed, shown in Fig. 6.1 with dashed lines. The RZ data format was applied. The differential mode requires a delayed and attenuated signal traveling in the lower arm to cancel the long tailing edge of the phase shift in the CW due to the slow SOA recovery time. The output data width and shape are determined by the delay time and the optical power difference between the data signals in the separate arms of the MZI. Due to the random nature of the data pattern, the two data pulse streams require bit-level synchronization.

6.3 Simulation modeling and results

VPItransmissionMaker™ *WDM* simulator is used to carry out simulations of MWC at 10 Gb/s and 40 Gb/s. The SOA-MZI wavelength converter in *VPI* deploys a standard traveling wave SOA model [127–129]. This model assumes a polarization-independent SOA that can handle signals with arbitrary polarization states. Besides, this model neglects *SOA gain dispersion* and *internal ASE noise*.

Neglecting *SOA gain dispersion* means that the SOA gain spectrum is independent of the wavelength, which is valid as long as the bandwidth of the optical signals is significantly smaller than the amplification bandwidth. Typically the SOA amplification bandwidth is in the order of several tens of nanometers. Most standard SOAs have a gain spectrum of around 30 nm when used as wavelength converters. This sets one limitation on the maximum possible number of channels for MWC, because the input data signal and the CW probes to be injected into the SOA-MZI must be within this range. For our simulations with up to eight channels at 200 GHz channel spacing, this condition is always fulfilled. Simulations with more than eight channels at both 100 and 200 GHz channel spacing have also been carried out, however, with more than eight channels, the simulations demand so much computing power that the *VPI* could not measure all the MWC channel performance simultaneously. Thus the results of more than eight MWC channels are not as reliable.

The *SOA internal ASE noise* is not critical for our MWC scheme. Although neglecting the ASE noise can result in overoptimistic estimation of the optical signal-to-noise ratios (OSNRs), it is not an influencing factor for the MWC system performance. ASE can be critical in systems where several ASE sources are cascaded, in which case the degraded OSNRs of the optical signals can affect significantly the correct detecting of the signals at the receiver.

The longest available PRBS signal pattern length in *VPI* is 2^{23}-1, which was employed in all simulations. The physical parameters of the simulated SOA-MZI in *VPI* are specified in [126, 130], which are also given in Table B.1. Other simulation parameters are summarized in Table 6.1.

6.3.1 MWC simulations at 10 Gb/s

The *VPI* simulation schematic for one-to-four MWC at 10 Gb/s follows the standard configuration illustrated in Fig. 6.1. Reference is made to Sec. B.2.1 for details of the VPI simulation setup. In all the simulations at 10 Gb/s bit rate, the

Table 6.1: Simulation parameters.

Data Rate	Channel Configuration	I_{bias} (mA)		P_{in} (dBm)	
		SOA1	SOA2	Data1/2	CW Total
10 Gb/s	200 GHz / 4CH	313	281	-1	0
	200 GHz / 8CH	300	270		
	100 GHz / 4CH	350	320		
40 Gb/s	200 GHz / 4-8CH	300	305	6.5/0.5	7

original signal channel wavelength was set to 1541.35 nm. The detuning of the CW channel that was closest to the signal channel was 400 GHz. The injection current to SOAs was optimized for each set of simulations to obtain the best MWC results, shown in Table 6.1.

a. 200 GHz channel spacing, one-to-four MWC

Fig. 6.2 (a) presents the simulated output spectrum of the MWC. The data in the original signal channel were copied onto all the CW probe wavelength channels. The SOA-MZI showed good conversion efficiency, because of the gain provided by the SOAs and the fact that the SOA-MZI converts phase modulation into amplitude modulation.

From Fig. 6.2 (a), several FWM contributions due to the SOA nonlinear effect can be seen aside the input channels. Although the out-of-band FWM satellite signals were significantly weaker than the MWC channels, the optical powers of the in-band FWM products were comparable to that of the MWC channels, which consequently influenced the BER performance and the eye opening of the converted channels, shown in Fig. 6.2 (b) and (c). In experiments, such FWM interference can be minimized by adjusting the polarizations of the input channels because FWM phase matching conditions are strongly polarization dependent.

In Fig. 6.2 (b), the BER results of the four converted channels as well as the original input channel are plotted. As we can see, the negative impact of the FWM byproducts on the four-channel MWC performance was not very pronounced, for the maximum power penalty among the four channels was around 0.5 dB. Nevertheless, the larger power penalties were related to the channel 1 (Ch1) and channel 4 (Ch4), the two outer channels that suffer most from the in-band FWM crosstalk.

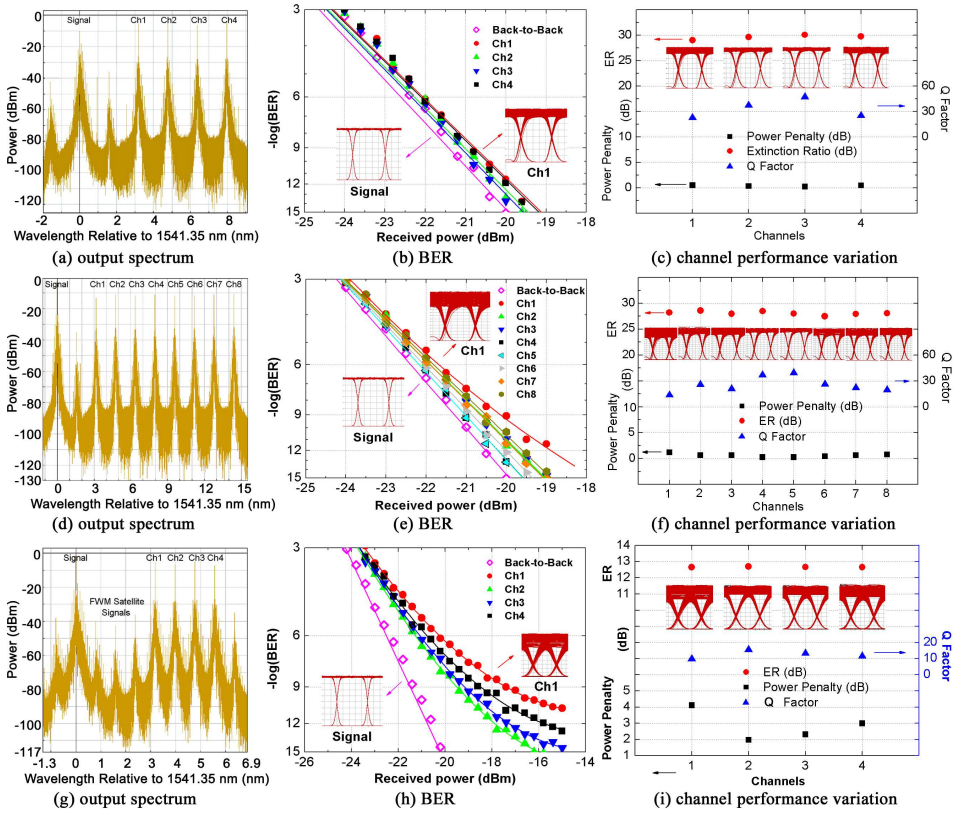

Figure 6.2: Simulation results at 10 Gb/s: (a)-(c) 200 GHz spacing, 4 channels; (d)-(f) 200 GHz spacing, 8 channels; (g)-(i) 100 GHz spacing, 4 channels.

These FWM components, which carry exactly the same data as the desired channels, were generated inside the bandwidth of each converted channel. However, the ones inside the outer channels were weaker than the ones in the central channels, and thus had lower amplitudes. This reduced the upper part of the eye opening of the outer channels, and therefore, caused eye distortion at the logical *one* level of the converted channels. The consequence of such distortion was that the converted eye diagrams had an obviously *thicker one* level, which is illustrated in the Ch1 eye diagram inset in Fig. 6.2 (b).

In Fig. 6.2 (c), the extinction ratios (ERs), power penalties and Q factors of the converted channels are presented. Note that due to the fact that in an ideal simulation environment, there is no external influence such as noise and temperature

fluctuations, or hardware imperfections such as loss and reflections, the absolute values of the ERs and Q cannot represent the performance of the system in realistic conditions. However, the relative values of these parameters can reflect channel- and simulation configuration-dependent performance characteristics, because free from other impacts, the simulation results reveal primarily the effects of the nonlinear interactions in the system.

Figure 6.2 (c) confirmed that the outer channels had worse eye quality. Nevertheless, all the four channels exhibited clear and open eye diagrams, which agrees with the error-free operation of the MWC and the low power penalties achieved.

b. 200 GHz channel spacing, one-to-eight MWC

Fig. 6.2 (d) presents the output spectrum. The output OSNRs were still high but the FWM satellite signals were much stronger now that there were more interacting channels. From the BER results in Fig. 6.2 (e) and channel parameters in Fig. 6.2 (f), it was observed that the impact of the in-band FWM products was also severer. Not only the power penalty of Ch1 increased to more than 1 dB, but a slight error floor tendency also appeared in Ch1. Comparing to the second worst channel, Ch8, Ch1 had an extra 0.5 dB penalty at the BER of 10^{-9}. Moreover, from the eye diagrams presented in Fig. 6.2 (f), Ch1 suffered more from the FWM contributions. This is because Ch1 was the closest channel to the high-power modulated input data channel, and thus more higher-order FWM byproducts were generated inside the bandwidth of Ch1, which resulted in a higher degree of eye closure and distortion.

Fig. 6.2 (f) reveals the same channel characteristics observed in the one-to-four MWC, in that the outer channels had worse quality than the central channels with respect to the Q values and power penalty. The ERs of the converted channels were not affected by the FWM contributions, though on average the ERs were slightly lower than those in the four-channel case. This is probably due to the fact that some energy from the desired MWC channels at logical 1 level was transferred to the increased number of FWM byproducts.

c. 100 GHz channel spacing, one-to-four MWC

Simulations were carried out with reduced channel spacing of 100 GHz. Fig. 6.2 (g) presents the output spectrum. With signal detuning still kept at 400 GHz, there are more FWM satellite signals due to the halved channel spacing. The BER

results in Fig. 6.2 (h) indicate obvious error floors in all the four channels, with the simulated power penalty increased to 2-4 dB at the BER of 10^{-9}. The eye patterns and channels parameters in Fig. 6.2 (i) show higher degrees of degradation due to stronger nonlinear interactions. The behavior of the channels is in accordance with the observations from the previous simulations, but the simulated values of ERs and Q were much lower. The degradation of the ERs and Q factors is in accordance to the worse BER results in Fig. 6.2 (h). By reducing the input power of the data signal and the CW probes, the performance of the 100 GHz spaced MWC could be improved, but the power penalties were still larger than those in the 200 GHz cases due to stronger FWM interactions.

Some other simulations were carried out at 100 GHz channel spacing with more than four MWC channels, but the results were much worse [130]. Those results are not included in this thesis. Reference is made to [130].

6.3.2 MWC simulations at 40 Gb/s

40 Gb/s MWC based on this SOA-MZI model had to be carried out under *differential mode* in order to avoid the effects of the slow SOA carrier dynamics [59]. The *VPI* simulation schematic is shown in Fig. B.2. This setup includes the differential mode that is indicated in Fig. 6.1. At 40 Gb/s, we did not obtain any numerical estimation on the MWC performance in terms of BER measurement because *VPI* did not yield any results with the differential configuration.

In these simulations, the original signal channel wavelength was set to 1556 nm. 400 GHz signal detuning and 200 GHz CW channel spacing were used. For 40 Gb/s RZ signals, these minimum spectral spacings between the adjacent channels are necessary to avoid significant inter-channel crosstalk. The corresponding delays on the two data paths were 4 ps and 10 ps, respectively. In the simulations, a minimum power difference of 6 dB between the two data paths was required to enable the proper operation of the differential mode, while increasing the power difference up to 10 dB did not have any visible influence on the switching performance based on eye pattern observation.

a. 200 GHz channel spacing, one-to-four MWC

The spectrum obtained at the output of the SOA-MZI is presented in Fig. 6.3 (a). The simulated RZ spectra of the converted channels are difficult to distinguish because of all the RZ discrete spectral tones at multiples of the clock frequency.

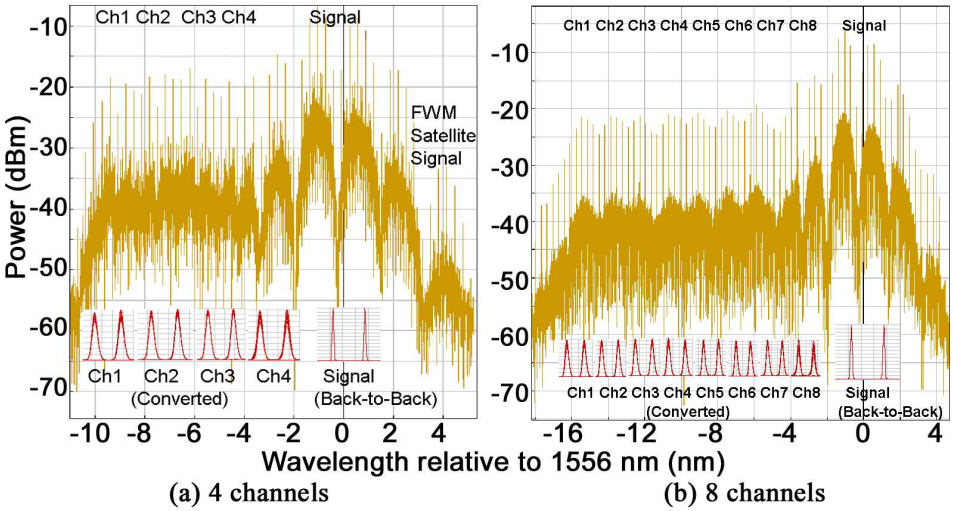

Figure 6.3: Simulation results at 40 Gb/s: optical spectrum at SOA-MZI output with eye diagram insets.

However, the eye diagram insets of the MWC signals, also shown in Fig. 6.3, are clear and open. As in the previous 10 Gb/s simulations with NRZ signals, we again perceived the FWM influence in degrading the outer channels (Ch1 and Ch4).

b. 200 GHz channel spacing, one-to-eight MWC

The eye patterns for one-to-eight MWC shown in Fig. 6.3 (b), are still clear and open. As before, the bordering channels were more affected by the in-band FWM byproducts, especially the channel that was closest to the input signal wavelength (Ch8).

6.3.3 Conclusions on simulation results

The presented simulation results indicate good feasibility of employing an SOA-MZI for MWC applications such as optical layer data multicast. At 10 Gb/s, the simulated power penalties were small, with clear and open converted eye patterns. At 40 Gb/s, widely open eye diagrams were also obtained with differential operation.

The observations in all the simulations lead to the following conclusions: i)

With increased number of channels and reduced channel spacing, the performance of the MWC tend to decrease. ii) Individual channel performance is strongly influenced by the in-band high-order FWM products, which is related to the position of the wavelength channel among all the input wavelengths. In general, the outer converted channels have the worse performance, with the two bordering channels suffering most from the FWM interference. Usually the MWC power penalty gradually decreases from the channel that is furthest from the input data channel, to a minimum value around the central channel, and then gradually increases again until it reaches a maximum value for the channel that is closest to the data signal. The Q factors of all the converted channels follows the opposite trend to that of the power penalty. iii) The in-band FWM byproducts degrade the converted eye diagrams by lowering the eye opening due to their comparably smaller optical amplitudes, therefore the influenced eye patterns have a thickened logical *one* level. However, such high-order FWM interference does not affect the ERs of converted signals. Therefore the ERs of all the converted channels generally retain a certain level if all input CW probes are injected with uniformed optical power.

The SOA model in the *VPI* does not take into account the internal ASE nose, which resulted in the overoptimistic estimation of the OSNR values of the MWC channels as shown in Fig. 6.2 (a) (d) (g), in which the OSNRs of the converted channels are mostly around 70 dB or more. Although these OSNR values are not realistic, it can be seen from the BER results and the eye diagrams in Fig. 6.2 that the major limiting factor of the MWC system performance is the significance of the physical impairments due to the FWM products. Therefore, employing such SOA model without ASE noise is reasonably realistic for our simulation purposes.

6.4 Experimental characterization and results

In order to validate the feasibility and assess the lab performance of SOA-MZI-based MWC, experiments at both 10 Gb/s and 40 Gb/s were carried out. All components employed in the experimental setups, including the integrated SOA-MZIs, are commercially available. In all experiments, ITU standard 200 GHz or 100 GHz spaced wavelengths were deployed. The input data signal was configured with PRBS of pattern length 2^{31}-1. Both SOA-MZIs we used were for 10 Gb/s standard operation speed. Other experimental parameters are summarized in Table 6.2.

At the output of the SOA-MZI, there are two VOAs. The first VOA right

Table 6.2: Experimental parameters.

Data Rate	Channel Configuration	I_{bias} (mA) / θ (V)		Ave. P_{in} (dBm)	
		SOA1	SOA2	Data1/2	CW Indiv.
10 Gb/s	200 GHz / P5	283.11	282.17	0.3	-6
	100 GHz / P5	323.60	312.50	-1.1	
	100 GHz / P4	242.96	310.95	-1.2	
40 Gb/s	600 GHz det.	400/7.8	400/0	7.3/-3.0	3.3∼6.1
	700 GHz det.	400/8.0	400/0	11.6/1.3	3.4∼5.0

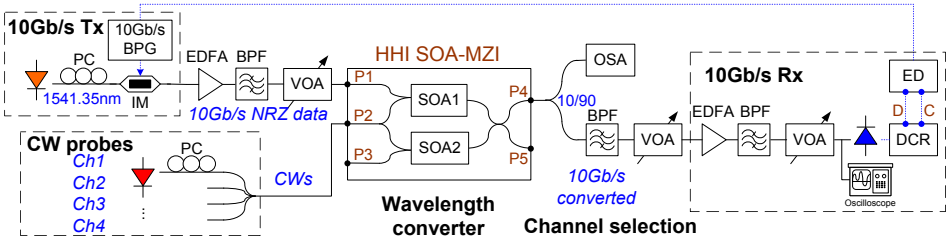

Figure 6.4: Experimental setup of MWC via an SOA-MZI at 10 Gb/s.

before the receiver was used to attenuate the selected MWC channel step by step for measuring the BER. The second VOA right before the PD is to reduce the optical signal power to around 0 dBm for the proper detection at the PD.

6.4.1 MWC experiments at 10 Gb/s

Fig. 6.4 shows the experimental setup for the 10 Gb/s MWC demonstration, where all-optical wavelength multicast via an SOA-MZI was achieved by launching a data signal and four CWs on the desired wavelength channels to the interferometric ports of the device. The monolithically-integrated SOA-MZI wavelength converter was manufactured by Heinrich Hertz Institut (HHI). Both SOAs were 1-mm long. The NRZ data signal was generated by externally modulating a tunable CW laser source tuned to 1541.35 nm. Four 200/100 GHz spaced CWs starting from 1544.53 nm were combined by a four-to-one coupler and launched in the co-propagating direction with the data signal. The total input power to P2 was around 0 dBm

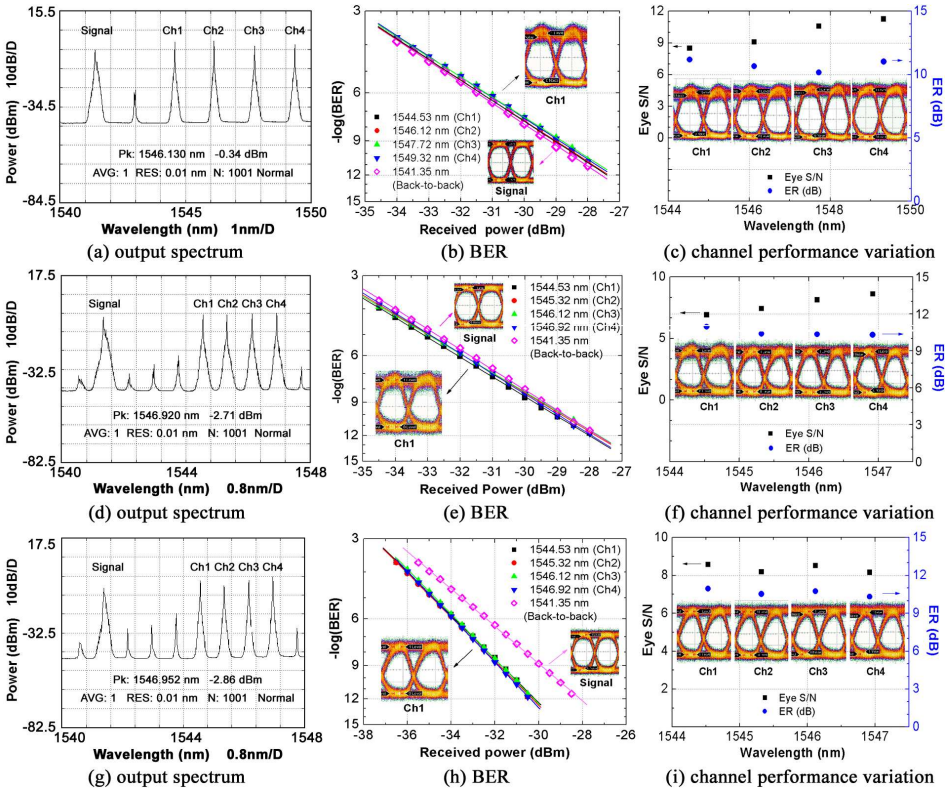

Figure 6.5: Experimental results at 10 Gb/s: (a)-(c) 200 GHz spacing, output P5; (d)-(f) 100 GHz spacing, output P5; (g)-(i) 100 GHz spacing, output P4.

at the output of the coupler with each individual CW channel alone adjusted to about -6 dBm. At the SOA-MZI output ports, a BPF of 0.3 nm narrow bandwidth was used for the channel selection. Simultaneously wavelength converted channels were obtained at both arms P4 and P5, and sent for the BER test. All the BER measurements, including the back-to-back one, were performed under the same default eye detection threshold level at the BER tester.

a. 200 GHz channel spacing, MZI output port P5

Fig. 6.5 (a) presents the output spectrum. The input signal had an ER of 12.33 dB. Its OSNR before the VOA was 56 dB, measured by an OSA with 0.01 nm resolution. The output OSNRs for the converted channels were within the range

of 40∼43 dB. Compared to the simulation results where an SOA model without internal ASE noise was used, the experimental OSNR values are generally worse because of the ASE noise from the SOAs [82]. The spectrum revealed an *average* 3.4 dB peak power ratio of the individual converted channels to the signal channel after the SOA-MZI MWC. Out-of-band FWM components were at least 25 dB weaker than the desired channels. Although the in-band FWM products were expected to be much stronger, their negative influence on the BER performance was negligible, as shown in Fig. 6.5 (b). The power penalties of the four channels at BER = 10^{-9} were within the range of 0.14∼0.39 dB.

The reasons that the experimental results were better than those in the simulations are: i) The SOA-MZI in *VPI* employs a basic standard SOA model with slow recovery time, while the HHI SOA-MZI we used in the experiments has an operation speed of 10 Gb/s up to 20 Gb/s; ii) The SOA model in the simulations is insensitive to the signal polarizations, however, in experiments, it is possible to optimize the output channel performance by adjusting the incoming signal polarizations so that the FWM degradation is minimized.

Fig. 6.5 (c) demonstrates the output eye signal-to-noise ratios (S/N) and ERs of the four simultaneously converted channels including their eye diagram snapshots, measured by an oscilloscope with 40-GHz bandwidth limit. All the channels showed clear and widely open eyes with eye S/N's ranging from 8.50 for Ch1 to 11.27 for Ch4, and an average ER of 10.76 dB.

b. 100 GHz channel spacing, MZI output port P5

The input signal and the converted channel OSNRs were 55 dB and 40∼41 dB, respectively. The input ER was 14.18 dB. After reducing the channel spacing to 100 GHz, as shown in Fig. 6.5 (d), the MWC did not exhibit noticeable BER performance degradation, plotted in Fig. 6.5 (e). The converted channels had negligible negative power penalties of 0.04∼0.30 dB at BER = 10^{-9}. The eye patterns insets in Fig. 6.5 (f) are still clear. However, compared to the 200 GHz spaced MWC, we observed a slightly smaller eye opening and more noise at both *zero* and *one* levels. The measured eye S/N's were lower, starting from 6.92 for Ch1 to 8.62 for Ch4. This is due to the stronger in-band FWM interference, a drawback of placing the channels closer to each other. The average ER of the converted channels was 10.49 dB.

c. 100 GHz channel spacing, MZI output port P4

In this experiment, we degraded the input signal OSNR to 21 dB. The input ER was 13.03 dB. All the BER measurements, including the back-to-back one, were performed keeping constant power of 0 dBm to the photo detector (PD). Even with the degraded input signal, the MWC channels at the output still had high OSNRs of 38∼43 dB. The SOA-MZI increased the original signal quality by modulating the signal phase and then translating the phase modulation into an amplitude modulation, which significantly cut down the noise level. The average peak power ratio of the individual converted channels to the signal channel after the SOA-MZI MWC was 4 dB. At the receiver, after the preamplifier EDFA and the second BPF employed to remove the out-of-band ASE, the OSNRs of all the extracted channels were within 41∼45 dB, with on average 22 dB enhancement over the input signal OSNR. This was The peak power ratio of the neighboring channels that were not completely suppressed by the filters to the selected channel was about −33 dB. By improving the OSNR of the original signals, the SOA-MZI MWC demonstrated its regeneration capability. The regeneration of the signal OSNRs were due to the redistribution of the noise in the SOA-MZI [124]. SOA-based interferometric wavelength converters have long been discovered to have the capability of reducing the noise level and hence improving the BER performance [124].

In Fig. 6.5 (h), the BER values indicated that the input data was converted to all the four channels with a receiver sensitivity improvement of 1.84 dB or more, while the sensitivity divergence among the four converted channels was measured to be no more than 0.14 dB. The observed negative power penalty confirmed once again the signal regeneration properties of the MWC.

In Fig. 6.5 (i), all the channels showed clear and widely open eyes with an average eye S/N of 8.36 and an average ER of 10.63 dB. The converted eye diagrams indicated a slightly lowered eye crossing point, which did not seem to have any negative influence on the system performance according to the BER. The clean multicast channels depicted by the eye snapshots further proved the excellent performance of the MWC for WDM applications.

6.4.2 MWC experiments at 40 Gb/s

The experimental setup for 40 Gb/s is shown in Fig. 6.6. MWC was achieved by a hybrid integrated SOA-MZI twin regenerator from the Centre of Integrated Photonics (CIP). The 40 Gb/s RZ data of 2-ps pulse width was generated by

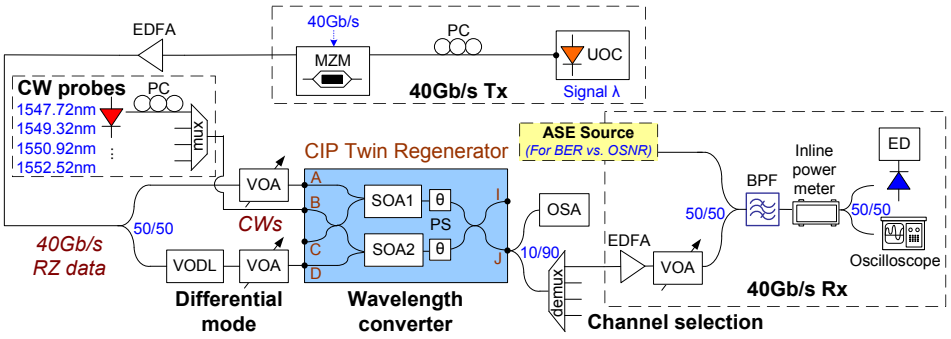

Figure 6.6: Experimental setup of MWC via an SOA-MZI at 40 Gb/s.

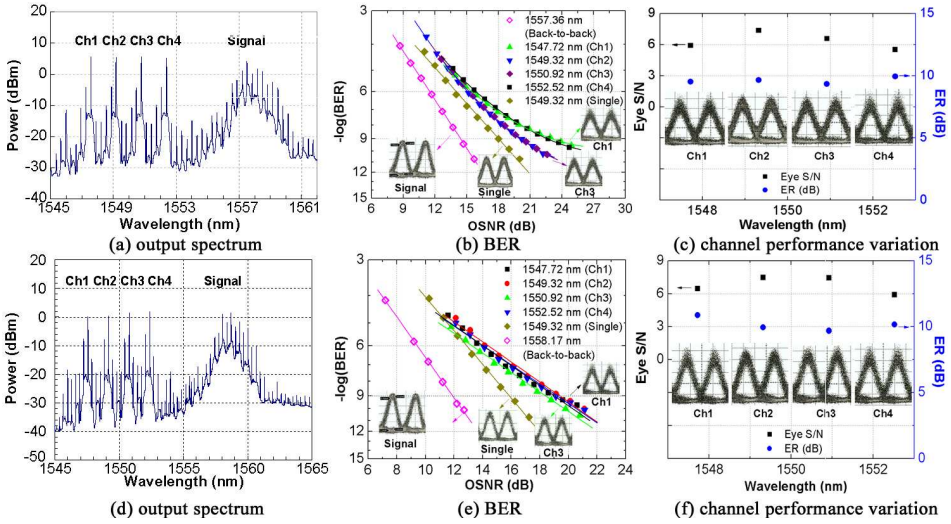

Figure 6.7: Experimental results at 40 Gb/s: (a)-(c) 600 GHz data detuning; (d)-(f) 700 GHz data detuning.

modulating a 40 GHz ultrafast optical clock (UOC) using a Mach-Zehnder modulator (MZM) with 40 Gb/s PRBS. An EDFA was used to compensate for the power loss in the modulation process. The data signal was tapped onto both of the SOA-MZI arms A and D using a 50/50 coupler, with the lower data path delayed by a VODL to achieve the differential mode. Four 200 GHz spaced CWs at wavelength 1547.72∼1552.52 nm were combined by a multiplexer and injected in the co-propagating direction into the SOA-MZI port B.

Both SOAs were pumped with 400 mA maximum allowed current to facilitate fast recovery time, while in the upper arm a phase shifter (PS) after the SOA1 was controlled with a voltage to obtain non-inverted output at MZI output *J*. After MWC, the converted data signals were demultiplexed and individually fed to a pre-amplified receiver and an ED. The -3 dB bandwidth of all the optical filters including the (de)multiplexers was 130 GHz. For the BER measurement, signal OSNR was degraded at the PD input by increasing the ASE noise level while keeping the signal power constant at -1 dBm to ensure linear operation of the electrical circuitry. The ASE noise was increased at the ASE source in Fig. 6.6, which in our case was an EDFA. The OSNR was taken using an inline power meter before the PD by disabling sequentially the signal or the ASE. The receiver had an electrical bandwidth of 37 GHz.

a. 200 GHz channel spacing, 600 GHz detuning

The 2-ps pulse source from the UOC was tuned to 1557.36 nm. The differential delay between the two data streams was around 6.5 ps. Fig. 6.7 (a) shows the output spectrum. The FWM satellite signals at both sides of the converted channels were at least 17 dB weaker than the converted channels. In Fig. 6.7 (b), the BER is plotted as a function of the OSNR at the PD input for the MWC channels, back-to-back reference as well as a single wavelength conversion (SWC). We observed a 3.6 dB OSNR penalty at BER of 10^{-9} for the SWC to 1549.32 nm. Since the input data signal had a very narrow pulse width with high OSNR and ER, the penalty was probably due to the change in the pulse shape inside the SOA-MZI which reduced the OSNR after the signal was converted. The MWC channels demonstrated a minimum 2 dB OSNR penalty with regard to the SWC. Ch1 and Ch4 also had a slight error floor, which caused the OSNR sensitivity variation of another 3 dB at BER of 10^{-9} from the two central channels. The worse performance of the outer channels due to the in-band FWM interference can also be observed from the eye snapshots presented in Fig. 6.7 (c). The average ER for the four channels was 9.61 dB, with the largest ER difference among two different channels no greater than 0.61 dB.

b. 200 GHz channel spacing, 700 GHz detuning

To reduce the crosstalk from the input signal, a second set of measurements was made with the data channel moved to 1558.17 nm. The lower data path was

delayed for 7.6 ps after optimization of the output eye quality and BER. Fig. 6.7 (d) presents the output spectrum. The out-of-band FWM by-products were more than 20 dB weaker. Fig. 6.7 (e) shows all the BER curves. The average OSNR penalties of the MWC channels at BER equal to 10^{-9} were 3.5 dB relative to the SWC, and 7 dB to the back-to-back reference. In this experiment, less than 1 dB OSNR sensitivity difference among all the MWC channels was achieved and no error-floor was observed. In Fig. 6.7 (f), a clear eye opening can be seen. The oscilloscope measured an average ER of 10.16 dB for the MWC channels, with the worst ER being 9.68 dB.

6.4.3 Conclusions on experimental results

The experimental results confirmed previous observations in simulations, and proved the promising performance of all-optical MWC by XPM in an SOA-MZI. Error free operation was achieved. Clear, open eye diagrams and negligible performance difference among all the MWC channels at both 10 Gb/s and 40 Gb/s were obtained. For the investigated experiment configurations, the FWM byproducts did not seem to be a limiting factor for the maximum number of channels, nor for the deployed channel spacing. By increasing the number of CW probes or reducing their channel spacing, the demonstrated schemes can accommodate more channels. With faster SOA dynamics, XPM-based wavelength converter can operate at higher bit rates up to 80 Gb/s [82].

However, unlike in simulations, experimental results are influenced by various optical and electrical noises, and the total CW power to the SOA-MZI is constrained by the maximum input power limit of the device. Due to the fact that such influences and limitations do not exist in our simulations, the maximum number of MWC channels in the simulations is only determined by the impairments caused by FWM, as discussed in Sec. 6.3.3. In the experiments, when increasing the number of CW channels, the optical power of each channel may need to be reduced accordingly, and thus the performance of each channel declines. Therefore, under realistic circumstances, the maximum number of MWC channels is determined by acceptable performance of all the channels under the combination of the following conditions: i) the narrow dynamic range of the total input CW power and data signal power to the device [82], usually no more than 10 dBm per port; ii) SOA gain spectrum, with typical usable bandwidth of less than 30 nm; iii) employed channel spacing, depending on the data bit rate and modulation format.

With the devices and experimental setups that *we* used, we expect the number of MWC channels can be increase to around eight or more at 200 GHz channel spacing for both 10 Gb/s and 40 Gb/s operation. However, at 40 Gb/s, a rather high penalty is expected if the number of MWC channels is more than four. In general, the maximum number of MWC channels achievable is highly dependent of the characteristics of the SOA-MZI device, other components in the setup, and the minimum performance requirements for the converted channels.

6.5 Summary and discussions

In this chapter, extensive simulation and experimental characterizations of single SOA-MZI-based MWC at both 10 Gb/s and 40 Gb/s bit rates are presented. The results confirm the promising performance of the MWC with standard ITU channel spacings for WDM applications in future high capacity, high transparency optical networks. Moreover, MWC system performance as well as channel-specific performance with different channel spacing and data rates are analyzed and discussed. Finally, the major restrictions on the maximum number of MWC channels and their wavelength configurations are identified and summarized.

The experimental results at 10 Gb/s reveal signal regeneration possibilities of an SOA-MZI for MWC. This feature is particularly desirable for WDM network nodes as in practice, optical cross-connects inside a network often do not receive clean input signals directly from the source, but degraded optical data channels with impaired OSNRs due to cascaded optical amplifiers they have passed through across long distances. Optical signal regeneration capabilities thus improve the quality of the incoming data to allow for further propagation in the optical layer without the necessity of OEO conversion and electronic regeneration.

SOA-MZIs are used for various functionalities and can be massively produced and integrated to reduce cost. Based on the results, it is believed that single SOA-MZI-based MWC is suitable for various applications in next generation all-optical infrastructures, where optical layer wavelength multicast is a most desirable feature for the increasing volume of multimedia on-demand data services.

Chapter 7

Fiber-based multi-wavelength conversion via four-wave mixing

Four-wave mixing (FWM) in nonlinear fibers has the potential for multi-wavelength conversion (MWC) of signals with any pulse shape at speeds of 1 Tb/s and beyond. Compared to FWM in semiconductor optical amplifiers, FWM in nonlinear fibers generally offers a much wider conversion bandwidth with a flatter conversion efficiency response. In this chapter, experimental performance evaluation of MWC by FWM in a commercially available dispersion-shifted fiber is presented at 10, 20 and 40 Gb/s. In particular, multiple-channel crosstalk induced by high-order FWM products and the general conditions of such crosstalk occurrence are analyzed. Moreover, the dependence of the optical power efficiency on the input probe wavelengths and probe power is characterized. Up to three-channel MWC at 40 Gb/s confirms the transparent and channel-independent MWC operation with good performance. The employed MWC scheme can make use of a noise compression effect at the logical zero level to achieve improved Q factors in the converted channels. However, strong inter-channel crosstalk occurs when the input channels are equally spaced in the frequency domain. Due to the limited laboratory resources, no bit error rate measurements can be shown. Parts of this chapter are based on publications.[1]

[1] See references [70, 101].

7.1 Introduction

Wave mixing is a widely explored nonlinear phenomenon and is at the moment the only wavelength conversion technique that provides strict data rate and modulation transparency [85]. Although with a proper semiconductor optical amplifier (SOA) design, four-wave mixing (FWM) in an SOA can possibly provide conventional wavelength conversion over a range of 80 nm [82], *multi-wavelength conversion (MWC)* by means of FWM in an SOA cannot make use of all this bandwidth because of the largely uneven and asymmetric conversion efficiency [85, 93]. Moreover, FWM in an SOA also suffers from the bit rate restriction due to the SOA operation speed and patterning effects [85, 90, 93, 98]. On the contrary, MWC by FWM in nonlinear fibers is believed to have no such limitations, and has attracted considerable interest since the 90's [85, 131–134]. Fibers with proper nonlinearity and length can accommodate a conversion range covering the entire gain bandwidth of standard C-band or L-band erbium-doped fiber amplifiers (EDFAs), or even realizing simultaneous conversion from one EDFA band to another, e.g. L-band to C-band [135].

In this chapter, experimental results on *fiber*-based MWC via FWM at 10, 20 and 40 Gb/s are presented. In the experiments, a commercially available dispersion-shifted fiber (DSF) is used for MWC to up to *three* channels at *varied* channel spacing. The number of MWC channels realized in the experiments were restricted by the available laser sources in the laboratory at the time of the experiments. For one-to-two MWC at 40 Gb/s, we analyze in particular the general conditions where multiple-channel crosstalk might occur to affect the converted signal quality, as FWM is induced by the nature of interaction between/among multiple waves. Moreover, as conversion efficiency is generally the major concern for FWM wavelength conversion, we investigated the dependence of channel conversion efficiency and converted signal Q factor on the input continuous wave (CW) power levels. In all measurements, the performance of a selected MWC channel was assessed using the Q factor, as no bit-error rate (BER) tester was available at the time of the experiments.

The chapter is organized as follows. In Sec. 7.2, the basics of the FWM scheme for conventional wavelength conversion are briefly reviewed and a MWC scheme is proposed. In Sec. 7.3, experimental results of the MWC employing the proposed scheme are presented. First, MWC at different bit rates and at varied channel spacing are demonstrated. Second, crosstalk interference caused by FWM satellite

signals is investigated and analyzed. Third, power efficiency of the FWM MWC scheme is measured. Finally, Sec. 7.4 summarizes and concludes the chapter.

7.2 Setup and operation principle

As illustrated in Fig. 4.9 (a), conventional FWM wavelength conversion is achieved by injecting a moderate-power data *signal* at frequency ω_s together with an intense CW *pump* at frequency ω_{cw} into the nonlinear medium where FWM occurs. With the input of these two waves, two first-order wavelength-converted replicas are generated, one adjacent to the pump at frequency $2\omega_{cw}-\omega_s$, and the other adjacent to the data signal at frequency $2\omega_s-\omega_{cw}$. When the CW *pump* has enough optical power to induce the nonlinearity of the medium, the copy that is adjacent to the *pump* starts to grow depleting the *pump* itself. This replica is mostly selected as the *converted* signal because it has higher optical power. The required pump power threshold to induce efficient FWM is dependent of the nonlinear medium and its nonlinear properties. However, in general, the conversion efficiency of FWM-based wavelength conversion is very low.

The *first-order* wavelength converted replicas are the results of the *direct* interaction of the input waves. In reality, these new waves can also interact with each other and with the existing waves, and hence generate *higher-order* replicas. In most cases, these high-order replicas have much weaker power.

To realize MWC using FWM, several CWs need to be employed. Based on the conventional FWM wavelength conversion scheme depicted in Fig. 4.9 (a) and also described above, the most straightforward method is to increase the number of pumps at frequencies $\omega_{cw(i)}$ ($i \in \mathbb{Z}$, $i > 1$), and select the replicas at frequencies $2\omega_{cw(i)} - \omega_s$ ($i \in \mathbb{Z}$, $i > 1$), as shown in Fig. 7.1 (a). However, MWC based on this conventional FWM wavelength conversion scheme is not suitable for multicast applications. In the following text, we discuss MWC using this conventional FWM wavelength conversion scheme illustrated in Fig. 7.1 (a), in comparison to a scheme in which the modulated *signal* at frequency ω_s is used as a *pump* and several *CWs* at frequencies $\omega_{cw(i)}$ ($i \in \mathbb{Z}$, $i > 1$) are employed as *probes*, as illustrated in Fig. 7.1 (b). In the scheme (b), the replicas at frequencies $2\omega_s - \omega_{cw(i)}$ ($i \in \mathbb{Z}$, $i > 1$) are selected as the *converted* signals.

Figure 7.1 visualizes the spectra of the two MWC schemes in nonlinear fibers. In this figure, several advantages of the scheme (b) over the scheme (a) can be seen:

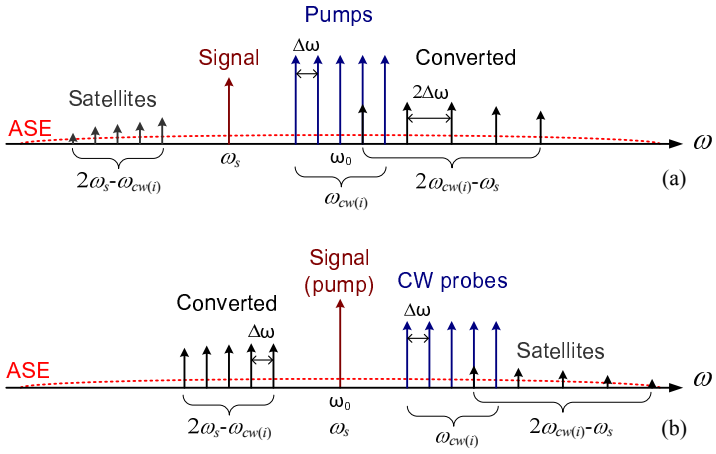

Figure 7.1: Spectra of MWC by FWM in nonlinear fibers using: (a) conventional FWM wavelength conversion scheme; (b) signal as pump scheme. (ω_0: zero-dispersion frequency of the nonlinear fiber; $\Delta\omega$: frequency spacing between MWC channels.)

– *Firstly*, the pump, which in this case is the data signal, can be easily placed at the zero-dispersion wavelength of the nonlinear fiber to achieve maximum phase-matching of the FWM process for all the wavelength channels.

– *Secondly*, the latter scheme accommodates simultaneous conversion of many more channels with lower channel interference and flatter conversion efficiency. This is because in the first scheme, as the number of the CW pumps increases, the CW pumps start to overlap with some of the converted channels, as shown in Fig. 7.1 (a). This makes it impossible to extract such a converted channel with an intense CW pump on the same wavelength. Therefore, interference between the CW pump and the converted channel occurs. Besides, flatter conversion efficiency can be achieved in the scheme (b) because the converted channels are separated in frequency by $\Delta\omega$ instead of $2\Delta\omega$, therefore these channels can take advantage of the flatter conversion bandwidth closer to the zero-dispersion wavelength of the fiber.

– *Thirdly*, the channel spacing of the converted signals in the second scheme is the same as the input CW spacing, which is twice as efficient as the first one, and allows more economical and convenient wavelength management as more wavelengths can

be converted simultaneously in the same fiber.
– *Fourthly*, instead of amplifying all *CW* channels for pump purposes as shown in Fig. 7.1 (a), only the power of the modulated *signal* channel needs to be boosted.
– *Finally*, it is theoretically and experimentally proven that the second scheme also provides a certain signal regeneration effect on the multi-wavelength converted channels [70], as discussed previously in Sec. 5.4.1. The signal regeneration is due to the quadratic nature of the MWC replicas selected at frequencies $2\omega_s - \omega_{cw(i)}$ ($i \in \mathbb{Z},\ i > 1$), whose power is proportional to the square of the data signal power [93]. This quadratic effect suppresses the noise at the logical *zero* level, as for $0 < x \ll 1$, $x^2 < x$.

In the following section, the second scheme is investigated experimentally, in which the first-order FWM replicas generated closer to the *modulated signal pump* are selected as *converted channels* as they have much higher power than the ones closer to the *CW probes*.

7.3 Experimental characterization and results

7.3.1 Experimental setup

The experimental setup is illustrated in Fig. 7.2. A commercially available International Telecommunication Union (ITU) G.653 standard single-mode dispersion-shifted fiber (DSF) of 8,859 meters long was utilized as the nonlinear wavelength conversion medium. The output signal from a tunable external cavity laser (ECL) at 1547.72 nm, the zero-dispersion wavelength of the DSF, was encoded with $2^{31}-1$ pseudorandom bit sequence (PRBS) data by a Mach-Zehnder interferometer (MZI) intensity modulator to form the 10/20/40 Gb/s nonreturn-to-zero (NRZ) data signals. The output was then boosted by an erbium-doped fiber amplifier (EDFA), and passed through an optical band-pass filter (BPF) centered at the same wavelength in order to remove the out-of-band amplified spontaneous emission (ASE) noise. The filtered signal served as the *modulated pump*.

Two other tunable ECL lasers for the multicast channels operated in CW mode as the *probe* inputs. Polarization controllers (PCs) were included to adjust the polarization of each laser at the input in order to maximize the phase-matching for the FWM process among all the channels in the DSF [94]. Two 50/50 couplers combining the optical sources provided the flexibility of tuning the CW wavelengths along the ITU 100 GHz spacing channels within the measured 3-dB effective wavelength

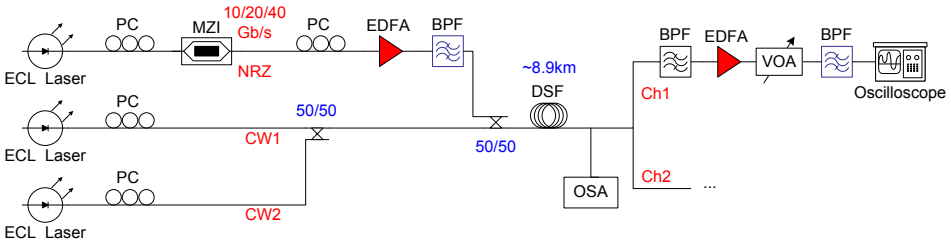

Figure 7.2: Experimental setup of MWC by FWM in DSF at 10/20/40 Gb/s.

conversion range between 1541.35∼1554.13 nm. During the MWC measurements, the CWs were operating simultaneously.

To determine the effective wavelength conversion range, a pump wave is fixed at the zero-dispersion wavelength of the fiber, while a second input wave is moved gradually in the wavelength domain further away from the pump wave. At each step, the conversion efficiency of the FWM is taken. The 3-dB effective wavelength conversion range is the wavelength range in which the conversion efficiency remains within 3 dB difference from the best conversion efficiency. Fig. 4.6 shows an example of such measurement.

After the DSF, an optical spectrum analyzer (OSA) monitored the output spectrum of the fiber. Another EDFA was used for the converted signal to allow proper detection via an oscilloscope. The first tunable BPF right after the DSF was to select the MWC channel, while the second one placed after the EDFA was to remove the out-of-band ASE noise. At the time of the experiments, there was no BER test equipment available. Therefore, only the Q factors of the output MWC channels were measured.

In the experiments, the output power of all the ECL lasers was set to be 7 dBm. After the EDFA, the data signal power was boosted to 13∼14 dBm. The MZI used was fabricated for 40 Gb/s operation. A 40 Gb/s pattern generator generated the 10/20/40 Gb/s data.

7.3.2 MWC experiments at varied channel spacing

a. One-to-two MWC at 10/20/40 Gb/s

Figure 7.3 shows the source and one of the converted channel eye diagrams under optimized polarization conditions at 20 Gb/s and 40 Gb/s. All the output channels

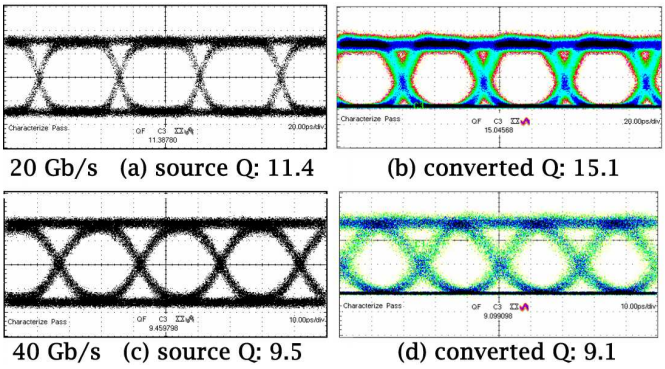

Figure 7.3: Source and converted eye diagrams with polarization optimization: (a)-(b) 20 Gb/s, 20 ps/div; (c)-(d) 40 Gb/s, 10 ps/div.

presented a clear eye opening. With MWC at 10 Gb/s and 20 Gb/s, the converted signal has higher Q factors than the source signal. The increase of Q factor was due to the quadratic nature of the FWM process, which caused the signal regeneration effect at the logical *zero* level, as previously explained in Sec. 5.4.1 in Chapter 5. While for the 40 Gb/s operation, the Q factors of the converted and source signals did not exhibit visible regeneration effect, because the speed limitation of the other devices in the setup has influenced the converted eye shape. Nevertheless, the noise compression at the *zero* level was obvious in the converted eye diagrams regardless of the high operation speed.

Figure 7.4 illustrates the spectra at the DSF output and converted eye diagrams at 10, 20 and 40 Gb/s without polarization optimization. The average Q factors for the converted channel C1 were 11.6, 11.2 and 6.2, respectively. The clear and open converted eye patterns with noise suppression at the *zero* level indicated the promising performance of the MWC. When there was no crosstalk due to the higher-order generation FWM products, the C1 Q factor fluctuations resulted from CW2 position shifting in the wavelength domain were less than 0.5 at 10 Gb/s and 20 Gb/s between 1542.92∼1544.53 nm, and less than 0.3 at 40 Gb/s between 1541.35∼1544.53 nm. The measured average MWC conversion efficiency, in this case defined as the ratio of the converted signal power to the CW power, was around −13.5 dB within the wavelength range from 1543.73∼1551.72 nm. By switching an individual CW channel off, no measurable change in the efficiency was observed. This should also hold when more than two CW channels are present,

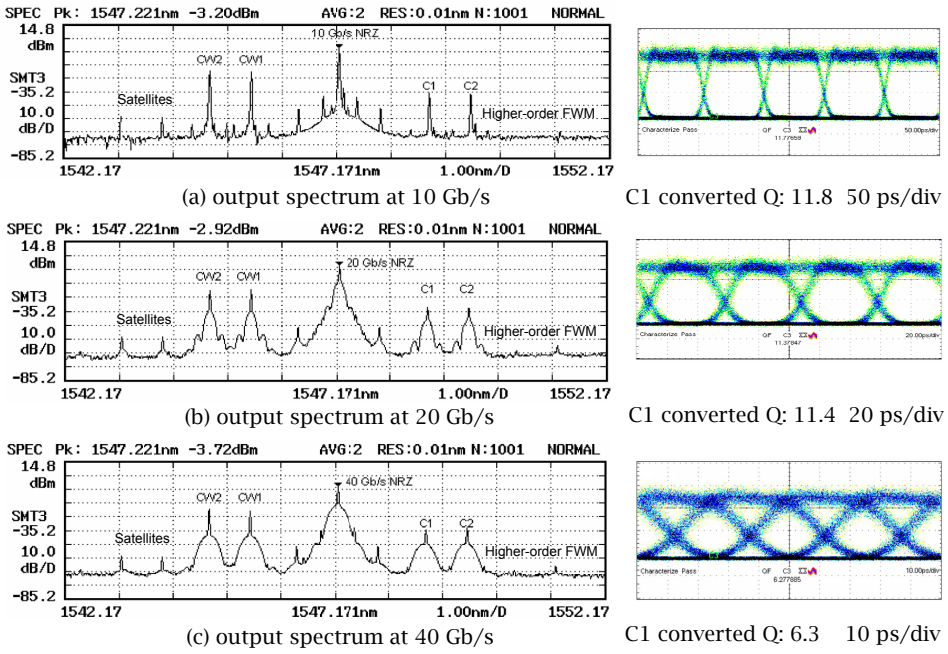

Figure 7.4: Output spectra and C1 converted eye diagrams without polarization optimization.

as the conversion efficiency of the FWM in a nonlinear fiber is dependent of the conversion efficiency response of the fiber around the zero-dispersion wavelength, not of the presence or absence of the other CW channels.

b. One-to-three MWC at 40 Gb/s

In order to test this channel independency of the FWM MWC process, a third laser was added to the setup via another optical coupler. Fig. 7.5 (a) presents the output spectrum of the one-to-three MWC at 40 Gb/s. Due to the unequal coupling, CW3 had higher power than the other two CWs. It was not possible to lower the CW3 power further. Therefore, at the output of the DSF, the corresponding MWC copy C3 also exhibited higher power than C1 and C2, as shown in Fig. 7.5 (a). The inclusion of a third MWC channel did not affect the conversion efficiency of the existing two MWC channels.

Figure 7.5 (b) shows the MWC eye diagrams of the three simultaneously con-

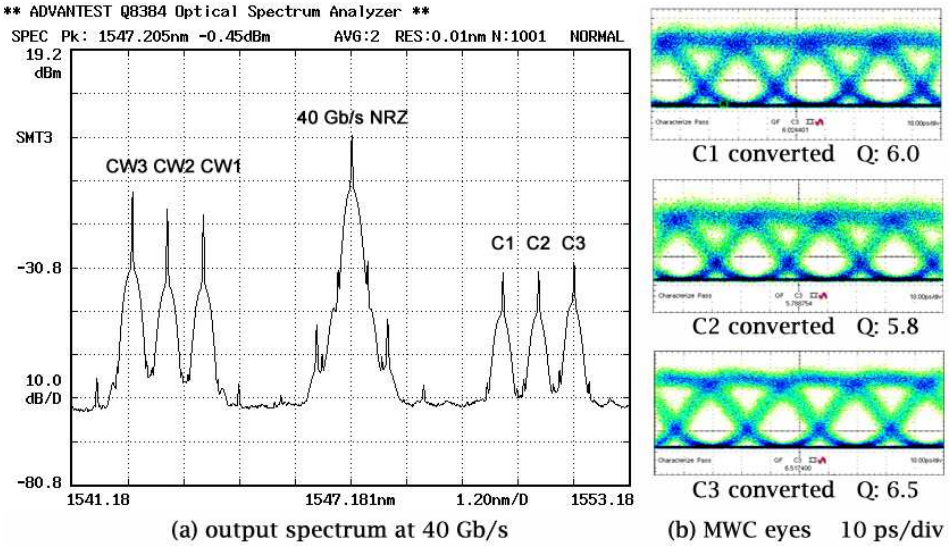

Figure 7.5: Output spectrum and all converted eye diagrams without polarization optimization.

verted channels. Without any adjustments or optimization in the setup, after switching on the third laser, all the three channels still demonstrated clear and open eye patterns with noise suppression at the *zero* level. Similar values of the Q factors to the one-to-two MWC were also obtained for all the channels. Neither the conversion efficiency nor the converted signal quality was affected by the inclusion of a third CW probe signal.

7.3.3 Crosstalk characterization

In WDM communication systems, multiple wavelength channels are generally equally spaced following the ITU standard. Due to this fact, there could be an interference phenomenon resulting from the crosstalk terms due to FWM [82]. Second or higher-order generation FWM products from the nonlinear interactions among the CW channels and the input signal channel could be generated inside the filtering bandwidth of the desired first-order replicas, which are going to be extracted together with converted copies. Consequently, an interference phenomenon resulting from crosstalk terms occurs. This degrades the eye qualities of the af-

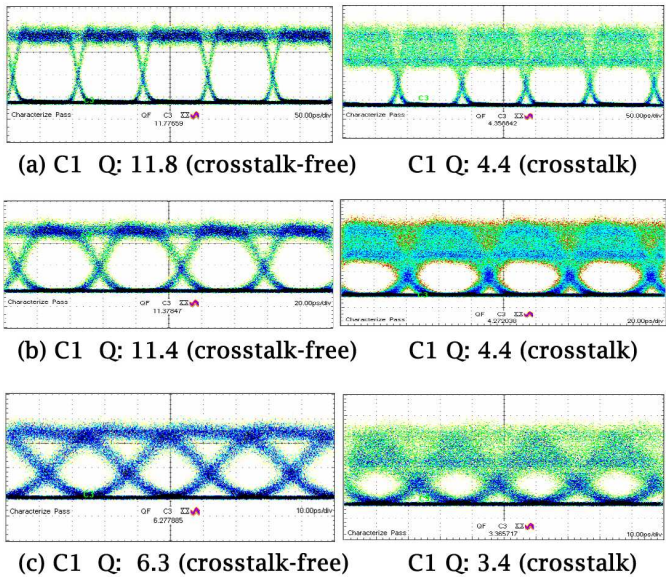

Figure 7.6: Converted eye diagrams without and with crosstalk: (a) 10 Gb/s, 50 ps/div; (b) 20 Gb/s, 20 ps/div; (c) 40 Gb/s, 10 ps/div.

fected converted channels.

Theoretically, it was then expected that in this setup, the crosstalk effect would be the worst when the signal channel and the two CW channels were placed with equal frequency spacing.

a. Crosstalk measurements at different bit rates

In Fig. 7.4, the spectra at the DSF output and normal converted eyes free of crosstalk interference are presented, at respectively 10, 20 and 40 Gb/s. The snapshots were taken when CW1 was on 1545.32 nm while CW2 was on 1544.53 nm, a crosstalk-free case. However, when CW2 was around 1543.73 nm, one of the satellite signals was generated inside the filtering bandwidth of the copy C1, which caused significant Q degradation on C1. In Fig. 7.6, converted eye diagrams of C1 are compared in the cases of no crosstalk influence and of strong crosstalk interference.

The eye patterns in Fig. 7.6 indicated that the Q degradation was mainly caused by another signal with the same data on the wavelength of the desired

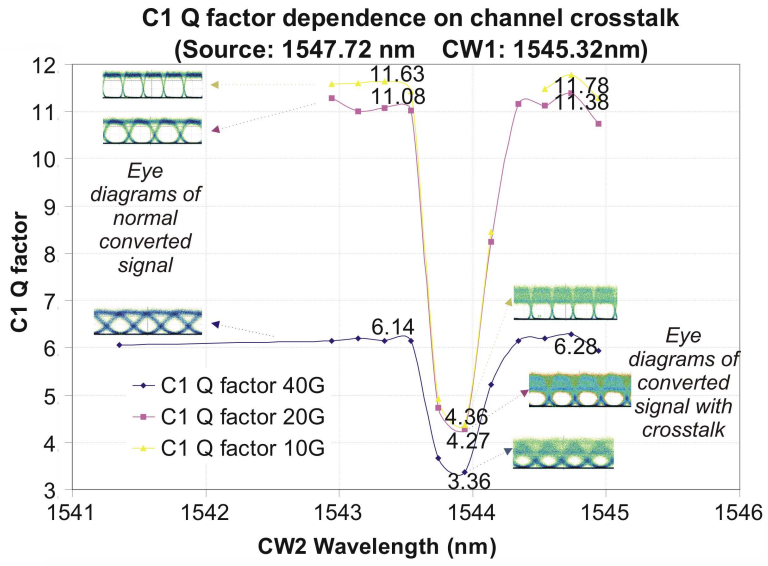

Figure 7.7: Crosstalk measurements at 10/20/40 Gb/s based on C1 Q factor.

copy, but with a different amplitude. This can be explained by the nature of the FWM process: the satellite signals carried the same information as the modulated source, and were higher-generation copies of it. Their power was much lower so that their logical *one*'s had much lower amplitude than the logical *one*'s from the first-order replicas. The quadratic nature of FWM further amplified the difference at the *one* level, which caused the closure of the upper part of the eyes. External noise played a negligible role here.

Therefore, the investigation into the crosstalk influence on the performance of one-to-two MWC at different bit rates was carried out. The evaluation was done by fixing the wavelength of CW1 while moving CW2 away from CW1 by a step of 0.2 nm along the effective wavelength conversion range of the DSF, and observing the converted C1 eye diagrams with Q measurements. Fig. 7.7 presents the C1 Q factor dependence on the crosstalk at 10, 20 and 40 Gb/s. It can be seen that when one of the satellite signals was inside the wavelength range of the modulated copy, the Q factor of its eye diagram dropped dramatically, which was about 6.8 for 10/20 Gb/s operation, and about 2.8 for 40 Gb/s operation.

From Fig. 7.7, MWC at 10 Gb/s performed the best among the three bit rates deployed, but with only about 0.5 higher Q value than the MWC at 20 Gb/s when

there was no crosstalk. In the 40 Gb/s case, the average Q factor of the converted signal was above 6.1 without interference. The big performance difference between the 40 Gb/s MWC and the 10/20 Gb/s ones was mainly because at 40 Gb/s, the operation speed of the other devices in the setup, such as the MZI modulator and the receiver, were pushed to their limit.

b. Crosstalk measurements at different channel spacing

The efficiency of the FWM process strongly depends on the spacing between the interacting waves [94]. Therefore, it is expected that when the channels are placed farther from each other, the crosstalk terms become weaker, and the performance degradation resulted in from the interference becomes less strong.

To exam the characteristics of crosstalk-related signal degradation at different channel spacing, four sets of measurements were carried out, with CW1 wavelength fixed respectively at 1546.92 nm, 1546.12 nm, 1545.32 nm and 1544.53 nm. During each set of measurements, we moved CW2 further away by a step of 0.2 nm in the wavelength domain from the fixed CW1 and the signal pump, and observed the crosstalk effect experienced by C1. By measuring the C1 Q factor with every wavelength combination, we found out the operating points that were subject most to the crosstalk terms and thus were able to identify more general crosstalk characteristics of multiple channel conversion by FWM in nonlinear fibers.

Fig. 7.8 presents the C1 Q factor dependence on the crosstalk terms with the four CW1 positions. Two complete sets of points were taken with CW1 on 1545.32 nm and 1546.12 nm. Regarding the other two CW1 wavelengths, by monitoring the spectra, only the Q factor where crosstalk took place was noted. With each set of measurements while CW1 wavelength was fixed, C1 Q factor stayed within a fluctuation range of about 0.3 with an average of 6.1 unless crosstalk occurred, where C1 Q factor dropped considerably. An average converted eye diagram without crosstalk and the worst crosstalk influenced eye diagrams from each set of measurement are shown as insets. From the figure we can see the closer the CW1 was placed to the pump signal, the more the crosstalk degraded the affected copy. When CW1 was positioned at 1544.53 nm, thus 3.2 nm away from the pump signal, the crosstalk related C1 Q factor degradation was already within the fluctuation range and the worst measured converted eye was still widely open. When CW1 was at 1545.32 nm, 2.4 nm away from the pump, the worst eye affected by the crosstalk terms was also clear and open, but with a Q degradation of about 0.9

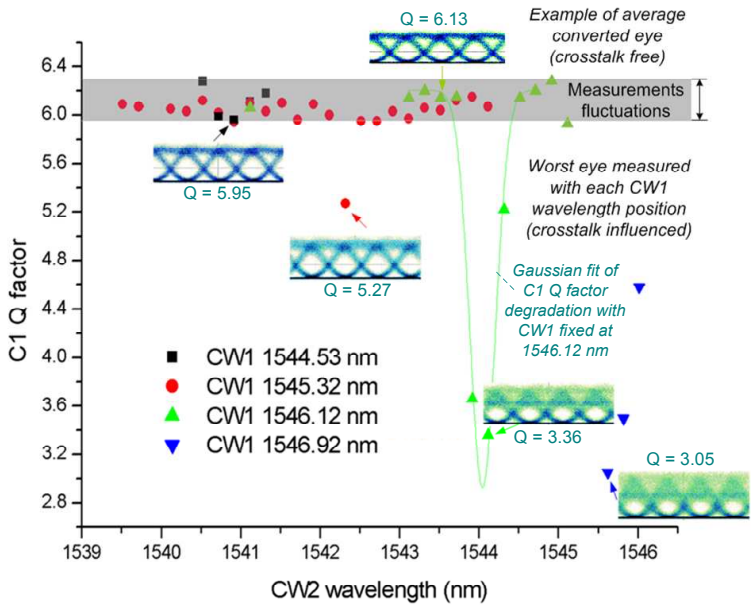

Figure 7.8: Crosstalk measurements at different channel spacings based on C1 Q factor.

from the average of no crosstalk. If CW1 was placed within 200 GHz away from the pump on either side, crosstalk would result in an eye closure of more than half of the mark amplitude. Therefore, to lower the crosstalk impact, it should be avoided to assign CW wavelengths too close to the pump signal.

In Fig. 7.8, for the data series of CW1 at 1546.12 nm, a Gaussian fit of C1 Q factor degradation with crosstalk is shown as an example of the estimated trend. The curve suggests that the measured worst point from the crosstalk interference may not be the worst case but with a small margin from where the crosstalk terms are generated exactly in the center of the desired wavelength channel.

c. Conditions of crosstalk occurrence

The measurements presented previously indicated that the generation of the crosstalk is bit-rate independent, which can be expected from the fact that FWM process itself is data rate transparent. However, crosstalk occurs at certain channel spacings of the interacting waves, which are directly related to the input wavelengths

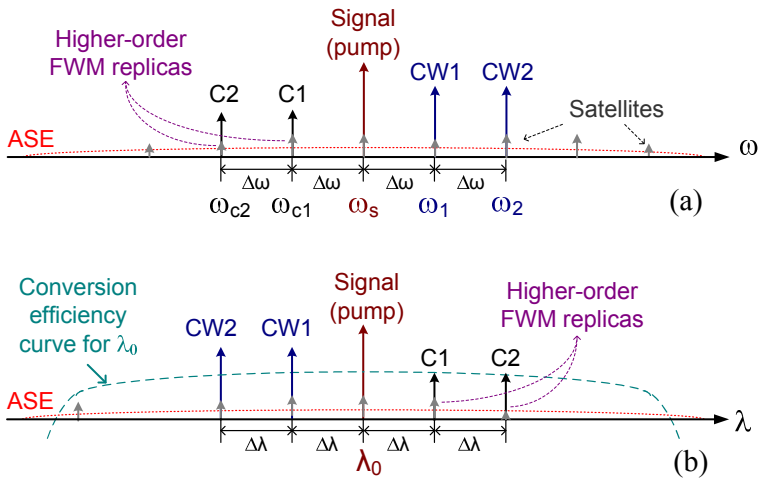

Figure 7.9: Conditions of crosstalk occurrence.

of the all the channels, as also proved in Fig. 7.8.

Denoting ω_s, ω_1 and ω_2 the frequencies of the pump, CW1 and CW2, the frequencies of C1 and C2 are: $\omega_{c1} = 2\omega_s - \omega_1$ and $\omega_{c2} = 2\omega_s - \omega_2$.

As discussed in Sec. 7.2, these first-order FWM products can also interact with the existing waves. Among others, a strong second-order interaction occurs between the input data signal channel at the frequency ω_s and the first-order product at the frequency ω_{c1}, as they are adjacent to each other and have considerable power levels. This interaction generates two new waves at the frequencies ω_{cc1} and $\omega_{cc1'}$, where

$$\omega_{cc1} = 2\omega_{c1} - \omega_s = 2(2\omega_s - \omega_1) - \omega_s = 3\omega_s - 2\omega_1. \tag{7.1}$$

As FWM products are generated at equally spaced frequency distance to the input channel spacing as shown in Fig. 4.9, in theory, the strongest crosstalk occurs when all the input channels are at equal frequency spacing. Under the experimental conditions, this happens when

$$\omega_2 - \omega_1 = \omega_1 - \omega_s = \Delta\omega. \tag{7.2}$$

From Eq. 7.2, we obtain $2\omega_1 = \omega_2 + \omega_s$. Consequently, Eq. 7.1 becomes

$$\omega_{cc1} = 3\omega_s - 2\omega_1 = 3\omega_s - (\omega_2 + \omega_s) = 2\omega_s - \omega_2. \tag{7.3}$$

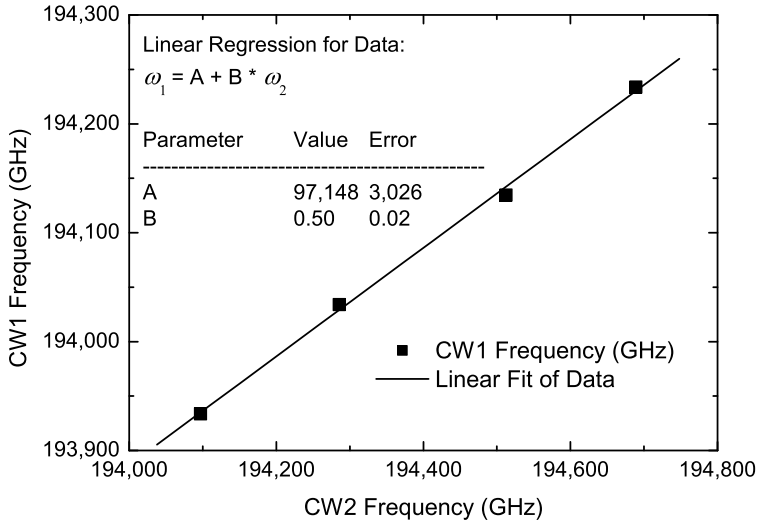

Figure 7.10: CW1 as function of CW2 when measured crosstalk was severest.

Therefore, the second-order replica at the frequency ω_{cc1} is generated *exactly* on the same frequency of the first-order converted channel at the frequency ω_{c2}.

The above example is just *one* of the many instances like this. What happens in reality is far more complicated, simply because every existing or new wave can be interacting with all the other waves. Especially at equal frequency spacing, inter-channel crosstalk is maximized. In this case there could be more than one high-order FWM products in each WDM channel, as shown in Fig. 7.9 (a).

This condition of crosstalk occurrence is confirmed by the experimental data. Based on the wavelength and frequency relation:

$$\omega = \frac{c}{\lambda}, \tag{7.4}$$

where c denotes the speed of light in free space, the frequencies of the CWs can be obtained. To prove the above assumptions on the general conditions of the crosstalk occurrence, in Fig. 7.10, CW1 frequencies were plotted against CW2 frequencies at the four points in Fig. 7.8 when the C1 Q factor was measured worst due to the channel crosstalk.

Note that all parameters are referred to vacuum free space, in which the velocity of the light is 3×10^8 m/s. This frequency-wavelength relation is also employed for ITU grid channel standards. The actual speed of light in fiber is closer to 2×10^8

m/s because of its effective refractive index [17].

In Fig. 7.10, the measurements presented a linear relation between the two CWs where crosstalk occurs. The linear fit of the data had a function of:

$$\omega_2 = 2\omega_1 - 194,296. \tag{7.5}$$

Converting the frequency value of 194,296 GHz back to the wavelength domain, we obtained 1544.03 nm. This can be understood as the pump signal wavelength within an error margin of 3.69 nm, which is reasonable considering the error margins of the linear fit, the approximations of the worst case wavelengths and the mis-calibration of the experimental equipment. Therefore, Eq. 7.5 became:

$$\omega_2 = 2\omega_1 - \omega_p. \tag{7.6}$$

This proved our expectation that when the channels are located with equal frequency spacing, the crosstalk is the strongest, as the case illustrated in Fig. 7.9 (a), where higher-order FWM replicas are generated on top of the input signals and first-order copies.

Interesting about channel spacing is that by differentiating Eq. 7.4 around a center wavelength λ_0, the relationship between the frequency spacing $\Delta\omega$ and the wavelength spacing $\Delta\lambda$ can be obtained as:

$$\Delta\omega = -\frac{c}{\lambda_0^2}\Delta\lambda. \tag{7.7}$$

Equation 7.7 suggests a linear relationship between the frequency spacing and the wavelength spacing. This is accurate as long as the wavelength or frequency spacing is small compared to the actual channel wavelength or spacing, which is usually the case in optical communication systems [17]. Around a center wavelength $\lambda_0 = 1550$ nm, a frequency spacing of 100 GHz corresponds to a wavelength spacing of 0.8 nm.

In general, if multiple channels are spaced apart equally in frequency, they are not spaced apart exactly equally in wavelength, and vice versa. However, in this case, where the farthest channels were only a few nanometers away from each other, according to Eq. 7.7, it can also be concluded that the above frequency conditions of the crosstalk occurrence also holds for the wavelength domain, as shown in Fig. 7.9 (b). In fact, this was observed in the experiments as well.

Figure 7.11 presents the spectra snapshots when CW1 was placed on 1546.92 nm. This was the case where crosstalk terms were most visible as the CW1 was

only 100 GHz away from the signal pump. The signal power at the input of the DSF remained the same, which was around 13∼14 dBm. From Fig. 7.11 (a) we see that high-order FWM replicas were generated, but since the channel spacing was not equal, they were out of band and could be eventually filtered out. Fig. 7.11 (b) and (c) showed that when the wavelength channels were evenly spaced, a high-order FWM product appeared inside the filtering bandwidth of the desired channel; therefore, the affected channel suffered from signal degradation, and the filtered copy experienced eye closure because of the same data of a smaller amplitude.

7.3.4 Power efficiency characterization

a. Power efficiency dependence on CW wavelengths

Optical power efficiency is an important factor for all-optical multicast. Although FWM is not the most power efficient wavelength conversion method, MWC by FWM in fiber offers the advantage of a flat conversion efficiency response within a wide wavelength range at both sides of the zero-dispersion wavelength of the nonlinear fiber. This wavelength range depends on the nonlinearity of the fiber – the higher nonlinearity the fiber has, the wider wavelength conversion range it accommodates [85]. Moreover, as FWM is transparent, the presence or absence of individual channels does not affect the power efficiency of the other channels.

Therefore, characterization of the DSF for one-to-two MWC was carried out. For this purpose, we fixed the CW1 wavelength, and moved CW2 in the wavelength domain by steps of 1 nm away from the CW1 and the signal, measuring the optical power of all the channels for calculating the power efficiency of the wavelength conversion. In order to observe the channel-independent characteristic of the conversion efficiency, with each step, the optical power levels were measured for all the wavelength channels with and without the presence of one CW channel or the other.

Measurements were taken with the CWs placed at both sides of the signal channel, as shown in spectrum insets in Fig. 7.12. The curves in Fig. 7.12 show the power of the signal, CWs and the converted channels dependency on the CW2 wavelength.

It can be seen that with FWM one-to-two MWC, the optical power of one wavelength channel is independent of the absence or presence of the other wavelength channel. As CW2 moved away from the signal and CW1, the power of C2 decreases. Outside the effective conversion range between 1541.35∼1554.13 nm,

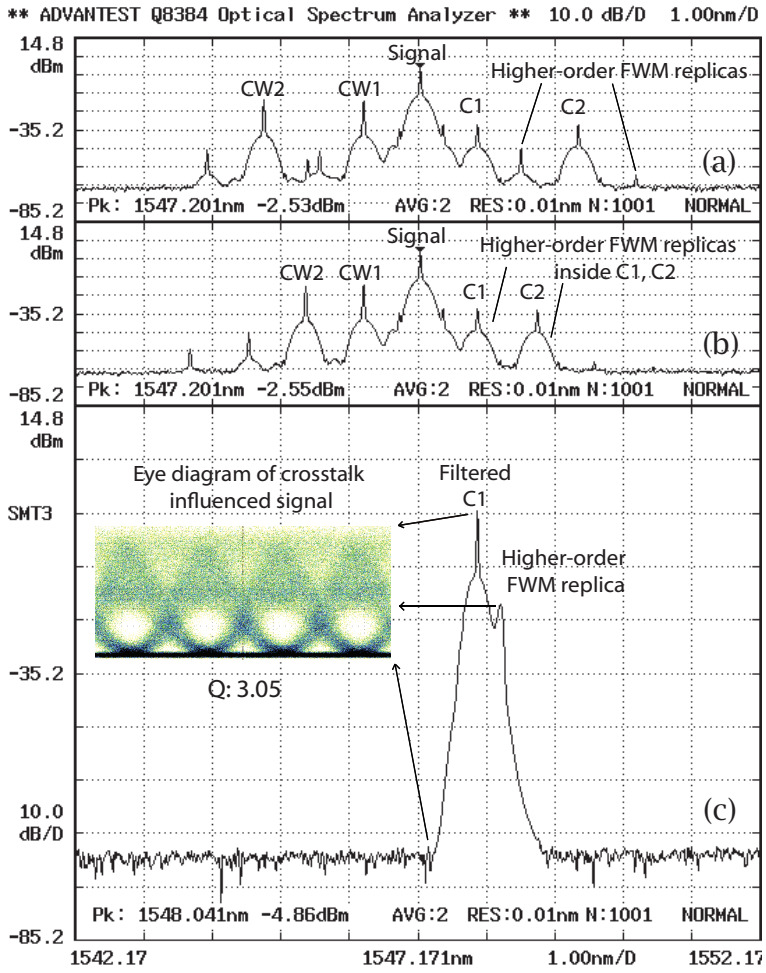

Figure 7.11: Spectra snapshots with CW1 fixed on 1546.92 nm: (a) unequal channel spacing where higher-order FWM replicas were generated outside desired copies; (b) nearly equal channel spacing where higher-order FWM replicas were generated inside the filtering bandwidth; (c) filtered C1 and eye degradation with visible crosstalk.

the C2 power drops rapidly. From Fig. 7.12 we also noticed a slight decrease in the powers of the signal, CW1, CW2 and C1 channels, this is probably due to the increased channel spacing from the CW2 to the CW1 and the signal channels,

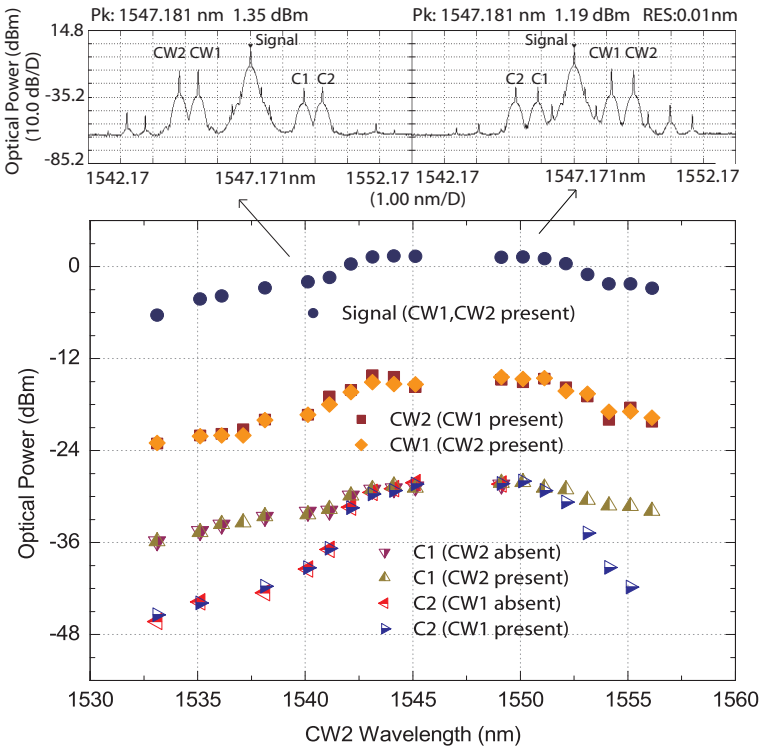

Figure 7.12: Optical power levels of all channels as function of CW2 wavelength.

more power is depleted from the other channels in order to transfer onto the C2.

In Fig. 7.13, optical power efficiency of C1 and C2 is presented as a function of the CW2 wavelength. It shows that also the efficiency of each MWC channel is independent of the absence or presence of the other. The best efficiency concerning the power ratio of the converted copy to the signal at the OSA was about −29.34 dB. When CW2 was out of the effective conversion range of the DSF, the conversion efficiency of C1 was not affected, while the conversion efficiency of C2 declined rapidly. The curves of the C2 efficiency indicated that the 3-dB conversion bandwidth of fiber was more than 11 nm from 1542.14∼1552.52 nm.

b. Power efficiency dependence on CW power

In this FWM scheme for MWC, the optical power of the CW probes has direct impact on the converted signal quality. However, unlike MWC by cross-gain modu-

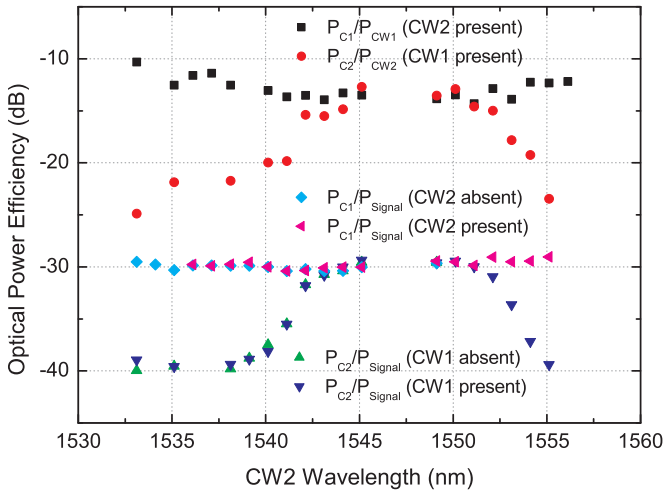

Figure 7.13: Optical power efficiency of C1 and C2 as function of CW2 wavelength.

lation (XGM) or cross-phase modulation (XPM) [59, 71, 102, 108], which generally require regulation of individual and total CW power, MWC by FWM in fiber is strictly transparent. Neither conversion efficiency nor converted Q factor degradation was observed when switching individual CW channel off, without compensating the total CW input power to the fiber. The main disadvantage of the FWM scheme compared to the others is its low conversion efficiency.

Nevertheless, it is expected that when lowering the CW power, the Q factor of the converted signal will also decrease. In all the previous measurements, both CW powers were set as 7 dBm at the laser sources. In this experiment, CW1 and CW2 were set around 1544.34 nm and 1545.53 nm, and their power were both varied from 0∼7 dBm in parallel. To find out the influence of the CW probe power on the converted Q factor and optical power efficiency, the C1 Q factor and the power efficiency of the converted channels over the CW probe power and pump signal power were measured while gradually reducing both CW power by 1 dB a step at the laser sources.

Figure 7.14 presents the results. The left axis shows the optical power efficiency scale, and the right axis shows the C1 Q factor scale. The optical spectrum when the CW power is 7 dBm, as well as two eye diagrams when the CW power is

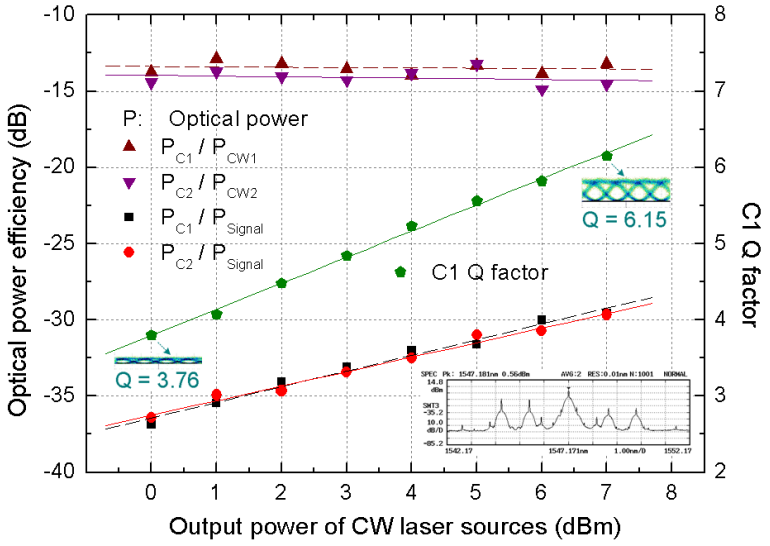

Figure 7.14: Optical power efficiency (left axis) and C1 Q factor (right axis) dependence on CW power.

respectively at 0 dBm and 7 dBm, are included as insets. The signal power at the input of the DSF is kept all the time at 13∼14 dBm. We can see that as the CW power increases, the C1 Q factor increases linearly. This can be explained theoretically. The eye diagrams indicates that as the CW power rises, the average mark level rises, but the noise levels remains almost the same as they are largely suppressed due to the quadratic effect that the selected FWM replicas experience. Therefore, C1 Q factor becomes proportional to the optical power of C1. Since the optical power of the converted signal is also proportional to the optical power of the CW, the C1 Q factor in this case has then a linear relation to the CW power.

Figure 7.14 suggests that also the power ratio of the copies to the pump signal increased linearly with the CW power, and the power efficiency of the copies was rather independent of the CW power. The former can be explained by the fact that the input signal power did not change, therefore the ratio increased linearly. The latter was also expected because of the linear relation of the converted power to the corresponding input CW power.

7.3.5 Conclusions on experimental results

In this section, MWC by FWM in a DSF is presented based on a simple scheme for up to three channels. The approach offers not only strict conversion transparency, but also signal regeneration in the converted channels due to the noise compression effect on the spaces. These advantages are supported by both theoretical analysis [70] and experimental demonstration.

In reality, operating bit rates can often be limited by other components in the system, as the case shown in the 40 Gb/s measurements. Eliminating such limitations is key to improve experimental performance at high bit rates.

Limited by the laser resources in the lab at the time of the experiments, it was not possible to test the scheme with more than three channels, nor with BER measurements. However, observing the results of one-to-two and one-to-three conversion, MWC by FWM implementing the proposed scheme has the following characteristics:

i) *The flat conversion bandwidth around the zero-dispersion wavelength λ_0 can be most effectively used by placing the signal as the pump at λ_0.*

The DSF employed in the experiment has the λ_0 around 1547.72 nm. Its 1-dB conversion bandwidth was about $9 \sim 10$ nm from $1542.4 \sim 1552.2$ nm. Its 3-dB conversion bandwidth was more than 11 nm from $1541.7 \sim 1552.9$ nm. However, these are rather moderate values as the nonlinearity of this fiber is not very high. Highly nonlinear fibers (HNLFs) can easily have 3-dB conversion bandwidth of $70 \sim 90$ nm [85, 93].

ii) *The MWC scheme exhibited efficiency and performance independency of the number of channels within the effective wavelength conversion bandwidth of the nonlinear fibers.*

According to the power efficiency measurements, MWC conversion efficiency does not depend on how many channels are simultaneously on. This is based on the fact that in the experiment, the MWC conversion efficiency did not degrade when more CWs were added. Moreover, measurements of the efficiency of the one-to-two MWC were made with and without the presence of the other CW, and no degradation was noticed when one more CW is added. When upgrading the scheme by adding a third channel without modifying any settings on the existing setup, no change in the existing channel performance and efficiency was perceived, and the third channel demonstrated similar performance and efficiency as the existing two channels. It was observed that the Q factors of the converted signals

also did not depend on the number of channels applied.

iii) *Both the power ratios of the converted channels to the pump and the converted Q factors have a positive linear relation to the power levels of the CWs injected into the fiber.*

In the experiments, the power levels of the CW sources were decreased from 7 dBm to 0 dBm. As a result, the power efficiency of the two copies to the input signal channel decreased linearly from around -29 dB to -37 dB. The measured Q factor of the copy C1 decreased linearly from 6.15 to 3.76.

iv) *When crosstalk between the MWC channels occurs, the Q factors of the converted channels are degraded. This happens if some of the channels are placed equally apart, and these channels are at the same time close enough so that higher-order FWM copies are generated inside the filtering bandwidth of the desired MWC channels.*

The beating of high-order replicas causes Q factor degradation of the extracted copies. From the eye diagrams of the measured worst cases, it can be easily seen that the filtered signal consists of the same data at different amplitudes.

v) *The severeness of the crosstalk depends on the channel spacing between the CWs and their spacing from the high-power signal.*

The closer the CWs are to the signal, the more effective the FWM is, and thus the stronger the beating is. In the crosstalk measurements at different channel spacing at 40 Gb/s, beating caused C2's Q factor to drop to less than half when CW1 was $100 \sim 200$ GHz away from the signal. When CW1 was 300 GHz away from the signal, beating only causes Q degradation of 0.8. When CW1 was 400 GHz away from the signal, beating was not so serious as the Q variation was only about 0.3. If crosstalk happens when the CWs are further away from each other, its negative influence is also less.

Therefore, the CWs should not be placed too close to the high-power signal to avoid channel crosstalk, but neither should they be placed too far, otherwise the conversion efficiency and the converted Q will degrade rapidly.

For the DSF tested in the experiments, CWs should be positioned $2 \sim 6$ nm away from the high-power signal. This gives an indication of the maximum number of channels that can be applied for MWC. If 200GHz (1.6nm) channel spacing between the CWs is used, the maximum number of channels for this fiber is only 4. If 100GHz (0.8nm) channel spacing between the CWs is used, the maximum number of channels for this fiber becomes $7 \sim 8$.

7.4 Summary and discussions

In theory, FWM-based MWC provides transparent operation concerning both data modulation format and operating bit rate. In this chapter, major issues related to the experimental performance of MWC by FWM in nonlinear fibers are analyzed. Important factors that influence the MWC performance are identified.

It is observed that this method for multicast is advantageous for its conversion transparency and wide conversion bandwidth, providing proper wavelength positioning of the multiple channels. Individual channel conversion efficiency does not depend on the number of the channels that are switched on at a time, unless crosstalk occurs. Crosstalk generally greatly impacts the desired channel performance on the conditions that the channels are close enough and the spacing between the channels are nearly equal taking into account of the channel filtering bandwidth. With crosstalk-free MWC, the converted Q factors are not affected by the presence of other channels.

In the CW power dependency characterization, it is observed that both conversion efficiency and converted signal Q factor depend on the optical power levels of the CWs injected into the nonlinear fiber. Converted signal Q factors and optical power efficiency of both converted copies over the pump signal have linear relations to the input CW power levels.

However, FWM in fibers does not offer full flexibility in wavelength due to two facts: i) the pump signal must be placed around the zero-dispersion wavelength of the fiber, or a dispersion-flattened fiber must be used; ii) there are limits in setting the channel wavelengths so that no crosstalk interference from the satellite copies could degrade the converted signal quality. Moreover, compared to the XGM and XPM techniques, FWM requires boosting of signal power to more than 10 dBm and its conversion efficiency is rather low, often below -10 dB. The length of the nonlinear fiber required for MWC depends on the nonlinearity of the fiber but it is generally a few hundred meters or more, which makes the setup bulky and impossible to integrate.

Nevertheless, FWM for MWC is still attractive for its conversion transparency and its signal regeneration effect at the logical *zero* level. Moreover, MWC by FWM in fiber offers a large wavelength conversion range around the zero-dispersion wavelength of the fiber. Further increasing the nonlinearity of the wavelength conversion media by using HNLFs can also improve the conversion efficiency and enlarge the useable wavelength span.

Chapter 8

Contention resolution for all-optical label switching nodes

In optical packet switched networks, contention occurs in optical switching nodes whenever two or more optical packets try to leave the same switch output port on the same wavelength at the same time. In electronic packet switching networks, such contention is resolved using a store-and-forward technique, by keeping the packets in a memory bank, such as an electronic random-access memory (RAM), until the desired output port becomes available. However, there is no equivalent optical RAM technology. All-optical contention resolution needs to explore the possibilities in time, wavelength or space domain, or a combination of them. How to implement buffering for node contention resolution is an important aspect to consider. In this chapter, output-buffered contention resolution for the all-optical label switching (AOLS) nodes is investigated. In particular, two buffering strategies for the AOLS nodes are evaluated and compared through traffic performance simulations. These two strategies are based on introducing more buffers and increasing the buffer size, respectively. The results show dependent performance on the input traffic characteristics. With self-similar traffic, these two strategies are equally efficient. With Bernoulli traffic, it is more practical to introduce more buffers. Parts of this chapter are based on publications.[1]

[1]See references [1, 136].

8.1 Optical contention resolution

As introduced in Chapter 1, all-optical contention resolution can be realized in the *wavelength*, *time* or *space* domain [5, 64].

For optical packet switching nodes, in the *wavelength* domain, one can use extra wavelengths to carry the optical data packets, and use wavelength conversion to avoid wavelength collision.

In the *time* domain, optical buffering is normally employed by sending the optical data packets into optical delay lines (ODLs). Note that in practice, ODLs as optical buffers have many short-comings. First, ODLs offer very limited flexibility in buffering. Because of their fixed lengths, once a packet enters an ODL, it is impossible to retrieve the whole packet before a fixed duration of time, which is determined by the packet *data rate*, packet *length* and the *refraction index* of the fiber. Second, ODLs are not efficient enough to provide adequate buffering on an integrable size. A 512-byte packet, which is the average Internet protocol (IP) packet size, requires 20.48 *meters* of fiber for the packet to be buffered *once*, not including the guard bands between the packets. To provide the same amount of buffering in the optical domain as in current electronic routers, *thousands of kilometers* of fibers are needed. However, the ODL buffering concept is simple and fibers are widely available, which has made ODLs the most commonly employed method for optical buffering at the time of writing. In this thesis, ODLs are assumed to be the medium for optical buffering and delay purposes.

As explained in Sec. 1.3.2, optical buffering for contention resolution can be implemented either at *input* or *output* side of the node, referred to as *input-buffering* and *output-buffering*, respectively. There have been research activities on both input-buffered and output-buffered photonic packet switches with electronic packet processing and electronic control for contention resolution [137, 138].

In the *space* domain, space deflection provides separate routes for the optical data packets to prevent contention. Contention resolution by deflection routing generally requires higher-layer monitoring, traffic control and management.

In real situations where optical contention resolution is needed, usually a *combination* of the above methods is employed [5, 64, 137–140]. The EPSRC-funded project WASPNET (wavelength switched packet network) did extensive work using multiple wavelengths to help resolve packet contention and to reduce the size of necessary optical buffers [141, 142].

As outlined in Sec. 1.3.2, as far as only time domain is concerned, output

queuing is generally more efficient than input-queuing, as it avoids the head-of-line (HOL) blocking effect. Unlike input-buffering, output-buffering is generally on an *on-demand* basis, especially for the buffering strategy of having several buffer ports. On the other hand, input-buffering is generally implemented in order to *avoid* contention, in which case may result in *unnecessary* buffering or *over* buffering. Moreover, a HOL packet being buffered *blocks* all the packets behind it, even if those packets are to be forwarded to a contention-free output port.

This chapter presents an output-buffered contention resolution scheme for all-optical label switching (AOLS) nodes using combined methods in the *wavelength* and *time* domain. In Sec. 8.2, different buffering strategies for output-buffered contention resolution scheme are investigated and compared, with their traffic performance evaluated using computer simulations. In Sec. 8.3, practical issues concerning the output-buffered contention resolution scheme are discussed, and main conclusions from the performance simulation results are summarized.

8.2 Output-buffered node contention resolution

8.2.1 Node architecture

Figure 8.1 presents the 2×2 AOLS unicast node investigated in the LASAGNE project. The LASAGNE AOLS node employs *output-buffered* contention resolution scheme. In Fig. 8.1, optical packet contention can occur near the output fiber ports of the AOLS packet switch when more than *one* optical packet tries to exit through one output fiber at the same time on the same wavelength; or when more than *four* optical packets try to exit through one output fiber at the same time, as four is the number of available wavelength channels per output fiber port. The contention resolution blocks are introduced to solve this problem.

As described in Sec. 2.2, such a contention resolution block requires *three* basic functions: packet *synchronization* (syn), variable optical packet *buffering* (Δt) and tunable *wavelength converters* (TWCs).

As packets arrive at each output fiber port from different input ports, they may experience slightly different delays due to the different optical paths they have traveled. One of the main causes for such delay difference is the wiring matrices between the arrayed waveguide gratings (AWGs) and output fiber ports. Measures can be taken to minimize such delay difference by making the optical paths, either *fibers* or *waveguides*, all the same length from any AWG output to

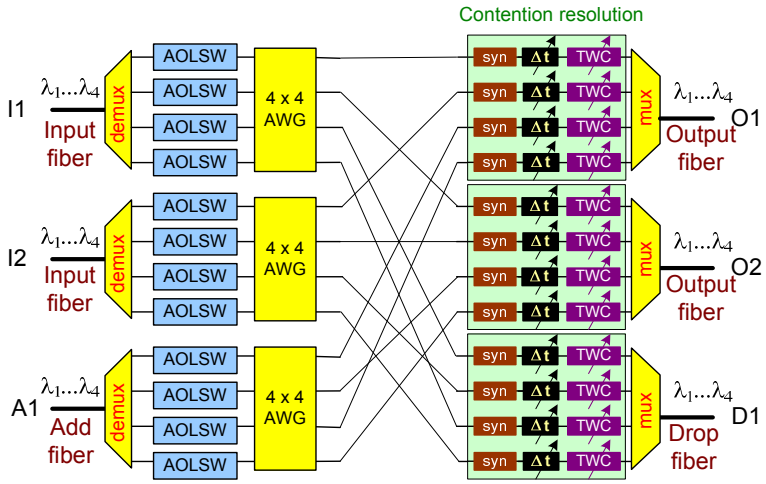

Figure 8.1: Output-buffered AOLS node. (AOLSW: all-optical label swapper; AWG: arrayed waveguide grating; syn: synchronization; Δt: variable time delay; TWC: tunable wavelength converter.)

any contention resolution block input. In such a case, optical packets may arrive at the contention resolution blocks already *"synchronized"* allowing small guardband margins, and the *synchronization* stage of the output contention resolution can be avoided.

After synchronization of the outgoing packets, *two* of the optical contention resolution methods can be used for prevention of possible packet collision: optical buffering in the *time* domain and wavelength conversion in the *wavelength* domain. In Chapters 2 and 3, the effectiveness of the wavelength conversion and one-slot optical buffering are evaluated by means of traffic performance simulations. The simulation results show that under bursty traffic conditions, wavelength conversion is much more efficient in solving packet contention than one-slot optical buffering, especially at low network loads. In practice, in case of contention, a node usually *first* seeks an *available output wavelength channel*; when all the available output wavelengths channels are occupied, the contended packet can be *then* forwarded to an *optical buffer*, if there is any.

Note that the *space*-domain packet contention resolution is not applicable here, as it involves either overall *network* control to route the contended packet via a different label-switched path (LSP) programmed by the label edge routers (LERs),

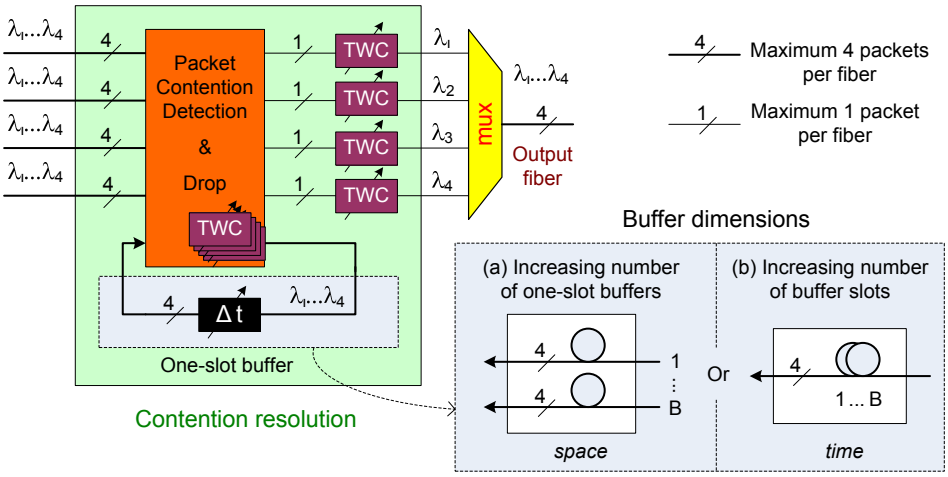

Figure 8.2: Contention resolution block for output-buffered AOLS nodes.

or overall AOLS *node* control to route the contended packet to a node feedback loop so that it can be forwarded to the desired output fiber port at the next available time slot. Because contention resolution by space deflection routing requires upper-layer management, it is generally applied at the *network* level or *node* level, but *not* at the output *port* level.

a. Contention resolution block

Figure 8.2 shows an example of a possible contention resolution block inner structure, which is implemented for the performance simulations presented in Chapters 2 and 3. This block is situated at every output of the AOLS node in Fig. 8.1, and includes the following functional stages: a *contention detection and drop* (*CDD*) module, *TWCs*, *variable optical buffering* Δt and a *wavelength multiplexer* (mux).

The operation principle of this contention resolution block is the following: At each input of the contention resolution block, which is connected to an output of an AWG, maximum *four* optical packets on *four* different wavelengths may enter. If no contention resolution (`NoCR`) is implemented, the CDD module only passes *maximum one* packet *per wavelength* to *each* of its four outputs that are connected to the output fiber, and drops all the other packets. The TWCs are not included for the `NoCR` situation. When wavelength conversion (`WC`) is implemented, the CDD module passes *maximum one* packet to *each* of its four outputs that are connected

to the output fiber, thus *maximum four* packets in total, and drops the rest of the packets. Note that as mentioned in Sec. 2.5, a policy is applied here that the optical packets on shorter wavelengths get higher priority to be forwarded. The TWCs before the multiplexer then convert the packets into different wavelengths for the output fiber. When both wavelength conversion and one-slot buffering (`WCFB`) are implemented, apart from letting *maximum four* packets through to the output fiber, the CDD can also further buffer *maximum four* optical packets for one time slot in its feedback ODL. In the next time slot, the packets that are in the buffer shall have higher priority to be forwarded to the output fiber than the new incoming packets arrive at the CDD module.

One can dedicate separate ODLs for every *single* packet, in which case each ODL carries just *one* wavelength. Or, as in our simulations, an ODL unit can be allocated for carrying *four* wavelengths, and thus maximum *four* packets can be stored at a time. To store up to four packets in one ODL unit, wavelength converters need to be employed to convert these packets into different wavelengths, as shown in Fig. 8.2 *before* the feedback buffering structure. Packets that cannot be sent because of lack of vacant wavelengths in both output fiber and the ODL unit are dropped, resulting in packet losses.

b. Buffering strategies

In previous chapters, only *one* packet duration optical buffering has been considered in the traffic performance evaluation of output-buffered contention resolution schemes. In order to explore further in the *time* dimension to reduce packet loss ratio (PLR) and improve network throughput (NT), this section investigates *two* different strategies for increasing the buffer size. As shown in Fig. 8.2, these two strategies concern two ways of providing more buffer, by increasing the number of *one-slot buffers* in *space*, and by increasing the number of *buffer slots* in *time*. The former strategy allows in each time slot more packets to be buffered. The second strategy allows each contended packet to be buffered longer.

Figure 8.3 illustrates a flow chart of the contention resolution algorithm implemented in the CDD module for the performance simulations of output-buffered AOLS nodes. As described earlier, wavelength conversion is employed when necessary to convert the contended packets into appropriate vacant wavelengths for the output fibers and ODL buffers.

Whether a packet will be forwarded, buffered or dropped depends on the time

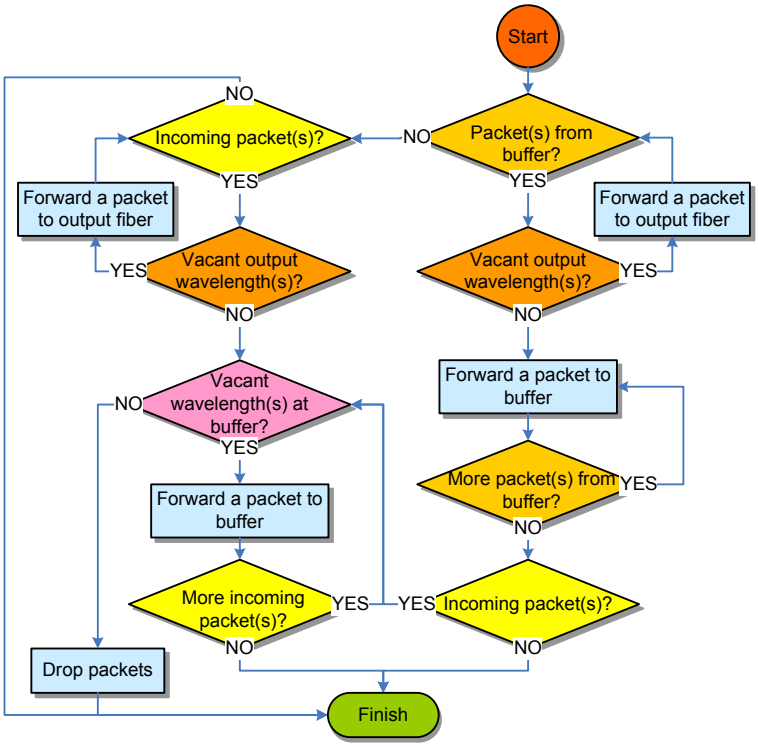

Figure 8.3: Contention resolution algorithm for output-buffered AOLS nodes.

the packet has already spent in the buffer. The packets that has stayed in the contention resolution block for the longest time get highest priority to be forwarded to the output fiber, among the other packets that are in the buffer and the incoming packets. In this way, we prevent the same packets keeping being recirculated in the buffer. Among the packets that has stayed in the buffer for the same amount of time, the policy that packets on shorter wavelengths get higher priority is then applied.

8.2.2 Unicast traffic performance evaluation

In this section, unicast traffic performance evaluation for the output-buffered AOLS nodes as in Fig. 8.1 is presented. As in previous chapters, *PLR* and *NT* of the node under Bernoulli and self-similar traffic are assessed. Wavelength conversion is implemented for contention resolution in all cases. An ODL buffering unit

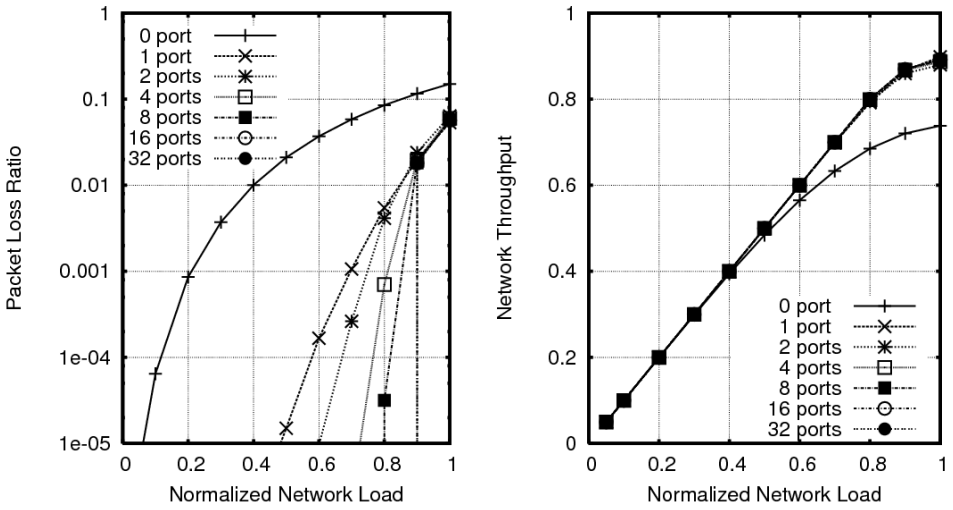

Figure 8.4: Simulation results of output-buffered unicast node performance under Bernoulli traffic - increasing number of buffer ports.

here refers to *one*-slot packet buffer of *four* wavelengths. Thus each ODL unit can buffer maximum four optical packet for one packet duration, as shown in Fig. 8.2 as the one-slot buffer. To investigate the effect of increasing buffer dimensions, simulations are carried out for various buffer sizes from 0 to 32, in both space and time dimension, as shown in Fig. 8.2 (a) and (b).

a. Increasing one-slot buffer ports

Figures 8.4 and 8.5 present the simulation results of the output-buffered unicast AOLS node with different number of buffer ports under Bernoulli and self-similar traffic, respectively. In both figures, the curve "`0 port`" is the result when no buffering is implemented and it is plotted as a baseline for comparison.

As expected, including more buffer ports reduces the *PLR*, although the level of improvement is highly dependent on the traffic characteristics. Adding more buffer ports to resolve contention for Bernoulli traffic is very effective because of the homogeneity in its traffic pattern. As explained in previous chapters, Bernoulli traffic spreads the network load over all the simulation time slots and avoids the creation of bursts. Packets can *smoothly* be forwarded, or, at higher network loads, be stored and then forwarded to the output fibers. As much as the buffer

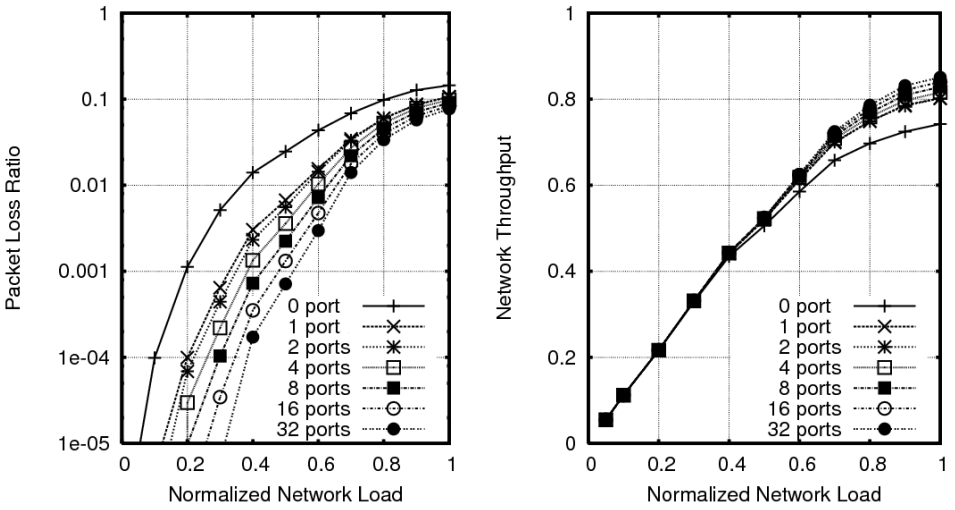

Figure 8.5: Simulation results of output-buffered unicast node performance under self-similar traffic - increasing number of buffer ports.

size allows, most packets can be either forwarded or stored, and few of them get dropped. When the AOLS node receives more packets at a steady rate than what the node can forward and buffer, the *PLR* starts to increase steeply.

As for self-similar traffic driven results, the margin of improvement in the *PLR* is significantly less than that for Bernoulli traffic. This is because self-similar traffic sends bursts of packets to the AOLS node. During an ON period with group of packets, the buffer can overflow and the incoming packets have to be discarded. On the other hand, the more buffer ports a contention resolution block contains, the more packets it can buffer at the arrival of a burst of packets, and the less incoming packets are dropped. Therefore, by increasing the number of one-slot buffer ports, the AOLS node does experience less packet losses, and the node *NT* improves accordingly.

For self-similar traffic, the margin of improvement for *PLR* by introducing more buffer ports becomes gradually less towards high network loads. This is because at high loads, the number of packets per burst is higher, so is the probability of receiving a new burst before clearing up all the stored packets. Under such situation, the switch tends to lose more packets as it cannot handle the amount of traffic *during a burst*, and neither can it empty its buffers *in between the bursts*.

The *NT* is a good complement to the *PLR* because it has a direct relationship

to the *PLR*, as explained in Chapter 2. *NT* can can reveal more subtle performance differences under high loads, while *PLR* can reveal more subtle performance differences under light loads [64]. For Bernoulli traffic, the *NT* does not experience much improvement when increasing the number of buffer ports. The traffic situation of Bernoulli at a certain load is steady and the load is well spread out over the whole simulation period. This is the most favored traffic shape for the AOLS nodes. Under such traffic conditions, the AOLS node operates at its highest efficiency in delivering packets. When more buffer ports are introduced, although less packets are dropped because of the increased buffer dimension, most of these packets stay in the buffer and cannot be delivered as the output capacity of the AOLS node remains the same. Consequently, the amount of packet *delivered* still remains almost at the same level and *NT* shows little appreciation of the increased buffer ports.

This situation, however, is different if the traffic is self-similar. Due to its bursty nature, self-similar traffic sends packets in an ON/OFF fashion. Packets being stored in the buffers have the chance of being delivered during the OFF periods. Therefore, the more buffer ports, the more buffering capacity is there to keep the packets until they can be forwarded to the output ports. Thus the amount of delivered traffic is higher, resulting in better throughput with increased buffer ports. However, with bursty traffic, the AOLS node does not operate at its highest efficiency in delivering packets because of the *un-shaped* traffic at its inputs, which can be seen from the Fig. 8.4 and Fig. 8.5 that even with 32 buffer ports, the *NT* of the AOLS node under self-similar traffic is still less than that in the case of Bernoulli traffic.

b. Increasing buffer slots

In this section, lengthening the ODLs by increasing the number of buffer time slots is considered. This can be seen as putting several one-slot buffer shown in Fig. 8.2 in *serial*, or increasing the buffer dimension in *time*. The results under Bernoulli and self-similar traffic are presented in Fig.s 8.6 and 8.7, respectively. In these figures, the curves "`0 slot`" are the results with no buffering, plotted as a baseline. Note that the results of *no buffering* "`0 slot`" and *one one-slot ODL buffer* "`1 slot`" are the same as the simulation results of "`0 port`" and "`1 port`" in the previous section, as they are taken under the same buffering conditions.

From Fig. 8.6, it can be seen that increasing the number of buffer slots does

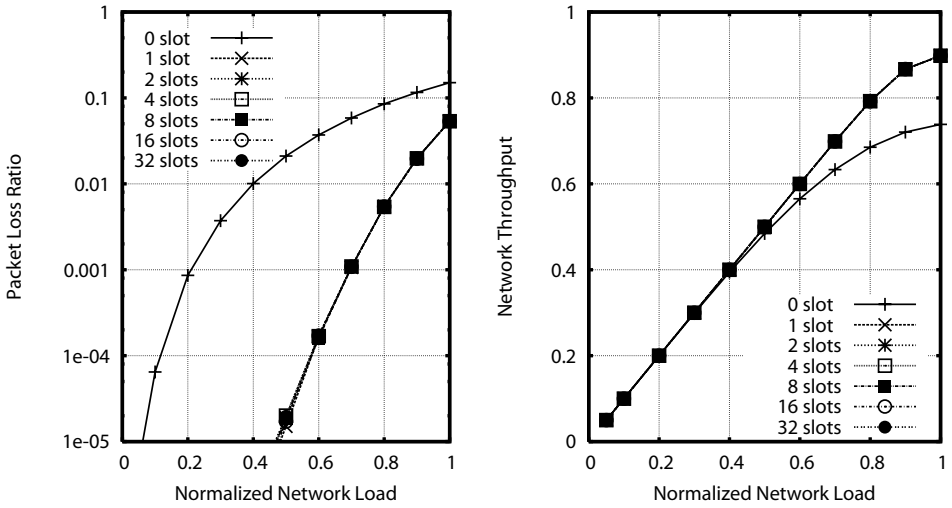

Figure 8.6: Simulation results of output-buffered unicast node performance under Bernoulli traffic - increasing number of buffer slots.

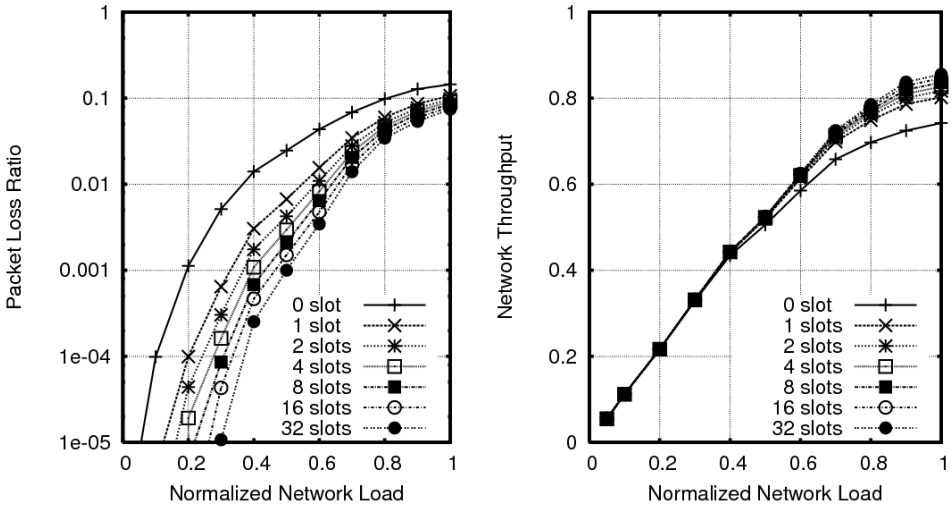

Figure 8.7: Simulation results of output-buffered unicast node performance under self-similar traffic - increasing number of buffer slots.

not show any advantage for Bernoulli traffic. Because of the homogeneous characteristic of the Bernoulli traffic, under a certain load, the probability of getting

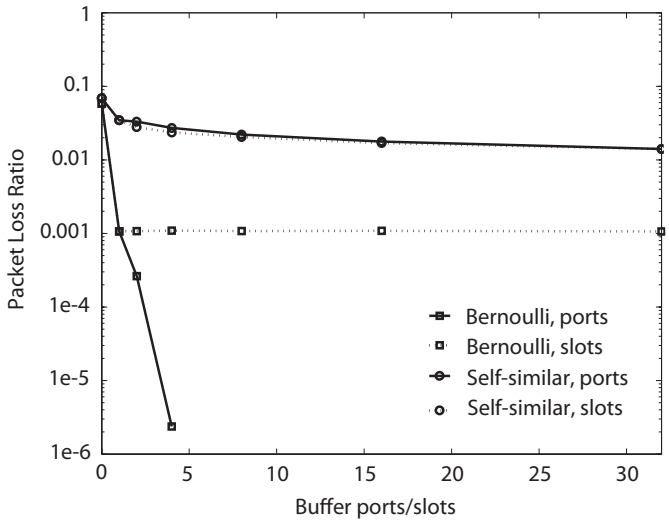

Figure 8.8: Packet loss ratio of output buffering strategies at network load of 0.7 (a) increasing one-slot buffer ports, and (b) increasing buffer slots.

incoming traffic is the same for the total simulation period, no matter after how long the packets stay in the buffer. When the buffered packets come out in the next time slot, in principle they causes the same amount of losses in the incoming packets as when they come out at any time slot after. While for self-similar traffic, packets tend to group together. Therefore the more slots the buffer has, the longer the packets stay in the buffer, and the higher probability that they come out of the buffer during an OFF period. This way, the stored packets in the ODLs can be sent without contending with the new incoming packets, reducing packet loss and increasing successful delivery. Consequently, better results are yielded for the *PLR* and *NT* under self-similar traffic condition.

c. Comparison of output buffering strategies

In Fig. 8.8, the *PLR* of the two buffering strategies is compared with both Bernoulli and self-similar traffic inputs for a load of 0.7. For self-similar traffic, the two strategies has almost the same effectiveness in reducing the *PLR*. For Bernoulli traffic, increasing the number of one-slot buffer ports seems to be much more effective than increasing buffer slots, which shows more than *two* orders of magnitude in *PLR* for one-slot buffer unit number higher than *four*.

8.3 Summary and discussions

Contention resolution for optical switches is an issue that commonly involves a great depth of complicated optical component design and electronics. To the best of the author's knowledge, at the time of writing there is no known *all-optical* solution for a complete contention resolution block design on the AOLS node level, which requires *all-optical* packet contention detection, *all-optical* control for the variable optical delay and *all-optical* control of the tunable wavelength conversion. *Electronic* control is a requisite to realize the contention resolution for the AOLS nodes presented in this chapter.

For implementation of the CDD module in Fig. 8.2, centralized monitoring and control via electronics are necessary at the each AOLS output fiber port. This means that the high-speed all-optical label processing at the all-optical label swapper stage will not show any advantages for the overal AOLS node performance as the contention resolution control still has to be realized in the *electrical* domain. Consequently, the optical transparency of the data signal is lost at the output contention resolution stage of the packet forwarding.

Regarding the performance of the two buffering strategies investigated in this chapter, the traffic shape at the AOLS node inputs has a great impact on the efficiency of different buffering strategies. For Bernoulli traffic with a homogeneous nature, increasing buffer ports is far more efficient than increasing buffer slots; while for self-similar traffic with a bursty nature, the two strategies have almost the same performance, although increasing buffer slots shows negligibly lower *PLR*'s for buffer dimensions between 2 and 8. In general, with the same buffering strategy and buffer dimension, Bernoulli traffic at the AOLS inputs results in at least one order of magnitude lower *PLR* than self-similar traffic.

As for practical issues concerning these two buffering strategies, increasing buffer ports at the CDD module means more computational complexity and larger dimension of the module, which at this moment can only be realized with electronics. On the other hand, the strategy of increasing the buffer slots means lengthening the ODL, which has the disadvantage of physical impairments of the signal such as attenuation of the signal power, crosstalk among wavelength channels, etc. Therefore, making the ODL longer also results in more expensive implementation of the node architecture due to the need for optical amplification and regeneration [64].

Chapter 9

Towards scalable optical multicast nodes

The all-optical label swapper (AOLSW) is the core of the all-optical label switching (AOLS) nodes. In the AOLSW, all-optical label processing takes place, and the optical packet is converted to a suitable internal wavelength to be forwarded passively by the arrayed waveguide grating (AWG) to the desired output port(s). Although in principle, the AOLSW presented in Chapter 2 is technically feasible, high optical complexity, costly components, and good interworking among the subsystems are required. Moreover, the number of the label bits that can be processed by each AOLSW is limited by the capabilities of the label comparison subsystem. The footprint of the label comparison subsystem shall increase exponentially with the label bit-length. These implementation difficulties significantly impact the commercial outlook of the AOLS nodes. In this chapter, a simple and scalable all-optical label processing scheme for AWG-based optical label switching nodes is proposed. It can be applied to any optical-pulse-based labels regardless of label length. It also supports optical layer feed-forward multicast (FFM). As shown in this chapter, FFM offers good scalability with the up-scaling of the AOLS nodes and the increase of the multicast traffic loads.

9.1 Introduction

Despite the ample advancements in various optical labeling techniques and several successful all-optical label switching (AOLS) subsystem proof-of-principle demonstrations [11, 12, 14, 48], a practical limitation for the AOLS implementation is the lack of a scalable label processing technique supporting multicast functionality. Especially for time-serial labels, the number of active switching components required for bit-correlating label processing techniques reported so far is exponentially related to the label length n [13, 15], let alone the high power losses due to the label splitting for parallel correlation.

The chapter is organized as follows. In Sec. 9.2, a simple and highly scalable all-optical processing concept for passive waveguide-based optical label switching nodes is proposed. It can be applied with different labeling techniques regardless of label length. Furthermore, it supports optical layer self-routing packet feed-forward multicast (FFM) [46, 65], which has been proved to be a faster, more efficient and economical multicast approach than the conventional feedback multicast [2, 13, 16, 22] exploited in most proposed optical label switching and AOLS nodes. In Sec. 9.3, scalability performance evaluation on such multicast-capable nodes is investigated by Bernoulli-traffic-driven simulations for different node dimensions and different multicast traffic loads. In Sec. 9.4, the main conclusions are summarized.

9.2 All-optical spatial label processing

The proposed all-optical spatial label processing scheme works with optical labels consisting of optical pulses. The most commonly used labeling encoding techniques are time-serial return-to-zero (RZ) labels as employed in [13] or wavelength labels as in [12, 143]. Further explanation and discussions will be based on these two examples.

9.2.1 Labeling concept and techniques

The labeling concept is straightforward and self-explanatory: each label bit corresponds to an AOLS output port; bit "1" means the packet is destined for that output port while bit "0" indicates that the packet is not meant for that output port. The general guidelines for this labeling concept is summarized in Table 9.1.

Table 9.1: Labeling concept.

Type of traffic	Labeling principle	Examples
Unicast traffic	One 1 among s series of 0's	0100, 00010, etc.
Multicast traffic	Multiple 1's among 0's	0101, 11001, 10111, etc.
Broadcast traffic	A series of 1's	11...1

According to this labeling concept, each label contains full information of how the packet should be forwarded. If the dimension of the arrayed waveguide grating (AWG) for each output port is equal to the AOLS node dimension, with a proper wiring matrix between the AWG and the output ports, the label pattern presents exactly to which output port(s) of the node the packet is intended. In this case, label 0100 means that the packet is a unicast packet for the second of the four logically-ordered output ports of the node, while label 11001 means that the packet is a multicast packet for the first, second and the last of the five logically-ordered output ports of the node. In each label, "1's" are represented by the presence of optical pulses, while the"0's" are represented by the absence of optical pulses.

To apply optical time-serial labeling, an amplitude-modulated optical pulse sequence on the same wavelength as the optical packet is used, usually separated from the packet payload by a guard time period [13]. To apply wavelength labels, optical pulses on different wavelengths can be placed in-band or out-of-band of the packet wavelength [12, 143]. These labeling techniques are illustrated in Fig. 9.1 and will be discussed in more details in the following sections.

9.2.2 Spatial label processing

The proposed all-optical label processor is based on an optical serial-to-parallel conversion (SPC), all-optical flip-flops (AOFFs) [14, 52], and a multi-wavelength converter (MWC) [60, 68, 70], as illustrated in Fig. 9.2. The SPC can be realized either by an optical time division multiplexing (OTDM) demultiplexer [144–146] for *time-serial labels*, or by a wavelength division multiplexing (WDM) demultiplexer for *wavelength labels*. The SPC performs the function of converting a series of optical pulses into spatial parallel bits. Each AOFF is optically controlled by optical pulses to switch between possible wavelength states. Outputs of the AOFFs serve as probe signals for the MWC, which can convert the optical packet onto single or

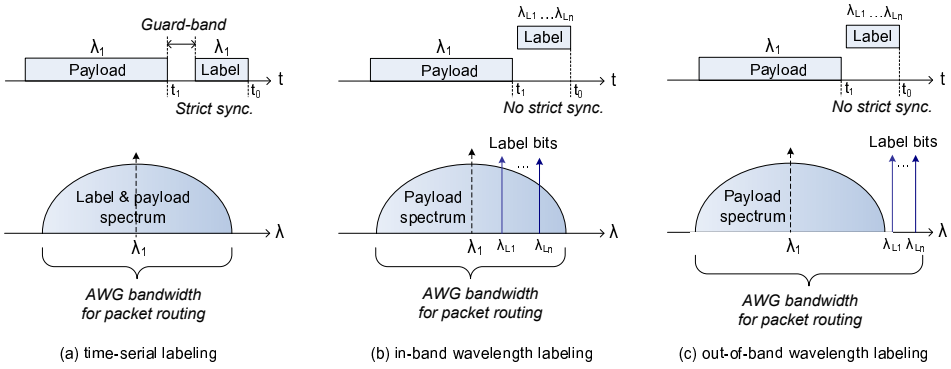

Figure 9.1: Three labeling techniques.

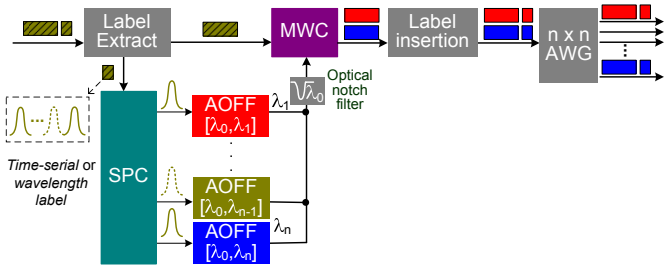

Figure 9.2: All-optical packet processor or all-optical label swapper (AOLSW) with AWG. (SPC: serial-to-parallel conversion; AOFF: all-optical flip-flop; MWC: multi-wavelength conversion; AWG: arrayed-waveguide grating.)

multiple wavelength(s) in order to be passively forwarded to different output ports of the node by an AWG, as shown in Fig. 9.3. According to the packet format and labeling techniques, different SPC and MWC technologies can be employed, summarized in Table 9.2.

9.2.3 Comparison of label processing schemes

As labeling schemes and label processing subsystems are generally the major bottlenecks of AOLS node scalability, here we discuss further how our labeling concept in Table 9.1 and the implementation of the SPC, can provide significant improvement for time-serial and wavelength labels with respect to the AOLS node

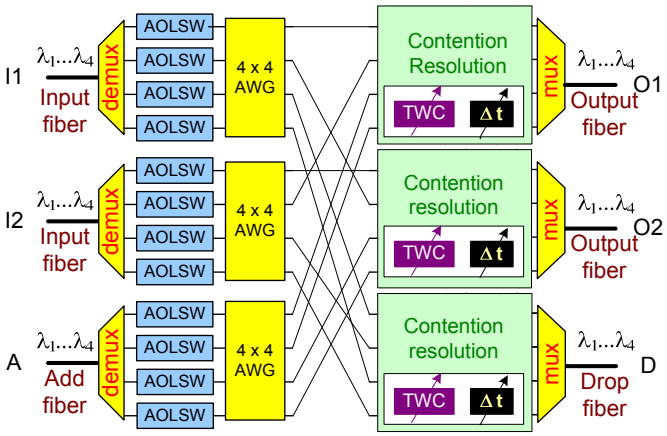

Figure 9.3: 3-port AOLS node architecture.

Table 9.2: All-optical label processor subsystems.

Type of traffic	Labeling principle	Examples
Label SPC	*Time-serial*	All-optical circuit [144] or nonlinear crystals [145, 146]
	Wavelength	Narrow-band AWG or filters
Payload MWC	*Intensity modulated*	cross modulation or gating, wave mixing, etc. [60, 68, 70]
	Other modulation	Wave mixing [70]

complexity and scalability .

i) *Time-serial labels*: AOLS nodes for optical intensity-modulated packets with time-serial labels as investigated in [13] can be greatly simplified employing our scheme. Table 9.3 summarizes the normalized minimum resources required for different time-serial label processing techniques. In this table, active switching units refer to active components with switching functionality, such as semiconductor optical amplifiers (SOAs) and SOA–Mach-Zehnder interferometers (SOA-MZIs); fixed gating inputs refer to continuous wave (CW) or optical gating pulse inputs.

Using spatial label processing by SPC, significant scalability improvement over

Table 9.3: Minimum resource requirement per AOLSW using different label processing schemes.

Time-serial labeling	*Active switching units*	*Gating inputs*	*AOFFs*
Parallel comparison [13]	$n \times 2^n$	2^n	2^n
Sequential recognition [15]	$6n + 2^n - 2$	$n - 1 + 2^n$	2^n
Spatial processing by SPC	Independent of n	n	n

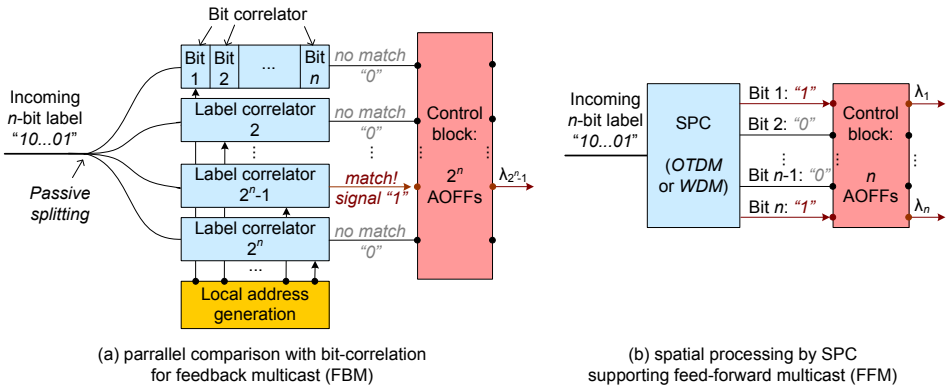

Figure 9.4: Comparison of two label processing schemes.

the previously reported methods can be achieved, since only the dimension of the label processor regarding the number of its outputs increases with n, while the active switching units for the SPC [144–146] remain the same regardless of n. Moreover, other necessary resources such as fixed gating inputs and AOFFs are also downsized from 2^n to n. Finally, this scheme also eliminates the *local address generation* in the other proposed AOLS schemes in Table 9.3 as the label processing no longer relies on bit-correlation. Fig. 9.4 shows a schematic comparison of the parallel bit-correlation approach and the spatial label processing approach.

ii) *Wavelength labels*: short-pulse wavelength labels allow further simplification of the label processing by offering several advantages over time-serial labels [12, 143]: they do not require strict synchronization with the payload as labels can be placed in-band of the payload [12]; and SPC can be simply and inexpensively realized by a passive narrow-band AWG.

For in-band labeling as shown in Fig. 9.1 (b), in each label, "1's" and "0's" are represented by the presence and absence of the optical pulses on particular wavelengths inside the bandwidth of the payload. The higher the payload bit rate, the wider the bandwidth, and hence more labels can be accommodated. The AWG used for packet routing needs to have a wider band covering the bandwidth of the payload. A disadvantage of the in-band wavelength labeling technique is the crosstalk between the label and payload.

To avoid label-payload crosstalk, the label bits can be placed on wavelengths outside the bandwidth of the payload, as illustrated in Fig. 9.1 (c). This technique has lower spectral efficiency as it consumes more bandwidth outside the payload bandwidth. The AWGs for packet routing also need to have sufficient bandwidth covering both the label and the payload spectrum.

9.3 Feed-forward multicast scalability with regard to performance

The proposed all-optical label processing scheme supports optical layer self-routing FFM. In this section, traffic performance simulation results on the scalability of the FFM AOLS nodes are presented. First, we investigate the FFM scalability in terms of performance for increased AOLS node dimensions. Second, we investigate the FFM scalability in terms of performance under increased multicast traffic loads. The multicast performance simulations were carried out assessing the *network throughput (NT)* of the node [46, 64], as defined in Chapter 2 and Chapter 3, based on the Bernoulli traffic model. The probability of generating a multicast packet is configured as on average one multicast packet in every three packets generated. Three contention resolution schemes at the outputs were assessed: no contention resolution (`NoCR`), wavelength conversion (`WC`) and wavelength conversion plus one-slot packet buffering (`WCFB`).

9.3.1 Increasing AOLS node dimension

In this set of simulations, we compare the FFM AOLS node performance of three dimensions: 3 ports, 4 ports, and 5 ports. 3-port and 4-port AOLS node architectures are illustrated in Fig. 9.3 and Fig. 9.5. A 5-port AOLS node has five pair of input and output ports, including one pair of add/drop ports.

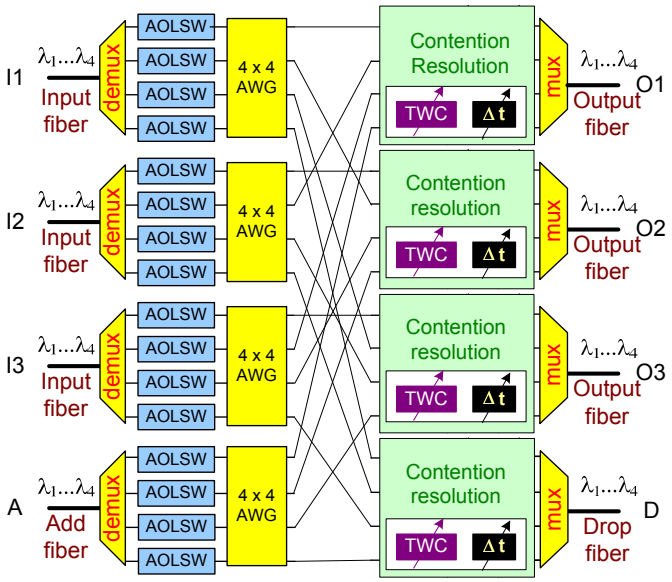

Figure 9.5: 4-port AOLS node architecture.

Figure 9.6 presents two sets of simulation results, with different multicast conditions. Fig. 9.6 (a) presents the NT of the AOLS nodes when each multicast packet is only sent to *two* output ports, thus a *multicast factor* of 2. Fig. 9.6 (b) presents the NT of the AOLS nodes when each multicast packet can be sent to *two* output ports or *more*, thus a *multicast factor* greater than 2.

When the multicast factor is 2 for all the 3-port, 4-port and 5-port AOLS nodes, all these AOLS nodes of different dimensions experience the same offered network load per port. From Fig. 9.6 (a), we observe that for the case of `NoCR`, the 3-port AOLS node has the highest NT. This is because as the number of ports increases for an AOLS node, the chance that an output port receives multicast packets is higher. Without any contention resolution, more packets are discarded. Therefore, AOLS nodes with more ports have slightly lower NT in this case. When `WC` is introduced, the dimension of the AOLS node has almost no effect on the NT. If we further implement fiber buffering, the AOLS nodes with more ports have higher NT. This is because when `WCFB` contention resolution is implemented, overall traffic throughput per port is the same for different AOLS node dimensions. An AOLS node with more ports allows more traffic through the node, thus a higher

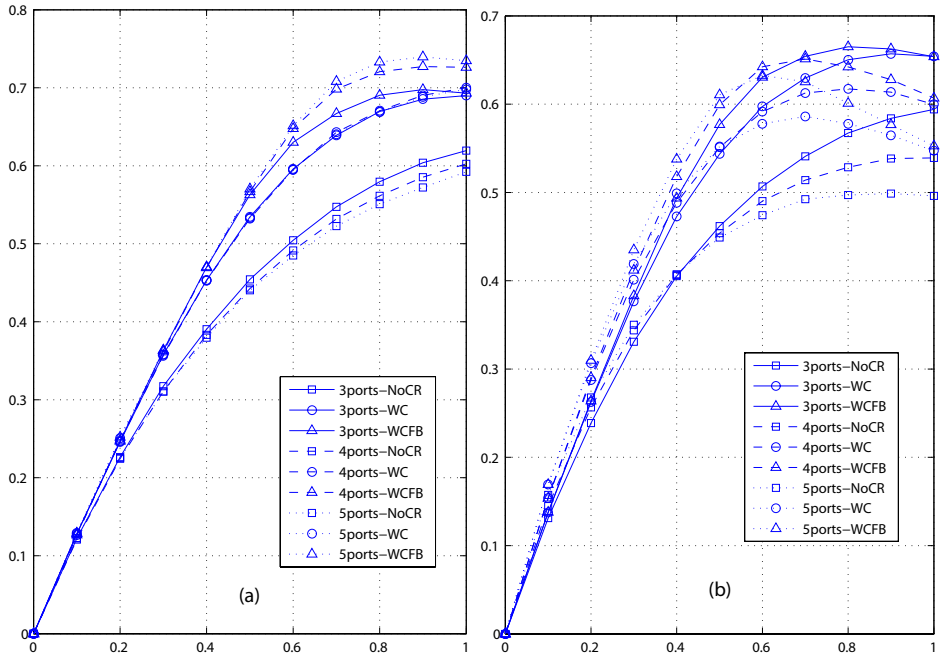

Figure 9.6: Network throughput comparison of FFM AOLS nodes with different node dimensions. The x-axis indicates the normalized network load. (a): multicast factor is 2; (b): multicast factor is greater than 2.

NT. Moreover, Fig. 9.6 (a) suggests that as the number of ports per AOLS node P increases, the difference in NT for a $(P+1)$-port AOLS node and a P-port AOLS node becomes less.

Figure 9.6 (b) presents the results when multicast factor is random for all the AOLS nodes. When a multicast packet is received, it is sent to *at least* two of the output ports. Therefore, for a 3-port AOLS node, a multicast packet can be duplicated or tripled. For a 4-port AOLS node, a multicast packet can be duplicated, tripled, or quadruplicated. For a 5-port AOLS node, a multicast packet can be duplicated, tripled, quadruplicated or quintuplicated. Under this random condition, as the AOLS node dimension increases, the AOLS node experience more multicast traffic, and the offered network load per port increases. Fig. 9.6 (b) shows that in the case of `NoCR`, the AOLS nodes with less ports have higher NT at a network load higher than 0.4, as they experience less multicast traffic and thus have a higher packet delivery success rate. At the network load of 0.8, the difference in

NT for different AOLS node dimensions in this case is four to five times greater than the case in Fig. 9.6 (a). When `WC` is implemented, the *NT* in general is higher for all the AOLS node dimensions, and the AOLS nodes with less ports have more throughput at a network load higher than 0.55. Now that contention resolution is introduced, the AOLS nodes start to experience *NT* saturation after the network load reaches 0.7. With `WCFB`, the *NT* in general is further improved for all the AOLS node dimensions, and the AOLS nodes with less ports have higher *NT* at a network load higher than 0.6. It is worth mentioning that after the *NT* saturation for the given contention resolution scheme, the throughput of the AOLS nodes starts to decrease, and can become worse than a smaller-dimension AOLS node with a weaker contention resolution scheme. For example, if the network load is higher than 0.9, a 5-port AOLS node with `WCFB` has lower *NT* than a 3-port node without any contention resolution, due to the much higher multicast traffic for the 5-port node.

In general, Fig. 9.6 suggests that the FFM scheme offers good node scalability, even if the multicast factor increases with the AOLS node dimension. In Fig. 9.6 (b), the *NT* decreases at most about 0.05 at a *full* network load of 1. The FFM AOLS nodes are scalable in traffic performance because it allows parallel multicast packet forwarding as each multicast packet is directly converted onto suitable wavelengths by the AOLSW implementing all-optical spatial processing. Conventional feedback multicast (FBM) architecture [2, 13, 16, 22, 23] scales poorly as it relies on the feedback loops for recirculation of the multicast packets to be further processed, and thus only *one* multicast packet *per loop* can be handled at a time [46, 65].

9.3.2 Increasing multicast traffic loads

In this set of simulations, the AOLS node dimension is fixed, and the impact from the increased multicast traffic load on the AOLS node performance is investigated.

Figure 9.7 shows the simulation results. It can be seen that with the increased traffic load without more output exits, the *NT* becomes lower. With an increased multicast factor, the NT tends to saturate at a lower network load. At high network loads after reaching the saturation point, the fiber buffering becomes less effective as the buffers are constantly loaded and the new packets generated due to the increased network load have to be dropped.

In general, Fig. 9.7 indicates that the FFM AOLS node is also scalable as the

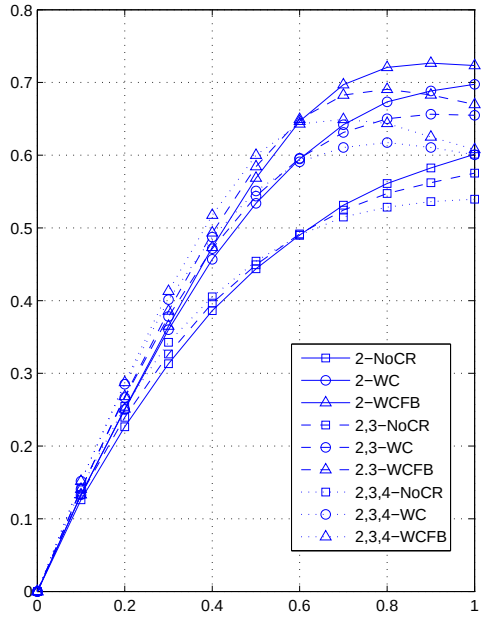

Figure 9.7: Network throughput comparison of a 4-port AOLS node with different multicast traffic loads. The numbers in the legend indicates possible multicast factors. The x-axis indicates the normalized network load.

multicast traffic loads increases. Under the same contention resolution scheme, with the increase of the multicast load the NT decreases between 0.025$\sim$ 0.06 at a *full* network load of 1 for a 4-port AOLS node.

9.4 Summary and discussions

In this chapter, a highly scalable all-optical spatial label processing scheme with a self-explanatory labeling concept is proposed. It can be employed for various optical-pulse based labeling techniques with different packet formats, regardless of the label bit-length n. For time-serial labels, the active switching components for the label processing are transparent to the label length; while the number of fixed gating inputs and required optical flip-flops can be reduced from 2^n to n. For wavelength labels, no active component is needed for label processing. Thus, it further simplifies the packet processor, lowers the power consumption, reduces hardware footprints, and consequently provides even higher AOLS node scalability.

Therefore, we consider wavelength labeling to be generally more suitable than time-serial labeling for practical AOLS networks.

However, wavelength labeling also has its disadvantages. The disadvantages depends on where the wavelength labels are placed. In-band labeling has good spectral efficiency but label-payload crosstalk is an important issue. Out-of-band labeling avoids possible label-payload crosstalk but requires extra spectrum for accommodating the labels. In general, when the optical packets are to be sent over long distance through dispersive fiber links, wavelength labels may also need additional dispersion control.

The SPC label processing scheme proposed in this chapter supports optical layer self-routing feed-forward packet multicast, which is considerably more efficient, scalable and economical than the conventional feedback multicast. Bernoulli traffic driven simulations indicate that the multicast node performance is not much affected by the node scaling from 3 ports to 5 ports, with maximum 0.05 decrease in the NT at a full network load for random multicast factors. This decrease in NT is due to the increasing multicast traffic in the AOLS nodes as the number of input ports increases, as each input port has the same probability of receiving multicast packets, which is 1/3.

An FFM AOLS node is also scalable when the multicast factor increases for a fixed AOLS node dimension. The maximum decrease in the NT due to the increased multicast traffic load is in the range of 0.025$\sim$ 0.06 at a *full* network load for a 4-port AOLS node. The decrease in the NT is due to the fact that more multicast packets are being multiplied in the AOLS node. After the NT reaches the saturation point for the defined contention resolution scheme, the packet loss starts to increase so the success rate for the packet delivery becomes lower.

Chapter 10

Conclusions and recommendations

All-optical label switching (AOLS) technologies are believed to be key for increasing the throughput of future optical packet switched networks for fiber line-rate data communications. The new constraints and realities imposed by the optical layer and wavelength division multiplexing technologies are already influencing many telecommunication standards that have been originally developed for mostly opaque optical networks. With the increasing amount of multicast applications such as multimedia streaming, high-definition TV, multi-party online games, video conferencing and optical storage area networks, AOLS with multicast becomes an important and exciting research subject that is likely to play an essential role in the next generation optical Internet and telecommunications infrastructure. Switching and multicasting in the optical layer will eliminate the electronic bottleneck and enable truly transparent optical networks taking full advantage of the available fiber bandwidth, developing towards future bit-rate-, protocol- and data-format-independent optical highways. In this chapter, the contributions and the main conclusions of this thesis are summarized, and recommendations for future research are given.

10.1 Summary of the LASAGNE project

The research presented in this thesis was initiated by the European Commission (EC) funded IST-LASAGNE (all-optical label-swapping employing optical logic gates in network nodes) project. In the LASAGNE project [13, 16, 38], an all-optical label switching (AOLS) node architecture with an all-optical label processor employing semiconductor optical amplifier – Mach-Zehnder interferometers (SOA-MZIs) was proposed. The main objective of the project was to verify the basic function of switching optical packets solely in the optical domain, without any electronic processing. The all-optical switching scheme will be particularly beneficial for transparent high-speed optical packet switching and forwarding at fiber line-rates in future *heterogeneous* optical packet networks that support various data and multimedia services and applications.

10.1.1 Project achievements

The AOLS node and network architecture investigated in the LASAGNE project were designed to perform wavelength division multiplexing (WDM) simultaneous all-optical time-serial label swapping for packet switching and forwarding. The revolutionary aspect of the study and trial of the AOLS node was to advance and combine the existing technologies for a completely all-optical WDM packet switching node that can switch and forward fixed-length optical packets directly in the optical layer. No electronics were involved in the switching/forwarding decision making.

At the completion of the project, all-optical packet *unicast* switching based on *two-bit* optical *time-serial* labels was demonstrated [14, 48]. The LASAGNE demonstrator included a working model of *four* out of the *six* proposed subsystems of the all-optical label processor, i.e. all-optical label swapper (AOLSW) (For details on the AOLSW, reference is made to Chapter 2). These *four* AOLSW subsystems were: *label extraction*, *label comparison*, *control block* and *wavelength conversion*. The other two AOLSW subsystems, namely *new label generation* and *label insertion*, were not demonstrated.

10.1.2 Issues not addressed in the project

The LASAGNE project focused on *unicast* operation of optical packets, although in the original proposal a *feedback multicast (FBM)* solution was included in the

node architecture [13]. Multicast operation of optical packets was neither investigated nor demonstrated in the LASAGNE project.

Contention resolution for the AOLS nodes was also not among the core objectives of the LASAGNE project. The LASAGNE project did not address a contention resolution scheme for solving optical packet contention at the AOLS *node* level, although during the project some proposals were raised for solving packet contention between two optical packets by means of wavelength conversion or optical buffering.

10.2 Contributions of this thesis

This thesis mainly contributes to the *multicast* aspects of the AOLS nodes in terms of *node architecture design*, *traffic performance analyses* under different *contention resolution schemes*, and physical layer *all-optical multicast technologies*. Apart from that, *unicast* AOLS node *traffic performance analyses* under different *contention resolution schemes* are also presented. In particular, the following issues of the AOLS nodes are the original contributions of this thesis:

1. Unicast AOLS nodes
   (a) Proposed an alternative AOLSW design with label and keyword generation based on external modulation (Sec. 2.3).
   (b) Evaluated traffic performance of a unicast AOLS node architecture with different contention resolution schemes including wavelength conversion and one-slot buffering, via computer simulations (Sec. 2.5).
   (c) Evaluated traffic performance of two buffering strategies for unicast AOLS nodes contention resolution, via computer simulations (Sec. 8.2).
2. Multicast AOLS nodes
   (a) Proposed a feed-forward multicast (FFM) scheme for the AOLS nodes (Sec. 3.2).
   (b) Compared and analyzed hardware requirements for the FFM and FBM schemes per AOLS node (Sec. 3.3).
   (c) Evaluated traffic performance of both FFM and FBM AOLS node architecture under different contention resolution schemes including wavelength conversion and one-slot buffering, as well as with different multicast traffic load and conditions, via computer simulations (Sec. 3.4).

(d) Proposed a simple, novel optical labeling scheme and a scalable all-optical spatial label processing scheme that support AOLS multicast (Sec. 9.2).

(e) Evaluated traffic performance of FFM AOLS nodes with different AOLS node dimension under different contention resolution schemes including wavelength conversion and one-slot buffering, as well as with different multicast traffic load and conditions, via computer simulations (Sec. 9.3).

3. Multi-wavelength conversion (MWC) technologies

(a) Researched and proposed possible MWC techniques for realizing AOLS FFM multicast (Sec. 4.3, Sec. 5.2, Sec.5.3).

(b) Experimentally evaluated laboratory performance of four promising MWC techniques (Sec. 5.4).

(c) Proposed a number of MWC-enabled new applications (Sec. 5.5).

(d) Extensively investigated on the MWC technique based on cross-phase modulation (XPM) in a single SOA-MZI, via computer simulations and laboratory experiments (Sec. 6.3, Sec. 6.4).

(e) Extensively investigated on the MWC technique based on four-wave mixing (FWM) in a nonlinear fiber, via laboratory experiments (Sec. 7.3).

As a summary, in 1, unicast AOLS node architecture and traffic performance are evaluated as a baseline. In 2, multicast AOLS node design and traffic performance are discussed. In 3, the physical-layer feasibility and performance of the multicast techniques for the AOLS nodes are investigated.

10.3 Main conclusions

AOLS nodes should considerably improve packet forwarding speeds compared to electronic processing switching nodes, however at this moment only at the cost of a high optical complexity, although the switch footprint can be relaxed by small-to-medium scale optical integration, which was further pursued in the EC-funded IST-MUFINS (multi-functional integrated arrays of interferometric switches) project.

Due to the complexity of the AOLS nodes, at the moment it is not possible to build and experimentally test the node performance. Therefore, in the research

framework, we have designed and developed our own simulator `AOLSim` using the C++ language. The current simulator can perform isolated AOLS node unicast traffic simulations, AOLS unicast network topology simulations up to 9 nodes and isolated AOLS multicast traffic simulations. The simulated isolated nodes have the size of 3×3 or 4×4 (no. of fiber line ports) and four wavelengths per port.

10.3.1 Unicast all-optical label switching nodes

For unicast AOLS nodes, traffic performance shows that the node packet loss ratio (PLR) and network throughput (NT) are considerably influenced by the implemented contention resolution scheme. For realistic bursty traffic patterns such as self-similar traffic, wavelength conversion (`WC`) proves to be much more efficient than optical fiber buffering (`FB`). However, when all the output wavelengths are occupied, optical buffering can further improve the node performance, but the effect is measurably lower. For example, at a network load of 0.8, `WC` improves the NT by about 20%, while further introducing one-slot `FB` only improves NT by about 5% more. – Chapter 2

Employing different buffering strategies has a certain impact on the AOLS node traffic performance. However, for self-similar traffic with a bursty nature, the difference of increasing the number of one-slot buffers and increasing the number of time slots in one buffer is hardly noticeable. For Bernoulli traffic with a homogeneous nature, increasing the number of one-slot buffers is far more efficient in reducing the PLR than increasing the number of time slots in one buffer, for buffer size *larger than one*. – Chapter 8

10.3.2 Multicast all-optical label switching nodes

As for multicast AOLS nodes, FFM is proven to be more efficient, economical and scalable than the conventional FBM approach. A hardware analysis shows that FFM requires considerably less physical resources than the FBM. For a 2×2 AOLS node, among other things, the FFM approach can save 20 all-optical flip-flops per node compared to the FBM approach. – Chapter 3

The traffic performance evaluation indicates that for the same AOLS node dimension, a FFM node performs similar to a unicast node, due to the similarity in their node architectures. The FFM node, however, has a slightly higher PLR and a lower NT. The higher PLR is due to the fact that there are more packets in the multicast AOLS nodes, so that more packets are likely to be lost because

of traffic congestion. The NT of the FFM node is lower because the FFM node duplicates effectively every multicast packet at the label processing stage, and not all of these packets can be successfully delivered, and the success rate is lower due to the increased traffic load compared to the unicast case. The NT also exhibits a saturation effect when the FFM AOLS node is operating at its maximum node capacity for the defined contention resolution scheme. – Chapter 3

Comparing the FFM and the FBM approach for the same AOLS node dimension, the FFM node *without* any contention resolution already performs similar to the FBM node *with* wavelength conversion and buffering. When wavelength conversion and buffering is introduced for the FFM node, its performance improves significantly. At low network loads, this improvement is several orders of magnitude. The limited performance of the FBM node is due to the fact that it can *only* process *one* multicast packet per time slot for its limited number of feedback loops, while the FFM node can *process* as many multicast packets as required and deliver *most* of them at the best of the AOLS node capacity under the specific contention resolution scheme. – Chapter 3.

AOLS node and network scalability is an important issue and a major concern for the proposed AOLS scheme in the LASAGNE project. The originally proposed AOLS scheme in the LASAGNE project requires $n \times 2^n$ SOA-MZIs *per* $AOLSW$ for comparing the incoming n-bit label with all 2^n possible addresses. If n increases with the up-dimensioning of AOLS nodes and networks, this approach is hardly scalable. This thesis proposes a novel labeling concept and a label processing scheme exploring the *space* domain of the label bits. The labeling concept and the spatial label processing scheme together enables a efficient self-routing AOLS node supporting both unicast and multicast operations. The dimension of the *label processor* is only proportional to n, and can be realized with a passive arrayed waveguide grating when wavelength labels are employed. The spatial label processing scheme is simple and its resource savings compared to previously proposed and investigated schemes are significant. – Chapter 9

10.3.3 Multi-wavelength conversion for all-optical multicast

MWC is essential for realizing FFM. This thesis reviews and summarizes the state-of-the-art MWC technologies and organizes them into categories according to their underlying principles and nonlinear processes. – Chapter 4

Four MWC techniques are evaluated through laboratory experiments, based

on FWM in a nonlinear fiber, FWM in a semiconductor optical amplifier (SOA), cross-gain modulation (XGM) in an SOA, and XPM in an SOA-MZI. FWM can offer format- and bit-rate- transparent MWC, as well as channel-independent operation when the input wavelength channels are positioned properly in the spectral domain, but it has very low conversion efficiency. The performance of XGM MWC is strongly dependent on the number of channels and the output extinction ratios decrease measurably with the increase of the number of MWC channels. The XPM-based MWC technique seems to be promising for intensity-modulated (IM) signals. Its good performance and the compact and integrable MWC medium, SOA-MZI, also make this technique more attractive compared to the others. – Chapter 5.

The experimental trials narrowed our MWC focuses to the compact and well-performed scheme based on XPM in an SOA-MZI, and the only format-transparent scheme based on FWM in a nonlinear fiber. Regarding the former scheme, simulations showed good performance for MWC to up to eight channels at both 10 Gb/s and 40 Gb/s. Experiments confirmed the excellent performance of this scheme for one-to-four non-return-to-zero (NRZ) MWC at 10 Gb/s with negligible or even negative penalties. At 40 Gb/s in a differential mode, one-to-four return-to-zero (RZ) MWC experienced higher power penalties but error-free operation up to bit-error rate of 10^{-9} was achieved. The simulation and experimental results suggested that with current SOA-MZI technologies, this approach can be *possibly* used for MWC of IM signals for up to one-to-eight MWC with 200 GHz channel spacing at 40 Gb/s bit rate, or even at higher bit rates up to 60∼80 Gb/s but with a lower number of MWC channels. One of the main factor that limits the maximum number of MWC channels is the signal degradation in some of the MWC channels due to the FWM interference at equal channel spacing. – Chapter 6

Up to one-to-three MWC by FWM in a dispersion-shifted fiber (DSF) was investigated in the laboratory. This technique also suffers from inter-channel crosstalk when input channels are spaced equally in the frequency domain or nearly equally in the wavelength domain. Such crosstalk may seriously affect the converted signal quality and causes converted eye closure at logical *one* level due to the superposition of the converted signal and lower-power FWM high-order products. Apart from that, this technique exhibited a noise compression effect contributed by the quadratic nature of the FWM replicas selected. This effect can improve the Q factor of the converted signal and thus provides signal regeneration of the converted channels. In general, this technique does not offer much

wavelength flexibility of the input channels as the data signal needs to be placed at the zero-dispersion wavelength of the fiber. With a highly-nonlinear fiber, the maximum possible number of channels for MWC can be potentially higher than the XPM approach, but its conversion efficiency is much lower. – Chapter 7

10.4 Recommendations

Concerning unicast AOLS nodes, issues for further study may include a more practical design of the optical switch building blocks, module and system integration, as well as analysis of the network performance and the scaling properties. In particular, all-optical verification and implementation of the contention resolution blocks based on all-optical logic functions will be essential for realizing fully transparent optical packet forwarding at fiber line-rates.

For multicast AOLS nodes, scalable node technologies such as the proposed all-optical spatial label processing scheme deserves further investigation. FFM AOLS nodes should be looked into, as they show superior performance to the FBM AOLS nodes, and require considerably less physical resources. Studies on the traffic performance of the FFM AOLS networks need to be carried out to determine the most efficient node and network dimension, as well as network topologies. Two lines of future research may assess the node performance under different traffic conditions with various AOLS dimensions and structures, and network performance evaluation of mixed AOLS unicast and multicast nodes in ring, mesh or other network topologies.

For physical layer multicast technologies based on MWC, one can exploit the investigated XPM and FWM schemes for converting a higher number of channels. However, for simultaneous MWC to more than eight to ten channels, different MWC techniques may be required. A recent demonstration shows that up to one-to-forty MWC can be achieved in a parametric amplifier [147], although this approach necessitates high-power pumps at the input to provide gain to the converted channels, and its conversion efficiency varies from channel to channel.

Appendix A

Traffic models

A.1 Bernoulli traffic

Bernoulli is the simplest traffic pattern for packet switched networks. When it comes to traffic performance evaluation, it is common to start with the simplest possible traffic scenario. Moreover, analytical results exist for Bernoulli traffic models [148]. It is important to implement this model to test the simulation engine and platform [43]. For Bernoulli traffic, there is a probability $\rho \in (0, 1)$ that in any time slot, any input will be receiving a packet on a certain wavelength. This probability is *constant* and *independent* of whether there have been packets on previous time slots and/or at other inputs. For a $\rho = 0.8$, the probability that a packet is generated in a random time slot on a certain wavelength at a node input is simply 0.8. With a $\rho = 0.5$, it is like the case of repeatedly tossing a coin: the probability of "heads" appearing is always 0.5, independent of whether "heads" have come up on any previous tosses of the coin [149].

The probability ρ follows a *Bernoulli distribution*, which is defined by the following equations:

$$p(x) = \begin{cases} 1-\rho & x = 0 \\ \rho & x = 1 \\ 0 & x \neq 0, x \neq 1 \end{cases} \tag{A.1}$$

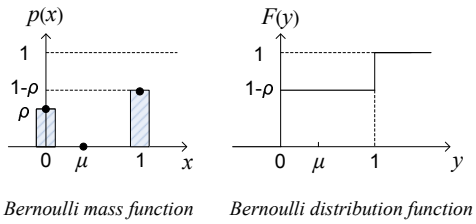

Figure A.1: Bernoulli distribution.

$$F(y) = p(x < y) = \begin{cases} 0 & y < 0 \\ 1 - \rho & 0 \leq y < 1 \\ 1 & 1 \leq y \end{cases} \tag{A.2}$$

$$\mu = \sum_i x_i p(x_i) = 0 \times (1 - \rho) + 1 \times \rho = \rho \tag{A.3}$$

In probability theory, Eq. A.1 is the *probability mass function*, also referred to as the *probability density function* or *frequency function*, which is the probability of an event giving a certain result. Eq. A.2 is the *probability distribution function*, also referred to as the *cumulative distribution function* or just *distribution function*, which is the probability that the result of an event x is smaller than a real number y. Eq. A.3 gives the *mean* value of the probability distribution. The above functions are plotted in Fig. A.1.

To generate Bernoulli traffic, in every time slot, a uniformly distributed random variable $u \in (0, 1)$ is created. If $u \leq \rho$, then $x = 1$, and a packet is generated. Otherwise, $x = 0$ and no packet is generated [43, 44]. Such a simple model clearly has limitations, since real traffic, particularly data traffic, is often bursty, i.e., the data packets tend to group together in time.

A.2 Self-similar traffic

Self-similarity is the property of objects called fractals and refers to the unchanged appearance regardless of the scale at which they are viewed. In Fig. A.2, a self-similar object *fractal* is presented.

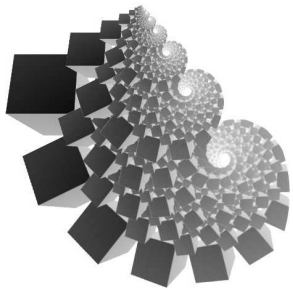

Figure A.2: Self–similarity in a 3D figure.

Historically, traffic modeling has its origins in conventional telephony, and has been based almost exclusively on *Poisson* or more generally, *Markovian* assumptions about traffic arrival patterns, and on *exponential* assumptions about resource holding requirements [73]. However, the emergence of modern high-speed packet networks combines drastically new and different transmission and switching technologies with dramatically heterogeneous mixtures of services and applications. As a result, packet traffic is generally expected to be more complex or bursty than voice traffic, simply because it is spanning vastly different time scales, from microseconds to seconds and minutes.

Classical traffic models such as *Bernoulli* and *geometric* were used to convey the autocorrelation or short-range dependence (SRD) found in bursty empirical traffic traces. In the early 90's, researchers found evidence of long-range dependence (LRD) in empirical traffic traces. This raised serious doubts about modeling network arrivals using *Poisson* and *Markov*-modulated processes, as these cannot convey LRD if stationary. There is convincing evidence that LRD is present in many types of network traffic, including: Ethernet LAN traffic, WAN traffic, coded video traffic, frame-relay traffic, asynchronous transfer mode (ATM) WAN traffic, narrow-band integrated services digital network (ISDN) traffic, telnet packet arrivals, the sizes of file transfer protocol (FTP) bursts, and some types of world-wide web (WWW) traffic [150].

LRD greatly lengthens the tail of queue waiting time distributions, so ignoring LRD can lead to overly optimistic estimates of performance in buffer dimensioning. This can result in more frequent buffer overflow in finite queues, in delays an order of magnitude longer than expected in some queues, and/or other manifestations of poor performance [72]. LRD is a characteristic of self-similar processes, so

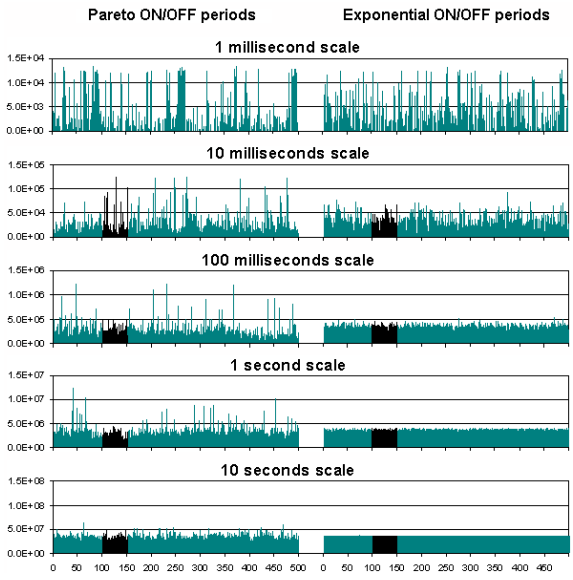

Figure A.3: Comparison between self-similar and exponential traffic [151].

self-similar processes are often used to generate synthetic arrivals in simulations when LRD is an important trait. In the case of traffic, self-similarity is used in a distributional sense: when viewed at different scales, the correlation structure of the traffic remains unchanged. Fig. A.3 shows a comparison between *exponential* and *self-similar* traffic [151]. In contrast to exponential traffic, the distribution of self-similar traffic exhibits a high variability even at large scales.

Because self-similar traffic has proven to represent realistic network traffic characteristics, such as Internet traffic [72–74], generating synthetic self-similar traffic is important to achieve credible simulation results. There exist many methods of creating self-similar traffic [73, 150–152]. One way is to multiplex multiple sources of a number of individual ON/OFF sources with infinite variance distribution, i.e. heavy-tailed distribution, for the lengths of their ON/OFF periods [73]. In the context of a packet switched network, the ON periods correspond to continuous packet trains, and OFF periods correspond to silence between packet trains [73].

The simplest heavy-tailed distribution is the *Pareto distribution*, defined by the following probability density function $p(x)$, distribution function $F(y)$, and mean value μ:

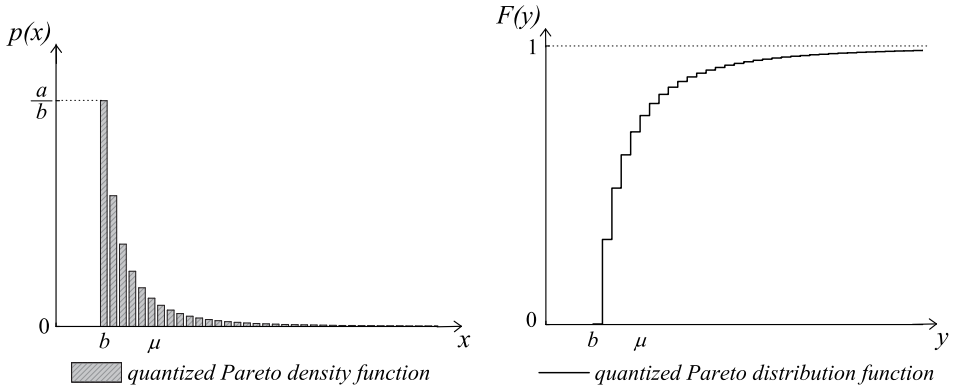

Figure A.4: Quantized Pareto distribution.

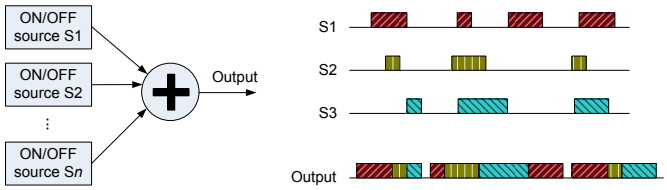

Figure A.5: Aggregation of Pareto ON/OFF traffic to form self-similar traffic [43, 44].

$$p(x) = \frac{ab^a}{x^{a+1}} \qquad a, b > 0, x \geq b \tag{A.4}$$

$$F(y) = p(x < y) = 1 - \left(\frac{b}{y}\right)^a \qquad a, b > 0, y \geq b \tag{A.5}$$

$$\mu = \frac{ab}{a-1} \tag{A.6}$$

In `AOLSim`, self-similar traffic is generated using a superposition of *Pareto*-distributed ON/OFF periods [43, 44]. However, the Pareto distribution is *continuous*, which means a Pareto random variable can be any decimal value from 0 to infinity. Because the simulation is *discrete*, in which a burst of packets occupies an integer number of slots of time, a quantized version of the Pareto distribution is applied, as plotted in Fig. A.4, where the simulated values are rounded up to the next integers [43, 44]. Aggregation of Pareto traffic is shown in Figure A.5.

Appendix B

VPI simulation parameters and schematics

B.1 Simulation parameters

Table B.1 summarizes the simulated physical parameters for semiconductor optical amplifier – Mach-Zehnder interferometer (SOA-MZI) in *VPI* in Chapter 6 [126, 130].

B.2 Simulation schematics

B.2.1 XPM MWC simulations at 10 Gb/s

In the multi-wavelength conversion (MWC) simulation at 10 Gb/s shown in Fig. B.1, an externally modulated *transmitter* was used for the original data channel and a variable number of continuous wave (CW) lasers was multiplexed into the central port of the SOA-MZI as the probe channels. The inclusion of the polarization controllers (PCs) for the data and CW channels was not necessary for the SOA-MZI model used in the simulations presented in Chapter 6, but for testing other wavelength conversion models. They had no effect on the simulation results. At the output of the SOA-MZI, the simultaneously converted channels were separated by a basic *demultiplexer* in *VPI*, which is an attenuator with standard third-order filters configured with 40 GHz bandwidth. After demultiplexing, each converted

Table B.1: Simulated physical parameters for semiconductor optical amplifier – Mach-Zehnder interferometer (SOA-MZI) in *VPI* [126, 130].

Parameter	Value		Units
	10 Gb/s	40 Gb/s	
SOA length	1	0.5	mm
SOA width	1	0.3	μm
SOA height	0.2		μm
optical confinement factor Γ	0.3		
fixed internal losses	3000		1/m
differential gain (gain cross section σ_g [82])	2.8e-20	3e-20	m^2
carrier density at transparency	1.4e24		$1/m^3$
IndexToGainCoupling α	3	1	
linear recombination constant (A)	1.43e8		1/s
biomolecular recombination constant (B)	1.0e-16		m^3/s
Auger recombination constant (C)	1.3e-41	3.0e-41	m^6/s
initial carrier density	2.0e24		$1/m^3$

channel was amplified by an erbium-doped fiber amplifier (EDFA), and then filtered by a band-pass filter (BPF) to remove the out-of-band amplified spontaneous emission (ASE) noise. Finally, the signals were sent to three different modules: i) an *ideal optical to electrical converter* followed by an *electrical signal analyzer* that calculates the eye extinction ratio (ER) illustrated in a *text visualizer*; ii) a *bit-error rate (BER) measuring block* together with a *power meter* for measuring BER as a function of the received optical power; iii) a *clock recovery circuit* followed by a *scope* for eye pattern visualization. The outputs of all the *BER* modules, including one for the original signal channel, were plotted in an *XY visualizer* to generate the BER curves.

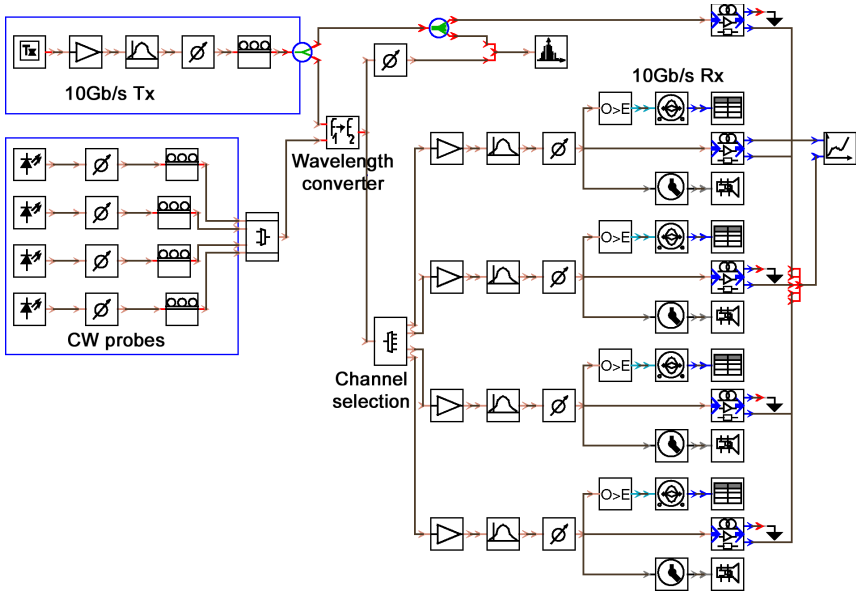

Figure B.1: *VPI* simulation schematic of MWC via a SOA-MZI at 10 Gb/s.

B.2.2 XPM MWC simulations at 40 Gb/s

In the *VPI* simulation scheme shown in Fig. B.2, a *Gaussian pulse transmitter* was used as a data generator to produce the 40 Gb/s return-to-zero (RZ) pulse train. The *full width at half maximum (FWHM)* of the source pulse is around 2 ps. In optical communications, FWHM can be used to describe the duration of pulse waveforms or the spectral width of optical sources used for the resolution of a spectrometer such as an optical spectrum analyzer (OSA). In the former case, a FWHM is typically quoted in units of time duration, e.g. picoseconds (ps). In the latter case, a FWHM is typically quoted in units of very small length, e.g. nanometers (nm). A FWHM of an optical pulse is given by the pulse width at half of the maximum pulse energy.

In the differential mode, the *push* data pulses were sent into one arm of the MZI inducing a nonlinear phase shift within the SOA. This nonlinearity was offset by inducing a similar effect within the SOA of the other arm by the delayed *pull* pulses. All the filters were configured with 130 GHz bandwidth to accommodate the wide 40 Gb/s RZ spectrum. Each extracted and pre-amplified channel was sent to a *scope* for eye pattern visualization.

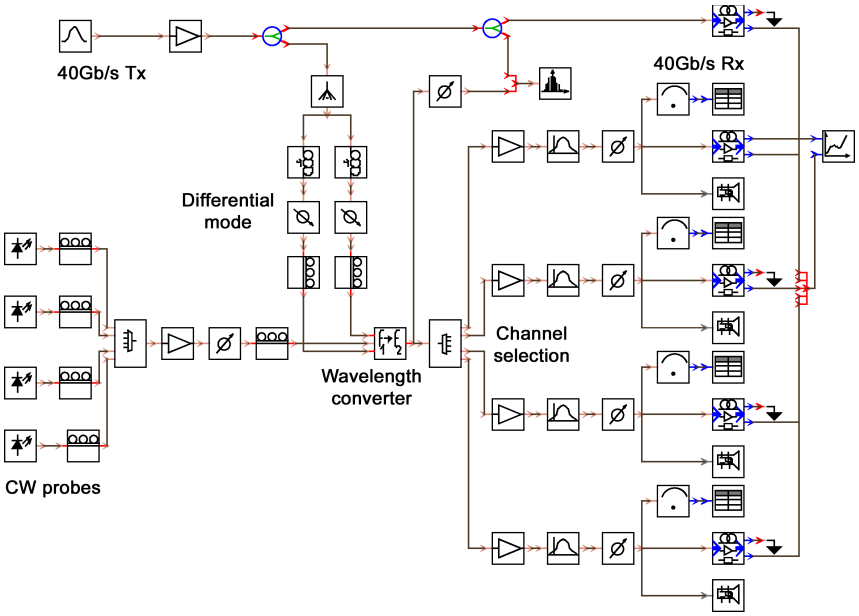

Figure B.2: *VPI* simulation schematic of MWC via a SOA-MZI at 40 Gb/s.

References

[1] N. Yan, I. Tafur Monroy, and A. M. J. Koonen, "All-optical label swapping node architectures and contention resolution," in *Proc. Int. Conf. on Optical Networking Design and Modeling (ONDM)*, pp. 1–9, Milan, Italy, Feb. 2005.

[2] A. M. J. Koonen, N. Yan, J. J. Vegas Olmos, I. Tafur Monroy, C. Peucheret, E. van Breusegem and E. Zouganeli, "Label-controlled optical packet routing - technologies and applications," *IEEE J. Select. Topics in Quantum Electron.*, vol. 13, pp. 1540–1549, Sept./Oct. 2007.

[3] A. S. Tanenbaum, *Computer networks.* Prentice Hall PTR, 3rd ed., 1996.

[4] L. L. Peterson and B. S. Davie, *Computer networks - a systems approach.* Morgan Kaufmann Publishers, 3rd ed., 2003.

[5] S. S. Dixit, *IP over WDM: building the next generation optical Internet.* USA: John Wiley & Sons, 2003.

[6] J.-P. Laude, *DWDM fundamentals, components, and applications.* USA: Artech House, 2002.

[7] D. Chiaroni, "Packet switching matrix: a key element for the backbone and the metro," *IEEE J. Select. Areas in Comm.*, vol. 21, pp. 1018–1025, Sept. 2003.

[8] B. Davie and Y. Rekhter, *MPLS technology and applications.* USA: Academic Press, 2000.

[9] P. Tomsu and G. Wieser, *MPLS-based VPNs.* USA: Prentice Hall PTR, 2002.

[10] S. V. Kartalopoulos, *DWDM networks, devices, and technology.* IEEE Press, John Wiley & Sons, Inc., 2003. ch. 5, Sec. 5.1, pp. 390.

[11] W. Wang, L. G. Rau, and D. J. Blumenthal, "160 Gb/s variable length packet / 10 Gb/s-label all-optical label switching with wavelength conversion and unicast/multicast operation," *IEEE/OSA J. Lightwave Technol.*, vol. 23, pp. 211–218, Jan. 2005.

[12] J. Herrera, O. Raz, E. Tangdiongga, Y. Liu, J. Marti, F. Ramos, G. Maxwell, A. Poustie, H. C. Mulvad, M. T. Hill, H. de Waardt, D. G. Khoe, A. M. J. Koonen, and H. J. S. Dorren, "160 Gb/s all-optical packet switched network operation over 110 km of field installed fiber," Anaheim, CA, USA, PDP5, Mar. 2007.

[13] F. Ramos, E. Kehayas, J. M. Martinez, R. Clavero, J. Marti, L. Stampoulidis, D. Tsiokos, H. Avramopoulos, J. Zhang, P. V. Holm-Nielsen, N. Chi, P. Jeppesen, N. Yan, I. Tafur Monroy, A. M. J. Koonen, M. T. Hill, Y. Liu, H. J. S. Dorren, R. V. Caenegem, D. Colle, M. Pickavet, and B. Riposati, "IST-LASAGNE: towards all-optical label swapping employing optical logic gates and optical flip-flop," *IEEE/OSA J. Lightwave Technol.*, vol. 23, pp. 2993–3011, Oct. 2005.

[14] J. Seoane, P. V. Holm-Nielsen, P. Jeppesen, E. Kehayas, H. Avramopoulos, Y. Liu, S. Zhang, H. J. S. Dorren, J. M. Martinez, J. Herrera, F. Ramos, J. Marti, R. McDougall, and G. D. Maxwell, "Towards transparent all-optical label-swapped networks: 40 Gb/s ultra-fast dynamic wavelength routing using integrated devices," in *Proc. European Conf. on Optical Comm. (ECOC)*, vol. 3, pp. 91–92, Cannes, France, Sept. 2006.

[15] R. van Caenegem, D. Colle, M. Pickavet, and P. Demeester, "AOLS node with sequential address generation and label recognition," in *Proc. European Conf. on Optical Comm. (ECOC)*, no. 1.6.6, pp. 99–100, Sept. 2007.

[16] R. van Caenegem, D. Colle, M. Pickavet, P. Demeester, K. Christodoulopoulos, K. Vlachos, E. Varvarigos, L. Stampoulidis, D. Roccato, and R. Vilar, "The design of an all-optical packet switching network," *IEEE Comm. Magazine*, vol. 45, pp. 52–61, Nov. 2007.

[17] R. Ramaswami and K. N. Sivarajan, *Optical networks: a practical perspective.* Morgan Kaufmann Publishers, 2nd ed., 2002. ch. 1, Sec. 1.7, pp. 28-30.

[18] S. J. B. Yoo, "Optical-label switching, MPLS, MPLambdaS, and GMPLS," *Opt. Netw. Mag.*, vol. 4, pp. 17–31, May/Jun. 2003.

[19] B. Meagher, G. K. Chang, G. Ellinas, Y. M. Lin, W. Xin, T. F. Chen, X. Yang, A. Chowdhury, J. Young, S. J. Yoo, C. Lee, M. Z. Igbal, T. Robe, H. Dai, Y. J. Chen, and W. I. Way, "Design and implementation of ultra-low latency optical label switching for packet-switched WDM networks," *IEEE/OSA J. Lightwave Technol.*, vol. 18, pp. 1978–1987, Dec. 2000.

[20] Z. Zhu, V. J. Hernandez, M. Y. Jeon, J. Cao, Z. Pan, and S. J. B. Yoo, "RF photonics signal processing in subcarrier multiplexed optical-label switching communication systems," *IEEE/OSA J. Lightwave Technol.*, vol. 21, pp. 3155–3166, Dec. 2003.

[21] D. J. Blumenthal, B.-E. Olsson, G. Rossi, T. E. Dimmick, L. Rau, M. Masanovic, O. Lavrova, R. Doshi, O. Jerphagnon, J. E. Bowers, V. Kaman, L. A. Coldren, and J. Barton, "All-optical label swapping networks and technologies," *IEEE/OSA J. Lightwave Technol.*, vol. 18, pp. 2058 – 2075, Dec. 2000.

[22] Z. Pan, H. Yang, J. Yang, J. Hu, Z. Zhu, J. Cao, K. Okamoto, S. Yamano, V. Akella, and S. J. B. Yoo, "Advanced optical-label routing system supporting multicast, optical TTL, and multimedia applications," *IEEE/OSA J. Lightwave Technol.*, vol. 23, pp. 3270–3281, Oct. 2005.

[23] K. G. Vlachos, I. Tafur Monroy, A. M. J. Koonen, C. Peucheret, and P. Jeppesen, "STOLAS: switching technologies for optically labeled signals," *IEEE Comm. Magazine*, vol. 41, pp. S9–15, Nov. 2003.

[24] I. Tafur Monroy, E. van Breusegem, A. M. J. Koonen, J. J. Vegas Olmos, J. van Berkel, J. Jennen, C. Peucheret, and Evi Zouganeli, "Optical labeled switched networks: laboratory trial and network emulator in the IST-STOLAS project," *IEEE Comm. Magazine*, pp. 43–51, Aug. 2006.

[25] D. J. Blumenthal, A. Carena, L. Rau, V. Curri, and S. Humphries, "All-optical label swapping with wavelength conversion for WDM-IP networks with subcarrier multiplexed addressing," *IEEE Photon. Technol. Lett.*, vol. 11, pp. 1497–1499, Nov. 1999.

[26] T. Fjelde, A. Kloch, D. Wolfson, B. Dagens, A. Coquelin, I. Guillemot, F. Gaborit, F. Poingt, and M. Renaud, "All optical fiber 2 + 1 auxiliary carrier trransponder-regenerator," *IEEE Photon. Technol. Lett.*, vol. 13, pp. 750–752, July 2001.

[27] D. Gurkan, S. Kumar, A. E. Willner, K. R. Parameswaran, and M. M. Fejer, "Simultaneous label swapping and wavelength conversion of multiple independent WDM channels in an all-optical MPLS network using PPLN waveguides as wavelength converters," *IEEE/OSA J. Lightwave Technol.*, vol. 21, pp. 2739–2744, Nov. 2003.

[28] O. Moriwaki, T. Sakamoto, A. Okada, and M. Matsuoka, "Demonstration of optical label processing with timing pulse generator," *IET Electron. Lett.*, vol. 39, pp. 730–731, May 2003.

[29] E. Udvary and T. Berceli, "Optical subcarrier label swapping by semiconductor optical amplifiers," *IEEE/OSA J. Lightwave Technol.*, vol. 21, pp. 3221–3225, Dec. 2003.

[30] S. J. B. Yoo, F. Xue, Y. Bansal, J. Taylor, Z. Pan, J. Cao, M. Jeon, T. Nady, G. Goncher, K. Boyer, K. Okamoto, S. Kamei, and V. Akella, "High-performance optical-label switching packet routers and smart edge routers for the next-generation Internet," *IEEE J. Select. Areas in Comm.*, vol. 21, pp. 1041–1051, Sept. 2003.

[31] M. Y. Jeon, Z. Pan, J. Cao, Y. Bansal, J. Tayllor, Z. Wang, V. Akella, K. Okamoto, S. Kamei, J. Pan, and S. J. B. Yoo, "Demonstration of all-optical packet switching routers with optical label swapping and 2R regeneration for scalable optical label switching network applications," *IEEE/OSA J. Lightwave Technol.*, vol. 21, pp. 2723–2733, Nov. 2003.

[32] K. Kitayama, "Code division multiplexing lightwave networks based upon optical code conversion," *IEEE J. Select. Areas in Comm.*, vol. 16, pp. 1309–1319, Sept. 1998.

[33] K.-I. Kitayama, N. Wada, and H. Sotobayashi, "Architectural considerations for photonic IP router based upon optical code correlation," *IEEE/OSA J. Lightwave Technol.*, vol. 18, pp. 1834–1844, Dec. 2000.

[34] K.-I. Kitayama and M. Murata, "Versatile optical code-based MPLS for circuit, burst, and packet switchings," *IEEE/OSA J. Lightwave Technol.*, vol. 21, pp. 2753–2764, Nov. 2003.

[35] V. J. Hernandez, Y. Du, W. Cong, R. P. Scott, K. Li, J. P. Heritage, Z. Ding, B. H. Kolner, and S. J. B. Yoo, "Spectral phase-encoded time-spreading (SPECTS) optical code-division multiple access for terabit optical access networks," *IEEE/OSA J. Lightwave Technol.*, vol. 22, pp. 2671–2679, Nov. 2004.

[36] N. Wada, H. Harai, W. Chujo, and F. Kubota, "80G to 10G bit/s variable rate photonic packet routing based on multi-wavelength label switch," in *Proc. European Conf. on Optical Comm. (ECOC)*, vol. 3, pp. 308–309, Amsterdam, Netherlands, Sept./Oct. 2001.

[37] N. Wada, H. Harai, W. Chujo, and F. Kubota, "Multi-hop, 40 Gbit/s variable length photonic packet routing based on multi-wavelength label switching, waveband routing, and label swapping," in *Proc. Optical Fiber Comm. Conf. (OFC)*, pp. 216–217, Anaheim, CA, USA, Mar. 2002.

[38] http://www.ist-lasagne.org/.

[39] J. M. Martinez, J. Herrera, F. Ramos, and J. Marti, "All-optical correlation using cascaded logic XOR gates based on active Mach-Zehnder interferometers," in *Proc. European Conf. on Optical Comm. (ECOC)*, vol. 1, pp. 103–104, Glasgow, Scotland, Sept. 2005.

[40] L. Dittmann, C. Develder, D. Chiaroni, F. Neri, F. Callegati, W. Koerber, A. Stavdas, M. Renaud, A. Rafel, J. Sole Pareta, W. Cerroni, N. Leligou, L. Dembeck, B. Mortensen, M. Pickavet, N. Le Sauze, M. Mahony, B. Berde, and G. Eilenberger, "The European IST project DAVID: a viable approach toward optical packet switching," *IEEE J. Select. Areas in Comm.*, vol. 21, pp. 1026–1040, Sept. 2003.

[41] L. Dittmann, "Optical packet networks - conclusions from the IST DAVID project," in *Proc. Optical Fiber Comm. Conf. (OFC)*, no. TuQ1, Los Angeles, USA, Feb. 2004.

[42] G. C. Sackett and C. Y. Metz, *ATM and multiprotocol networking.* USA: McGraw-Hill, 1997.

[43] J. M. Delgado-Mendinueta, "Traffic performance simulation of all-optical label swapping nodes," Master's thesis, Eindhoven University of Technology, June 2006. Electro-Optical Communications Group, Dept. of Electrical Engineering.

[44] A. Alcaide García, "Performance evaluation of all-optical label swapping nodes," Master's thesis, Eindhoven University of Technology, June 2007. Electro-Optical Communications Group, Dept. of Electrical Engineering.

[45] N. Yan, I. Tafur Monroy, and A. M. J. Koonen, "All-optical label swapping technologies and node architecture," in *Proc. London Communication Symp. (LCS)*, pp. 85–88, London, UK, Sept. 2004.

[46] N. Yan, A. Alcaide, J. M. D. Mendinueta, E. Tangdiongga, and A. M. J. Koonen, "Traffic performance evaluation of optical label switching nodes with optical layer multicast," in *Proc. Asia-Pasific Optical Comm. Conf. (APOC)*, vol. 6783, Wuhan, China, Nov. 2007.

[47] J. M. D. Mendinueta, I. Tafur Monroy, J. J. Vegas Olmos, N. Yan, Y. Dimitriadis, I. de Miguel Jimenez, and A. M. J. Koonen, "Traffic performance study of all-optical label swapping isolated and full network topologies," in *Proc. European Conf. on Networks and Optical Communications (NOC)*, pp. 387–394, Berlin, Germany, July 2006.

[48] J. M. Martinez Canet, R. Clavero Galindo, J. Herrera Llorente, F. Ramos, Y. Liu, A. M. J. Koonen, H. J. S. Dorren, and J. Marti, "All-optical latching circuit controlled by a 2-bit all-optical correlator," in *Proc. European Conf. on Optical Comm. (ECOC)*, vol. 1, pp. 97–98, Berlin, Germany, Sept. 2007.

[49] O. Zouraraki, D. Petrantonakis, D. Apostolopoulos, E. Kehayas, N. Pieros, and H. Avramopoulos, "A 40 Gbps all-optical label/payload separation circuit using hybrid integrated MZI switches," in *Proc. European Conf. on Optical Comm. (ECOC)*, vol. 4, pp. 27–28, Cannes, France, Sept. 2006.

[50] D. C. Rogers, J. V. Collins, C. W. Ford, J. Lucek, M. Shabeer, G. Sherlock, D. Cotter, K. Smith, C. M. Peed, A. E. Kelly, P. Gunning, D. Nesset, and I. F. Lealman, "Optical pulse pattern generation for self-synchronizing 100 Gbit/s networks," in *Proc. Optical Fiber Comm. Conf. (OFC)*, pp. 98–99, 1996.

[51] L. Stampoulidis, E. Kehayas, H. Avramopoulos, Y. Liu, E. Tangdiongga, and H. J. S. Dorren, "40 Gb/s fast-locking all-optical packet clock recovery," in *Proc. Optical Fiber Comm. Conf. (OFC)*, vol. 4, Anaheim, CA, USA, Mar. 2005.

[52] R. McDougall, G. Maxwell, R. Harmon, L. Rivers, A. Poustie, Y. Liu, M. T. Hill, S. Zhang, F. Huijskens, and H. J. S. Dorren, "Hybrid integrated, all-optical flip-flop memory element for optical packet networks," in *Proc. European Conf. on Optical Comm. (ECOC)*, vol. 4, pp. 35–36, Cannes, France, Sept. 2006.

[53] M. L. Nielsen, M. Nord, M. N. Petersen, B. Dagens, A. Labrousse, R. Brenot, B. Martin, S. Squedin, and M. Renaud, "40 Gbit/s standard-mode wavelength conversion in all-active MZI with very fast response," *IET Electron. Lett.*, vol. 39, pp. 385–386, Feb. 2003.

[54] K. Sato, "Semiconductor light sources for 40-Gb/s transmission systems," *IEEE/OSA J. Lightwave Technol.*, vol. 20, pp. 2035–2043, Dec. 2002.

[55] L. Kazovsky, S. Benedetto, and A. Willner, *Optical fiber communication systems.* Artech House, 1996. pp. 514-515, 164.

[56] T. Otsuji, M. Yaita, T. Nagatsuma, and E. Sano, "10-80-Gb/s highly extinctive electrooptic pulse pattern generation," *IEEE J. Select. Topics in Quantum Electron.*, vol. 2, pp. 643–649, Sept. 1996.

[57] K. L. Hall and K. A. Rauschenbach, "All-optical bit pattern generation and matching," *IET Electron. Lett.*, vol. 32, pp. 1214–1215, June 1996.

[58] D. Wolfson, A. Kloch, T. Fjelde, C. Janz, B. Dagens and M. Renaud, "40-Gb/s all-optical wavelength conversion, regeneration, and demultiplexing in an SOA-based all-active Mach-Zehnder interferometer," *IEEE Photon. Technol. Lett.*, vol. 12, pp. 332–334, Mar. 2000.

[59] D. Reading-Picopoulos, F. Wang, Y.J. Chai, R.V. Penty, I.H. White, "10 Gb/s and 40 Gb/s WDM multi-casting using a hybrid integrated Mach-Zehnder interferometer," in *Proc. Optical Fiber Comm. Conf. (OFC)*, no. OFP2, Anaheim, CA, USA, Mar. 2006.

[60] N. Yan, T. Silveira, A. Teixeira, A. Ferreira, E. Tangdiongga, P. Monteiro, and A. M. J. Koonen, "40 Gbits/s wavelength multicast via SOA-MZI and applications," *IET Electron. Lett.*, vol. 43, p. 1300, Nov. 2007.

[61] Y. Liu, E. Tangdiongga, Z. Li, H. de Waardt, A. M. J. Koonen, G. D. Khoe and H. J. S. Dorren, "Error-free 320 Gb/s SOA-based wavelength conversion using optical filtering," in *Proc. Optical Fiber Comm. Conf. (OFC)*, p. PDP28, Anaheim, CA, USA, Mar. 2006.

[62] J. Herrera Llorente, E. Tangdiongga, H. de Waardt, O. Raz, G.-D. Khoe, A. M. J. Koonen, H. J. S. Dorren, Y. Liu, J. Marti, and F. Ramos, "160 Gb/s error-free transmission through a 100-km fibre link with mid-span all-optical SOA-based wavelength conversion," in *Proc. European Conf. on Optical Comm. (ECOC)*, no. 1.3.4, pp. 57–58, Berlin, Germany, Sept. 2007.

[63] J. Herrera, E. Tangdiongga, Y. Liu, M. T. Hill, R. McDougall, A. Poustie, G. Maxwell, F. Ramos, J. Marti, H. de Waardt, G. D. Khoe, A. M. J. Koonen, and H. J. S. Dorren, "160 Gb/s all-optical packet switching employing in-band wavelength labelling and a hybrid-integrated optical flip-flop," in *Proc. European Conf. on Optical Comm. (ECOC)*, no. PDP, Cannes, France, Sept. 2006.

[64] S. Yao, B. Mukherjee, S. J. B. Yoo, and S. Dixit, "A unified study of contention-resolution schemes in optical packet-switched networks," *IEEE/OSA J. Lightwave Technol.*, vol. 21, Mar. 2003.

[65] N. Yan, A. Alcaide, J. M. D. Mendinueta, E. Tangdiongga, and A. M. J. Koonen, "Cost reduction and traffic performance improvement using direct forward optical layer multicast in optical label switching nodes," in *Proc. European Conf. on Optical Comm. (ECOC)*, vol. 2, pp. 39–40, Berlin, Germany, Sept. 2007.

[66] A. Misawa and M. Tsukada, "Broadcast-and-select photonic ATM switch with frequency division multiplexed output buffers," *IEEE/OSA J. Lightwave Technol.*, vol. 15, pp. 1769–1777, Oct. 1997.

[67] N. Yan, H.-D. Jung, I. Tafur Monroy, H. de Waardt, and A. M. J. Koonen, "All-optical multi-wavelength conversion with negative power penalty by a commercial SOA-MZI for WDM wavelength multicast," in *Proc. Optical Fiber Comm. Conf. (OFC)*, p. JWA36, Anaheim, CA, USA, Mar. 2007.

[68] N. Yan, E. Tangdiongga, H.-D. Jung, I. T. Monroy, H. de Waardt, and A. M. J. Koonen, "Regenerative all-optical wavelength multicast for next generation wdm network and system applications," *Photon. Network Comm.*, vol. 1387-974X(print), Sept. 2007.

[69] N. Yan, T. Silveira, A. Teixeira, A. Ferreira, E. Tangdiongga, P. Monteiro, and A. M. J. Koonen, "40 Gb/s all-optical multi-wavelength conversion via a single SOA-MZI for WDM wavelength multicast," in *Proc. Optoelectronics and Communications Conf. (OECC)*, pp. 530–531, Yokohama, Japan, July 2007.

[70] N. Yan, A. Teixeira, T. Silveira, G.M. Tosi Beleffi, F. Curti, D. Forin, F. Dalla Longa, I. Tafur Monroy, P. Monteiro, and A. M. J. Koonen, "Theoretical and experimental performance evaluation of all-optical multi-wavelength conversion by four-wave mixing in fiber at 10/20/40 Gb/s for optical layer multicast," *Micro. and Optic. Technol. Lett.*, vol. 49, pp. 1067–1071, May 2007.

[71] H. S. Chung, R. Inohara, K. Nishimura, and M. Usami, "All-optical multi-wavelength conversion of 10 Gbit/s NRZ/RZ signals based on SOA-MZI for WDM multicasting," *IET Electron. Lett.*, vol. 41, pp. 432–433, Mar. 2005.

[72] W. E. Leland, M. S. Taqqu, W. Willinger, and D. V. Wilson, "On the self–similar nature of Ethernet traffic (extended version)," *IEEE/ACM Transactions on Networking*, vol. 2, Feb. 1994.

[73] W. Willinger, M. S. Taqqu, R. Sherman, and D. V. Wilson, "Proof of a fundamental result in self-similar traffic modeling," *IEEE/ACM Transactions on Networking*, vol. 5, Feb. 1997.

[74] M. E. Crovella and A. Bestavros, "Self-similarity in World Wide Web traffic: evidence and possible causes," *IEEE/ACM Transactions on Networking*, vol. 5, Dec. 1997.

[75] N. Yan, A. Teixeira, T. Silveira, A. M. J. Koonen, I. Tafur Monroy, P. Monteiro, G. Tosi Beleffi, and D. Forin, "Simultaneous multi-wavelength signal conversion for transparent optical multicast," in *Proc. European Conf. on Networks and Optical Communications (NOC)*, pp. 155–162, London, UK, July 2005.

[76] G. N. Rouskas, "Optical layer multicast: rationale, building blocks, and challenges," *IEEE Networks*, pp. 60–65, Jan./Feb. 2003.

[77] C. W. Chow, C. S. Wong and H. K. Tsang, "All-optical modulation format conversion and multicasting using injection-locked laser diodes," *IEEE/OSA J. Lightwave Technol.*, vol. 22, pp. 2386–2392, Nov. 2004.

[78] G. Contestabile, M. Presi, and E. Ciaramella, "Multiple wavelength conversion for WDM multicasting by FWM in an SOA," *IEEE Photon. Technol. Lett.*, vol. 16, pp. 1775–1777, July 2004.

[79] A. M. J. Koonen, "Fiber to the Home/Fiber to the Premises: What, Where, and When?," *Proc. IEEE*, vol. 94, pp. 911–934, May 2006.

[80] J. L. Miller and E. Friedman, *Optical communications rules of thumb.* McGraw-Hill, 2003.

[81] S. V. Kartalopoulos, *Optical bit error rate - an estimation methodology.* IEEE Press, John Wiley & Sons, Inc., 2004.

[82] G. P. Agrawal, *Fiber-optic communication systems.* John Wiley & Sons, Inc., 3rd ed., 2002.

[83] G. Keiser, *Optical fiber communications.* McGraw-Hill, 3rd ed., 2000.

[84] D. Derickson and M. Müller, *Digital communications test and measurement.* Prentice Hall, 2008.

[85] S. J. B. Yoo, "Wavelength conversion technologies for WDM network applications," *IEEE/OSA J. Lightwave Technol.*, vol. 14, pp. 955–966, June 1996.

[86] M. Asghari, I. H. White and R. V. Penty, "Wavelength conversion using semiconductor optical amplifiers," *IEEE/OSA J. Lightwave Technol.*, vol. 15, pp. 1181–1190, July 1997.

[87] H. Suche, G. Schreiber, Y. L. Lee, V. Quiring, R. Ricken, W. Sohler, A. Paoletti, F. Carbone, D. Caccioli, and A. Schiffini, "Efficient Ti: PPLN multiwavelength converter for high bitrate WDM-transmission systems," in *Proc. European Conf. on Optical Comm. (ECOC)*, pp. 42–43, Amsterdam, Netherlands, Oct. 2001.

[88] Y. W. Lee, F. C. Fan, B. Z. Dong, B. Y. Gu, and Y. C. Huang, "Aperiodic optical superlattice in lithium niobate for multi-wavelength conversion," in *Proc. Conf. on Lasers and Electro-optics (CLEO)*, 2002.

[89] S. J. B. Yoo, C. Caneau, R. Bhat, and M. A. Koza, "Wavelength conversion by quasi-phase-matched difference frequency generation in AlGaAs waveguides," in *Proc. Optical Fiber Comm. Conf. (OFC)*, pp. 377–380, San Diego, CA, USA, Feb./Mar. 1995.

[90] C. Gosset and G.-H. Duan, "Multi-wavelength conversion and resynchronization of wavelength division multiplexed signals by use of four-wave mixing in a semiconductor optical amplifier," in *Proc. Optical Fiber Comm. Conf. (OFC)*, pp. 706–707, Anaheim, CA, USA, Mar. 2002.

[91] Antònio L. J. Teixeira and Rogério Nogueira and Mário J. N. Lima and Paulo S. B. André and J. L. Pinto and J. R. F. da Rocha, "Multi-wavelength conversion based on a semiconductor optical amplifier self pumped converter," in *Proc. IEEE Int. Conf. on Telecommunications*, pp. 661–664, Papeete, French Polynesia, Feb. 2003.

[92] S. Watanabe, S. Takeda, G. Ishikawa, H. Ooi, J. G. Nielsen, and C. Sonne, "Simultaneous wavelength conversion and optical phase conjugation of 200 Gb/s (5×40 Gb/s) WDM signal using a highly nonlinear fiber four-wave mixer," in *Proc. European Conf. on Optical Comm. (ECOC)*, vol. 5, pp. 1–4, Edinburgh, UK, Sept. 1997.

[93] H. Ishikawa, S. Watanabe, and H. Kuwatsuka, "Wavelength conversion technologies for photonic network systems," *Fujitsu Sci. Tech. J.*, vol. 35, pp. 126–138, July 1999.

[94] G. P. Agrawal, *Nonlinear fiber optics.* Academic Press, 3rd ed., 2001.

[95] H. Simos, A. Bogris, and D. Syvridis, "Investigation of a 2R all-optical regenerator based on four-wave mixing in a semiconductor optical amplifier," *IEEE/OSA J. Lightwave Technol.*, vol. 22, pp. 595–604, Feb. 2004.

[96] W. S. C. Chang, *Principle of lasers and optics.* Cambridge University Press, 2005.

[97] A. Yariv, *Optical electronics.* Saunders College Publishing, 4th ed., 1991.

[98] J. Zhou, N. Park, K. J. Vahala, M. Newkirk, and B. I. Miller, "Four-wave mixing wavelength conversion efficiency in semiconductor traveling-wave amplifiers measured to 65 nm of wavelength shift," *IEEE Photon. Technol. Lett.*, vol. 6, pp. 984–987, Aug. 1994.

[99] M. Karasek, J. Kanka, P. Honzatko, J. Vojtech and J. Radil, "10 Gb/s and 40 Gb/s multi-wavelength conversion based on nonlinear effects in HNLF," in *Proc. Int. Conf. on Transparent Optical Networks (ICTON)*, pp. 155–161, Nottingham, UK, Tu.D1.7, June 2005.

[100] G. Kalogerakis, M. E. Marhic, and L. G. Kazovsky, "Multiple-wavelength conversion with gain by a high-repetition-rate pulsed-pump fiber OPA," *IEEE/OSA J. Lightwave Technol.*, vol. 23, pp. 2954–2960, Oct. 2005.

[101] N. Yan, A. Teixeira, T. Silveira, I. Tafur Monroy, P. Monteiro, G. Tosi Beleffi, and A. M. J. Koonen, "Optical multicasting performance evaluation using multi-wavelength conversion by four-wave mixing in DSF at 10/20/40 Gb/s," in *Proc. IEEE Int. Conf. on Photonics in Switching (PS)*, no. O 14.2, pp. 181–183, Herakleion, Crete, Greece, Oct. 2006.

[102] J. L. Pleumeekers, J. Leuthold, M. Kauer, P. G. Bernasconi, C. A. Burrus, M. Cappuzzo, E. Chen, L. Gomez and E. Laskowski, "All-optical wavelength conversion and broadcasting to eight separate channels by a single semiconductor optical amplifier delay interferometer," in *Proc. Optical Fiber Comm. Conf. (OFC)*, pp. 596–597, Anaheim, CA, USA, ThDD4, 2002.

[103] N. Yan, H.-D. Jung, I. T. Monroy, and A. M. J. Koonen, "Simultaneous one-to-four multi-wavelength conversion using a single SOA-MZI," in *Proc. European Conf. on Networks and Optical Communications (NOC)*, pp. 375–380, Berlin, Germany, July 2006.

[104] N. Yan, A. Teixeira, T. Silveira, I. Tafur Monroy, H.-D. Jung, and A. M. J. Koonen, "Optical multicast technologies by multi-wavelength conversion for optical routers," in *Prof. IEEE Int. Conf. on Communication Technology (ICCT)*, vol. SRGN, Guilin, China, Nov. 2006.

[105] B.-E. Olsson, P. Öhlén, L. Rau, and D. J. Blumenthal, "A simple and robust 40-Gb/s wavelength converter using fiber cross-phase modulation and optical filtering," *IEEE Photon. Technol. Lett.*, vol. 12, pp. 846–848, July 2000.

[106] L. Rau, B.-E. Olsson, and D. J. Blumenthal, "Wavelength multicasting using an ultra high-speed all-optical wavelength converter," in *Proc. Optical Fiber Comm. Conf. (OFC)*, pp. WDD52–1–WDD52–4, Anaheim, CA, USA, Mar. 2001.

[107] W. Mao, P. A. Andrekson, and J. Toulouse, "All-optical wavelength conversion based on sinusoidal cross-phase modulation in optical fibers," *IEEE Photon. Technol. Lett.*, vol. 17, pp. 420–422, Feb. 2005.

[108] G. Contestabile, N. Calabretta, R. Proietti and E. Ciaramella, "Double-stage cross-gain modulation in SOAs: an effective technique for WDM multicasting," *IEEE Photon. Technol. Lett.*, vol. 18, pp. 181–183, Jan. 2006.

[109] B. H. L. Lee, R. Mohamad and K. Dimyati, "Performance of all-optical multicasting via dual-stage XGM in SOA for grid networking," *IEEE Photon. Technol. Lett.*, vol. 18, pp. 2215–2217, Nov. 2006.

[110] D. Liu, N. J. Hong, and C. Lu, "Wavelength conversion based on cross-gain modulation of ASE spectrum of SOA," *IEEE Photon. Technol. Lett.*, vol. 12, pp. 1222–1224, Sept. 2000.

[111] Y. Shen, J. H. Ng, C. Lu, T. H. Cheng, and M. K. Rao, "Single to multi wavelength conversion using amplified spontaneous emission of semiconductor optical amplifier," in *Proc. Optical Fiber Comm. Conf. (OFC)*, vol. 1, Anaheim, CA, USA, Mar. 2001.

[112] X. Zhang, D. Huang, J. Sun, and D. Liu, "Single to 16-channel wavelength conversion at 10 Gb/s based on cross-gain modulation of ASE spectrum in SOA," *J. Optical and Quantum Electronics*, pp. 627–634, 2004.

[113] L. Xu, N. Chi, K. Yvind, L.J. Christiansen, L.K. Oxenløwe, J. Mørk, P. Jeppesen and J. Hanberg, "8×40 Gb/s RZ all-optical broadcasting utilizing an electroabsorption modulator," in *Proc. Optical Fiber Comm. Conf. (OFC)*, p. MF71, Los Angeles, USA, Feb. 2004.

[114] L. Xu, N. Chi, K. Yvind, L. J. Christiansen, L. K. Oxenløwe, J. Mørk, P. Jeppesen, and J. Hanberg, "7×40 Gb/s base-rate RZ all-optical broadcasting utilizing an electroabsorption modulator," *OSA Optics Express*, vol. 12, pp. 416–420, 2004.

[115] K. K. Chow and C. Shu, "All-optical wavelength conversion with multicasting at 6/*times*10 Gbit/s using electroabsorption modulator," *IET Electron. Lett.*, vol. 39, pp. 1395–1397, Sept. 2003.

[116] K. K. Chow and C. Shu, "All-optical signal regeneration with wavelength multicasting at 6×10 Gb/s using a single electroabsorption modulator," *OSA Optics Express*, vol. 12, no. 13, pp. 3050–3054, 2004.

[117] G. Contestabile, N. Calabretta, M. Presi and E. Ciaramella, "Single and multicast wavlength conversion at 40 Gb/s by means of fast nonlinear polarization switching in an SOA," *IEEE Photon. Technol. Lett.*, vol. 17, pp. 2652–2654, Dec. 2005.

[118] K. Morioka, K. Mori, S. Kawanishi, and M. Saruwatari, "Pulse-width tunable, self-frequency conversion of short optical pulses over 200 nm based on supercontinuum generation," *IET Electron. Lett.*, vol. 30, pp. 1960–1962, Nov. 1994.

[119] F. Futami, R. Okabe, Y. Takita, and S. Watanabe, "Transparent wavelength conversion at up to 160 Gb/s by using supercontinuum generation in a nonlinear fiber," in *Proc. OSA Optical Amplifiers and their Applications (OAA)*, no. MD07, Otaru, Japan, July 2003.

[120] G. Contestabile, F. Martelli, A. Mecozzi, L. Graziani, A. D'Ottavi, P. Spano, G. Guekos, R. Dall'Ara, and J. Eckner, "Efficiency flattening and equalization of frequency up- and down-conversion using four-wave mixing in semiconductor optical amplifiers," *IEEE Photon. Technol. Lett.*, vol. 10, pp. 1398–1400, Oct. 1998.

[121] T. Durhuus, B. Mikkelsen, C. Joergensen, S. L. Danielsen, and K. E. Stubkjaer, "All-optical wavelength conversion by semiconductor optical amplfiers," *IEEE/OSA J. Lightwave Technol.*, vol. 14, pp. 942–954, June 1996.

[122] J. M. H. Elmirghani and H. T. Mouftah, "All-optical wavelength conversion: technologies and applications in DWDM networks," *IEEE Comm. Magazine*, pp. 86–92, Mar. 2000.

[123] T. Schneider, *Nonlinear optics in telecommunications.* Springer, 2004.

[124] B. Mikkelsen, S. L. Danielsen, C. Joergensen, R. J. S. Pedersen, H. N. Poulsen, and K. E. Stubkjaer, "All-optical noise reduction capability of interferometric wavelength converters," *IET Electron. Lett.*, vol. 32, pp. 566–567, Mar. 1996.

[125] T. G. Silveira, P. M. N. P. Monteiro, A. L. J. Teixeira, and G. M. T. Beleffi, "Cross-gain modulation bandwidth enhancement in semiconductor optical amplifiers by means of detuned optical filter," *IET Electron. Lett.*, vol. 41, pp. 761–763, June 2005.

[126] J. del Val Puente, N. Yan, E. Tangdiongga, and A. M. J. Koonen, "Performance comparison of multi-wavelength conversion using SOA-MZI and DSF for optical wavelength multicast," in *Proc. Int. Conf. on Optical Networking Design and Modeling (ONDM)*, pp. 1–10, Athens, Greece, May 2007.

[127] A.A.M. Saleh, "Nonlinear models of travelling-wave optical amplifiers," *IET Electron. Lett.*, vol. 24, pp. 835–837, 1988.

[128] S. Shimada and H. Ishio, *Optical amplifiers and their applications.* Chichester, Ch. 3: John Wiley, 1994.

[129] G.P. Agrawal and N.K. Dutta, *Long-wavelength semiconductor lasers.* New York: Van Nostrand Reinhold, 1986.

[130] J. del Val Puente, "Multi-wavelength conversion using SOA-MZI, SOA and DSF for optical wavelength multicast," Master's thesis, Eindhoven University of Technology, June 2007. Electro-Optical Communications Group, Dept. of Electrical Engineering.

[131] R. Thompson and R. Roy, "Nonlinear dynamics of multiple four-wave mixing processes in a single-mode fiber," *Phys. Rev. A*, vol. 43, pp. 4987–4996, May 1991.

[132] R. Thompson and R. Roy, "Statistical fluctuations in multiple four-wave mixing in a single-mode optical fiber," *Phys. Rev. A*, vol. 44, pp. 7605–7614, Dec. 1991.

[133] E. Ciaramella, F. Curti, and S. Trillo, "All-optical signal reshaping by means of four-wave mixing in optical fibers," *IEEE Photon. Technol. Lett.*, vol. 13, pp. 142–144, Feb. 2001.

[134] D. M. Forin, F. Curti, G. M. T. Beleffi, and F. Matera, "All optical fiber 2 + 1 auxiliary carrier trransponder-regenerator," *IEEE Photon. Technol. Lett.*, vol. 17, pp. 429–431, Feb. 2005.

[135] O. Aso, S.-I. Arai, T. Yagi, M. Tadakuma, Y. Suzuki, and S. Namiki, "Broadband four-wave mixing generation in short optical fibers," *IET Electron. Lett.*, vol. 36, pp. 709–710, Apr. 2000.

[136] A. Alcaide, N. Yan, E. Tangdiongga, and A. M. J. Koonen, "Buffering strategies for contention resolution in all-optical label swapping switches," in *Proc. European Conf. on Networks and Optical Communications (NOC)*, Stockholm, Sweden, June 2007.

[137] W. D. Zhong and R. S. Tucker, "Wavelength routing-based photonic packet buffers and their applications in photonic packet switching systems," *IEEE/OSA J. Lightwave Technol.*, vol. 16, pp. 1737–1745, Oct. 1998.

[138] P. Pavon-Marino, J. Garcia-Haro, J. Malgosa-Sanahuja, and F. Cerdan, "Maximal matching characterization of optical packet input-buffered wavelength routed switches," in *Proc. IEEE Conf. High Performance Switching and Routing (HPSR)*, pp. 55–60, June 2003.

[139] F. Xue, Z. Pan, Y. Bansal, J. Cao, M. Jeon, K. Okamoto, S. Kamei, V. Akella, and S. J. B. Yoo, "End-to-end contention resolution schemes for an optical packet switching network with enhanced edge routers," *IEEE/OSA J. Lightwave Technol.*, vol. 21, pp. 2595–2604, Nov. 2003.

[140] S. Rangarajan, Z. Hu, L. Rau, and D. J. Blumenthal, "All-optical contention resolution with wavelength conversion for asynchronous variable-length 40 Gb/s optical packets," *IEEE Photon. Technol. Lett.*, vol. 16, pp. 689–691, Feb. 2004.

[141] D. K. Hunter, M. H. M. Nizam, K. M. Guild, J. D. Bainbridge, M. C. Chia, A. Tzanakaki, M. J. O'Mahony, L. D. Bainbridge, M. F. C. Stephens, R. V. Penty, and I. H. White, "WASPNET: a wavelength switched packet network," *IEEE Comm. Magazine*, vol. 37, pp. 120–129, Mar. 1999.

[142] M. C. Chia, D. K. Hunter, I. Andonovic, P. Ball, I. Wright, S. P. Ferguson, K. M. Guild, and M. J. O'Mahony, "Packet loss and delay performance of feedback and feed-forward arrayed-waveguide gratings-based optical packet

switches with WDM inputs-outputs," *IEEE/OSA J. Lightwave Technol.*, vol. 19, pp. 1241–1254, Sept. 2001.

[143] P. Seddighian, J. B. Rosas-Fernández, S. Ayotte, L. A. Rusch, S. LaRochelle, and A. Leon-Garcia, "Low-cost, scalable optical packet switching networks with multi-wavelength labels," in *Proc. Optical Fiber Comm. Conf. (OFC)*, no. OThF5, Anaheim, CA, USA, Mar. 2007.

[144] N. Calabretta, M. Presi, G. Contestabile, and E. Ciaramella, "Asynchronous all-optical circuit for serial-to-parallel conversion of label bits of DPSK packets," in *Proc. Optical Fiber Comm. Conf. (OFC)*, no. OTuB5, Anaheim, CA, USA, Mar. 2007.

[145] R. Urata, R. Takahashi, T. Yasui, T. Suemitsu, T. Nakahara, and H. Suzuki, "All-optical and optoelectronic serial-to-parallel conversion of high-speed, asynchronous optical packets," in *Proc. IEEE Lasers & Electro-Optics Society Annual Meeting (LEOS)*, vol. 2, pp. 747–748, Montreal, Que, Oct. 2006.

[146] R. Itoh, T. Konishi, and K. Itoh, "Arbitrary wavelength- and time-selective reconfigurable optical add/drop multiplexer (ROADM) using a time-space conversion and a MEMS optical switch," in *Proc. European Conf. on Optical Comm. (ECOC)*, no. We3.P.99, pp. 319–320, Cannes, France, Sept. 2006.

[147] C. Bres, N. Alic, E. Myslivets, S. Radic, "1-to-40 multicasting and amplification of 40 Gbps channels in wideband parametric amplifier," in *Proc. Optical Fiber Comm. Conf. (OFC)*, no. PDP16, Feb. 2008.

[148] J. P. Tomillo, "Analysis of optical switching fabrics based on AWGs using switchable delay lines as buffers," Master's thesis, Eindhoven University of Technology, June 2003. Electro-Optical Communications Group, Dept. of Electrical Engineering.

[149] D. K. Hunter, M. C. Chia, and I. Andonovic, "Buffering in optical packet switches," *IEEE/OSA J. Lightwave Technol.*, vol. 16, pp. 2081–2094, Dec. 1998.

[150] A. Bragg, "Generating self-similar traffic for OPNET simulations," tech. rep., Fujitsu Network Communications, Inc., 1999.

[151] G. Kramer, "Generator of self-similar network traffic." University of California Davis, June 2006. http://www.csif.cs.ucdavis.edu/∼kramer/code/trf_gen1.html.

[152] V. Paxson, "Fast, approximate synthesis of fractional gaussian noise for generating self-similar network traffic," *Computer Communication Review*, vol. 27, Oct. 1997.

List of abbreviations

AOFF	all-optical flip-flops
AOLS	all-optical label switching
AOLSW	all-optical label swapper
AOWC	all-optical wavelength conversion
ASE	amplified spontaneous emission
ATM	asynchronous transfer mode
AWG	arrayed-waveguide grating
BER	bit error rate
BPF	band-pass filter
CIP	Centre of Integrated Photonics
CoS	cost of service
CR	contention resolution
CW	continuous wave
DCR	digital clock recovery
DFG	difference frequency generation
DSF	dispersion-shifted fiber
EAM	electroabsorption modulator
ECL	extended cavity laser
ED	error detector
EDFA	erbium-doped fiber amplifier
ER	extinction ratio
FBG	fiber Bragg grating
FBM	feedback multicast
FDL	fiber delay line
FEC	forward equivalent class
FFM	feed-forward multicast

FM	frequency modulation
FP	Fabry-Pérot
FSK	frequency shift keying
FTP	file transfer protocol
FWHM	full width at half maximum
FWM	four-wave mixing
GMPLS	generalized multi-protocol label switching
HHI	Heinrich Hertz Institut
HNL	highly-nonlinear
HOL	head-of-line
HNLF	highly nonlinear fiber
HTTP	hypertext transfer protocol
IM	intensity modulator/modulation
IP	Internet protocol
IPv4	Internet protocol version 4
IPv6	Internet protocol version 6
ISDN	integrated services digital network
ITU	International Telecommunication Union
LAN	local area network
LASAGNE	all-optical label-swapping employing optical logic gates in network nodes
LD	laser diode
LER	label edge router
LiNbO	lithium niobate
λSP	λ switched path
LN-MZ	LiNbO3-based Mach-Zehnder modulator
LRD	long-range dependence
LSP	label-switched path
LSR	label switching router
MAN	metropolitan area network
MPLS	multi-protocol label switching
MPλS	multi-protocol lambda switching
MWC	multi-wavelength conversion
MZI	Mach-Zehnder interferometer
MZM	Mach-Zehnder modulator
NL	network load

NNL	normalized network load
NoCR	no contention resolution
NPS	nonlinear polarization switching
NRZ	nonreturn-to-zero
NT	network throughput
OCDM	optical code division multiplexing
OCS	optical circuit switching
OBS	optical burst switching
ODL	optical delay line
OEO	optic-electronic-optic
OLS	optical label switching
OPA	optical parametric amplification/amplifier
OPS	optical packet switching
OSA	optical spectrum analyzer
OSI	open systems interconnection
OSNR	optical signal-to-noise ratio
OTDM	optical time division multiplexing
PBS	polarization beam splitter
PC	polarization controller
PD	photo detector
PG	pattern generator
PLR	packet loss ratio
PM	phase modulation
PON	passive optical networks
PPLN	periodically poled $LiNbO_3$
PRBS	pseudorandom binary sequence
PS	phase shifter
Q factor	quality factor
QoS	quality of service
RAM	random-access memory
RF	radio frequency
Rx	receiver
RZ	return-to-zero
SC	supercontinuum
SCM	subcarrier multiplexing
SMF	single mode fiber

SMTP	simple mail transfer protocol
S/N	signal-to-noise ratio
SNR	signal-to-noise ratio
SOA	semiconductor optical amplifier
SPC	serial-to-parallel converter
SPM	self-phase modulation
SRD	short-range dependence
STOLAS	switching technologies for optically labeled signals
SWC	single wavelength conversion
TCP	Transmission Control Protocol
TDM	time-domain multiplexing
TDMA	time-division multiple access
TE	transverse electric
TLS	tunable laser source
TM	transverse magnetic
ToS	type of services
TTL	time-to-live
TW	traveling wave
TWC	tunable wavelength converter
Tx	transmitter
UOC	ultrafast optical clock
VOA	variable optical attenuator
VODL	variable optical delay line
VPN	virtual private network
WAN	wide area network
WC	wavelength conversion
WCFB	wavelength conversion with fiber buffering
WDM	wavelength division multiplexing
WWW	world-wide web
XAM	cross-absorption modulation
XGM	cross-gain modulation
XOR	eXclusive OR
XPM	cross-phase modulation

List of publications

Journal papers

1. N. Yan, J. del Val Puente, T. Silveira, A. Teixeira, A. Ferreira, E. Tangdiongga, P. Monteiro, and A. M. J. Koonen, "Simulation and experimental characterization of SOA-MZI-based multi-wavelength conversion," *IEEE/OSA J. Lightwave Technol.*, submitted.

2. N. Yan, T. Silveira, A. Teixeira, A. Ferreira, E. Tangdiongga, P. Monteiro, and A. M. J. Koonen, "40 Gbits/s wavelength multicast via SOA-MZI and applications," *IET Electron. Lett.*, vol. 43, no. 23, pp. 1300, 8 Nov. 2007.

3. N. Yan, E. Tangdiongga, H.-D. Jung, I. Tafur Monroy, H. de Waardt, A. M. J. Koonen, "Regenerative all-optical wavelength multicast for next generation WDM network and system applications," *Photon. Network Comm.*, 1387-974X (print), 1572-8188 (online), DOI 10.1007/s11107-007-0077-y, 14 Sept. 2007.

4. N. Yan, A. Teixeira, T. Silveira, G.M. Tosi Beleffi, F. Curti, D. Forin, F. Dalla Longa, I. Tafur Monroy, P. Monteiro, and A. M. J. Koonen, "Theoretical and experimental performance evaluation of all-optical multi-wavelength conversion by four-wave mixing in fiber at 10/20/40 Gb/s for optical layer multicast," *Micro. and Optic. Technol. Lett.*, vol 49, no. 5, pp. 1067-1071, May 2007.

5. A. M. J. Koonen, N. Yan, J. J. Vegas Olmos, I. Tafur Monroy, C. Peucheret, E. van Breusegem and E. Zouganeli, "Label-controlled optical packet routing – technologies and applications," *Invited paper*, *Special Issue IEEE J. Select.*

Topics in Quantum Electron., vol. 13, no. 5, pp. 1540-1549, Sept./Oct. 2007.

6. F. Ramos, E. Kehayas, J. M. Martinez, R. Clavero, J. Marti, L. Stampoulidis, D. Tsiokos, H. Avramopoulos, J. Zhang, P. V. Holm-Nielsen, N. Chi, P. Jeppesen, N. Yan, I. Tafur Monroy, A. M. J. Koonen, M. T. Hill, Y. Liu, H. J. S. Dorren, R. V. Caenegem, D. Colle, M. Pickavet, and B. Riposati, "IST-LASAGNE: towards all-optical label swapping employing optical logic gates and optical flip-flop," *Special Issue IEEE/OSA J. Lightwave Technol.*, vol. 23, no. 10, pp. 2993-3011, Oct. 2005.

International conference papers

7. N. Yan, A. Alcaide, J. M. D. Mendinueta, E. Tangdiongga, and A. M. J. Koonen, "Traffic performance evaluation of optical label switching nodes with optical layer multicast," in *Proc. Asia-Pacific Optical Comm. Conf. (APOC'07)*, vol. 6783, no. 21, Wuhan, China, 1-5 Nov. 2007.

8. N. Yan, A. Alcaide, J. M. D. Mendinueta, E. Tangdiongga, and A. M. J. Koonen, "Cost reduction and traffic performance improvement using direct forward optical layer multicast in optical label switching nodes," in *Proc.* 33^{rd} *European Conf. on Optical Comm. (ECOC'07)*, vol. 2, no. 3.2.2, Berlin, Germany, pp. 39-40, 16-20 Sept. 2007.

9. N. Yan, T. Silveira, A. Teixeira, A. Ferreira, E. Tangdiongga, P. Monteiro, and A. M. J. Koonen, "40 Gb/s all-optical multi-wavelength conversion via a single SOA-MZI for WDM wavelength multicast," *Best Paper Award*, in *Proc. Optoelectronics and Communications Conf. /* 16^{th} *Int. Conf. on Integrated Optics and Optical Fiber Communication (OECC/IOOC'07)*, Yokohama, Japan, pp. 530-531, 9-13 Jul. 2007.

10. N. Yan, H.-D. Jung, I. Tafur Monroy, H. de Waardt, and A. M. J. Koonen, "All-optical multi-wavelength conversion with negative power penalty by a commercial SOA-MZI for WDM wavelength multicast," in *Proc. Optical Fiber Comm. Conf. (OFC'07)*, JWA36, Anaheim, CA, USA, 25-29 Mar. 2007.

11. N. Yan, A. Teixeira, T. Silveira, I. Tafur Monroy, H.-D. Jung, and A. M. J. Koonen, "Optical multicast technologies by multi-wavelength conversion for optical routers," in *Prof. IEEE* 10^{th} *Int. Conf. on Communication Technology (ICCT'06)*, vol. SRGN, no. 2006072901, Guilin, China, 27-30 Nov. 2006.

12. N. Yan, A. Teixeira, T. Silveira, I. Tafur Monroy, P. Monteiro, G. Tosi Beleffi, and A. M. J. Koonen, "Optical multicasting performance evaluation using multi-wavelength conversion by four-wave mixing in DSF at 10/20/40 Gb/s," in *Proc. IEEE Int. Conf. on Photonics in Switching (PS'06)*, O 14.2, Herakleion, Crete, Greece, pp. 181-183, 16-18 Oct. 2006.

13. N. Yan, H.-D. Jung, I. Tafur Monroy, and A. M. J. Koonen, "Simultaneous one-to-four multi-wavelength conversion using a single SOA-MZI," in *Proc.* 11^{th} *European Conf. on Networks and Optical Communications (NOC'06)*, Berlin, Germany, pp. 375-380, 11-13 Jul. 2006.

14. N. Yan, A. Teixeira, T. Silveira, A. M. J. Koonen, I. Tafur Monroy, P. Monteiro, G. Tosi Beleffi, and D. Forin, "Simultaneous multi-wavelength signal conversion for transparent optical multicast," in *Proc.* 10^{th} *European Conf. on Networks and Optical Communications (NOC'05)*, London, UK, pp. 155-162, 5-7 Jul. 2005.

15. N. Yan, I. Tafur Monroy, and A. M. J. Koonen, "All-optical label swapping node architectures and contention resolution," in *Proc.* 9^{th} *Int. Conf. on Optical Networking Design and Modeling (ONDM'05)*, Milan, Italy, pp. 1-9, 7-9 Feb. 2005.

16. A. Alcaide, N. Yan, E. Tangdiongga, and A. M. J. Koonen, "Buffering strategies for contention resolution in all-optical label swapping switches," in *Proc.* 12^{th} *European Conf. on Networks and Optical Communications (NOC'07)*, Stockholm, Sweden, 19-21 Jun. 2007.

17. J. del Val Puente, N. Yan, E. Tangdiongga, and A. M. J. Koonen, "Performance comparison of multi-wavelength conversion using SOA-MZI and DSF for optical wavelength multicast," in *Proc.* 11^{th} *Int. Conf. on Optical Networking Design and Modeling (ONDM'07)*, Athens, Greece, pp. 1-10, 29-31 May 2007.

18. J. M. D. Mendinueta, I. Tafur Monroy, J. J. Vegas Olmos, N. Yan, Y. Dimitriadis, I. de Miguel, and A. M. J. Koonen, "Traffic performance study of all-optical label swapping isolated and full network topologies," in *Proc. 11^{th} European Conf. on Networks and Optical Communications (NOC'06)*, Berlin, Germany, pp. 387-394, 11-13 Jul. 2006.

19. I. Tafur Monroy, A. M. J. Koonen, J. J. Vegas Olmos, N. Yan, J. J. Jennen, C. Peucheret, and E. van Breusegem, "Optical label switching functionalities employing semiconductor optical amplifiers," *Invited paper*, in *Proc. OSA Optical Amplifiers and their Applications (OAA'06)*, Whistler, Canada, 26-28 Jun. 2006.

Regional conference papers

20. N. Yan, I. Tafur Monroy, and A. M. J. Koonen, "All-optical label swapping node architecture and contention resolution," in *Proc. ePhoton/ONe Winter School on Optical Core Network Technologies*, Aveiro, Portugal, pp. C75-C80, 23-25 Feb. 2005.

21. N. Yan, I. Tafur Monroy, A. M. J. Koonen, and D. Khoe, "All-optical label swapping node architectures and contention resolution," in *Proc. IEEE/LEOS Symp. Benelux Chapter*, Ghent, Belgium, pp. 183–186, 2-3 Dec. 2004.

22. N. Yan, I. Tafur Monroy, and A. M. J. Koonen, "All-optical label swapping technologies and node architecture," in *Proc. London Communication Symp. (LCS'04)*, London, UK, pp. 85-88, 13-14 Sept. 2004.

23. J. J. Vegas Olmos, E. J. M. Verdurmen, I. Tafur Monroy, J. P. Turkiewicz, N. Yan, H. de Waardt, and A. M. J. Koonen, "Wavelength conversion with multicasting capabilities deploying highly nonlinear fiber for time-serial labeled networks," in *Proc. IEEE/LEOS Symp. Benelux Chapter*, Mons, Belgium, pp. 181–184, 1-2 Dec. 2005.

Referable work

24. N. Yan, "Simulation of 4×4 optical packet space switch array," in *Proc. London Communication Symp. (LCS'03)*, London, UK, pp. 121-124, 8-9

Sept. 2003.

25. N. Yan, "Future IP/WDM optical switching technologies & networks," *Distinction, MSc. Telecommunications Final Project Dissertation*, Dept. of Electronic & Electrical Engineering, University College London, London, UK, Sept. 2003.

26. N. Yan, "Integrated network management system for SDH – client module design," *BSc./BEng. Communication Engineering Final Project Dissertation*, Siemens Transmission Systems Co. Ltd., & Dept. of Electrical Engineering, Zhongshan University, Guangzhou, China, June 2001.

Acknowledgement

In the last four months of continuous writing and revising my thesis, I have never come across any parts of the thesis that I found so difficult to begin. To reach this point of finalizing my doctoral thesis, I owe so many people for their great help and support throughout my PhD project. Were it not for them, I would never have made it here.

First of all, I would like to thank my promotor Prof. Ton Koonen for offering me this opportunity to conduct my research in the Electro-Optical Communication (ECO) group at Eindhoven University of Technology (TU/e) over the last four years. I am also very grateful to him for providing valuable comments on some of my papers, my draft thesis and two of the rewritten chapters. During the course of my PhD, I have been supervised by Dr. Idelfonso Tafur Monroy and Dr. Eduward Tangdiongga. I am thankful to Idelfonso for always being encouraging, especially when I was trying to find my way in my research project. I would like to thank Eduward for showing me the world of the physical-layer research and sharing his in-depth knowledge on laboratory experiments. I am very grateful to both of them for reading my thesis and giving their insightful comments, especially to Eduward who revised some of the chapters twice.

A large part of this thesis would not have existed were it not for Dr. Antonio Teixeira, who I first met at the ePhoton/ONe summer school in 2004. Thanks to our encounter, the laboratory of his group at Instituto de Telecomunicações (IT) in Aveiro, Portugal, became where I carried out my very first experiments. During my two-month stay, Antonio spent a considerable amount of time in the lab assisting me on the experiments. I am indebted to him for his guidance, support, as well as efforts to arrange the Siemens lab facilities for me in Lisbon and Aveiro. For the success of these experiments, I shall also thank Dr. Paulo Monteiro for hosting me in the Siemens lab and lending me their lab resources.

I would like to express my gratitude to Tiago Silveira, a PhD student at IT Aveiro and Siemens, who taught me a lot and stayed with me for many late evenings trying to make the setup working. For my second experiment at IT, Tiago and Ana Ferreira, another PhD student, spent two days in the lab taking the measurements for me after I took my scheduled flight back to the Netherlands. These fruitful measurements resulted in our Best Paper Award at the OECC conference in Japan and a paper published in Electronic Letters. I owe a great deal to both of them, with whom I had such an enjoyable time doing experiments, as well as spending some of our leisure hours in many places around Aveiro. I shall certainly also thank the other friends and colleagues that I met at IT Aveiro and Siemens, especially Ruben Sousa, Luis Teixeira, Ruben Luis, Daneil Fonseca, Rogério Nunes Nogueira and Paulo André.

During my PhD studies, I have supervised and worked together with five international Master students. From my first Erasmus student Marco Orallo Rodriguez, followed by Jose Manuel Delgado Mendinueta, Aleida Alcaide García, and Jorge Del Val Puente, to my most recent student Li Pu, all of them contributed in one way or another to the many simulation results that are included in this thesis in support of my research ideas. Next to that, I also learnt a lot from their expertise on the simulation environment. I would like to thank them all for their useful inputs to this thesis and for our many inspiring discussions.

My PhD project is in the framework of the European Commission funded IST-LASAGNE project. During the three years of the LASAGNE project, I had the opportunity to meet and share ideas with many of our academic and industrial project partners and fellow PhD students. I am thankful to all of them for the fruitful discussions and the pleasant time we spent together. Special thanks are given to our project coordinator Prof. Javier Martí for coordinating various project meetings and keep the project running to its successful completion; to Monica Teruel for all the hard administrative work; to Ruth van Caenegem, Didier Colle, Efstratios Kehayas, Leontis Stampoulidis, Jose M. Martinez, Pablo V. Holm-Nielsen, Marco Schiano, Idelfonso, Harm Dorren, Liu Yong, Graeme Maxwell, and all the other names that I cannot list exhaustively here, for the productive interactions within the project.

There is one person that, although not directly related to my work, has always made me believe in myself and my decisions, and strongly motivated me in pursuing what I want to achieve. This person is Prof. Izzat Darwazeh. Izzat was a great lecturer teaching at my Master course in MSc. Telecommunications at University

College London (UCL). He gave me much support and encouragement during the first years of my PhD and introduced me to many of his academic acquaintances including Antonio. I am indebted to him for helping me to establish my way and my own network. Next to him, I would like to thank Dr. John Mitchell and Dr. Robert Kelly, also involved in my Master programme at UCL, for always being encouraging when we met again at various occasions.

I am thankful to all my doctorate committee members for participating in my defense, and their interest in my work. I appreciate the expert comments from my external committee members, Prof. Javier Martí and Prof. Mario Pickavet, on the first draft of my thesis. I am grateful to Prof. Jan Bergmans for his detailed revision. I would also like to thank Prof. Harm Dorren and Prof. Onno Boxma for sparing valuable time-slots from their busy agenda to discuss specific parts of my thesis.

My officemates are the ones that have been sharing my everyday happiness and all the ups and downs during the last four years. For most of my PhD I have been seated in the room PT 11.06, at my lovely window-side. Here I have had many laughters, chats, and discussions with Bas Huiszoon, Archi Delphinanto, Johan van Berkel, Patryk Urban, and most recently Karen Solis Trapala. Among us, Bas is a great source of information for, e.g. from general queries of "Dutch culture and language" to specific research-relevant tips; Archi is the expert of regulations concerning social welfare and tax-returns, and as a young father, has given me a lot of useful tips related to childcare; Patryk can bargain almost like a Dutch, and he and his girlfriend Marta have a great hospitality; Karen, my new and very welcomed female companion, is a motivated young lady who enjoys fruits, good food and exercise, although due to the tight schedule we have, our daily (or weekly) exercise plans did not work out quite persistently. I would like to thank you all for the lovely time we have had, as well as our mutual understanding and help.

There are also many other ECO-members that I shall heartily acknowledge. Just to name a few, I am thankful to Prof. Djan Khoe for his comments on some of my papers; Dr. Huug de Waardt for his availability whenever I went for questions and suggestions concerning my papers and my thesis; our secretaries Susan de Leeuw, Els Holleman, and José Hakkens for all their arrangements and diligent administrative work; Dr. Kevin Williams for revising two of my thesis chapters; Christos Tsekrekos and Maria García Larrodé for our peer experience sharing and discussions; Nicola Calabretta and Hyun-Do Jung for always being cheerful and positive; Johan van Zantvoort and Frans Huijskens for their active participation

in Beugelen; all the Chinese colleagues for creating a nice and warm "home" atmosphere; Aaron Albores Mejia as a daily and pleasant visitor to our office at lunch and off-work times; Jeffrey Lee for his frequent greetings at conferences; as well as many ex-colleagues such as Javier Molina, Liu Yong, Shaoxian Zhang, Zhonggui Li, Erwin Verdurmen, René Kramer, Kun Wang, Sander Lars Jansen, and Anthony Ng'oma. I would also like to thank Tim Schenk, formerly from the ECR group, for his extensive interactions with our ECO members, especially the ones on the 11^{th} floor.

Eindhoven is a technical and international city. I have had made many new friends during these years but most of them moved away after the completion of their contracts or assignments. Among all my friends here, special thanks to Alke and Luna, two of my best friends over these four years, and Alke's whole family Erna, Justus, and Karmijn, who always make me feel at home. I would also like to thank Therry for her sincere friendship; Rosemarie for the great time we had together; Günter and Waltraud for their hospitality whenever we were in their neighborhood; Javier and Estelle for our delightful outings and dinners; Fred for sharing our thoughts about career and development; René for his nice "call for events"; and Huiyu for her lovely spontaneousness. And I should certainly not forget to acknowledge our newly-acquainted neighbors Christoph and Aya, who are always willing to offer a hand, as the old Chinese saying says: *Having a close neighbor is better than having a relative who lives far away.*

Last but not least, I would like to address all my family members. My parents, though at almost the other end of the globe, have always been there for me, and been proud of me. Francesco, without his constant support, all the sacrifice he has made, and all his love and affection, I would still be washing the dishes, running the laundry and vacuum-cleaning the house. Everyday a new surprise with her master of English, Dutch, Chinese and a little bit of Italian, our little Angela Shijia is a wonder, and is the biggest achievement that I have had during my PhD and my whole life. Francesco's parents Mari and Giacomo, had to fly over from Italy many many times helping us "sorting out" our rather messy lifestyle coping awkwardly with a little running citizen having her own opinions. Elisa, Francesco's sister and Angela's "MY aunt!!!", is a magnet for Angela's full attention, and thus indirectly "contributed" to the production of many chapters in this book.

Curriculum vitæ

Ni Yan was born in Wuhan, China, in January 1979. In June 2001, she received her *B.Eng. in Communication Engineering* degree from Zhongshan University in Guangzhou, China. During her Bachelor studies, she conduced two one-month industrial internship at China Telecom and China Mobile, on setting up a local area network with a Cisco router and fiber splicing. Between February and June 2001, she carried out her Bachelor final project at Siemens Transmission Systems Co. Ltd. on the subject of "Design of Integrated Network Management System for Synchronous Digital Hierarchy", in the Technical Assistant Center II Department. During her undergraduate studies, she attained *IBM Certified Specialist certificate as AS/400 Associate System Operator* and *Cisco Certified Network Associate (CCNA)* certificate, respectively in October 2000 and March 2001.

From June 2001 to September 2002, she worked as a *project implementation engineer* in the Project Implementation Department at Siemens Transmission Systems Co. Ltd., in Guangzhou, the headquarters of Siemens Information & Communications Networks in China. She participated in two national projects setting up the Chinese backbone optical networks for China Mobile and China Unicom, which lasted three to six months each, and two provincial and one local projects for China Telecom, which lasted one to two months each. She received the Telecommunication Network Management System (TNMS) Primary Acceptance Certificate with her successful completion of the TNMS network installation and configuration at three sites in Guangdong Province in a national project for China Mobile.

In September 2003, she received her *M.Sc. in Telecommunications* degree with

Distinction from University College London (UCL) in London, UK. She conducted her Master final project, also with *Distinction*, on the topic of "Future IP/WDM Optical Switching Technologies & Networks", in the Optical Networks Group and Telecommunications Group at the Department of Electrical & Electronic Engineering. Between October and December 2003, she worked part-time as a facilitator in the Department of Education and Professional Development at UCL, facilitating individuals and teams in various postgraduate development courses and activities.

Since January 2004, she has been working as a *Ph.D. researcher* in the Electro-Optical Communication (ECO) Systems group within the Cobra Research Institute at Eindhoven University of Technology, the Netherlands. She was involved in the European Commission funded IST-LASAGNE (all-optical LAbel SwApping employing optical logic Gates in NEtwork nodes) project (http://www.ist-lasagne.org/) and IST-STOLAS (Switching Technologies for Optically LAbelled Signals) project (http://www.ist-stolas.org/). Upon the completion of this thesis, she has published 12 first-authored and 6 co-authored international journal and conference papers, and has presented her work at the world's major international conferences in Europe, the United States and Asia. She has also served as a peer-reviewer for Electronic Letters from the Institution of Engineering and Technology (IET), an internationally renowned journal that publishes high-quality, short original research papers.

In November 2006, she and Francesco Dalla Longa together won the first prize of the STW Business Challenge with their business proposal in Delft, the Netherlands, during the two-day workshop of Orientation on Entrepreneurship, co-organized by the Technologiestichting STW and the Wageningen Business School. In July 2007, she received the Best Paper Award in Yokohama, Japan, at the International OptoElectronics and Communications Conference (OECC), technically co-sponsored by the Institute of Electrical and Electronics Engineers (IEEE), Optical Society of America (OSA) and the International Society for Optical Engineering (SPIE).

Her current research interests mainly include optical label switching node architectures, optical packet switches, all-optical multi-wavelength conversion technologies and applications. She is also interested in computer networks and information security.

"...to make an end is to make a beginning.

The end is where we start from"

T. S. Eliot, *Little Gidding*